VISUALISING THE MYCOBACTERIAL MUTASOME

by

Michael Anton Reiche
RCHMIC017

Submitted to the University of Cape Town
Faculty of Health Sciences
Department of Pathology

In fulfilment of the requirements for the degree

DOCTOR OF PHILOSOPHY in MEDICAL MICROBIOLOGY

February 2018

The financial assistance of the National Research Foundation (NRF) towards this research is hereby acknowledged. Opinions expressed, and conclusions arrived at, are those of the author and are not necessarily to be attributed to the NRF.

ABSTRACT

An SOS-inducible DNA repair system has been linked to transient hypermutation and the development of drug resistance in *Mycobacterium tuberculosis*. Previous work has established that this "mycobacterial mutasome" comprises the specialist DNA polymerase, DnaE2, and accessory factors of unknown function, ImuA′ and ImuB. However, the molecular interactions and subcellular recruitment dynamics enabling mutasome function remain poorly understood. Here, a panel of fluorescent strains of *M. smegmatis* was developed to investigate expression and subcellular localization of ImuA′ and ImuB in live mycobacteria exposed to genotoxic agents. Using fluorescence microscopy, it was observed that, during prolonged genotoxic stress, single *M. smegmatis* cells exhibited an elongated cell phenotype and apparent aneuploidy – potentially providing an environment for recombination between differentially mutated chromosomes. Furthermore, ImuB was seen to associate with the *dnaN*-encoded β clamp in discrete foci during mutagenic DNA repair. In contrast, ImuA′ did not exhibit similar localization and instead appeared to diffuse throughout the bacillus. A mutant ImuB protein deficient in the β clamp-binding motif failed to co-localize with the β clamp, reinforcing the inferred essentiality of the ImuB-β clamp protein-protein interaction for mutasome recruitment and induced mutagenesis. Additionally, exposure of *M. smegmatis* to griselimycin, a novel β clamp-targeting natural product antibiotic, prevented ImuB-β clamp co-localization during SOS induced mutagenesis, an observation confirmed by superresolution, three-dimensional interferometric photo-activated light microscopy. These results establish the capacity of griselimycin to inhibit DNA replication as well as prevent DNA damage-induced mutagenesis by disrupting mutasome assembly and activity. Notably, this

differentiates griselimycin from other inhibitors of DNA metabolic function which carry the often-unavoidable liability of accelerating drug-resistance by inducing mutagenic DNA repair. In turn, it suggests the potential application of griselimycin as an anti-evolution agent in novel therapeutic regimens designed to protect existing anti-tuberculosis drugs.

DECLARATION OF ORIGINALITY

This thesis has been submitted to the *Turnitin* module (or equivalent similarity and originality checking software) and I confirm that my supervisor has seen my report and any concerns revealed by such have been resolved with my supervisor.

Name: **Michael Reiche**

Student number: **RCHMIC017**

Signature: Signed by candidate

Date: **16 February 2018**

DEDICATION

This thesis is dedicated to my late grandfather,
Colyn Kilton Else, who shared with me his incredible
passion and love for science and knowledge.

ACKNOWLEDGEMENTS

I would like to take the time to acknowledge all those that have contributed to this work in some way and thank everyone who has helped me through the course of this degree, which started with a Master's degree, was upgraded to a PhD, and finally culminated in the completion of this thesis.

First and foremost, I would like to thank my beloved family. Thank you, Mom. Thank you, Dad. Thank you, Sam. Thank you for the unrelenting support and always being there for me through the good and bad times. Mom and Dad, thank you for your support (of all kinds) which has allowed me to reach for my dreams – I sincerely hope I have made you both very proud.

Single-handedly the most important person involved in this thesis is Prof. Digby Warner. Thank you for always going beyond what is expected of a supervisor. Thank you for your knowledge and wisdom. Thank you for guiding me and brainstorming with me. Thank you for the opportunities you introduced to me and helped me pursue. Thank you for giving me the opportunity to work in the MMRU where I have been exposed to amazing science and wonderful people. It has been a remarkable honour to have you as a mentor and a PhD supervisor.

In a similar vein, I am also grateful to Prof. Valerie Mizrahi. Thank you for your time and expertise and for always holding the members of the MMRU to an exceptionally high standard. I am always grateful for the wisdom and knowledge you have imparted to me, either personally, or as a member of the laboratory. Without your hard work and passion for science, much of what I have done, experienced, learned, and been exposed to would never have been possible.

To all the (old and new) members of the MMRU, I am so grateful for everything you have done with me – whether it be big or small. Thank you for teaching me tips and tricks in the lab. Thank you for all the brainstorming and problem solving. Thank you for critiquing my work and giving me advice. And thank you for always being great people to be around – both inside and outside the lab.

To Dr Sophia Gessner, I practically cannot list here all the aspects of our friendship I am grateful for – all I can say is that I am grateful for all of it. Thank you, Simon Broadley, for making everything we did together so much fun. Dr Zanele Ditse, thank you for teaching me so many things. Dr Atica Moosa, I am incredibly grateful to you for all of your support and wisdom and for helping me with difficult decisions. Dr Anastasia Koch, thank you for always being caring, kind, and willing to help – you helped me more than you realise. To Dr Vinayak Singh, Dr Joanna Evans, and Dr Krupa Naran, thank you for your technical help and advice in the lab. I am also deeply thankful to Ndalo Katywa and Elrico Jooste for their work in the lab that made it easier to focus on experiments.

To Prof. Dirk Lang and Susan Cooper, thank you for your time, effort, and help with the confocal microscope and for teaching me everything you did. Similarly, thank you to Erica Smith for helping and assisting me with the flow

cytometry. I am incredibly grateful to Dr Jesse Aaron, Dr Teng-Leong Chew, and Satya Khuon for your insight, knowledge, and help during my stay at the HHMI – I cannot express how honoured I am to have spent time at Janelia working on the iPALM. My time at the AIC was one of my favourite scientific experiences.

Thank you to Prof. John McKinney, Dr Neraj Dhar, Dr Isabella Santi, and Prof. Dr Rolf Müller for supplying me with some of the molecular and chemical tools I used during my research.

Finally, I would like to thank Carla Collins for always being excited for me during my thesis write-up. Thank you to Debbie Lopes for helping and supporting me during my PhD. Thank you to all my friends that made my time outside of academics so much fun and giving me excuses to break away from work. Thank you to Douglas and Kim Else for being there for me from the beginning.

Thank you to the following sources of funding for their support:

- US National Institute of Child Health and Human Development (USA): grant no. U01HD085531-02, awarded to Prof. Digby Warner and Dr Roger Woodgate.
- Howard Hughes Medical Institute (USA): Senior International Research Scholars grant (grant no. 55007649), awarded to Prof. Valerie Mizrahi.
- The Department of Science and Technology (ZA) and National Research Foundation (ZA), awarded to Prof. Valerie Mizrahi.
- The South African Medical Research Council (ZA), awarded to Prof. Valerie Mizrahi.
- The Research Council of Norway (NOR), INTPART and AMR-PART, awarded to Prof. Digby Warner.
- National Research Foundation (ZA): Free-standing Scarce Skills Master's (2014) and Doctorate (2016) Scholarships (grant no. 104683).
- National Research Foundation (ZA): Student Travel Grant (linked to grant no. 104683), 2015 and 2017.
- Whitehead Scientific (ZA): Travel Award, 2016.

LIST OF ABBREVIATIONS, ACRONYMS, SYMBOLS, AND UNITS

2YT	Two yeast tryptone
2D	Two-dimension
3D	Three-dimension
A	Adenosine
AAAAG(G)	Mutant β-binding domain sequence of ImuB
AIA	Mutant catalytic site sequence of DnaE2
AFU	Arbitrary fluorescence unit
AMI	Aminoglycoside
Am^R	Ampicillin-resistance
ATP	Adenosine triphosphate
BDQ	Bedaquiline
BLAST	*Basic Local Alignment Search Tool*
bp	Base pair
BRTC	BRCA1 C-terminal
BSA	Bovine serum albumin
C	Cytosine
C. crescentus	*Caulobacter crescentus*
$CD4^+$	Cluster of differentiation 4-positive
CFU	Colony forming unit
CFZ	Clofazamine
CI	Confidence interval
CIP	Ciprofloxacin
cm^2	Square centimetre
dATP	Deoxyadenosine triphosphate
dCTP	Deoxycytidine triphosphate
dGTP	Deoxyguanosine triphosphate
dH_2O	Distilled water
DIC	Differential interference contrast
DMSO	Dimethyl sulfoxide
DNA	Deoxyribose nucleic acid
DnaE1	DnaE1 replicative polymerase, encoded by *dnaE1*
DnaE2	DnaE2 polymerase, encoded by *dnaE2*
DnaN	DnaN protein, encoded by *dnaN*
dNTP	Deoxyribonucleotide triphosphate
dTTP	Deoxythymidine triphosphate
E. coli	*Escherichia coli*
EDTA	Ethylenediaminetetraacetic acid
EGFP	Enhanced green fluorescent protein
EM	Electron-multiplying
EMB	Ethambutol

EMCCD	Electron-multiplying charge coupled device
ESX	ESAT6-protein family secretion system
EtBr	Ethidium Bromide
ETH	Ethionamide
Et al.	*Et alia*
FLQ	Fluoroquinolone
FP	Fluorescent protein
FSC	Forward-scatter
G	Guanine
g	Gram
GC	Guanine-cytosine
GENT	Gentamycin
GFP	Green fluorescent protein
Gm^R	Gentamycin-resistance
GRS	Griselimycin
h	Hour(s)
H37Rv	Wild-type laboratory strain of *Mycobacterium tuberculosis*
HGT	Horizontal gene transfer
HIV	Human Immunodeficiency Virus
I.e.	*Id est*
ImuA′	Inducible mutation protein A-prime, encoded by *imuA′*
ImuABC	Mutagenic cassette proteins ImuA, ImuB, and ImuC
ImuB	Inducible mutation protein B, encoded by *imuB*
Indel	Insertion and/or deletion
INF-γ	Interferon gamma
INH	Isoniazid
iPALM	Interferometric photo-activated light microscopy
IQR	Interquartile range
KAN	Kanamycin
Km^R	Kanamycin-resistance
kD	Kilodalton
LB	Luria-Bertani
LexA	LexA repressor, encoded by *lexA*
M	Molar
MCherry	MCherry fluorescent protein, encoded by *mCherry*
MCS	Multiple cloning site
MDR	Multi-drug resistant
MEos4a	MEos4a fluorescent protein, encoded by *mEos4a*
Met	Methionine
mg	Milligram
MIC	Minimum inhibitory concentration
MIMF	Mean inducible mutation frequency
min	Minute(s)

mJ	Millijoule
ml	Millilitre
mM	Millimolar
mm	Millimetre
MMC	Mitomycin C
MMS	Methyl methanesulfonate
MOX	Moxifloxacin
mRNA	Messenger RNA
ms	Millisecond(s)
Msm	*Mycobacterium smegmatis*
Mtb	*Mycobacterium tuberculosis*
n	Number
NA	Numerical aperture
NCBI	*National Center for Biotechnology Information*
NER	Nucleotide excision repair
ng	Nanogram
NHEJ	Non-homologous end-joining
NK	Natural Killer
nm	Nanometre
NQO	4-Nitroquinoline 1-oxide
NRG	Nargenicin
NVB	Novobiocin
OADC	Oxidase-albumin-dextrose-catalase
OD_{600}	Optical density at 600 nm wavelength light
ORF	Open reading frame
P('*gene*')	Promoter of gene
PAS	Para-aminosalisylic acid
PBS	Phosphate-buffered saline
PCR	Polymerase chain reaction
PHP	Polyhistidinol phosphatase
Pol	Polymerase
PPI	Protein-protein interaction
PSOS('*gene*')	SOS promoter of gene
PZA	Pyrazinamide
QLPLWG	Wild-type β-binding domain sequence of ImuB
qRT-PCR	Quantitative, reverse transcription PCR
RBS	Ribosome binding site
rcf	Relative centrifugal force
RE	Restriction endonuclease
RecA	RecA protein, encoded by *recA*
RecA*	Activated nucleoprotein filament of RecA
RIF	Rifampicin
Rif^{200}	200 μg/ml rifampicin

RNA	Ribonucleic Acid
RNI	Reactive nitrogen intermediates
ROS	Reactive oxygen species
rpm	Revolutions per minute
RRDR	Rifampicin-resistance determining region
s	Second(s)
S. aureus	*Staphylococcus aureus*
S. typhimurium	*Salmonella enterica* serovar Typhimurium
SD	Standard deviation
SEM	Standard error of the mean
Seq.	Sequence
SM	Streptomycin
SNP	Single nucleotide polymorphism
spp.	*Species pluralis*
SSA	Single-stranded annealing
SSB	Single-stranded binding protein, encoded by *ssb*
SSC	Side-scatter
ssDNA	Single-stranded DNA
T	Thymine
T_A	Annealing temperature
TAE	Tris base, acetic acid, and EDTA
T_AOPT	Optimal annealing temperature
TB	Tuberculosis
TFB	Transformation buffer
Th1	T helper class one
TIRF	Total internal reflection fluorescence
TLS	Translesion DNA Synthesis
TNF-α	Tumour necrosis factor alpha
U	Enzyme unit
UK	United Kingdom
UmuD	Polymerase V subunit UmuD, encoded by *umuD*
USA	United States of America
UV	Ultraviolet
V	Volt
v/v	Volume-per-volume
VFP	Venus fluorescent protein
w/v	Weight-per-volume
Wag31	Wag31 protein, encoded by *wag31*
WHO	World Health Organisation
WT	Wild-type
wt	Wild-type allele
XDR	Extensively drug resistant
Y2H	Yeast two-hybrid

ZA	South Africa
Δ'*gene*'	Deletion mutant or knockout of gene
λ	Wavelength
μ	Time constant
μF	Microfarad
μg	Microgram
μl	Microlitre
μm	Micrometre
μM	Micromolar
β [clamp]	Homodimer of DnaN, encoded by *dnaN*
λ	Wavelength
Ω	Ohm
°C	Degree Celsius
⊗	Digested with
→	Changes to
± and ~	Approximately

THESIS OUTLINE

Please refer to the table of contents, list of figures, and list of tables for each chapter presented at the beginning of each chapter for a detailed page list

CHAPTER I: LITERATURE REVIEW

Table of Contents: **Page**

List of Tables: **Page**

List of Figures: **Page**

1. Introduction

Mycobacterium tuberculosis (*Mtb*) is the etiological agent of tuberculosis (TB), a disease which is prevalent in 1 % of the global population and caused the death of 1.67 million people in 2016 (WHO, 2017). Moreover, it is estimated that between one third and one quarter of the global population is infected with latent *Mtb* (Dye, *et al.,* 2002; Houben and Dodd, 2016). In alignment with the global occurrence of latent *Mtb* infection, active TB disease presents a large healthcare problem in southern Africa and, together with Human Immunodeficiency Virus (HIV) infections, continues to exact a massive toll on public health programs in the region (Gandhi, *et al.,* 2006; Dheda, *et al.*, 2014, 2017). This co-morbidity is contributed to by a multitude of socioeconomic and biological factors including the dysregulation of the anti-TB immune response caused by the depletion of immune cells, in particular $CD4^+$ T-cells, as a result of infection with HIV (Miedema, *et al.*, 1988; Brenchley, *et al.*, 2004; Dheda, *et al.*, 2017); treatment with corticosteroids; diabetes mellitus (Dheda, *et al.*, 2017); vitamin D deficiency; poor nutrition; smoking; over-crowding; and alcohol or drug abuse. As such, TB is considered one of the largest global health issues together with other infectious diseases such as malaria and HIV. As a result, TB continues to affect a large number of people both within South Africa and throughout the world.

The reasons for the continued impact of *Mtb* infection are multiple and complex and include environmental as well as biological factors. Among the latter is the genetic malleability of the microorganism, which is epitomized by the rapid development of drug resistance globally (Dheda, *et al.*, 2017). The micro-evolution and adaptation of *Mtb* against chemotherapy illustrates a core

property responsible for the success of this pathogenic organism which seemingly transcends the ability of modern medicine to restrict it – thereby threatening the major pillar of TB control efforts globally (Andrei and Platon, 2017). As a result, patients infected with multi-drug resistant (MDR) or extensively drug resistant (XDR) strains of *Mtb* are often unable to be effectively cured of TB (Dheda, *et al.*, 2017). The increasing proportion of MDR – rifampicin (RIF) and isoniazid (INH) resistance – and XDR – resistance to RIF, INH, any fluoroquinolone (FLQ), as well as an injectable aminoglycoside (AMI) – cases of TB underscores the need to develop new and effective anti-TB drugs. Furthermore, anti-TB drugs are often highly toxic to patients (Zheng and Av-Gay, 2016; Yee, *et al.*, 2003; Forget and Menzies, 2006; Yew and Leung, 2006; Bloss, *et al.*, 2010; Falzon, *et al.*, 2012), particularly in combination (WHO, 2013), further justifying the need for new anti-TB drugs. However, drug discovery and development are expensive, time-consuming, and often fail to yield suitable drug options that translate into clinical use (reviewed by Ma, *et al.*, 2010; Koul, *et al.*, 2011; Mikušová and Ekins, 2017; Zheng and Av-Gay, 2016; Butler, *et al.*, 2016).

Drug resistance occurs in *Mtb* through the random acquisition of nucleotide sequence changes within the gene encoding the protein target of the antibiotic (or proteins involved in the uptake or activation of the compound). Such mutations can result in the loss of susceptibility to a compound at concentrations that would normally result in the cessation of growth (bacteriostatic) or bacillary death (bactericidal) (Kaur, *et al.*, 2015). In the majority of cases, microbes develop drug resistance through the acquisition of drug-resistance cassettes via horizontal gene transfer (HGT) mechanisms

(Ochman, *et al.*, 2000; Gogarten, *et al.*, 2002) such as plasmid acquisition, insertion sequences, or phage infection, which allows the distribution of drug-resistance genes throughout a microbial population. Such gene transfers often result in the recombination, deletion, or duplication of operons, genes, or gene segments that consequently confer drug resistance by a number of mechanisms (review by Munita and Arias, 2016; and Blair, *et al.*, 2015). However, drug resistance mutations can also occur through the *de novo* acquisition of single nucleotide polymorphisms (SNPs) (discussed in detail in subsequent sections), insertions and deletions (indels), and gene duplication by recombination (Zhang, 2003; Gevers, *et al.*, 2004; Serres, *et al.*, 2009). However, unlike other bacteria, intra- and inter-species HGT is uncommon in members of the *Mtb* complex, with the exception of *Mycobacterium canettii* (Boritsch, *et al.*, 2016; Eldholm and Balloux, 2016). This fact is exemplified by the closed genome of *Mtb* which does not include significantly large pangenomic regions that vary between different strains (Cole, *et al.*, 1998; Ochman, *et al.*, 2000; Borrell and Gagneux, 2011). This is likely associated with the significant physical barrier of entry to environmental DNA molecules caused by the complex and highly specialized mycobacterial cell wall – the same factor that renders *Mtb* intrinsically tolerant to many compounds that exhibit *in vitro* target efficacy (reviewed by Jarlier and Nikaido, 1994; Jankute, *et al.*, 2015). This is potentially further confounded by the 'genetic isolation' associated with pulmonary alveoli, granulomas, and phagosomes where *Mtb* naturally occurs during infection resulting in very limited opportunity to interact and transfer DNA with other bacteria within the relatively sterile environments. However, it should be noted here that conjugation has been identified to be dependent on functional ESAT6-protein family secretion system (ESX)-1- and ESX-4-

mediated pathways in *Mycobacterium smegmatis* (*Msm*) (Parsons, *et al.*, 1998; Coros, *et al.*, 2008; Gray, *et al.*, 2016) and in *Mycobacterium canettii* but is absent in other strains of the *Mtb* complex (Boritsch, *et al.*, 2016). Regardless, drug resistance appears to occur exclusively as a result of *de novo* mutation in clonal *Mtb* (Dos Vultos, *et al.*, 2008). These resistance-conferring mutations consist predominantly of SNPs within specific genes and have been linked to the resistance of almost all anti-TB drugs (as discussed in subsequent sections). In addition, the development of MDR strains has been observed to occur by the step-wise acquisition of mutations (Manson, *et al.*, 2016; Borrell, *et al.*, 2013; Saunders, *et al.*, 2011; Merker, *et al.*, 2013; Trindade, *et al.*, 2009; Bergval, *et al.*, 2012) – both in terms of resistance-associated and compensatory mutations (Comas, *et al.*, 2012; de Vos, *et al.*, 2013; Casali, *et al.*, 2014; Brandis and Hughes, 2013). This information highlights the requirement for endogenous mutations for the success of *Mtb* and suggests a potential weak link due to the complete dependence on mutation for adaptive evolution.

Within mycobacteria and *Mtb* in particular, *de novo* mutations can occur by a number of processes. However, the focus of this thesis is on the mechanism known as inducible mutagenesis, which is characterized by the increase in mutation rate following DNA damage. A mutagenic DNA repair pathway has been identified to be responsible for this phenomenon in *Mtb* and *Msm* (Boshoff, *et al.*, 2003) and consists of a C family polymerase, encoded by the gene *dnaE2*, capable of synthesizing new DNA across lesions induced by ultraviolet (UV) irradiation, such as cyclobutane pyrimidine dimers and 6-4 pyrimidine-pyrimidone adducts (Beggs, 2002), or mitomycin C (MMC), which results in inter- and intra-strand DNA cross-linking (Tomasz, *et al.*, 1988).

Repair of such lesions occurs through the process known as translesion DNA synthesis (TLS), which is a phenomenon that has been identified in eukaryotes as well as prokaryotes (reviewed by Goodman and Woodgate, 2013). Although some TLS polymerases are able to repair DNA lesions in a non-mutagenic fashion (*i.e.*, Takeiri, *et al.*, 2014; and reviewed by McCulloch and Kunkel, 2008), in the case of DnaE2, DNA synthesis is associated with the generation of mutations (Boshoff, *et al.*, 2003).

In a later development, the accessory factors ImuA' and ImuB were determined to be essential to the function of DnaE2 (Warner, *et al.*, 2010). Together, the three-component, SOS-dependent mechanism, known as the 'mycobacterial mutasome', contributes to the *in vitro* (and potentially *in vivo*) tolerance of DNA damage as well as DNA damage-inducible mutagenesis (Boshoff, *et al.*, 2003; Warner, *et al.*, 2010). The term 'mutasome' refers to the complex of proteins associated with a stalled replication fork during mutagenic TLS (Echols and Goodman, 1990). Importantly, this mycobacterial mutasome is the only inducible mutagenesis pathway identified in *Mtb* and is highly conserved in the model organism, *Msm* (Warner, *et al.*, 2010).

Despite the significant contribution of the mycobacterial mutasome to the mutagenic capacity and micro-evolution of *Mtb*, the precise molecular mechanisms enabling mutasome function remain largely unknown. To this end, this literature review will explore associated literature and knowledge surrounding bacterial inducible mutagenesis, drug resistance in *Mtb*, as well as the knowledge of the mycobacterial mutasome and similar mutagenic pathways in other bacteria. The aim is to synthesize all available evidence into

a composite review that details DNA replication dynamics; the utility of the mycobacterial mutasome during infection of *Mtb*; and explores the potential for targeting the mycobacterial mutasome to reduce the micro-evolution of drug resistance.

1.1. Host Responses and Conditions Associated with Genotoxic Stresses in *Mtb*

TB is an airborne disease and is transmitted by aerosol via the respiratory tract. Here, *Mtb* bacilli are inhaled deep into lung alveoli where they are taken up by pulmonary macrophages that initiate a series of immunological events resulting in the formation of a granuloma, consisting of macrophages, foamy macrophages, Langerhans cells, antibody-producing B-cells, dendritic cells, natural killer (NK) cells, epithelioid cells, fibroblasts, and T-lymphocytes (reviewed by Russell, 2007; Ramakrishnan, 2012; and Cadena, *et al.*, 2017). One of the responses of mononucleated phagocytes following uptake of *Mtb* is an oxidative burst. Here, macrophages generate reactive oxygen species (ROS) such as hydrogen peroxide and superoxide (Adams, *et al.*, 1997). In parallel, reactive nitrogen intermediates (RNI), such as nitric oxide, nitroxyl, nitrogen dioxide, and nitrate, are generated by nitric oxide synthase as a result of interferon gamma (IFN-γ) and tumor necrosis factor alpha (TNF-α) produced by associated Th1 lymphocytes (Adams, *et al.*, 1997). However, a recent study from the Sassetti laboratory has suggested that nitric oxide plays a subtler role during *Mtb* infection by regulating anti-inflammatory responses (specifically of neutrophils) rather than by direct antibacterial activity (Mishra, *et al.*, 2017). Regardless of the role of nitric oxide, it is theorized that the resulting oxidative conditions mediated by ROS within the site of infection represent one of the

main innate immune responses to *Mtb* infection in an attempt to clear intracellular bacterial infection. These oxidizing agents are able to damage macromolecules such as proteins, lipids, and the genetic material of the intracellular *Mtb*, ultimately leading to bacterial death (Nathan and Shiloh, 2000; Burney, *et al.*, 1999). It is important to reiterate that DNA damage may therefore occur as a result of infection and the host immune response. Correspondingly, it has been long thought that the generation of oxidative stress plays an important role in the bactericidal effect of antibiotics (see Zhao, *et al.*, 2014a; and Kohanski, *et al.*, 2007). However, this idea is highly disputed (Liu and Imlay, 2013; Keren, *et al.*, 2013) and fails to provide a functional mechanism of antibiotic killing during anaerobic conditions, although oxidation of dCTP has been linked to antibiotic killing of stationary phase *Mtb* (Fan, *et al.*, 2018). Regardless, it is evident that both exogenously- and endogenously-derived DNA-damaging oxidative stress is present within *Mtb* during infection.

1.2. Antitubercular Drug Therapy

In addition to the host-derived defences, *Mtb* encounters other factors that influence not only the propagation of the pathogen but the integrity of the genome as well. Following diagnosis of active *Mtb* infection, standard combination therapy is administered and consists of treatment with INH, RIF, ethambutol (EMB), and pyrazinamide (PZA) for two months followed by a further four months of treatment with only INH and RIF. Previously treated (and unresponsive) cases of TB are treated for three months with INH, RIF, EMB and PZA, followed by a further five months of INH, RIF, and EMB chemotherapy. Cases suspected of drug resistance are treated for a total of 18

months with a combination of PZA or EMB, an injectable AMI, and a FLQ (Reviewed by Müller, *et al.*, 2013). However, treatment courses for MDR-TB in some countries last in excess of 20 months and require daily administration of drugs which are generally less effective and often cause side-effects (Shehzad, *et al.*, 2013; WHO, 2017). Such scenarios may contribute to patient non-adherence which is commonly associated with treatment failure (Frieden and Sbarbaro, 2007; Volmink and Garner, 2007; Hirpa, *et al.*, 2013; Ormerod, 2005; Moonan, *et al.*, 2011). In addition, the exposure of anti-TB compounds to mycobacteria has numerous effects on bacilli physiology that may or may not result in the clearance of the pathogen. Recent studies have reported that *Escherichia coli* (*E. coli*) developed antibiotic tolerance during intermittent ampicillin exposure *in vitro* (Fridman, *et al.*, 2014; van den Bergh, *et al.*, 2016) which was eventually followed by the development of drug resistance (Levin-Reisman, *et al.*, 2017). The formation of drug-tolerant persister (or slow growing) *Mtb* bacilli has previously been observed *in vitro* (Deb, *et al.*, 2009; Torrey, *et al.*, 2016), therefore it is possible this also plays a role in the development of drug resistant TB during drug therapy (see review: Fisher, *et al.*, 2017). This further reinforces the need to discover novel anti-TB compounds capable of shortening treatment and effectively sterilizing infection.

1.3. The Mycobacterial Replication Machinery

A very promising category of novel therapeutics against TB includes those that target DNA replication and synthesis in *Mtb* (as reviewed by Reiche, *et al.*, 2017). However, it is necessary to discuss the mechanism of genome replication in mycobacteria, in particular the *dnaN*-encoded β sliding clamp, which links DNA replication with DNA repair.

The mechanism of DNA replication is well understood in model organisms such as *E. coli*, *Caulobacter crescentus* (*C. crescentus*), as well as *Bacillus subtilis*. The orthologous systems in other bacteria such as mycobacteria are also understood, albeit to a lesser extent. The multi-protein complex involved in DNA synthesis and replication fork progression consists of a variety of proteins. The constituents of the holoenzyme include DNA polymerase – consisting of an α subunit (PolC or DnaE), ε subunit (DnaQ), and θ subunit (HolE); the β sliding clamp processivity factor (DnaN); the clamp loading units – consisting of τ subunit (DnaX) and δ and δ' (HolA and HolC, respectively); a helicase (DnaB); a primase (DnaG); and a topoisomerase (TopA) or DNA gyrase (GyrAB) in addition to other proteins such as χ (HolB) (Beattie, *et al.*, 2017; Reyes-Lamothe, *et al.*, 2010; reviewed in van Oijen and Loparo, 2010; reviewed by Pomerantz and O'Donnell, 2007). In addition, these processes must be finely controlled and orchestrated both spatially and temporally in order to prevent lethal events such as improper chromosomal segregation or chromosome cleavage.

In this vein, the replisome is thought to be largely stationary within *E. coli* during DNA replication and functions like a 'factory' whereby the DNA is pulled through the holoenzyme as DNA synthesis occurs (Lemon and Grossman, 1998). However, this observation was contradicted by Reyes-Lamothe and colleagues who showed that independent replication fork progression is dictated by chromosomal DNA only and that the position of the replisome is only dependent on the dynamics of the chromosome itself (Reyes-Lamothe, *et al.*, 2008). Additionally, replication of the chromosome in *C.*

crescentus occurs by the movement of the replisome along the chromosome (Jensen, *et al.*, 2001). Irrespective, the β sliding clamp is essential to mediate polymerase access to the replication fork during DNA synthesis (Burgers, *et al.*, 1981). Furthermore, it was recently suggested that β promotes the stability of the replication fork and maintains a longer association to the replication fork in *E. coli* than other replisome components (Beattie, *et al.*, 2017). As a result, it is thought that this allows the β clamp to act as a base to which different polymerases can rapidly associate and dissociate (Beattie, *et al.*, 2017), indicating that β serves a critically important, multi-faceted function in DNA replication.

1.3.1. The β Sliding Clamp

Studies in *Msm* have elucidated the dynamics of β in live cells, indicating the highly dynamic nature of the replication fork through observations of DnaN (Santi, *et al.*, 2013, Santi and McKinney, 2015; Trojanowski, *et al.*, 2015, 2017). Using fluorescent microscopy to study live bacilli, the formation of foci of constitutively expressed, fluorescently labelled DnaN proteins is thought to correlate with the formation of the replication fork and initiation of the 140 minute long C-phase (DNA synthesis) of the *Msm* cell cycle. This phase accounted for 77.78 % of the total cell replication time (Santi, *et al.*, 2013). In addition, chromosome replication occurred immediately after cell division of the parental cell into two daughter cells where the B-phase (from the end of cell division to the initiation of DNA replication) was largely absent (Santi, *et al.*, 2013). Therefore it can be deduced that DNA replication contributed to a large portion of the time between cell division events. Trojanowski and colleagues further showed that mycobacteria are capable of multi-fork chromosome

replication, indicating heterogeneity in whether successive rounds of DNA replication occur before or after termination of the previous round (Trojanowski, *et al.*, 2017). This implied that in instances where cell division is slowed down or inhibited, resultant daughter cells can inherit partially duplicated chromosomes.

Indeed, the replisome is highly dynamic within mycobacteria as multiple replication forks can be observed within single *Msm* cells, where it was reported that 35.5 % of exponentially growing cells exhibit two DnaN foci (Trojanowski, *et al.*, 2015). In the same study, it was observed that the replisome does not assemble and that DNA replication does not occur during stationary phase (Trojanowski, *et al.*, 2015). Similarly, Santi *et al.* observed that 13 % of all cells contained no DnaN foci and attributed this to cell division corresponding to the B-phase in short cells and D-phase (from the end of DNA replication to cell division) in long cells (Santi, *et al.*, 2015). However, the location of DnaN did not exclusively indicate the location of the replication fork, as previous studies have suggested multiple roles played by β during DNA repair (de Saro and O'Donnell, 2001; Simmons, *et al.*, 2008a; Pillon, *et al.*, 2015; Grompone, *et al.*, 2002). It is therefore possible that, in addition to the one or two 'replicative' foci observed in *Msm*, the non-replicative foci ('denoted as minor foci in Trojanowski, *et al.*, 2015, and observed as 'dim' foci in Santi, *et al.*, 2015) may indicate locations of non-replicative DNA processing such as DNA repair.

The precise dynamics and localization of DnaN during cell growth were assessed by Santi and colleagues, where DnaN foci were observed to form at the midcell during the initiation of the C-phase, during which the majority of

DnaN foci remained as a single focus (Santi, *et al.*, 2015). However, the foci were observed to be highly dynamic and underwent multiple splitting and re-joining events with time. As these experiments were not conducted in three-dimensions (3D), it is unclear if the dynamic foci represented completely separate replisome complexes that stochastically occupy the same lateral position within the cell or complexes that actively merge and split from one another. Regardless, it remains unclear how these processes relate to DNA damage repair, highlighting the gap in knowledge that exists regarding the dynamics of DnaN and the contribution of this protein to DNA repair.

1.4. Understudied Anti-TB Drugs

The development of drug resistance in *Mtb* is of particular relevance to the global TB control programme and thus is of special interest to TB drug discovery and development research. Recently, a number of unapproved, novel, and promising antitubercular compounds have been identified which target bacillary processes involved in genome replication and DNA synthesis (Reiche, *et al.*, 2017), namely griselimycin (GRS) (Kling, *et al.*, 2015), nargenicin (NRG) (International Patent Number: WO 2016 064982 A1; Young, *et al.*, 2016), and moxifloxacin (MOX) (Xu, *et al.*, 2017). The implications of these drugs on the mutagenic capacity of mycobacteria and their potential contribution to the development of drug resistance is under-explored. In the past, other drugs that have been shown to induce the SOS response in other organisms have also shown a resulting increase in mutagenesis and genetic diversity (reviewed by Galhardo, *et al.*, 2007; Couce and Blázquez, 2009; Blázquez, *et al.*, 2012). For example, ciprofloxacin (CIP), which induces the SOS response in *Staphylococcus aureus* (*S. aureus*) (Cirz, *et al.*, 2007), has been shown to increase the mutation

rate of *Mycobacterium fortuitum* (Gillespie, *et al.*, 2005) as well as induce the SOS response in *Mtb* (O'Sullivan, *et al.*, 2008) and *Msm* (Fan, *et al.*, 2018). Importantly, the use of FLQs was shown to induce the development of drug resistance in *Msm* and *Mtb* (Malik, *et al.*, 2012). Indeed, earlier it was shown that the development of *E. coli* drug resistance *in vivo* and *in vitro* was dependent on the induction of the SOS response (Cirz, *et al.*, 2005). Therefore, if any of the novel compounds that target DNA replication result in DNA lesions that induce expression of the mutagenic DNA repair mechanism, there may be an associated increase in inducible mutagenesis associated with therapeutic treatment comprising MOX, GRS, or NRG. Such an implication is of significant concern and warrants investigation in the early stages of drug development.

1.4.1. Nargenicin

NRG is a natural product antibiotic that has efficacy against *E. coli* as well as *S. aureus* and was determined to have a novel mode of action in the latter that involves the specific inhibition of DnaE (Painter, *et al.*, 2015). Such a compound would hold potential promise for the treatment of TB if it were to act via the same mechanism as *dnaE1* is essential within *Mtb* and is also a previously un-explored drug target (Reiche, *et al.*, 2017). Although no report in the scientific literature has confirmed the efficacy of NRG as a sterilizing agent against *Mtb*, a patent published in 2016 has signposted the potential use of NRG as a novel antitubercular (Young, *et al.*, 2016). However, it must be noted here that the compound may not be suitable as an anti-TB therapeutic as exposure of this compound to *E. coli* resulted in the induction of the SOS response and caused cell elongation (Painter, *et al.*, 2015). As a potential consequence of the activation of the SOS response, it is possible that the mutasome is induced

during NRG-exposure of *Mtb*, which could ultimately contribute to increased levels of mutagenesis and the development of drug resistance. However, there exists an intriguing possibility that NRG may simultaneously inhibit DnaE2 in addition to the replicative DnaE1 subunit based on the shared homology between the two proteins (Boshoff, *et al.*, 2003), which could limit DnaE2-mediated mutagenesis. The potential impact of NRG on mutagenesis in mycobacteria is unknown and warrants investigation.

1.4.2. Moxifloxacin

MOX is a fourth-generation FLQ that shows increased antibacterial activity and serum half-life and decreased toxicity when compared to earlier generation FLQs (Stass, *et al.,* 1998). This antimicrobial agent shows promise in treating TB disease as it inhibits DNA gyrase ($GyrA_2B_2$), a topoisomerase critically involved in the structural maintenance of the mycobacterial chromosome by controlling negative supercoiling ahead of the replication fork (Reece and Maxwell, 1991; Ashley, *et al.*, 2017). Considerable effort has been made to determine the efficacy of MOX in both reducing treatment duration (Nuermberger, *et al.*, 2004a,b; Burman, *et al.*, 2006; Conde, *et al.*, 2009, 2016; Dorman, *et al.*, 2009; Gillespie, *et al.*, 2014; Li, *et al.*, 2017; Moodley and Godec, 2016) and treating resistant cases of TB (Murray, *et al.*, 2016; Kang, *et al.*, 2016), making MOX a drug of high interest. Of further interest within the scope of this work, inhibition of DNA gyrase results in the development of double-stranded DNA breaks which contributes to the lethality of FLQs in *Mtb* (Mduli and Ma, 2007), which may imply the potential for mutagenic DNA repair as a direct result of MOX exposure. This possibility is supported by the observation that MOX induced the SOS response and expression of the $UmuD_2C'$ mutasome in

S. aureus at sub-inhibitory concentrations (Mesak, *et al.,* 2008). Therefore, it is imperative to investigate the concern regarding the mutagenicity of MOX if it is to be used as a successful anti-TB drug in the future.

1.4.3. Griselimycin

The natural product, GRS, is a cyclic peptide antibiotic isolated from *Streptomyces spp*. (Terlain and Thomas, 1971) which was found to have potent activity against mycobacteria (Kling, *et al.,* 2015). The target of this drug was recently elucidated to be the *dnaN*-encoded β clamp, which, as previously indicated, is an essential component of the DNA replication machinery (Kling, *et al.,* 2015; Reiche, *et al.*, 2017). Furthermore, GRS was shown to have a high binding affinity to, and low dissociation constant for, the β clamp to which it binds via the hydrophobic cleft of domains II and III known to be required for polymerase binding (Bunting, *et al.*, 2003; Burnouf, *et al.*, 2004). Additionally, an Ames test conducted with GRS on *Salmonella enterica* serovar Typhimurium (*S. typhimurium*) indicated no mutagenicity (Kling, *et al.*, 2015); however, induction of the SOS response by GRS may potentially indicate activity of the mutagenic DNA repair pathway in mycobacteria, although there is no evidence, as yet, to support this. Given the inhibition of DnaN by the compound, specifically the interruption of replicative and repair processes, it remains possible though that, at inhibitory concentrations, the mutasome is unable to function despite formation of the complex at the replication fork. Thus, the effect of DnaN inhibition by GRS on inducible mutagenesis remains unknown. This represents a knowledge gap that must be addressed to determine whether this represents a positive feature or drawback of this drug candidate.

2. Drug Resistance and Mutations in Mycobacteria

In 2014, the World Health Organization (WHO) reported that 3.6 % of new and 20.2 % of recurring TB patients were estimated to have MDR-TB (WHO, 2014). Furthermore, in 2016, 8.1 % of global TB cases were reported as MDR/RIF-resistant (WHO, 2017). With regard to mortality, 170,000 deaths resulted from the 350,000 reported cases of MDR-TB in 2014 (WHO, 2014). Subsequent acquisition of resistance to a FLQ and an AMI in MDR-TB leads to XDR-TB, a highly-resistant form of TB that has a very poor treatment success rate of only 28-30 % versus 52-54 % and 83 % in MDR-TB and drug-susceptible TB, respectively (WHO, 2014, 2016, 2017). XDR-TB has been reported in 117 countries world-wide (WHO, 2016), indicating that this is an issue of global concern.

Drug-resistance mutations include SNPs that occur within specific regions of a target (or antibiotic processing- or uptake-related) gene, thereby affecting the molecular affinity of the compound to the corresponding binding site within the target protein. As an example, RIF, discovered in 1959, is a highly utilized, first-line anti-TB drug and, together with the resistance mechanisms against it (Wehrli, 1983), represents one of the best studied anti-TB drugs (Koch, *et al.*, 2014). Resistance to RIF is conferred by SNPs that occur within the rifampicin-resistance determining region (RRDR) of *rpoB*, the gene that encodes the target of RIF, DNA-dependent RNA polymerase subunit β (Ramaswamy and Musser, 1998).

In addition to the list of mutations that directly influence the efficacy of drugs against *Mtb*, the acquisition of SNPs within mycobacteria also poses a

significant threat to global health through the function of indirect, compensatory mutations. Mutations that confer a high level of drug resistance usually incur a significant fitness cost associated with the altered gene expression or altered amino acid sequence of the protein (Gagneux, *et al.*, 2006; Heym, *et al.*, 1995). The downstream effect a SNP has is not exclusively restricted to the antibiotic efficacy and can affect a variety of additional protein and physiological properties (reviewed by Hershberg, 2017). Although the mutation confers resistance to the drug (and therefore circumvents the large selective pressure of chemotherapy), it can also significantly reduce the overall, relative fitness of the bacterium – potentially reducing virulence or leading to a loss of the mutation within a population in the absence of the selective antibiotic (Andersson and Hughes, 2010; Koch, *et al.*, 2014). In some cases, the (beneficial) drug resistance conferred by a mutation may be overshadowed by the detrimental effects of that mutation, compromising the "success" of any strain containing the drug-resistance-conferring mutation and thus, preventing its fixation within a population (Levin, *et al.*, 2000). Despite the disadvantageous effects of most mutations, other genetic changes can result in the compensation of the detrimental effect associated with resistance mutations and render the resistant bacterium equally, or more, fit than the original, drug-sensitive strain – effectively ensuring the success of the otherwise deleterious resistance mutation through genetic linkage (Comas, *et al.*, 2012; Sherman, *et al.*, 1996; Heym, *et al.*, 1995; Koch, *et al.*, 2014; Durão, *et al.*, 2018). This renders the antibiotic unable to suppress antibacterial growth or impose a highly selective force. In such cases, mutations that occur at unrelated loci within the genome can alleviate the detrimental characteristic associated with previously fixed, resistance-conferring mutations and may even be a necessary precursor

before severely detrimental resistance mutations can be tolerated by the bacteria (*e.g.*, *rpoC* and *ahpC* mutations, as outlined in more detail below) (Trindade, *et al.*, 2009). Compensatory mutations are often an overlooked consequence of mutagenesis and mutation acquisition in mycobacteria despite being frequently linked to the development and success of MDR and XDR strains of *Mtb* (Trindade, *et al.*, 2009). Overall, the generation and acquisition of mutations in mycobacteria lead to the development of drug resistance as well as the accumulation of compensatory mutations that help propagate other drug-resistance mutations.

2.1. Drug Resistance-Conferring Mutations

Despite the dependence on chemotherapy to cure TB, subsequent to the development of RIF in 1967, bedaquiline (BDQ) (2012) is the only new anti-TB drug to be widely used against (MDR-)TB (Mahajan, 2013; Jain, *et al.*, 2008; Long, 1991; Wolfson, *et al.*, 2015; Udwadia, *et al.*, 2014). As a consequence of the considerable lack of new drugs in recent decades, a large proportion of the drugs available for use are ineffective due to the dramatic and sharp rise of MDR and XDR strains of *Mtb* that have accumulated in recent years (Yanling, *et al.*, 2006; WHO, 2017; Tessema, *et al.*, 2017; Dheda, *et al.*, 2017), culminating in a scenario where drug resistance occurs against almost all drugs (Gygli, *et al.*, 2017). A non-exhaustive list of drug resistance-conferring SNPs and indels within the genome of *Mtb* is presented in **Table 1-1**, and examples are described below.

Table 1-1 | Mutatable resistance-associated genes (including associated promoters) in *Mtb*

H37Rv gene	Antibiotic											
	AMI	BDQ	CFZ	EMB	ETH	FLQ	INH	PAS	PA-824	PZA	RIF	SM
accD6							+					
aphC							c					
atpE		+										
efpA							+					
eis	+											
embA				+								
embB				+			+				+	
embC				+								
embR				+								
ethA					+							
ethR					+							
fabD							+					
fabG							+					
fadE24							+					
fbpC							+					
fgd1									+			
folC								+				
furA							+					
gidB												+
gyrA						+						
gyrB						+						
inhA					+		+					
iniA				+			+					

iniB				+			+					
iniC				+			+					
kasA							+					
katG							+					
mabA							c					
mshA					+							
ndh							+					
nhoA							+					
oxyR							+					
rmlD				+								
pncA										+		
rpoA											+	
rpoB											+	
rpoC											c	
rpsL												+
rrs	+											+
Rv0340				+			+					
Rv0678		+	+									
Rv1592c							+					
Rv1772							+					
Rv1979c			+									
Rv3124				+								
Rv3125c				+								
Rv3126				+								
Rv3264c				+								
Rv3266c				+								

Rv3547						+
Rv3792		+				
Rv3806c		+				
srmR				+		
thyA					+	
tlyA	+					

Based off information from citations in text.
AMI, Aminoglycosides; BDQ, Bedaqualine; CFZ, Clofazamine; EMB, Ethambutol; ETH, Ethionamide; FLQ, Fluoroquinolones; INH, Isoniazid; PAS, Para-aminosalisylic Acid; PZA, Pyrazinamide; RIF, Rifampicin; SM, Streptomycin.
First-line, combination TB drugs are indicated in red.
c Rrepresents compensatory mutations that contribute to resistance

Mtb becomes refractory to standard RIF treatment following the acquisition of mutations (usually SNPs) in *rpoB* that result in amino acid changes within the RRDR of the translated protein – thereby reducing the binding affinity of the compound to the essential target RNA polymerase (Campbell, *et al.*, 2001; Feklistov, *et al.*, 2008). The two most frequent SNPs that confer RIF-resistance to *Mtb in vitro* and *in vivo* are substitutions that cause amino acid changes either from a serine to a leucine at the 450th position of RpoB (S450L) or a TCG→TTG transition mutation that changes the serine to a leucine at position 531 (S531L) (Morlock, *et al.*, 2000). Mutations such as those that occur in the RRDR result in conformational changes of RpoB that reduce the binding affinity of RIF, thereby preventing the inhibitory effect on the protein (Telenti, *et al.*, 1993; Campbell, *et al.*, 2001). In addition to this, many other SNPs outside of the RRDR contribute to RIF-resistance (Siu, *et al.*, 2011). These include mutations in *rpoA* as well as *rpoC*; however, these mutations do not contribute directly to the mechanism of resistance and rather are associated with the restoration of fitness in strains of *Mtb* that contain RIF-resistance-conferring mutations in *rpoB*, allowing for greater success of the pathogen (Comas, *et al.*, 2011; de Vos, *et al.*, 2013; Brandis and Hughes, 2013; Koch, *et al.*, 2014).

In the case of PZA, resistant strains are usually associated with SNPs in a single gene, *pncA*, which encodes the pyrazinamidase enzyme responsible for converting the prodrug into the active form, pyrazinoic acid (Scorpio and Zhang, 1996; Juréen, *et al.*, 2008). PZA resistance-associated SNPs are abundant throughout the *pncA* gene and all result in either the loss of protein function or a decrease in expression levels (Yadon, *et al.*, 2017). Similarly, INH-resistance occurs mainly as a result of resistance-conferring non-synonymous SNPs in a

number of genes (Zhang, *et al.*, 1992; Ramaswamy, *et al.*, 2003; Seifert, *et al.*, 2015). However, in a similar fashion to that of RIF, fitness compensation mutations are also found in INH-resistant strains. Here, mutations in the promoter of the *ahpC* gene in strains resistant to INH allow for greater survival and transmission of the bacillus (Sherman, *et al.*, 1996; Heym, *et al.*, 1997). A similar change of *ahpC* regulation is associated with a silent, compensatory-conferring SNP within *mabA* (Ando, *et al.*, 2014). In a similar example, 89 % of EMB-resistant *Mtb* strains are associated with SNPs that replace the canonical methionine residue at position 306 of the translated EmbB protein, which is thought to prevent drug-protein binding (Sreevatsan, *et al.*, 1997; Telenti, *et al.*, 1997). Adding complexity to this example and further highlighting the role of mutations in drug resistance, the level of resistance conferred in EMB-resistant strains is dependent on the number and type of mutations present in other genes involved in arabinogalactan production (Safi, *et al.*, 2008). In the last example, high-level SM-resistance is mediated by SNPs in *rpsL* (K43R and K88Q) and *rrs* (nucleotide position 530 and 915), while low level resistance is associated with mutations in *gidB* (Sreevatsan, *et al.*, 1996; Okamoto, *et al.*, 2007).

In addition to contributing to first-line drug resistance, mutations are also linked to resistance against second-line drugs. FLQ-resistance is associated with SNPs in *gyrA* and *gyrB* (Takiff, *et al.*, 1997); AMI-resistance is associated with mutations in *rrs* (Alangaden, *et al.*, 1998; Suzuki, *et al.*, 1998; Stanley, *et al.*, 2010), *eis* (Zaunbrecher, *et al.*, 2009), and *tlyA* (Johansen, *et al.*, 2006). ETH-resistance occurs as a result of mutations in *inhA*, *ethA*, *ethR*, and *mshA* (Brossier, *et al.*, 2011; Vilchèze, *et al.*, 2008). Mutations in *thyA* and *folC* cause PAS-resistance (Rengarajan, *et al.*, 2004; Zhao, *et al.*, 2014b). While other

mutatable resistance-associated genes include *Rv0678* (CFZ and BDQ); *rplC* (linezolid); *atpE* (BDQ); *fdg1* (PA-824); as well as others (as reviewed by Palomino and Martin, 2014; Da Silva and Palomino, 2011; Sandgren, *et al.*, 2009; and Müller, *et al.*, 2013).

2.2. Acquisition of Mutations and the SOS Response

In addition to the presence of antibiotics during infection, pathogenic mycobacteria experience harsh physiochemical conditions due to hypoxia, the scarcity of nutrients, and the natural immune response of the host to clear the infection (Russell, 2001; Moore, *et al.*, 2017). Not only do these conditions select for more fit (or drug resistant) strains from the ever-diversifying population, but they also directly contribute to this genetic diversity through the induction and subsequent activity of the DNA damage-inducible mutagenic DNA repair pathway (Warner, *et al.*, 2010), which will be discussed below.

Bacteria have evolved a multitude of responses to stressful or suboptimal conditions (Storz, *et al.*, 2011). Environmental stresses that cause DNA damage (genotoxic stress), which include exogenous sources such as macrophage-generated ROS and chemotherapy, as well as endogenous production such as by-products of respiration and metabolism, are usually lethal to bacteria if left unrepaired. Bacteria have evolved a variety of mechanisms to deal with the DNA damage encountered during these conditions – one of which, the SOS response, is the primary response to DNA damage (Little and Mount, 1982). This response is a mechanism that tightly regulates the expression of a wide variety of genes (**Table 1-2**) in an attempt to ensure cell survival and viability when genome integrity is lost. Throughout the entire bacterial domain, genome

robustness is maintained during genotoxic stress through the function of a highly conserved array of pathways that act to limit and repair DNA damage (reviewed by Erill, *et al.*, 2007). Transcription of the DNA damage-responsive genes is often (but not exclusively) mediated by specific transcription operator elements known as SOS boxes that allow for highly dynamic regulation of multiple genes throughout the genome. The SOS box sequences are located directly upstream of the regulated genes to which a dimer of the LexA regulatory protein binds under normal cellular conditions (Davis, *et al.*, 2002a; Little, *et al.*, 1981; Brent and Ptashne, 1981). Binding of the LexA repressor prevents transcription initiation of the downstream gene by DNA-dependent RNA polymerases (Little, *et al.*, 1981; Brent and Ptashne, 1981; Durbach, *et al.*, 1997).

During genotoxic stress, single-stranded DNA (ssDNA) accumulates in the cell as a consequence of stalled replication forks caused by DNA damage lesions and a loss of chromosomal integrity (Moore, *et al.*, 1981; Sogo, *et al.*, 2002). A second regulatory protein, RecA, subsequently binds cytosolic ssDNA (in an ATP-dependent fashion) to form activated, multimeric, helical nucleoprotein filaments referred to as RecA* (Miura and Tomizawa, 1968; Friedberg, *et al.*, 1995). These RecA* filaments interact with LexA, causing the repressor to undergo proteolytic autocleavage (Little, 1984, 1993). Once LexA is cleaved and rendered non-functional, the repressor protein is no longer able to bind the SOS box and the down-stream SOS gene is de-repressed, allowing transcriptional initiatiation (Papavinasasundaram, *et al.*, 2001). The order of expression of the SOS genes corresponds with the level of DNA damage present in the cell and

Table 1-2 | DNA damage inducible (potential SOS) genes of *Mtb*

H37Rv gene	Gene Name	Davis, *et al.*, (2002a) RecA-dependent SOS box prediction	Rand, *et al.*, (2003) MMC-mediated upregulation	Gamulin, *et al.*, (2004) RecA-nondependent prediction	Smollett, *et al.*, (2012) ChIP-seq LexA binding site	Other experimental DNA damage references
Rv0054	*ssb*	-	Yes	Yes	-	
Rv0055	*rpsR*	-	Yes	-	-	
Rv0056	*rplI*	-	Yes	-	-	
Rv0058	*dnaB*	Yes	Yes	Yes	-	
Rv0071		Yes	Yes	-	Yes	
Rv0094c		-	Yes	-	-	
Rv0095c		-	Yes	Yes	Yes	
Rv0181c		-	Yes	-	-	
Rv0182c	*sigG*	-	Yes	Yes	-	
Rv0184		-	Yes	Yes	-	
Rv0185		-	Yes	-	-	
Rv0186	*bglS*	-	Yes	-	-	
Rv0335c	*pe6*	Yes	-	-	-	
Rv0336		Yes	Yes	-	Yes	
Rv0427c	*xthA*	-	Yes	Yes	-	
Rv0515		Yes	Yes	-	Yes	
Rv0516c		-	Yes	-	-	
Rv0605		-	Yes	Yes	-	
Rv0606		-	Yes	-	-	
Rv0607		-	Yes	-	-	
Rv0829		-	Yes	-	-	
Rv0848	*cysK2*	-	Yes	-	-	

Rv0921		-	Yes	-	-	
Rv0922		-	Yes	-	-	
Rv0991c		-	Yes	-	-	
Rv1000c		Yes	Yes	-	Yes	
Rv1001	*arcA*	Yes	-	-	-	
Rv1057		-	-	-	Yes	
Rv1128c		-	Yes	Yes	-	
Rv1148c		-	Yes	Yes	-	
Rv1169c	*lipX*	-	Yes	-	-	
Rv1277		-	Yes	Yes	-	
Rv1278		-	Yes	-	-	
Rv1317c	*alkA*	-	-	Yes	-	
Rv1376		-	Yes	-	-	
Rv1377c		Yes	Yes	-	-	
Rv1378c		Yes	Yes	-	Yes	
Rv1379	*pyrR*	Yes	-	-	-	
Rv1406	*fmt*	-	Yes	Yes	-	
Rv1407	*fmu*	-	Yes	-	-	
Rv1547	*dnaE1*	-	-	Yes	-	Boshoff, *et al.*, 2003
Rv1587c		-	Yes	-	-	
Rv1588c		-	Yes	Yes	Yes	
Rv1633	*uvrB*	-	Yes	Yes	-	
Rv1638	*uvrA*	-	Yes	Yes	-	
Rv1702c		Yes	Yes	-	Yes	
Rv1765c		-	Yes	Yes	-	
Rv1833c		-	Yes	Yes	-	

Rv1907c		-	-	Yes	-	
Rv1945		-	Yes	Yes	-	
Rv1948c		-	Yes	-	-	
Rv1955	*higB*	-	-	Yes	-	
Rv1961		-	Yes	-	-	
Rv2014		-	Yes	-	-	
Rv2015c		-	Yes	Yes	-	
Rv2016		-	-	Yes	-	
Rv2017		-	Yes	-	-	
Rv2018		Yes	-	-	-	
Rv2024c		-	Yes	Yes	-	
Rv2099c	*pe21*	Yes	-	-	-	
Rv2100		Yes	Yes	Yes	Yes	
Rv2119		-	-	Yes	-	
Rv2191		-	Yes	-	-	
Rv2428	*ahpC*	-	-	Yes	-	
Rv2517c		-	-	-	Yes	
Rv2578c		Yes	Yes	-	Yes	
Rv2579	*linB*	Yes	Yes	-	-	
Rv2592c	*ruvB*	Yes	Yes	-	-	
Rv2593c	*ruvA*	Yes	Yes	-	Yes	
Rv2594c	*ruvC*	Yes	Yes	Yes	Yes	Dawson, *et al.*, 2010
Rv2595	*vapB40*	Yes	-		-	
Rv2660c		-	Yes	-	-	
Rv2717c		Yes	Yes	-	-	
Rv2718c	*nrdR*	Yes	Yes	-	-	

Rv2719c		Yes	Yes	Yes	Yes	
Rv2720	*lexA*	Yes	Yes	-	Yes	
Rv2721c		-	-	-	-	Brooks, *et al.*, 2006
Rv2734		-	-	Yes	-	
Rv2735c		-	Yes	-	-	
Rv2737c	*recA*	Yes	Yes	Yes	Yes	
Rv2790c	*ltp1*	-	Yes	-	-	
Rv2791c		-	Yes	-	-	
Rv2792c		-	Yes	Yes	-	
Rv2884		-	Yes	-	-	
Rv2885c		-	Yes	-	-	
Rv2975c		-	Yes	Yes	-	
Rv2976c	*ung*	-	Yes	-	-	
Rv2977c	*thiL*	-	Yes	-	-	
Rv2978c		-	Yes	-	-	
Rv2979c		-	Yes	Yes	-	
Rv3048c	*nrdG/nrdF2*	-	Yes	Yes	-	
Rv3073c		Yes	-	-	-	
Rv3074		Yes	Yes	-	Yes	
Rv3164c	*moxR3*	Yes	-	-	-	
Rv3191c		-	Yes	-	-	
Rv3198c	*uvrD2*	-	Yes	Yes	-	
Rv3201c		-	Yes	-	-	
Rv3202c		-	Yes	-	-	
Rv3223c	*sigH*	-	-	Yes	-	
Rv3226c		-	Yes	Yes	-	

Rv3260c	*whiB2*	Yes	-	-	Yes	
Rv3261	*fbiA*	Yes	-	-	-	
Rv3263		-	-	Yes	-	
Rv3296	*lhr*	-	Yes	Yes	-	
Rv3297	*nei*	-	Yes	-	-	
Rv3370c	*dnaE2*	Yes	Yes	-	Yes	Boshoff, *et al.*, 2003;
Rv3371		Yes	-	-	-	
Rv3393	*iunH*	-	Yes	-	-	
Rv3394c	*imuB*	Yes	Yes	-	-	Warner, *et al.*, 2010
Rv3395c	*imuA'*	Yes	Yes	-	Yes	Warner, *et al.*, 2010;
Rv3466		-	Yes	Yes	-	
Rv3467		-	Yes		-	
Rv3517		-	Yes	Yes	-	
Rv3534c	*hsaF*	Yes	-	-	-	
Rv3554	*fdxB*	-	Yes	-	-	
Rv3555c		-	Yes	Yes	-	
Rv3585	*radA*	-	Yes	Yes	-	
Rv3644c		-	Yes	Yes	-	
Rv3714c		-	Yes	Yes	-	
Rv3776		Yes	Yes	-	Yes	
Rv3777		Yes	Yes	-	-	
Rv3827c		-	Yes	-	-	
Rv3828c		-	Yes	Yes	-	
Rv3914	*trxC*	-	Yes	-	-	

Genes in bold font are supported by two or more references

is modulated by the differential binding affinity of LexA to variable SOS box sequences controlling transcription of each gene (Friedberg, *et al.*, 1995; Friedman, *et al.*, 2005). Operator-binding affinity confers the level of repression exerted on the corresponding gene by LexA, with genes that have less detrimental effects on the cell having a lower LexA-binding affinity, allowing expression of these genes at lower levels of DNA damage (Kamenšek, *et al.*, 2010; Schnarr, *et al.*, 1991). The more severe and critical the damage encountered by the cell, the greater the extent that the SOS response is initiated and as a consequence, the more severe the secondary effects of the SOS response, such as mutagenesis (Schnarr, *et al.*, 1991; Friedman, *et al.*, 2005; reviewed by Simmons, *et al.*, 2008b). This cascade of events ultimately contributes to the survival of the cell by rigorous control of DNA repair pathways and limiting expression to appropriate levels corresponding to the conditions of genotoxic stress. Following the successful expression of the SOS-regulated genes, the resulting gene products function together, either dependently or independently of one another, to perform functions in an orchestrated and highly regulated manner to reduce the amount of genomic stress and allow the survival of the cell. Thereafter, in the absence of active RecA*, newly expressed LexA is free to bind to the SOS boxes and prevent further downstream transcription of the responding genes, thereby turning off the SOS response.

The SOS response as a whole (RecA-dependent and -independent pathways) consists of multiple mechanisms, ranging from nucleotide excision repair (NER) to mutagenic DNA repair, non-homologous end-joining (NHEJ) to single-strand annealing (SSA), and cell division inhibition to recombination

(reviewed by Simmons, *et al.*, 2008b). Error-free repair mechanisms such as NER are induced early during the response due to weak LexA-binding promoters (Schnarr, *et al.*, 1991). If the level of DNA damage is too extensive to be repaired by NER alone, homologous recombination machinery is expressed to help repair damaged DNA (Hedge, *et al.*, 1996). In addition, cell division inhibitors such as SulA and MinC in *E. coli* or YneA in *B. subtilis* remodel cell division timing to allow repair and segregation of the chromosome before cell division occurs (Bi and Lutkenhaus, 1993; Kawai, *et al.*, 2003). Finally, if the DNA damage is too extensive to be repaired by non-mutagenic mechanisms, mutagenic polymerases (such as Pol V) are expressed in order to avoid lethal interruptions to DNA synthesis; however, expression of UmuDC (Pol V) in *E. coli* requires extensive post-translational regulation (Erdem, *et al.*, 2014) in addition to a strong LexA-binding operator (Burckhardt, *et al.*, 1988; Shinagawa, *et al.*, 1988; Friedman, *et al.*, 2005). It has also been shown more recently that UmuC activity is additionally regulated by spatial sequestration of the protein to the cell membrane in *E. coli* (Robinson, *et al.*, 2015).

In the specific example of the *E. coli* SOS response, varying strengths of the SOS promoters co-ordinates the induction of the different pathways (Kamenšek, *et al.*, 2010; Schnarr, *et al.*, 1991). Thus, following DNA damage, the weaker regulator sequences allow expression of the corresponding genes first, as low levels of non-cleaved LexA disassociate from the sequence more frequently (Kamenšek, *et al.*, 2010; Schnarr, *et al.*, 1991). Because highly pleiotropic effects such as the expression and engagement of mutagenic TLS polymerases need to be tightly regulated in order to prevent unnecessary mutations when cell viability is not jeopardized, the stronger promoters controlling these genes are

further repressed as more LexA is expressed as part of this SOS response (Tippin, *et al.*, 2004). Repression of the tightly regulated genes is maintained until such time that the DNA damage is too extensive and the high concentration of ssDNA and newly synthesized RecA* results in the cleavage of the vast majority of LexA repressors within the cell.

The mycobacterial SOS response shares many similarities with the SOS response regulons in other bacteria and is largely similar to that of the *E. coli* model organism, as described above. The SOS response of *Mycobacterium spp*. is only functional after induction of gene expression following DNA damage and thus does not function under normal growth conditions (Davis, *et al.*, 2002a; Boshoff, *et al.*, 2003; Warner, *et al.*, 2010; Durbach, *et al.*, 1997; Brooks *et al.*, 2001). In *Mtb*, genes of the SOS regulon are controlled by SOS boxes with the consensus sequence of 5′-TCGAACACATGTTCGA-3′, to which LexA is able to bind (Davis, *et al.*, 2002a). However, there are also distinct differences between the model organism and the mycobacterial SOS response that need to be noted. In addition to the canonical SOS response, mycobacteria also contain a set of genes that are expressed during DNA damage but are not regulated by LexA. These so-called 'RecA-nondependent' genes are regulated by an unknown mechanism governed by a different promoter element (Gamulin, *et al.*, 2004; Davis, *et al.*, 2002b; Dawson, *et al.*, 2010; Brooks, *et al.*, 2001; Movahedzadeh, *et al.*, 1997) that likely includes the function of the ClpR protein (Wang, *et al.*, 2011), making it distinctly and differentially regulated in comparison to traditional RecA-LexA-regulated genes. Additionally, there are notable differences in the genes controlled by the SOS regulon between *E. coli*

and that of mycobacteria, which includes discrepancies in the presence of *E. coli* structural homologues such as UmuDC and MinBC (see **Table 1-2**).

2.2.1. Inducible DNA Mutagenesis and TLS

DNA-dependent DNA polymerase enzymes are required to copy and replicate the genome with a high degree of fidelity; however, the high degree of fidelity offered by replicative enzymes prevents the compact catalytic active site from accommodating DNA lesions often encountered on template strands during replication (Boudsocq, *et al.*, 2004; Yang and Woodgate, 2007; Wang and Yang, 2009; Wu, *et al.*, 2017). These lesions can result in stalled replication forks that can be lethal to the cell, thus necessitating the evolution of TLS polymerases that have more 'forgiving' catalytic sites that allow incorporation of deoxyribonucleotides (dNTPs) necessary to facilitate DNA synthesis opposite the lesion, such as observed in the case of human DNA Polymerase ι (Donigan, *et al.*, 2014), and allowing for the continuation of DNA replication. Polymerases that possess a less stringent active site allow for the polymerization of dNTPs in the presence of DNA lesions on the template strand by the process of TLS (**Table 1-3**), ultimately contributing to the continuation of chromosomal replication.

The primary role of TLS is to facilitate the continuation of genome replication and thus ensure the survival of the cell following severe genotoxic stress. In the case of mutagenic TLS, cell survival usually occurs as a trade-off against an increased mutation rate as a result of the incorporation of incorrect nucleotides opposite the DNA lesion by specialist TLS polymerases in an attempt to

Table 1-3 | Summary of bacterial DNA polymerases

Bacterial species	Encoded protein	SOS-regulation	TLS activity
E. coli	PolA (Pol I)		
	PolB (Pol II)	Yes	
	DnaE (Pol III)		Yes (non-mutagenic)
	DinB (Pol IV)	Yes	Yes (Moore, *et al.*, 2017)
	UmuC (Pol V)	Yes	Yes
Bacillus subtilis	DnaE	Yes	Yes (Le Chatelier, *et al.*, 2004)
Streptococcus pyogenes	DnaE		Yes (non-mutagenic; Bruck, *et al.*, 2003)
Msm	DnaE1	Yes	
	DnaE2	Yes	Yes (Boshoff, *et al.*, 2003)
	DinB		
	DinX		
	PolA	No	
Mtb	DnaE1	Yes	
	DnaE2	Yes	Yes (Boshoff, *et al.*, 2003)
	DinB	No	
	DinX	No	
	PolA	No	
C. crescentus	DnaE1		
	ImuC	Yes	
Pseudomonas spp.	ImuC	Yes	Yes (Jatsenko, *et al.*, 2017)
	DinB		Yes (Jatsenko, *et al.*, 2017)

continue DNA replication (Moore, *et al.*, 2017). This phenomenon of inducible mutagenesis (or adaptive mutagenesis) results in the generation of mutations within the region of repaired DNA (Tippin, *et al.*, 2004) and, as a consequence, allows for variation of mutation rate through the function of stress-induced, SOS-regulated, low-fidelity polymerases (Bruck, *et al.*, 2003). The ultimate evolutionary consequence of this mechanism is the generation of genomic heterogeneity during severely adverse environments, which may result in a subpopulation of cells enduring the stress (Radman, *et al.*, 1999; Bruck, *et al.*, 2003). It is postulated that inducible mutagenesis evolved as a result of a combination of second-order selection for a variable mutation rate, genetic drift due to rare selection events, as well as the proximal consequence of surviving the associated stress (MacLean, *et al.*, 2013). Regardless, the heterogeneity

generated as a result of inducible mutagenesis, although typically deleterious (Taddei, *et al.*, 1997), can lead to enough diversity in key genes to allow survival and endurance of a bacterial population through the harsh selective pressure associated with nutrient deprivation, genotoxic stress, and antibiotic chemotherapy (Warner, *et al.*, 2010; Moore, *et al.*, 2017). Although low mutation rates are beneficial on long time-scales, temporary periods of increased mutation can be beneficial to the organism. The increased mutagenesis associated with lesion bypass by random nucleotide insertion is a potential contributor to the micro-evolution of the bacterium and, in cases where the mutation has a non-deleterious effect on immediate cell survival, the error may become fixed overtime resulting in genetic diversity. Fixation is more likely to take place during selective conditions such as occurs during antibiotic exposure (Baym, *et al.*, 2016).

Mutagenic TLS polymerases contain a promiscuous active site that can accommodate an array of DNA lesions and adducts to be replicated past (Boudsocq, *et al.*, 2004; Goodman and Woodgate, 2013); however, due to the nature of the active site of these polymerases, nucleotide incorporation is not highly specific and accounts for the associated low fidelity and resultant highly error-prone DNA polymerization (Ling, *et al.*, 2001; Boudsocq, *et al.*, 2004). In organisms such as *E. coli*, the RecA-dependent, inducible mutagenic repair pathway consists of UmuD′$_2$C (Pol V) (Tang, *et al.*, 1998; Pham, *et al.*, 2001). DNA Pol V is a Y family polymerase that requires the activity of RecA to function (Jiang, *et al.*, 2009; Pham, *et al.*, 2001). In contrast, other bacteria such as *Mtb* and *C. crescentus* have different DNA-damage induced mutagenic repair machinery (**Table 1-4**). In these cases, C family polymerases such as DnaE2 are

responsible for TLS and mutagenesis following DNA damage (Boshoff, *et al.*, 2003; Galhardo, *et al.*, 2005) (**Table 1-3**).

Table 1-4 | Summary of the genes consituting the mutagenic cassette in various bacterial species

Bacterial species	ImuA′ orthologue	ImuB orthologue	DnaE2 orthologue
Msm	*MSMEG_1620*[1*]	*MSMEG_1622*[2]	*MSMEG_1633*
Mtb	*Rv3395c*[1*]	*Rv3394c*[2]	*Rv3370*
C. crescentus	*CC3213*[1]	*CC3212*[2]	*CC3211*[3]
Pseudomonas aeruginosa	*PA0671*[1]	*PA0670*[2]	*PA0669*[3]
Vibrio vulnificus	*VV1296*[1]	*VV1295*[2]	*VV1294*[3]
Vibrio parahaemolyticus	*VP2034*[1]	*VP2035*[2]	*VP2036*[3]
Ralstonia solanacaerum	*RSp0798*[1X]	*RSp0799*[2]	*RSp0800*[3]
Bordetella bronchisceptica	*BB3086*[1]	*BB3087*[2]	*BB3088*[3]
Bordetella parapertussis	*BPP1642*[1]	*BPP1641*[2]	*BPP1640*[3]
Pseudomonas putida	*PP3117*[1]	*PP3118*[2]	*PP3119*[3]
Methylococcus capsulatus	*MCA2166*[1]	*MCA2165*[2]	*MCA2164*[3]
Pseudomonas syringae	*PSPTO_2793*[1]	*PSPTO_2794*[2]	*PSPTO_2795*[3]
Xanthomonas campestris	*XCC1099*[1]	*XCC1100*[2]	*XCC1101*[3]
Xanthomonas axonopodis	*XAC1197*[1]	*XAC1198*[2]	*XAC1199*[3]
Corynebacterium glutamicum	*NCgl0590*[1]	*NCgl0591*[2]	*NCgl0611*
Sinorhizobium meliloti	*SMc03790*[1]	*SMc03789*[#2]	*SMc03788*[2]
Nocardia farcinia	*Nfa9059*[1]	*Nfa9060*[2]	*Nfa9150*
Rhodopirellula baltica	*RB11894*[1]	*RB11891*[2]	*RB1262*
Streptomyces avermitilis	-	*SAV6556*[#1]	*SAV6555*[2]
Propionibacterium acnes	*PPA1652*[1*]	*PPA1651*[2]	*PPA1650*[3]
Mycobacterium bovis	*Mb3427c*[1*]	*Mb3426c*[2]	*Mb3405c*
Agrobacterium tumefaciens	*AGR_L_3170*[1]	*AGR_L_3171*[1]	*AGR_L_3173*[3]

Adapted from Galhardo, *et al.*, 2005., Abella, *et al.*, 2004, and Clark, *et al.*, 2016.
Numerical superscript indicates the putative position of the gene within the predicted operon.
[*] RecA homologue
[#] DinB homologue
[X] Annotated as pseudogene

Within *E. coli*, all three SOS-regulated DNA polymerases (Pol II, Pol IV, and Pol V) are required to bypass DNA lesions of different kinds (Napolatino, *et al.*, 2000), with Pol V being the largest factor contributing to survival following UV irradiation (Courcelle, *et al.*, 2005). Maor-Shoshani and colleagues assessed the gap-filling replicative capacity of different combinations of proteins and

proposed that the *in vitro* activity of UmuC (Pol V) requires processed UmuD', RecA, as well as single-stranded binding protein (SSB) and is responsible for SOS-mediated, non-specific mutagenesis by TLS (Maor-Shoshani, *et al.*, 2000). Furthermore, multiple other interactions have been identified as being necessary for the complete function of this UmuD'$_2$C pathway in *E. coli*, including interactions between UmuD'$_2$C, the β clamp (Tang, *et al.*, 2000), Pol II, the γ clamp loader (Pham, *et al.*, 2001), as well as the co-factor ATP (Jiang, *et al.*, 2009). Overall, Pol V is tightly regulated by multiple levels of control at both pre-transcriptional and post-translational levels (briefly reviewed by Goodman, *et al.*, 2016). On the other-hand, the analogous ImuABC/DnaE2 mutagenic repair mechanism found in mycobacteria and *C. crescentus* is considerably less well studied and the detailed structure, function, and regulation of this mutasome is not completely understood.

2.2.1.1. *E. coli* UmuDC

In *E. coli*, three DNA polymerases contribute to TLS, namely Pol II, Pol IV, and Pol V (Napolitano *et al.*, 2000). In combination, these three polymerases are able to synthesize DNA while using a damaged DNA strand as a template for replication; however, it is Pol V that contributes the most to inducible mutagenesis (Courcelle, *et al.*, 2005). UV irradiation and chemicals such as 4-nitroquinoline 1-oxide (NQO) and methyl methanesulfonate (MMS) appear to cause mutagenesis as a result of TLS and requires DNA Pol III and the SOS-regulated proteins DinB, UmuD, UmuC and RecA (Friedberg, *et al.*, 1995). Kato and Shinoura screened *E. coli* mutants for a Umu-deficient, UV-nonmutatable phenotype and observed mutations in *umuA*, *umuB* and *umuC* (Kato and Shinoura, 1977). Although deficiencies in UmuA and UmuB resulted in slight

decreases in UV-inducible mutagenesis, UmuC was found to be more important to inducible mutagenesis as *umuC*-knockout strains were considerably more sensitive to UV irradiation and exhibited a considerable decrease in SOS induced mutagenesis (Kato and Shinoura, 1977). UmuC is a well conserved polymerase in prokaryotes, with a homologue in eukaryotes (Murakumo, *et al.*, 2001; and reviewed by Lawrence and Maher, 2001). In addition to UmuC, a second component of the *E. coli* inducible mutagnesis pathway was found to be UmuD (Shinagawa, *et al.*, 1983). Sequence data of UmuD allowed researchers to discover that the 45 kD protein shared homology with a region of LexA that is responsible for the autolytic cleavage of the repressor (Perry, *et al.*, 1985). This subsequently lead to the discovery that UmuD also underwent autocatalytic cleavage in a similar but distinct fashion to that of LexA (Burckhardt, *et al.*, 1988; Shinagawa, *et al.*, 1988). Once more, it was determined that RecA* nucleofilaments were responsible for protein autolytic cleavage, in this instance, resulting in the cleavage of the first 24 amino acid residues in UmuD to yield UmuD'. This processing was deemed essential to the function of the UmuDC pathway, as strains deficient in both LexA and RecA (UmuDC was still expressed but RecA was absent) failed to yield wild-type (WT) levels of induced mutagenesis following UV exposure (Nohmi, *et al.*, 1988). Furthermore, a strain of *E. coli* with a mutated copy of *recA* such that the encoded protein could no longer form nucleoprotein filaments also failed to exhibit any degree of UV-induced mutagenesis despite the production of processed UmuD' (Bailone, *et al.*, 1991; Dutreix, *et al.*, 1992). This further established an additional role of RecA in SOS-mediated DNA damage repair beyond the regulatory role of the protein.

Adding to the utility of RecA and the associated RecA* nucleoprotein filament, it was further determined that RecA* together with a bound ATP molecule is required to assemble with the rest of the Pol V complex for inducible mutagenesis to occur (Jiang, *et al.*, 2009). It was found that the presence of this RecA*-ATP molecule is required for a biochemical reason: to remotely recycle the Pol V complex by activation to the Pol V Mut state prior to TLS (Jiang, *et al.*, 2009). Here, RecA* was able to activate Pol V prior to the polymerase being purified and subsequently used to synthesize DNA in the absence of RecA*. Activation of Pol V occurs when the 3′-end of RecA* donates a RecA-ATP complex to UmuD′$_2$C to yield UmuD′$_2$C-RecA-ATP (Jiang, *et al.*, 2009). The UmuD′$_2$C-RecA-ATP complex is active and performs TLS until which point it becomes inactive following single primer extension of a single DNA template. It is postulated that the conversion from active to inactive Pol V Mut is associated with a conformational change of the UmuD′$_2$C complex and a repositioning of bound RecA-ATP from UmuD′$_2$ to UmuC (Jiang, *et al.*, 2009). This inactivation allows the bacterium to endure of the function of Pol V during the SOS response due to the decrease in mutational load associated with the rapid inactivation of Pol V (Jiang, *et al.*, 2009).

A further level of regulation and control of mutagenic polymerases exists beyond protein activity. Degradation of low-level Pol V expressed under conditions of minimal DNA damage (Frank, *et al.*, 1996) and sequestration of mutagenic polymerases to the cell membrane (Robinson, *et al.*, 2015) also contribute to the limited functionality of Pol V in *E. coli*. Therefore, error-prone DNA repair in *E. coli* is only fully functional if the DNA damage (and RecA*) persists beyond initial repair attempts by non-mutagenic pathways (Robinson,

et al., 2015). It is likely that this high level of regulation evolved to tightly control when the error-prone Pol V complex is functional, as evidenced by experiments by Caillet-Fauquet and colleagues in which *E. coli* cells containing the constitutively active *recA730* allele exhibited higher levels of spontaneous mutations without conditions of genotoxic stress (Caillet-Fauquet and Maenhaut-Michel, 1988). This phenotype was reversed following disruption of the *umuC* gene (thus eliminating Pol V function), suggesting that that Pol V has the capacity to introduce mutations into non-damaged DNA (Caillet-Fauquet and Maenhaut-Michel, 1988). This observation is reinforced by similar accounts of over-expressed SOS-dependent polymerases, such as DinB, resulting in increased mutational load in the absence of DNA damage (Kim, *et al.*, 1997).

2.2.1.2. *C. crescentus* ImuA, ImuB, and ImuC

Although *E. coli* is historically considered the 'gold standard' bacterial model, it differs significantly from other bacterial species, including, but not limited to, *Mtb* and *Msm*, in terms of metabolism and physiology. This generalization also applies to mutagenic repair and the error-prone polymerases, whereby, as discussed earlier, *E. coli* contains genes encoding the Pol V mutasome system. To this end, it is worthwhile to review another model organism, *C. crescentus*, which employs the more relevant *imuA-imuB-dnaE2* cassette-based mutagenesis mechanism (Galhardo, *et al.*, 2005). *C. crescentus* is UV-mutable but contains no homologues of the *E. coli* UmuD′$_2$C polymerase complex. Rather, *C. crescentus* contains genes encoding ImuA, ImuB, and ImuC (Galhardo, *et al.*, 2005). Here, DnaE2 is referred to as ImuC and completes the full array of the ImuABC cassette genes in the organism (Galhardo, *et al.*, 2005). The ImuABC proteins share no homology with components of UmuD′$_2$C pathways but are

thought to perform an analogous function. Furthermore, *imuC* (*CC3211*) is part of an SOS-regulated tricistronic operon within *C. crescentus* including *imuA* (*CC3213*), a homologue of *sulA*, as well as *imuB* (*CC3212*), a distant homologue of *dinB* (Galhardo, *et al.*, 2005). The regulation of the ImuABC system in *C. crescentus* has been shown to be mediated by a single $GTTCN_7GTTC$ SOS box located 66 bp upstream of *imuA* (Galhardo, *et al.*, 2005). The resultant mRNA molecule is present during normal cell growth but is strongly upregulated following UV irradiation and induction of RecA expression as part of the SOS response (Galhardo, *et al.*, 2005).

Homologues of *C. crescentus* ImuA in other bacteria, such as *Pseudomonas putida*, share sequence conservation with the corresponding SulA protein in that species; however genetic knockouts of *CC3213* did not indicate involvement in the SOS-dependent suppression of cell division during MMC exposure (Galhardo, *et al.*, 2005), indicating that ImuA does not contribute to the inhibition of cell division. The *CC3212* gene (*imuB*) shares homology with other DinB proteins and it is intriguing to note that all bacteria that encode ImuB also possess one or more genes encoding a DinB polymerase (Galhardo, *et al.*, 2005). However, phylogenetic analysis of ImuB and DinB proteins from a variety of organisms indicate highly divergent evolution – with the exception of *Streptomyces avermitilis*, which is also the only bacterium that encodes ImuB but lacks an *imuA* homologue (see **Table 1-4**) – suggesting that ImuB belongs to the UmuC superfamily (Galhardo, *et al.*, 2005). Similarly, what is evident from the strong co-evolution of the system is that DnaE2 polymerases from all bacterial backgrounds exhibit considerable divergent evolution from corresponding replicative DnaE(1) proteins (Galhardo, *et al.*, 2005). A large

proportion of α-proteobacteria (as well as other lineages such as Actinomycetales) exhibit marked divergence in sequence of the two *dnaE*-type genes, suggesting a gene duplication event in an extremely distant common ancestor (Galhado, *et al.*, 2005; Timinskas, *et al.*, 2013) (**Figure 1-1**). It is evident from this that DnaE2 performs a non-analogous and specialized function distinct from that of the distantly related replicative enzyme, DnaE1.

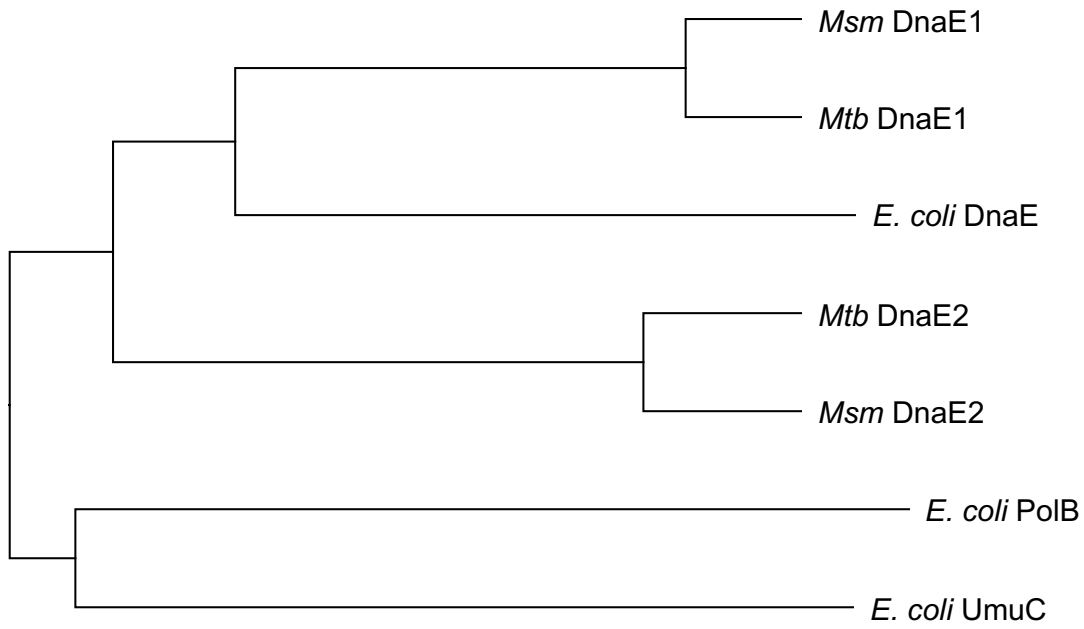

Figure 1-1 | Representative phylogenetic tree of the evolutionary relationship between DnaE2 and other polymerases from other model organisms

Single gene knockouts in *imuABC* showed a mild increase of UV sensitivity in *C. crescentus*, but double knockouts had no additive effect confirming that these proteins are involved in the same, non-redundant pathway (Galhardo, *et al.*, 2005). In the same vein, MMC and UV irradiation resistance as well as mutagenesis were negatively affected by the absence of any single *imuABC* open reading frame (ORF) – a phenotype that is recapitulated by double knockouts of the same genes (Galhardo, *et al.*, 2005). In addition to this, ImuABC contributed a very specific type of mutation during UV light-induced

mutagenic DNA repair that is underrepresented in pathway-deficient strains. When assessing RIF-selected, UV-induced RIF-resistance mutations within the *rpoB* gene of *C. crescentus*, Galhardo and colleagues identified that G:C→C:G transversion mutations were only present in WT strains and accounted for 28.5 % of SNPs present in these cases (Galhardo, *et al.*, 2005). Conversely, these transversions were completely absent in Δ*imuB* and Δ*imuC* strains. In the latter case, G:C→A:T transitions were much more abundant, contributing approximately 90 % of the SNPs in the knockout strain, but only accounting for 42.9 % of SNPs in WT (Galhardo, *et al.*, 2005). The preference for the G:C→C:G transversions by ImuABC differentiates the role of this mutagenic repair system from UmuD'$_2$C, which instead favours TC mutations from T(6-4)T photodimers following DNA damage by UV irradiation, and likely indicates a nucleotide preference during TLS as well as mechanistic differences between the two pathways (LeClerc, *et al.*, 1991; Napolitano *et al.*, 2000; Galhardo, *et al.*, 2005).

It is thought that following the formation of a DNA lesion which prevents the progression of the replicative DnaE polymerase, the resulting stalled replication fork induces expression of SOS-controlled genes. Thereafter, expressed ImuABC displaces the replicative polymerase and performs TLS for a limited number of bases (Galhardo, *et al.*, 2005; Moore, *et al.*, 2017). Beattie and colleagues have recently indicated that this 'polymerase swapping' occurs frequently, at a rate of turnover in the region of 10 s (Beattie, *et al.*, 2017). Furthermore, the swapping is predicted to be mediated by the more stable DNA-β clamp interaction and perhaps the *dnaB*-encoded helicase subunit (Galhardo, *et al.*, 2005; Beattie, *et al.*, 2017). Under this model, the mutagenic

repair polymerase is able to outcompete the replicative polymerase – particularly at stalled replication forks – and perform mutagenic TLS. However, the complete regulatory mechanism of TLS activation has not been elucidated in *C. crescentus* and it is likely that other factors influence the activity of ImuABC following expression. This is evidenced by the observation that SOS-level expression of ImuABC in the absence of genotoxic stress does not yield an increase in spontaneous or induced mutagenesis in *C. crescentus* (Alves, *et al.*, 2017). It is therefore possible that in the absence of lesion-specific factors (such as polymerase stalling), TLS cannot be successfully initiated by this pathway. This finding is in contrast to the observation that UmuD′$_2$C mutagenesis is functional in the absence of DNA damage during over-expression studies and highlights another key difference between the two mutagenic pathways (Caillet-Fauquet and Maenhaut-Michel, 1988; Tang, *et al.*, 2000). Additionally, Alves and colleagues provided evidence that RecA is not required for ImuABC function; therefore, it can be inferred that activated RecA* is not involved in ImuABC function (Alves, *et al.*, 2017), further identifying another dissimilarity to UmuD′$_2$C mutagenesis.

2.2.2. The Mycobacterial Mutasome

As with *E. coli* and *C. crescentus*, mycobacteria contain a complement of mutagenic DNA repair genes. The mutagenic DNA repair pathway in mycobacteria is encoded by the genes *imuA′*, *imuB* and *dnaE2* in a homologous pathway to that of *C. crescentus* (Boshoff, *et al.*, 2003; Warner, *et al.*, 2010). In further contrast to *E. coli*, which expresses three polymerases as part of the RecA-dependent response, DnaE1 and DnaE2 are the only known SOS-regulated polymerases identified in *Msm* and *Mtb* (Boshoff, *et al.*, 2003; Warner,

et al., 2010). The mycobacterial mutasome functions in an analogous manner to the previously discussed systems, namely, to continue DNA strand synthesis across DNA damage lesions on the template strand when the replicative polymerase stalls at a site of damage during replication of the chromosome. More specifically, the mycobacterial mutasome is thought to perform TLS across DNA lesions to allow the continuation of DNA replication during potentially lethal genotoxic stress (Boshoff, *et al.*, 2003).

Although the reason for the upregulation of the replicative DnaE1 during genotoxic stress is unknown, the expression of DnaE2 was determined to facilitate survival of lethal DNA damage lesions caused by UV irradiation, MMC or other genotoxins (Wang, 2001; Boshoff, *et al.*, 2003; Hanawalt, 2015). It was additionally established that the mycobacterial mutasome included the operonic accessory factors ImuA′ and ImuB, which are required for the phenotype of mutagenic DNA repair and damage tolerance (Warner, *et al.*, 2010). In *Mtb* and *Msm*, these three mutasome components are part of the split mutagenesis cassette, *imuA′-imuB/dnaE2*, and are controlled independently by two LexA-regulated promoters as part of the SOS response to DNA damage (Erill, *et al.*, 2006; Davis, *et al.*, 2002a; Boshoff, *et al.*, 2003; Warner, *et al.*, 2010; Galhardo, *et al.*, 2005).

The *imuA-imuB-dnaE2* mutagenic cassette is found in many bacteria (**Table 1-4**), but never in bacteria that encode Pol V-functioning UmuDC (Timinskas, *et al.*, 2013), suggesting that the proteins in each pathway perform analogous functions. Therefore, the mycobacterial mutasome is predicted to perform a function similar to that of $UmuD'_2C$ in *E. coli* (Jiang, *et al.*, 2009; Erill, *et al.*, 2006),

which has also been previously implicated in the development of drug resistance *in vivo* (Cirz, *et al.*, 2005). The mycobacterial mutasome, which represents the only inducible mutagenesis pathway in both *Mtb* and *Msm*, has DNA damage-inducible base-substitution mutagenesis activity (Warner, *et al.*, 2010), but induces a different spectrum of mutations from that observed in *C. crescentus* (Galhardo, *et al.*, 2005; Boshoff, *et al.*, 2003). Despite the non-essentiality of the pathway, it was previously shown that each of these three components is essential to the function of the mutasome and that strains individually deficient in functional DnaE2, ImuA', or ImuB are phenotypically identical and have markedly increased sensitivity to genotoxins such as MMC *in vitro* (Boshoff, *et al.*, 2003; Warner, *et al.*, 2010). Furthermore, an *Mtb* mutant strain deficient in DnaE2 was attenuated in a mouse infection model of TB, and exhibited a marked decrease in the ability to yield drug-resistant mutants during treatment with RIF *in muris* (Boshoff, *et al.*, 2003).

2.2.2.1. DnaE2

Unlike other bacteria, polymerase-encoding genes such as *dinB* and *dinX* are not known to be upregulated during DNA damage in mycobacteria (Brooks, *et al.*, 2001; Boshoff, *et al.*, 2003; see **Table 1-2** and **Table 1-3**); however, in addition to *dnaE1*, *dnaE2* (denoted as *MSMEG_1633* in *Msm* and *Rv3370c* in *Mtb*), is known to be the only other significantly upregulated polymerase in *Mtb* during exposure to genotoxic stressors (Boshoff, *et al.*, 2003). The associated induction of *dnaE2* is known to be controlled by the LexA repressor as *recA*-deficient strains did not exhibit increased expression of DnaE2 following DNA damage with UV, MMC or hydrogen peroxide (Boshoff, *et al.*, 2003). Strains of *Mtb* and *Msm* that are deficient in *dnaE2* phenocopy the inducible mutagenic capacity of

recA-deficient mutants and have considerably lower mutation frequencies following UV induction of the SOS response than WT (Boshoff, *et al.*, 2003), indicating that mutagenic DNA repair was completely dependent on the expression of DnaE2 in *Mtb* and *Msm*. Furthermore, the study by Boshoff and colleagues identified that DnaE2 was neither expressed *in vitro* under standard growth conditions nor functional outside of DNA damaging conditions as *dnaE2*-knockouts exhibited no associated fitness costs in addition to the fact that the mutants maintained a WT mutation rate during normal growth (Boshoff, *et al.*, 2003).

When compared to WT, Δ*dnaE2* strains failed to yield mutated pyrimidine dimers from sequential cytosine bases (CC→TT) when exposed to UV irradiation (Boshoff, *et al.*, 2003) indicating that this specific type of mutation was solely resultant of the function of DnaE2 in the WT background. Ultimately, the landmark study by Boshoff *et al.* identified that following a nine-month infection, the total number of Δ*dnaE2 Mtb* bacilli recovered from the lungs of infected C57BL/6 mice was 10-fold lower than that of WT (Boshoff, *et al.*, 2003). Additionally, the mice infected by aerosolized Δ*dnaE2 Mtb* exhibited exceptionally longer life-spans than the mice infected with WT (median survival time of 384 days and 222 days for mice infected with Δ*dnaE2* and WT, respectively) (Boshoff, *et al.*, 2003). Similarly, S3B6F1 mice infected with WT exhibited a 20 % mortality after 150 days while the counterpart mice infected with the Δ*dnaE2* mutant did not succumb to disease in the same period (Boshoff, *et al.*, 2003). This decrease in virulence illustrates the role that inducible mutagenic DNA repair plays in pathogenesis and in the survival of *Mtb* during infection, highlighting the potential benefits of DnaE2 inhibition by

chemotherapy. To further illustrate the mutagenic role of DnaE2, an experiment to determine the number of RIF-resistant mutants recovered from infected mice (although far from a conclusive result due to low statistical power) showed that *dnaE2*-deficient bacteria were less likely to develop resistance to RIF (Boshoff, *et al.*, 2003). Importantly, this work also provides evidence to suggest a link between the oxidative stress-induced role of DnaE2 and an environment that necessitates its function *in vivo*, and therefore suggests that *Mtb* does encounter a somewhat oxidative environment during infection (reviewed by Warner and Mizrahi, 2006). Overall, the results presented by Boshoff and colleagues provide evidence to suggest that DnaE2 (i) plays an integral role in mutagenic DNA repair during genotoxic stress; (ii) contributes to genotoxic stress survival and the mutagenic capacity of *Mtb in vivo*; and (iii) is involved in a non-redundant, SOS-regulated TLS pathway in *Mtb* and *Msm*.

DnaE2 is a C family DNA polymerase III α subunit and is homologous to the α-subunit of *E. coli* Pol III (**Figure 1-1**), except for the apparent loss of the τ clamp-loader subunit-binding region of the C-terminus region which may contribute to its low fidelity (Warner, *et al.*, 2010). In addition, when comparing mycobacterial DnaE2 to DnaE1, the former is missing both amino acids required for proof-reading activity (corresponding to the glutamate and aspartate residues at position 133 and 228, respectively, of *Mtb* DnaE1) as well as the polyhistidinol phosphatase (PHP) domain of replicative IIIα polymerases – likely further contributing to the low fidelity of DnaE2 (Warner, *et al.*, 2010; Wieczorek and McHenry, 2006; Nakane, *et al.*, 2009; Ditse, 2015). These key differences found in DnaE2 are likely necessary to allow the protein

to perform TLS and enhance the survival of the bacterium during genotoxic stress (Boshoff, *et al.*, 2003; Moore, *et al.*, 2017).

When analyzing the sequence information of DnaE2, it is evident that this C family polymerase does not contain the typical β clamp-binding domain with the sequence of QFDLF (Dalrymple, *et al.*, 2001), as is present in *Mtb* DnaE1 (Warner, *et al.*, 2010). The sequence in DnaE2 corresponding to the location of this binding site in DnaE1 is occupied by a conserved amino acid sequence of RPDRLPGVG not predicted to bind β (Warner, *et al.*, 2010). Therefore, as DnaE2 is thought not to contain a β clamp-binding domain, it is currently not known how DnaE2 is maintained at the replication fork during TLS. However, despite this discrepancy, DnaE2 does in fact include a catalytic active site suggesting its function as a type III*α* polymerase. The DnaE2 protein includes a series of three separated aspartic acid residues (at positions 439, 441, and 579 in *Mtb* or 441, 443, and 583 in *Msm*) that form the catalytic triad that is required for function by type III*α* polymerases (Warner, *et al.*, 2010; Bailey, *et al.*, 2006; Lamers, *et al.*, 2006). When this catalytic triad was disrupted by mutation of the 441st and 443rd amino acids from aspartic acid to alanine (^{441}DID^{443}→^{441}AIA^{443}) in *Msm*, UV-induced mutagenesis was restricted in the strain containing the chromosomal mutation in alignment with the phenotype of the *dnaE2*-deletion mutant (Warner, *et al.*, 2010). In addition, this *dnaE2*^{AIA} strain exhibited an associated increase in MMC sensitivity suggesting, together with the previous result, that polymerization of DNA is the biochemical function of DnaE2 during mutagenic DNA repair (Warner, *et al.*, 2010). However, the precise dynamics of DnaE2 activity following DNA damage remain unknown.

2.2.2.2. ImuA′ and ImuB

As described above, bacterial genomes that encode *dnaE2* invariably contain a gene encoding ImuB and occasionally a third protein denoted ImuA, constituting a three-component *imuA-imuB-dnaE2* mutagenic cassette (Erill, *et al.*, 2006) (**Table 1-4**). As expected, both *Mtb* and *Msm* encode a gene sharing considerable homology with the ImuB homologue found in *C. crescentus* (*Rv3394c* and *MSMEG_1622*, respectively) (Erill, *et al.*, 2006; Warner, *et al.*, 2010). Furthermore, the third component gene, which shares distant homology with *C. crescentus imuA*, is found in both mycobacterial species (*Mtb Rv3395c*; *Msm MSMEG_1620*), although here (and in other actinobacteria) it is denoted as *imuA*′ to indicate the reduced homology shared with the *imuA* gene found in proteobacteria (Erill, *et al.*, 2006; Galhardo, *et al.*, 2005). Both the accessory genes, *imuA*′ and *imuB*, were determined to be co-regulated following UV damage in exponentially growing *Mtb* (Warner, *et al.*, 2010) further identifying the cassette regulon which was previously identified to be LexA-repressible (Rand, *et al.*, 2003; Davis, *et al.*, 2002a). When each accessory protein was genetically inactivated in *Mtb* and *Msm*, a significant decrease in both inducible mutagenic capacity and genotoxic stress survival was observed (Warner, *et al.*, 2010). That is, *imuA*′ and *imuB* knockout mutants effectively phenocopy the *dnaE2* knockout, which suggests essential contributions of each protein to the function of DnaE2 during mutagenic DNA repair (Warner, *et al.*, 2010). Furthermore, the components were shown not to contribute to mutagenic DNA repair in an additive manner as a Δ*dnaE2* Δ*imuA*′ Δ*imuB* triple knockout mutant did not exhibit a further decrease in UV-induced mutation frequency and MMC-tolerance beyond that observed in individual knockout mutants (Warner, *et al.*, 2010). The results of Warner *et al.* (2010) confirmed that the

mycobacterial mutasome (i) consists of at least three components (ImuA′, ImuB, and DnaE2); (ii) is genetically related to that observed in *C. crescentus*; and (iii) perhaps functions in an analogous manner (Galhardo, *et al.*, 2005).

When looking at the ImuB component, phylogeny indicates that it is a distant member of the Y family polymerases which include DinB and other TLS polymerases (Galhardo, *et al.*, 2005); however, homology modeling indicates that the active site of ImuB does not include carboxylic acid residues which are required for DNA polymerization (Warner, *et al.*, 2010; Ling, *et al.*, 2001; Koorits, *et al.*, 2007). Despite this predicted loss-of-function, ImuB contains a putative β clamp-binding domain, represented by the QLPLWG amino acid sequence motif from position 354 to 359 in *Mtb* ImuB, a domain that is not observed in DnaE2 (Warner, *et al.*, 2010). Overall, these observations suggest that ImuB is not directly responsible for DNA polymerization during TLS but instead is thought to be essential to the ability of DnaE2 to catalyze TLS by an unknown mechanism (Warner, *et al.*, 2010).

Unlike the majority of ImuA proteins found in bacteria which are closely homologous to the respective SulA protein of each species, mycobacterial ImuA′ is more closely related to RecA than to either mycobacterial SulA or *C. crescentus* ImuA, indicating an early divergence from ImuA found in other bacterial species (**Figure 1-2**) (Warner, *et al.*, 2010; Galhardo, *et al.*, 2005). Although ImuA′ shares homology with *Mtb* RecA, it is missing the C-terminus and RecA-homologous regions that would allow it to perform homologous functions (Warner, *et al.*, 2010). Despite this, it is predicted that ImuA′ is able to bind to DNA as well as to ImuB, making it possible that it performs an

analogous function to RecA (Warner, *et al.*, 2010). However, the exact function of ImuA′ remains unknown.

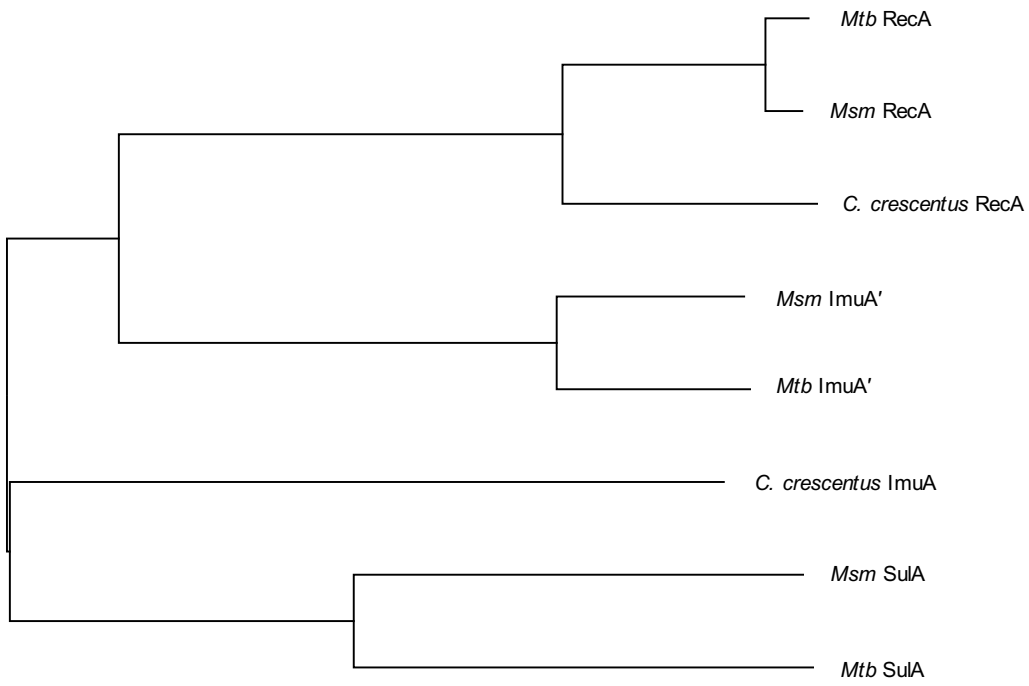

Figure 1-2 | Representation of the phylogenetic relationship between mycobacterial ImuA′ and related RecA and SulA proteins
There is a clear evolutionary divergence of mycobacterial ImuA′ proteins, which are more homologous to RecA proteins. In contrast, ImuA proteins found in bacteria such as *C. crescentus*, share more homology with SulA proteins.

2.2.2.3. Putative Protein Interactions within the Mycobacterial Mutasome and an Inferred Model

In addition to the fundamental genetic and microbiological analyses performed by Warner and colleagues, the authors also performed yeast two-hybrid (Y2H) analyses to identify possible protein-protein interactions (PPIs) between the identified components of the mycobacterial mutasome (**Figure 1-3**). ImuB was observed to interact with the greatest number of other proteins when tested in the heterologous yeast host, whereas ImuA′ and DnaE2 each only interacted with ImuB (Warner, *et al.*, 2010). Namely, ImuB-DnaN; ImuB-DnaE1; ImuB-

DnaE2; and ImuB-ImuA′ interactions were detected, in addition to an interaction between ImuB and another ImuB monomer (Warner, *et al.*, 2010). It makes intuitive sense that a DnaN-DnaE2 signal was not detected as the DnaE2 polymerase is predicted to lack the necessary β sliding clamp binding domain (Warner, *et al.*, 2010). Similarly, ImuB does contain a putative β sliding clamp binding domain, further supporting the PPIs detected by these analyses (Warner, *et al.*, 2010). Importantly, neither ImuA′ nor DnaE2 is predicted to interact with the *dnaN*-encoded β clamp, making ImuB the only mutagenic cassette protein to interact with DnaN in *Mtb* (Warner, *et al.*, 2010). This result highlights the essentiality of ImuB for mutasome function as it is possible the protein serves an indispensable central role in the function of the mutasome (**Figure 1-3**). In contrast, the ImuB-DnaE1 and ImuB-ImuB interactions inferred from the Y2H analysis are less intuitive and their roles in induced mutagenesis and DNA damage tolerance remain unclear. However, the use of a heterologous host, which provides a cytosolic environment distinct from that of mycobacteria, has the potential to detect false-positive PPIs (Vidal and Fields, 2014; Venkatesan, *et al.*, 2009). Therefore, it is necessary to support these hypotheses with evidence obtained from mycobacteria.

The Y2H interaction between ImuB and β was thought to be mediated by the previously mentioned DinB-specific (a Y family polymerase), conserved β clamp-binding motif of QLPLWG located within ImuB (Dalrymple, *et al.*, 2003; Warner, *et al.*, 2010). Indeed, a change in the amino acid residue at position 354 of ImuB from glutamine to alanine prevented the ImuB interaction with β but not ImuA′ nor DnaE2, suggesting the specificity of this site to binding DnaN

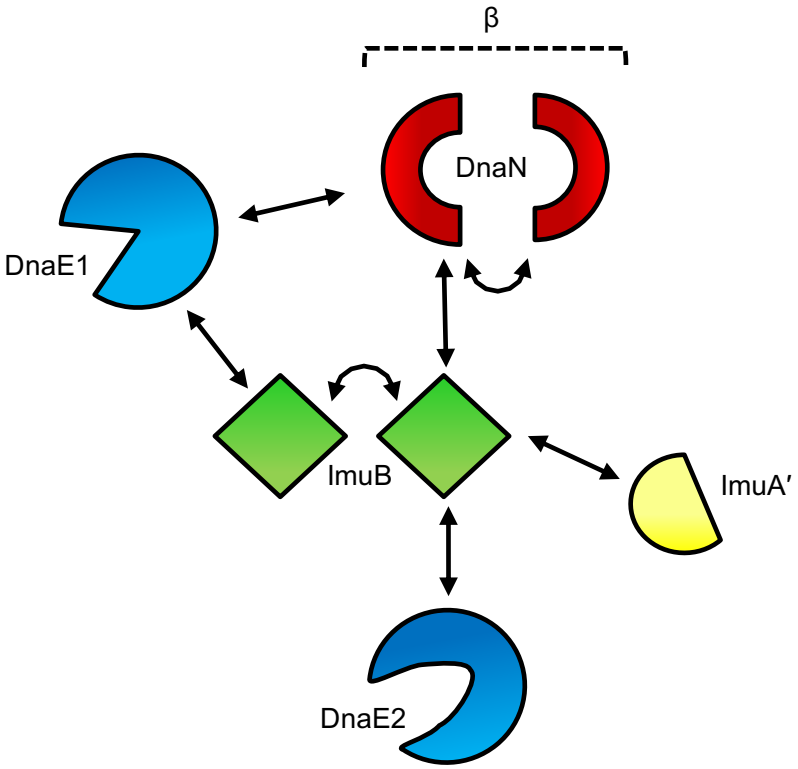

Figure 1-3 | The putative PPIs between the components of the mycobacterial mutasome
Y2H analyses by Warner, *et al.* (2010) identified potential interactions between ImuB and DnaN (the latter of which is known to form the β clamp dimer), as well as between ImuB and DnaE1, DnaE2, and ImuA'. Furthermore, ImuB was also detected to interact with itself.

(Warner, *et al.*, 2010). However, the corresponding change in *Msm* ImuB (Q352A) did not prevent a WT-level of UV-induced mutagenesis *in vitro* (Warner, *et al.*, 2010). In addition, substitution of the hydrophobic or aromatic amino acid residues in the putative β clamp-binding site did not affect the function of ImuB (Warner, *et al.*, 2010). However, alteration of the first five residues in the predicted *Msm* ImuB β-binding sequence (^{352}QLPLWG^{357} → ^{352}AAAAGG^{357}) rendered ImuB nonfunctional, as assessed in damage tolerance assays and UV-induced mutagenesis assays (Warner, *et al.*, 2010). The fact that *imuB*^{AAAAGG} phenocopied Δ*imuB* suggested that ImuB may interact with the β clamp through this putative site. It is likely that this interaction is tightly linked to the function of ImuB *in vivo* and that SOS-dependent mutagenic DNA repair necessitates the interaction between the β clamp and ImuB (Warner, *et al.*, 2010).

More specifically, it can be hypothesized that the putative interaction between ImuB and the β clamp is essential for the successful recruitment of the entire mutasome to the site of DNA damage, making the expression of *imuB* paramount to the function of DnaE2, the mutagenic function of the mutasome, and for the ability of the bacterium to survive DNA damage (Warner, *et al.*, 2010).

Furthermore, the C-terminal region of ImuB contains an extensive region containing structural disorder (Warner, *et al.*, 2010). These intrinsically unstructured protein regions are often an indicator of PPI sites (Dyson and Wright, 2005), suggesting that DnaE1, DnaE2, and ImuA′ may interact with the C-terminus of ImuB during mutagenic DNA repair. Indeed, when stop codons were introduce prematurely in the 3′-end of *Mtb imuB*, immediately preceding the putative β clamp binding site mentioned above (yielding *imuB*^{CB}), Y2H experiments failed to indicate interaction between ImuB and any previously identified protein partner (DnaE1, DnaE2, ImuA′, and β) excluding full-length ImuB, which indicated an interaction between the truncated ImuB and WT ImuB (**Figure 1-4**) (Warner, *et al.*, 2010). Conversely, stop mutations immediately after the β-binding site that removed the final 168 amino acids only yielded an interaction between ImuB^{C168} and β (Warner, *et al.*, 2010). This result further recapitulates the role of the ^{52}QLPLWG^{357} domain in binding with β, which was present in ImuB^{C168} but not in the ImuB^{CB} truncation. Together, these two results illustrate the association between the C-terminus of ImuB, which contains large segments of structural disorder, and the potential role it plays in binding other proteins involved in mutagenic DNA repair. Intriguingly, ImuB^{C168} was also identified to interact with full-length ImuB but

not with another ImuB^{C168} protein (Warner, *et al.*, 2010), suggesting that the C-terminus of ImuB interacts and binds the second ImuB outside the final 168 residues (**Figure 1-4**). Corresponding to the Y2H results, when *Msm* ImuB was truncated in a similar fashion, both ImuB^{CB} and ImuB^{C168} failed to restore the UV-induced mutagenic DNA repair and DNA damage tolerance phenotype of Δ*imuB in vitro* (Warner, *et al.*, 2010), once again highlighting the importance of PPIs with regard to mutasome function. Taken together, this identifies the essentiality of protein interactions between ImuB and the other components of the mutasome (and potentially proteins involved in replicative DNA synthesis) at the C-terminus of ImuB to the function of the mycobacterial mutasome.

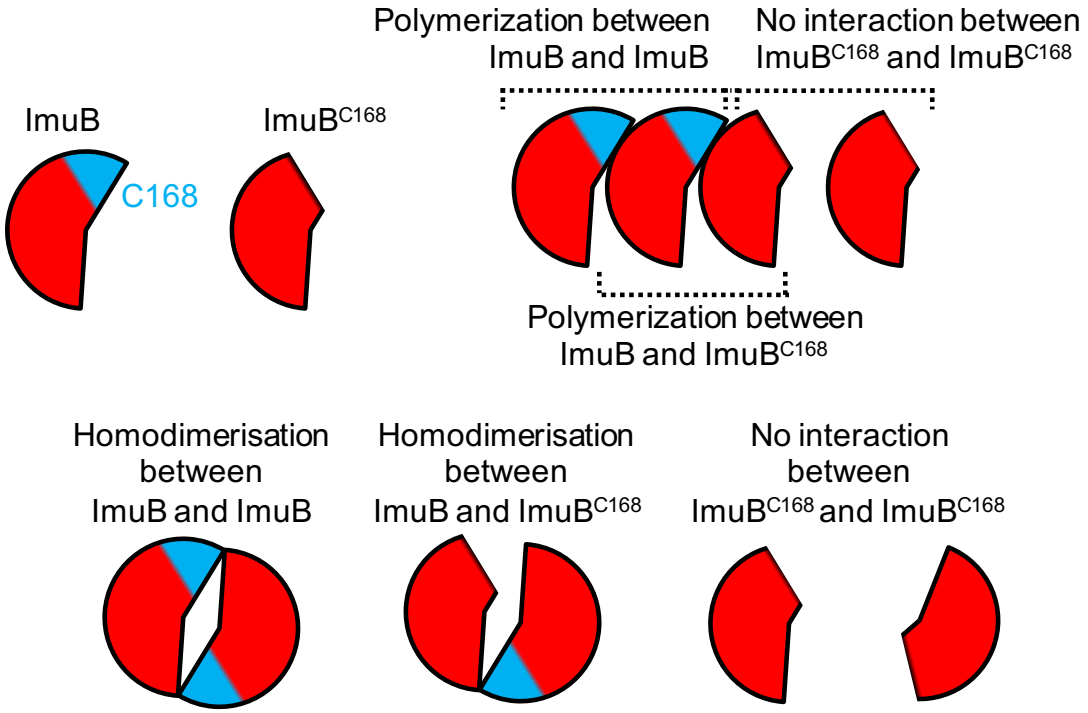

Figure 1-4 | Potential models of PPI between two ImuB components
The potential for C-terminus-dependent polymerization or dimerization is illustrated. ImuB with the final 168 amino acids truncated fail to contact the adjacent ImuB molecule; however, full-length ImuB is able to interact with any other ImuB molecule through the functional, structurally disordered C-terminus.

Given the genetic essentiality of *imuA′* for mutasome function, it was predicted that ImuA′ might interact with other mutasome components to form a functional complex that effects repair of DNA in a mutagenic fashion. This inference was supported by Y2H data in which ImuA′ was shown to interact solely with ImuB (Warner, *et al.*, 2010) (**Figure 1-3**). Notably, 48 amino acid N-terminal truncations of ImuA′ maintained the ability to bind to ImuB, whereas a truncated ImuA′ protein lacking the C-terminal 44 amino acids (ImuA′^{C44}) did not interact with ImuB during Y2H analysis (Warner, *et al.*, 2010). Similarly, when the Δ*imuA′* mutant strain of *Msm* containing the truncated *imuA′*^{C44} gene was exposed to UV irradiation or MMC *in vitro*, the phenotype did not differ from the *imuA′*-deficient background strain indicating that the C-terminus is involved with essential functions of ImuA′ and is involved with, or contributes to, an essential interaction with ImuB; however, the possibility that the N-terminus of ImuA′ plays another role in the function of ImuA′ *in vivo* cannot be excluded (Warner, *et al.*, 2010). Warner and colleagues also investigated the potential for ImuA′ to interact with itself, similar in fashion to RecA polymerization that occurs during the formation of a nucleoprotein filament; however, ImuA′ self-association was not detected by Y2H analysis, further differentiating it from the RecA homologue (Warner, *et al.*, 2010). Furthermore, mycobacterial ImuA′ does not contain a RecA-like nucleotide-binding domain nor a conserved DNA binding loop, which suggests that its function is specialized and distinctly different from that of RecA (Warner, *et al.*, 2010).

From the work conducted by Warner and colleagues (2010), a model of the mutasome can be constructed to allow insight into the key PPIs required for inducible mutagenic DNA repair in mycobacteria (**Figure 1-5**). This model

illustrates the essential interaction between the ImuB pseudopolymerase, which is predicted to be incapable of performing DNA polymerization and is likely to rather act as a central hub protein, and the β sliding clamp through the DinB-like β-binding domain located in the C-terminus of ImuB. This putative interaction potentially grants other components of the mutasome access to the replication fork. DnaE2, which lacks a conserved β binding domain, potentially interacts with ImuB through an unknown motif located in the C-terminus of ImuB (Warner, *et al.*, 2010). This putative PPI would allow DnaE2 access to the replication fork and allow the function of its conserved, homologous catalytic site to perform TLS. Furthermore, ImuA′ also interacts with ImuB through an interaction between the C-terminus of both proteins; however, the exact contribution and function of ImuA′ is unknown. According to this model, once the mutasome complex has formed, it would be able to perform TLS and

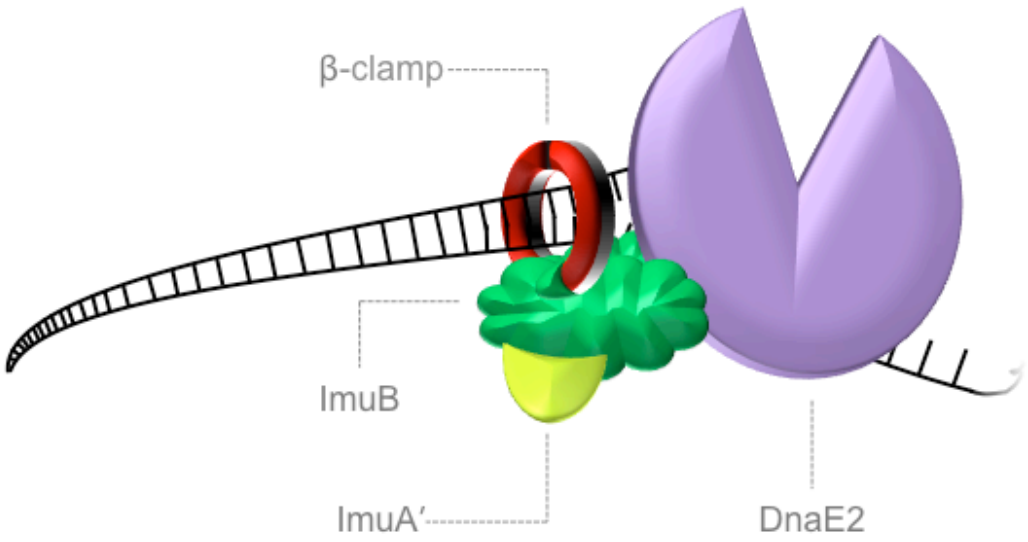

Figure 1-5 | A model of the mycobacterial mutasome
Here, a complete overview of the mycobacterial mutasome is presented. The β sliding clamp processivity factor (red) allows recruitment of the entire mutasome complex through an interaction with ImuB (green). Bound to ImuB is the additional accessory protein, ImuA′ (yellow) and the error-prone C family polymerase, DnaE2 (purple).

produce random mutations within the repaired DNA sequence. However, this model is far from complete and is based on a number of assumptions that warrant further investigation. Specifically, the PPIs identified by Y2H need further molecular validation within whole mycobacterial cells. Furthermore, the exact stoichiometry and order in which the mutasome components interact and how this is orchestrated requires elucidation. Similarly, the role, if any, of the putative ImuB-ImuB and DnaE1-ImuB interactions illustrates the complexity associated with the role of ImuB as a "hub" protein and raises the question of whether the mutasome interacts with other proteins of the replisome. Finally, the existence of other, unidentified mutasome components remains a possibility and requires further investigation in order to fully develop the mycobacterial mutasome model.

3. Aim and Objectives of this Study

The putative PPIs identified by Warner *et al*. (2010) provided the central axioms that guided the experimentation conducted in this work. Therefore, the interactions between ImuA', ImuB, and DnaE2 during DNA damage-inducible mutagenic DNA repair were investigated. At the inception of this work, efforts to express soluble proteins of all three mutasome components for downstream X-ray crystallographic modelling were largely unsuccessful. As a consequence of this, the primary aim of this work was to utilize alternative approaches to infer and investigate the PPIs predicted in the mycobacterial mutasome model (**Figure 1-5**). Specifically, the following objectives provided a basis for the experimental methods used:

(i) To visualize the location of ImuA', ImuB, and DnaE2 proteins within live mycobacterial cells;

(ii) To identify expression and localization dynamics that might indicate specialized function of each mutasome component and contribute to the development of the mutasome model;

(iii) To use the genetic evidence available (Boshoff, *et al*., 2003; Warner, *et al*., 2010), in combination with (i) above, to validate the essentiality of the putative PPIs within the mycobacterial mutasome;

(iv) To develop the foundation of high-throughput screening method for mycobacterial mutasome PPI inhibitors.

Upon initial investigation, fluorescence microscopy was selected as the most suitable method for achieving objectives (i), (ii), and (iv). Furthermore, preliminary results suggested the abandonment of the investigation of DnaE2, while correspondingly increasing the research focus of ImuB. Thereafter, the aim of this work was extended to include the following objectives:

(v) To investigate the potential implications of inducible mutagenesis on cell physiology and fate;

(vi) To investigate the effect of novel antitubercular agents on the mycobacterial mutasome with particular reference to expression and recruitment of ImuB.

4. Importance and Significance of this Research

The mycobacterial mutasome is of particular interest due to the associated decrease in virulence of *Mtb* strains lacking the mutasome in a mouse infection model of TB (Boshoff, *et al*., 2003), indicating the importance DNA damage repair plays during infection. This point alone underpins the value of studying the PPIs involved in the mycobacterial mutasome – which represents a

significant gap in the literature – with the potential of acquiring knowledge that will contribute to the discovery of chemical inhibitors targeted against the mutasome. Prior research has already demonstrated the consequences following the genetic disruption of the mutasome (Boshoff, *et al*., 2003; Warner, *et al*., 2010); however, further efforts are required to justify significant pursuit of chemical inhibitors, particularly by means of proof-of-concept experimentation within mycobacteria using non-genetic-based methods. The work conducted in this project represent the first steps undertaken in the development of an 'anti-evolution' chemotherapy for TB that specifically targets the mycobacterial mutasome. Such research might offer potentially significant downstream clinical and public health impacts with the ultimate goal of contributing toward the knowledge required to reduce the number of individuals that develop MDR- and XDR-TB in the future.

5. References:

Abella M, Erill I, Jara M, Mazón G, Campoy S, Barbé J. (2004) Widespread distribution of a lexA-regulated DNA damage-inducible multiple gene cassette in the Proteobacteria phylum. *Mol. Microbiol.* 54(1):212-222

Adams LB, Dinauer MC, Morgenstern DE, Krahenbuhl JL. (1997) Comparison of the roles of reactive oxygen and nitrogen intermediates in the host response to Mycobacterium tuberculosis using transgenic mice. *Tuber. Lung Dis.* 78(5&6):237-246

Alangaden GJ, Kreiswirth BN, Aouad A, Khetarpal M, Igno FR, Moghazeh SL, Manavathu EK, Lerner SA. (1998) Mechanism of Resistance to Amikacin and Kanamycin in Mycobacterium tuberculosis. *Antimicrob. Agents Chemother.* 42(5):1295-1297

Alves IR, Lima-Noronha MA, Silva LG, Fernández-Silva FS, Freitas AL, Marques MV, Galhardo RS. (2017) Effect of SOS-induced levels of imuABC on spontaneous and damage-induced mutagenesis in Caulobacter crescentus. *DNA Rep.* 59:20-6

Andersson DI, Hughes D. (2010) Antibiotic resistance and its cost: is it possible to reverse resistance? *Nat. Rev. Microbiol.* 8(4):260-71

Ando H, Miyoshi-Akiyama T, Watanabe S, Kirikae T. (2014) A silent mutation in mabA confers isoniazid resistance on Mycobacterium tuberculosis. *Mol. Microbiol.* 91(3):538-547

Andrei M, Platon E. (2017) Drug-resistant tuberculosis threatens WHO's End-TB strategy. *Lancet Infec. Dis.* (17)7:674-675

Ashley RE, Blower TR, Berger JM, Osheroff N. (2017) Recognition of DNA Supercoil Geometry by Mycobacterium tuberculosis Gyrase. *Biochem*. 56(40):5440-8

Bailey S, Wing RA, Steitz TA. (2006) The structure of T. aquaticus DNA polymerase III is distinct from eukaryotic replicative DNA polymerases. *Cell* 126:893-904

Bailone A, Sommer S, Knežević J, Dutreix M, Devoret R. (1991) A RecA protein mutant deficient in its interaction with the UmuDC complex. *Biochimie* 73:479-484

Baym M, Lieberman TD, Kelsic ED, Chait R, Gross R, Yelin I, Kishony R. (2016) Spatiotemporal microbial evolution on antibiotic landscapes. *Science* 353(6304):1147-1151

Beattie TR, Kapadia N, Nicolas E, Uphoff S, Wollman AJM, Leake MC, Reyes-Lamothe R. (2017) Frequent exchange of the DNA polymerase during bacterial chromosome replication. *eLife* e21763

Beggs CB. (2002) A quantitative method for evaluating the photoreactivation of ultraviolet damaged microorganisms. *Photochem. Photobiol. Sci.* 1(6):431-7

Bergval I, Kwok B, Schuitema A, Kremer K, van Soolingen D, Klaster P, Anthony R. (2012) Pre-Existing Isoniazid Resistance, but Not the Genotype of Mycobacterium Tuberculosis Drives Rifampicin Resistance Codon Preference in Vitro. *PLOS One* 7(1):e29108

Bi E, Lutkenhaus J. (1993) Cell division inhibitors SulA and MinCD prevent formation of the FtsZ ring. *J. Bacteriol.* 175:1118-1125

Blair JM, Webber MA, Baylay AJ, Ogbolu DO, Piddock LJ. (2015) Molecular mechanisms of antibiotic resistance. *Nat. Rev. Microbiol.* 13(1):42-51

Blázquez J, Couce A, Rodríguez-Beltrán J, Rodríguez-Rojas A. (2012) Antimicrobials as promoters of genetic variation. *Curr. Opin. Microbiol.* 15(5):561-9

Bloss E, Kukša L, Holtz TH, Riekstina V, Skripčonoka V, Kammerer S, Leimane V. (2010) Adverse events related to multidrug-resistant tuberculosis treatment, Latvia, 2000–2004. *Tuber. Lung Dis.* 14(3):275-81

Boritsch EC, Khanna V, Pawlik A, Honoré N, Navas VH, Ma L, Bouchier C, Seemann T, Supply P, Stinear TP, Brosch R. (2016) Key experimental evidence of chromosomal DNA transfer among selected tuberculosis-causing mycobacteria. *Proc. Natl. Acad. Sci. USA* 113(35):9876-81

Borrell S, Gagneux S. (2011) Strain diversity, epistasis and the evolution of drug resistance in Mycobacterium tuberculosis. *Clin. Microbiol. Infect.* 17(6):815-20

Borrell S, Teo Y, Giardina F, Streicher EM, Klopper M, Feldmann J, Müller B, Victor TC, Gagneux S. (2013) Epistasis between antibiotic resistance mutations drives the evolution of extensively drug-resistant tuberculosis. *Evol. Med. Public Health* 2013:65-74

Boshoff HIM, Reed BR, Barry III CE, Mizrahi V. (2003) DnaE2 polymerase contributes to in vivo survival and the emergence of drug resistance in Mycobacterium tuberculosis. *Cell* 113:183–193

Boudsocq F, Kokoska RJ, Plosky BS, Vaisman A, Ling H, Kunkel TA, Yang W, Woodgate R. (2004) Investigating the role of the little finger domain of Y-family

DNA polymerases in low fidelity synthesis and translesion replication. *J. Biol. Chem.* 279(31):32932-32940

Brandis G, Hughes D. (2013) Genetic characterization of compensatory evolution in strains carrying rpoB Ser531Leu, the rifampicin resistance mutation most frequently found in clinical isolates. *J. Antimicrob. Chemother.* 68:2493-2497

Brenchley JM, Schacker TW, Ruff LE, Price DA, Taylor JH, Beilman GJ, Nguyen PL, Khoruts A, Larson M, Haase AT, Douek DC. (2004) CD4+ T Cell Depletion during all Stages of HIV Disease Occurs Predominantly in the Gastrointestinal Tract. *J. Exp. Med.* 200(6):749-759

Brent R, Ptashne M. (1981) Mechanism of action of the lexA gene product. *Proc. Natl. Acad. Sci. USA* 78(7):4204-4208

Brooks PC, Movahedzadeh F, Davis EO. (2001) Identification of Some DNA Damage-Inducible Genes of Mycobacterium tuberculosis: Apparent Lack of Correlation with LexA Binding. *J. Bacteriol.* 183(15):4459-4467

Brossier F, Veziris N, Truffot-Pernot C, Jarlier V, Sougakoff W. (2011) Molecular Investigation of Resistance to the Antituberculous Drug Ethionamide in Multidrug-Resistant Clinical Isolates of Mycobacterium tuberculosis. *Antimicrob. Agents Chemother.* 55(1):355-360

Bruck I, Goodman MF, O'Donnell M. (2003) The Essential C Family DnaE Polymerase Is Error-prone and Efficient at Lesion Bypass. *J. Biol. Chem.* 278(45):44361-44368

Bunting KA, Roe SM, Pearl LH. (2003) Structural basis for recruitment of translesion DNA polymerase Pol IV/DinB to the β-clamp. *EMBO J.* 22(21):5883-92

Burckhardt SE, Woodgate R, Scheuermann RH, Echols H. (1988) UmuD mutagenesis protein of Escherichia coli: overproduction, purification, and cleavage by RecA. *Proc. Natl. Acad. Sci. USA* 85(6):1811-1815

Burgers PM, Kornberg A, Sakakibara Y. (1981) The dnaN gene codes for the beta subunit of DNA polymerase III holoenzyme of Escherichia coli. *Proc. Natl. Acad. Sci. USA* 78(9):5391-5

Burman WJ, Goldberg S, Johnson JL, Muzanye G, Engle M, Mosher AW, Choudhri S, Daley CL, Munsiff SS, Zhao Z, Vernon A. (2006) Moxifloxacin versus ethambutol in the first 2 months of treatment for pulmonary tuberculosis. *Am. J. Respir. Crit. Care Med.* 174(3):331-8

Burney S, Caulfield JL, Niles JC, Wishnok JS, Tannenbaum SR. (1999) The chemistry of DNA damage from nitric oxide and peroxynitrite. *Mutat. Res.* 424:37–49

Burnouf DY, Olieric V, Wagner J, Fujii S, Reinbolt J, Fuchs RP, Dumas P. (2004) Structural and biochemical analysis of sliding clamp/ligand interactions suggest a competition between replicative and translesion DNA polymerases. *J. Mol. Biol.* 335(5):1187-97

Butler MS, Blaskovich MA, Cooper MA. (2016) Antibiotics in the clinical pipeline at the end of 2015. *J. Antibiot.* 70:3–24

Cadena AM, Fortune SM, Flynn JL. (2017) Heterogeneity in tuberculosis. *Nat. Rev. Microbiol.* 17:691–702

Caillet-Fauquet P, Maenhaut-Michel G. (1988) Nature of the SOS mutator activity: genetic characterization of untargeted mutagenesis in Escherichia coli. *Molec. gen. Genet.* 213:491-498

Casali N, Nikolayevskyy V, Balabanova Y, Harris SR, Ignatyeva O, Kontsevaya I, Corander J, Bryant J, Parkhill J, Nejentsev S, Horstmann RD, Brown T, Drobniewski F. (2014) Evolution and transmission of drug-resistant tuberculosis in a Russian population. *Nat. Genet.* 46:279-286

Cirz RT, Chin JK, Andes DR, de Crécy-Lagard V, Craig WA, Romesberg FE. (2005) Inhibition of mutation and combating the evolution of antibiotic resistance. *PLOS Biol.* 3(6):e176

Cirz RT, Jones MB, Gingles NA, Minogue TD, Jarrahi B, Peterson SN, Romesberg FE. (2007) Complete and SOS-mediated response of Staphylococcus aureus to the antibiotic ciprofloxacin. *J. Bacteriol.* 189(2):531-9

Clark K, Karsch-Mizrachi I, Lipman DJ, Ostell J, Sayers EW. (2016) GenBank. *Nucleic Acids Res.* 44(Database issue):D67-D72

Comas I, Borrell S, Roetzer A, Rose G, Malla B, Kato-Maeda M, Galagan J, Niemann S, Gagneux S. (2012) Whole-genome sequencing of rifampicin-resistant Mycobacterium tuberculosis strains identifies compensatory mutations in RNA polymerase genes. *Nat. Genet.* 44(1):106-110

Conde MB, Efron A, Loredo C, De Souza GR, Graça NP, Cezar MC, Ram M, Chaudhary MA, Bishai WR, Kritski AL, Chaisson RE. (2009) Moxifloxacin versus ethambutol in the initial treatment of tuberculosis: a double-blind, randomised, controlled phase II trial. *Lancet* 373(9670):1183-9

Conde MB, Mello FC, Duarte RS, Cavalcante SC, Rolla V, Dalcolmo M, Loredo C, Durovni B, Armstrong DT, Efron A, Barnes GL. (2016) A phase 2 randomized trial of a rifapentine plus moxifloxacin-based regimen for treatment of pulmonary tuberculosis. *PLOS One* 11(5):e0154778

Coros A, Callahan B, Battaglioli E, Derbyshire KM. (2008) The specialized secretory apparatus ESX-1 is essential for DNA transfer in Mycobacterium smegmatis. *Mol. Microbiol.* 69(4):794-808

Couce A, Blázquez J. (2009) Side effects of antibiotics on genetic variability. *FEMS Microbiol. Rev.* 33(3):531-8

Courcelle CT, Belle JJ, Courcelle J. (2005) Nucleotide Excision Repair or Polymerase V-Mediated Lesion Bypass Can Act To Restore UV-Arrested Replication Forks in Escherichia coli. *J. Bacteriol.* 187(20):6953-6961

Da Silva PEA, Palomino JC. (2011) Molecular basis and mechanisms of drug resistance in Mycobacterium tuberculosis: classical and new drugs. *J. Antimicrob. Chemother.* 66:1417-1430

Dalrymple BP, Kongsuwan K, Wijffels G, Dixon NE, Jennings PA. (2001) A universal protein–protein interaction motif in the eubacterial DNA replication and repair systems. *Proc. Natl. Acad. Sci. USA* 98:11627–11632

Dalrymple BP, Wijffels G, Kongsuwan K, Jennings P. (2003) Towards an understanding of protein-protein interaction network heirarchies. Analysis of DnaN-binding peptide motifs in members of protein families interacting with the eubacterial processivity clamp, the subunit of DNA Polymerase III. pp 153–162

Davis EO, Dullaghan EM, Rand L. (2002a) Definition of the Mycobacterial SOS box and use to identify LexA-regulated genes in Mycobacterium tuberculosis. *J. Bacteriol.* 184:3287–3295

Davis EO, Springer E, Gopaul KK, Papavinasasundaram KG, Sander P, Böttger EC. (2002b) DNA damage induction of recA in Mycobacterium tuberculosis independently of RecA and LexA. *Mol. Microbiol.* 46(3):791-800

Dawson LF, Dillury J, Davis EO. (2010) RecA-Independent DNA Damage Induction of Mycobacterium tuberculosis ruvC Despite an Appropriately Located SOS Box. *J. Bacteriol.* 192(2):599-603

de Saro FJL, O'Donnell M. (2001) Interaction of the b sliding clamp with MutS, ligase, and DNA polymerase I. *Proc. Natl. Acad. Sci. USA* 98(15):8376-8380

de Vos M, Müller B, Borrell S, Black PA, van Helden PD, Warren RM, Gagneux S, Victor TC. (2013) Putative Compensatory Mutations in the rpoC Gene of Rifampin Resistant Mycobacterium tuberculosis Are Associated with Ongoing Transmission. *Antimicrob. Agents Chemother.* 57(2):827-832

Deb C, Lee CM, Dubey VS, Daniel J, Abomoelak B, Sirakova TD, Pawar S, Rogers L, Kolattukudy PE. (2009) A novel in vitro multiple-stress dormancy model for Mycobacterium tuberculosis generates a lipid-loaded, drug-tolerant, dormant pathogen. *PLOS One* 4(6):e6077

Dheda K, Gumbo T, Gandhi NR, Murray M, Theron G, Udwadia Z, Migliori GB, Warren R. (2014) Global control of tuberculosis: from extensively drug-resistant to untreatable tuberculosis. *Lancet Respir. Med.* 2(4):321-38

Dheda K, Gumbo T, Maartens G, Dooley KE, McNerney R, Murray M, Furin J, Nardell EA, London L, Lessem E, Theron G. (2017) The epidemiology, pathogenesis, transmission, diagnosis, and management of multidrug-resistant, extensively drug-resistant, and incurable tuberculosis. *Lancet Respir. Med.* 5(4):291-360

Ditse, Z. (2015) 'Replication fidelity in the mircroevolution of mycobacteria', PhD Medical Microbiology. *University of Cape Town*, Cape Town, South Africa

Donigan KA, McLenigan MP, Yang W, Goodman MF, Woodgate R. (2014) The steric gate of DNA polymerase ι regulates ribonucleotide incorporation and deoxyribonucleotide fidelity. *J. Biol. Chem.* 289(13):9136-45

Dorman SE, Johnson JL, Goldberg S, Muzanye G, Padayatchi N, Bozeman L, Heilig CM, Bernardo J, Choudhri S, Grosset JH, Guy E. (2009) Substitution of moxifloxacin for isoniazid during intensive phase treatment of pulmonary tuberculosis. *Am. J. Respir. Crit. Care Med.* 180(3):273-80

Dos Vultos T, Mestre O, Rauzier J, Golec M, Rastogi N, Rasolofo V, Tonjum T, Sola C, Matic I, Gicquel B. (2008) Evolution and diversity of clonal bacteria: the paradigm of Mycobacterium tuberculosis. *PLOS One* 3(2):e1538

Durão P, Balbontín R, Gordo I. (2018) Evolutionary Mechanisms Shaping the Maintenance of Antibiotic Resistance. *Trends Microbiol*. doi: 10.1016/j.tim.2018.01.005

Durbach SI, Andersen SJ, Mizrahi V. (1997) SOS induction in Mycobacteria: analysis of the DNA-binding activity of a LexA-like repressor and its role in DNA damage induction of the recA gene from Mycobacterium smegmatis. *Mol. Microbiol.* 26:643–653

Dutreix M, Burnett B, Bailone A, Radding CM, Devoret R. (1992) A partially deficient mutant, fecAl730, that fails to form normal nucleoprotein filaments. *Molec. gen. Genet.* 232:489-497

Dye C, Williams BG, Espinal MA, Raviglione MC. (2002) Erasing the world's slow stain: strategies to beat multidrug-resistant tuberculosis. *Science* 295:2042–2046

Dyson HJ, Wright PE. (2005) Intrinsically unstructured proteins and their functions. *Nat. Rev. Mol. Cell Biol.* 6:197-208

Echols H, Goodman MF. (1990) Mutation induced by DNA damage: a many protein affair. *Mutat. Res.* 236:301-311

Eldholm V, Balloux F. (2016) Antimicrobial resistance in Mycobacterium tuberculosis: the odd one out. *Trends Microbiol.* 24(8):637-48

Erdem AL, Jaszczur M, Bertram JG, Woodgate R, Cox MM, Goodman MF. (2014) DNA polymerase V activity is autoregulated by a novel intrinsic DNA-dependent ATPase. *Elife* 3:e02384

Erill I, Campoy S, Barbé J. (2007) Aeons of distress: an evolutionary perspective on the bacterial SOS response. *FEMS Microbiol. Rev.* 31(6):637-56

Erill I, Campoy S, Mazon G, Barbé J. (2006) Dispersal and regulation of an adaptive mutagenesis cassette in the bacteria domain. *Nucleic Acids Res.* 34:66–77

Falzon D, Gandhi N, Migliori GB, Sotgiu G, Cox H, Holtz TH, Hollm-Delgado MG, Keshavjee S, DeRiemer K, Centis R, D'Ambrosio L. (2012) Resistance to fluoroquinolones and second-line injectable drugs: impact on MDR-TB outcomes. *Eur. Respir. J.* erj01347-2012

Fan XY, Tang BK, Xu YY, Han AX, Shi KX, Wu YK, Ye Y, Wei ML, Niu C, Wong KW, Zhao GP. (2018) Oxidation of dCTP contributes to antibiotic lethality in stationary-phase mycobacteria. *Proc. Natl. Acad. Sci. USA* 30:201719627

Feklistov A, Mekler V, Jiang Q, Westblade LF, Irshik H, Jansen R, Mustaev A, Darst SA, Ebright RH. (2008) Rifamycins do not function by allosteric modulation of binding of Mg2+ to the RNA polymerase active center. *Proc. Natl. Acad. Sci. USA* 105:14820–5

Fisher RA, Gollan B, Helaine S. (2017) Persistent bacterial infections and persister cells. *Nat. Rev. Microbiol.* 15:453–464

Forget EJ, Menzies D. (2006) Adverse reactions to first-line antituberculosis drugs. *Expert Opin. Drug Saf.* 5(2):231-49

Frank EG, Ennis DG, Gonzalez M, Levine AS, Woodgate R. (1996) Regulation of SOS mutagenesis by proteolysis. *Proc. Natl. Acad. Sci. USA* 93(19):10291-6

Fridman O, Goldberg A, Ronin I, Shoresh N, Balaban NQ. (2014) Optimization of lag time underlies antibiotic tolerance in evolved bacterial populations. *Nature* 513(7518):418-21

Friedberg EC, Walker GC, Siede W. (1995) DNA Repair and Mutagenesis. *American Society for Microbiology Press* Washington DC

Frieden TR, Sbarbaro JA. (2007) Promoting adherence to treatment for tuberculosis: the importance of direct observation. *Bull. World Health Organ.* 85(5):407-9

Friedman N, Vardi S, Ronen M, Alon U, Stavans J. (2005) Precise temporal modulation in the response of the SOS DNA repair network in individual bacteria. *PLOS Biol.* 3(7):e238

Gagneux S, Long CD, Small PM, Van T, Schoolnik GK, Bohannan BJM. (2006) The Competitive Cost of Antibiotic Resistance in Mycobacterium tuberculosis. *Science* 312(5782):1944-1946

Galhardo RS, Hastings PJ, Rosenberg SM. (2007) Mutation as a stress response and the regulation of evolvability. *Crit. Rev. Biochem. Mol. Biol.* 42(5):399-435

Galhardo RS, Rocha RP, Marques MV, Menck CFM. (2005) An SOS-regulated operon involved in damage-inducible mutagenesis in Caulobacter crescentus. *Nucleic Acids Res.* 33:2603–2614

Gamulin V, Cetkovic H, Ahel I. (2004) Identification of a promoter motif regulating the major DNA damage response mechanism of Mycobacterium tuberculosis. *FEMS Microbiol. Lett.* 238:57-63

Gandhi NR, Moll A, Sturm AW, Pawinski R, Govender T, Lalloo U, Zeller K, Andrews A, Friedland G. (2006) Extensively drug-resistant tuberculosis as a cause of death in patients co-infected with Tuberculosis and HIV in a rural area of South Africa. *Lancet* 368:1575–1580

Gevers D, Vandepoele K, Simillion C, Van de Peer Y. (2004) Gene duplication and biased functional retention of paralogs in bacterial genomes. *Trends Microbiol.* 12(4):148-54

Gillespie SH, Basu S, Dickens AL, O'sullivan DM, McHugh TD. (2005) Effect of subinhibitory concentrations of ciprofloxacin on Mycobacterium fortuitum mutation rates. *Antimicrob. Agents Chemother.* 56(2):344-8

Gillespie SH, Crook AM, McHugh TD, Mendel CM, Meredith SK, Murray SR, Pappas F, Phillips PP, Nunn AJ. (2014) Four-month moxifloxacin-based regimens for drug-sensitive tuberculosis. *N. Engl. J. Med.* 371(17):1577-87

Gogarten JP, Doolittle WF, Lawrence JG. (2002) Prokaryotic evolution in light of gene transfer. *Mol. Biol. Evol.* 19(12):2226-38

Goodman MF, McDonald JP, Jaszczur MM, Woodgate R. (2016) Insights into the complex levels of regulation imposed on Escherichia coli DNA polymerase V. 44:42-50

Goodman MF, Woodgate R. (2013) Translesion DNA polymerases. *Cold Spring Harb. Perspect. Biol.* 5(10):a010363

Gray TA, Clark RR, Boucher N, Lapierre P, Smith C, Derbyshire KM. (2016) Intercellular communication and conjugation are mediated by ESX secretion systems in mycobacteria. *Science* 354(6310):347-50

Grompone G, Seigneur M, Ehrlich SD, Michel B. (2002) Replication fork reversal in DNA polymerase III mutants of Escherichia coli: a role for the β clamp. *Mol. Microbiol.* 44(5):1331-1339

Gygli SM, Borrell S, Trauner A, Gagneux S. (2017) Antimicrobial resistance in Mycobacterium tuberculosis: mechanistic and evolutionary perspectives. *FEMS Microbiol. Rev.* 41(3):354-73

Hanawalt PC. (2015) Historical perspective on the DNA damage response. *DNA Rep.* 36:2-7

Hegde SP, Qin MH, Li XH, Atkinson MA, Clark AJ, Rajagopalan M, Madiraju MV. (1996) Interactions of RecF protein with RecO, RecR, and single-stranded DNA binding proteins reveal roles for the RecF-RecO-RecR complex in DNA repair and recombination. *Proc. Natl. Acad. Sci. USA* 93:14468-14473

Hershberg R. (2017) Antibiotic-Independent Adaptive Effects of Antibiotic Resistance Mutations. *Trends Genet.* 33(8):521-528

Heym B, Stavropoulos E, Honoré N, Domenech P, Saint-Joanis B, Wilson TM, Collins DM, Colston MJ, Cole ST. (1997) Effects of Overexpression of the Alkyl Hydroperoxide Reductase AhpC on the Virulence and Isoniazid Resistance of Mycobacterium tuberculosis. *Infect. Immun.* 65(4):1395-1401

Hirpa S, Medhin G, Girma B, Melese M, Mekonen A, Suarez P, Ameni G. (2013) Determinants of multidrug-resistant tuberculosis in patients who underwent first-line treatment in Addis Ababa: a case control study. *BMC Public Health* 13(1):782

Houben RM, Dodd PJ. (2016) The global burden of latent tuberculosis infection: a re-estimation using mathematical modelling. *PLOS Med.* 13(10):e1002152

Jain SK, Lamichhane G, Nimmagadda S, Pomper MG, Bishai WR. (2008) Antibiotic treatment of Tuberculosis: Old problems, new solutions. *Microbe* 3:285–292

Jankute M, Cox JA, Harrison J, Besra GS. (2015) Assembly of the mycobacterial cell wall. *Annu. Rev. Microbiol*. 69:405-23

Jarlier V, Nikaido H. (1994) Mycobacterial cell wall: Structure and role in natural resistance to antibiotics. *FEMS Microbiol. Lett.* 123(1&2):11-18

Jatsenko T, Sidorenko J, Saumaa S, Kivisaar M. (2017) DNA Polymerases ImuC and DinB Are Involved in DNA Alkylation Damage Tolerance in Pseudomonas aeruginosa and Pseudomonas putida. *PLOS One* 12(1):e0170719

Jensen RB, Wang SC, Shapiro L. (2001) A moving DNA replication factory in Caulobacter crescentus. *EMBO J.* 20:4952-4963

Jiang Q, Karata K, Woodgate R, Cox MM, Goodman MF. (2009) The active form of DNA polymerase V is UmuD′2C-RecA-ATP. *Nature* 460:359–363

Johansen SK, Maus CE, Plikaytis BB, Douthwaite S. (2006) Capreomycin Binds across the Ribosomal Subunit Interface Using tlyA-Encoded 20 -O-Methylations in 16S and 23S rRNAs. *Mol. Cell* 23:173-182

Juréen P, Werngren J, Toro J-C, Hoffner S. (2008) Pyrazinamide Resistance and pncA Gene Mutations in Mycobacterium tuberculosis. *Antimicrob. Agents Chemother.* 52(5):1852-1854

Kamenšek S, Podlesek Z, Gillor O, Žgur-Bertok D. (2010) Genes regulated by the Escherichia coli SOS repressor LexA exhibit heterogenous expression. *BMC Microbiol.* 10:283

Kang YA, Shim TS, Koh WJ, Lee SH, Lee CH, Choi JC, Lee JH, Jang SH, Yoo KH, Jung KH, Kim KU. (2016) Choice between levofloxacin and moxifloxacin and multidrug-resistant tuberculosis treatment outcomes. *Ann. Am. Thorac. Soc.* 13(3):364-70

Kato T, Shinoura Y. (1977) Isolation and Characterization of Mutants of *Escherichia coli* Deficient in Induction of Mutations by Ultraviolet Light. *Molec. gen. Genet.* 156:121-131

Kaur P, Ghosh A, Krishnamurthy RV, Bhattacharjee DG, Achar V, Datta S, Narayanan S, Anbarasu A, Ramaiah S. (2015) A high-throughput cidality screen for Mycobacterium tuberculosis. *PLOS One* 10(2):e0117577

Kawai Y, Moriya S, Ogasawara N. (2003) Identification of a protein, YneA, responsible for cell division suppression during the SOS response in Bacillus subtilis. *Mol. Microbiol.* 47:1113-1122

Keren I, Wu Y, Inocencio J, Mulcahy LR, Lewis K. (2013) Killing by bactericidal antibiotics does not depend on reactive oxygen species. *Science* 339(6124):1213-6

Kim S-R, Maenhaut-Michel G, Yamada M, Yamamoto Y, Matsui K, Sofuni T, Nohmi T, Ohmori H. (1997) Multiple pathways for SOS-induced mutagenesis in Escherichia coli: An overexpression of dinB/dinP results in strongly enhancing mutagenesis in the absence of any exogenous treatment to damage DNA. *Proc. Natl. Acad. Sci. USA* 94:13792-13797

Kling A, Lukat P, Almeida DV, Bauer A, Fontaine E, Sordello S, Zaburannyi N, Herrmann J, Wenzel SC, König C, Ammerman NC, Barrio MB, Borchers K, Bordon-Pallier F, Brönstrup M, Courtemanche G, Gerlitz M, Geslin M, Hammann P, Heinz DW, Hoffmann H, Klieber S, Kohlmann M, Kurz M, Lair C, Matter H, Nuermberger E, Tyagi S, Fraisse L, Grosset JH, Lagrange S, Müller R. (2015) Targeting DnaN for tuberculosis therapy using novel griselimycins. *Science* 348(6239):1106-1112

Koch A, Mizrahi V, Warner DF. (2014) The impact of drug resistance on Mycobacterium tuberculosis physiology: what can we learn from rifampicin? *Emerg. Microbes Infect.* 3(3):e17

Kohanski MA, Dwyer DJ, Hayete B, Lawrence CA, Collins JJ. (2007) A common mechanism of cellular death induced by bactericidal antibiotics. *Cell* 130(5):797-810

Koorits L, Tegova R, Tark M, Tarassova K, Tover A, Kivisaar M. (2007) Study of involvement of ImuB and DnaE2 in stationary-phase mutagenesis in Pseudomonas putida. *DNA Repair* 6(6):863-8

Koul A, Arnoult E, Lounis N, Guillemont J, Andries K. (2011) The challenge of new drug discovery for tuberculosis. *Nature* 469(7331):483-90

Lamers MH, Georgescu RE, Lee SG, O'Donnell M, Kuriyan J. (2006) Crystal structure of the catalytic α subunit of E. coli replicative DNA polymerase III. *Cell* 126:881-892

Lawrence CW, Maher VM. (2001) Eukaryotic mutagenesis and translesion replication dependent on DNA polymerase ζ and Rev1 protein. *Biochem. Soc. Trans.* 29(2):187-191

Le Chatelier E, Bécherel OJ, d'Alençon E, Canceill D, Ehrlich SD, Fuchs RPP, Jannière L. (2004) Involvement of DnaE, the Second Replicative DNA Polymerase from Bacillus subtilis, in DNA Mutagenesis. *J. Biol. Chem.* 279(3):1757-1767

LeClerc JE, Borden A, Lawrence CW. (1991) The thymine-thymine pyrimidine-pyrimidone(6-4) ultraviolet light photoproduct is highly mutagenic and specifically induces 3' thymine-to-cytosine transitions in Escherichia coli. *Proc. Natl. Acad. Sci. USA* 88(21):9685-9689

Lemon KP, Grossman AD. (1998) Localization of Bacterial DNA Polymerase: Evidence for a Factory Model of Replication. *Science* 282(5393):1516-1519

Levin BR, Perrot V, Walker N. (2000) Compensatory Mutations, Antibiotic Resistance and the Population Genetics of Adaptive Evolution in Bacteria. *Genetics* 154:985-997

Levin-Reisman I, Ronin I, Gefen O, Braniss I, Shoresh N, Balaban NQ. (2017) Antibiotic tolerance facilitates the evolution of resistance. *Science* 9:eaaj2191

Li SY, Tasneen R, Tyagi S, Soni H, Converse PJ, Mdluli K, Nuermberger EL. (2017) Bactericidal and sterilizing activity of a novel regimen with bedaquiline, pretomanid, moxifloxacin, and pyrazinamide in a murine model of tuberculosis. *Antimicrob. Agents Chemother.* 61(9):e00913-17

Ling H, Boudsocq F, Woodgate R, Yang W. (2001) Crystal structure of a Y-family DNA polymerase in action: A mechanism for error-prone and lesion-bypass replication. *Cell* 107:91–102

Little JW, Mount DW, Yanisch-Perron CR. (1981) Purified lexA protein is a repressor of the recA and lexA genes. *Proc. Natl. Acad. Sci. USA* 78(7):4199-4203

Little JW, Mount DW. (1982) The SOS regulatory system of Escherichia coli. *Cell* 29:11-22

Little JW. (1993) LexA Cleavage and Other Self-Processing Reactions. *J. Bacteriol.* 175(16):4943-4950

Liu Y, Imlay JA. (2013) Cell death from antibiotics without the involvement of reactive oxygen species. *Science* 339(6124):1210-3

Long JW. (1991) In Essential guide to prescription drugs 1992. *Harper Collins Publishers, New York* Pages: 925–929

Ma Z, Lienhardt C, McIlleron H, Nunn AJ, Wang X. (2010) Global tuberculosis drug development pipeline: the need and the reality. *Lancet* 375:2100-2109

MacLean RC, Torres-Barceló C, Moxon R. (2013) Evaluating evolutionary models of stress-induced mutagenesis in bacteria. *Nat. Rev. Genet.* 14(3):221-7

Mahajan R. (2013) Bedaquiline: First FDA-approved tuberculosis drug in 40 years. *Int. J. App. Basic. Med. Res.* 3:1–2

Malik M, Chavda K, Zhao X, Shah N, Hussain S, Kurepina N, Kreiswirth BN, Kerns RJ, Drlica K. (2012) Induction of mycobacterial resistance to quinolone class antimicrobials. *Antimicrob. Agents Chemother.* 56(7):3879-87

Manson AL, Cohen KA, Abeel T, Desjardins CA, Armstrong DT, Barry CE III, Brand J, TBResist Global Genome Consortium, Chapman SB, Cho S-N, Gabrielian A, Gomez J, Jodals AM, Joloba M, Jureen P, Lee JS, Malinga L, Maiga M, Nordenberg D, Noroc E, Romanceno E, Salazar A, Ssengooba W, Velayati AA, Winglee K, Zalutskaya A, Via LE, Cassell GH, Dorman SE, Ellner J, Farnia P, Galagan JE, Rosenthal A, Crudu V, Homorodean D, Hsueh P-R, Narayanan S, Pym AS, Skrahina A, Swaminathan S, Van der Walt M, Alland D, Bishai WR, Cohen T, Hoffner S, Birren BW, Earl AM. (2016) Genomic analysis of globally diverse Mycobacterium tuberculosis strains provides insights into the emergence and spread of multidrug resistance. *Nat. Genet.* 49:295-402

Maor-Shoshani A, Reuven NB, Tomer G, Livneh Z. (2000) Highly mutagenic replication by DNA polymerase V (UmuC) provides a mechanistic basis for SOS untargeted mutagenesis. *Proc. Natl. Acad. Sci. USA* 97(2):565-570

McCulloch SD, Kunkel TA. (2008) The fidelity of DNA synthesis by eukaryotic replicative and translesion synthesis polymerases. *Cell Res.* 18(1):148-61.

Mduli K, Ma Z. (2007) Mycobacterium tuberculosis DNA Gyrase as a Target for Drug Discovery. *Infect. Disord. Drug Targets* 7(2):159-168

Merker M, Kohl TA, Roetzer A, Truebe L, Richter E, Rüsch-Gerdes S, Fattorini L, Oggioni MR, Cox H, Varaine F, Niemann S. (2013) Whole Genome Sequencing Reveals Complex Evolution Patterns of Multidrug-Resistant Mycobacterium tuberculosis Beijing Strains in Patients. *PLOS One* 8(12):e82551

Mesak LR, Miao V, Davies J. (2008) Effects of Subinhibitory Concentrations of Antibiotics on SOS and DNA Repair Gene Expression in Staphylococcus aureus. *Antimicrob. Agents Chemother.* 52(9):3394-3397

Miedema F, Petit AJC, Terpstra FG, Schattenkerk JKME, de Wolf F, Al BJM, Roos M, Lange JMA, Danner SA, Goudsmit J, Schellekens PTA. (1988) Immunological Abnormalities in Human Immunodeficiency Virus (HIV)-infected Asymptomatic Homosexual Men. *J. Clin. Invest.* 82:1908-1914

Mikušová K, Ekins S. (2017) Learning from the past for TB drug discovery in the future. *Drug Discov. Today* 22(3):534-45

Mishra BB, Lovewell RR, Olive AJ, Zhang G, Wang W, Eugenin E, Smith CM, Phuah JY, Long JE, Dubake ML, Palace SG, Goguen JD, Baker RE, Nambi S, Mishra R, Booty MG, Baer CE, Shaffer SA, Dartois V, McCormick BA, Chen X, Sassetti CM. (2017) Nitric oxide prevents a pathogen-permissive granulocytic inflammation during tuberculosis *Nat. Microbiol.* 2(7):17072

Miura A, Tomizawa J-I. (1968) Studies on Radiation-sensitive Mutants of E.coli. *Molec. gen. Genet.* 103:1-10

Moodley R, Godec TR. (2016) Short-course treatment for multidrug-resistant tuberculosis: the STREAM trials. *Eur. Respir. J.* 25(139):29-35

Moonan PK, Quitugua TN, Pogoda JM, Woo G, Drewyer G, Sahbazian B, Dunbar D, Jost KC, Wallace C, Weis SE. (2011) Does directly observed therapy (DOT) reduce drug resistant tuberculosis? *BMC Public Health* 11(1):19

Moore JM, Correa R, Rosenberg SM, Hastings PJ. (2017) Persistent damaged bases in DNA allow mutagenic break repair in Escherichia coli. *PLOS Genet.* 13(7):e1006733

Moore P, Bose KK, Rabkin SD, Strauss BS. (1981) Sites of termination of in vitro DNA synthesis on ultraviolet- and N-acetylaminofluorene-treated phi X174 templates by prokaryotic and eukaryotic DNA polymerases. *Proc. Natl. Acad. Sci. USA* 78(1):110-114

Morlock GP, Plikaytis BB, Crawford JT. (2000) Characterization of Spontaneous, In Vitro-Selected, Rifampin-Resistant Mutants of Mycobacterium tuberculosis Strain H37Rv. *Antimicrob. Agents Chemother.* 44(12):3298-3301

Movahedzadeh F, Colston MJ, Davis EO. (1997) Determination of DNA sequences required for regulated Mycobacterium tuberculosis RecA expression in response to DNA-damaging agents suggests that two modes of regulation exist. *J. Bacteriol.* 179(11):3509-3518

Müller B, Borrell S, Rose G, Gagneux S. (2013) The heterogeneous evolution of multidrug-resistant Mycobacterium tuberculosis. *Trends Genet.* 29(3):160-169

Munita JM, Arias CA. (2016) Mechanisms of Antibiotic Resistance. *Microbiol. Spectr.* 4(2):doi:10.1128

Murakumo Y, Ogura Y, Ishii H, Numata S-i, Ichihara M, Croce CM, Fishel R, Takahashi M. (2001) Interactions in the Error-prone Postreplication Repair Proteins hREV1, hREV3, and hREV7. *J. Biol. Chem.* 276(38):35644-35651

Murray S, Mendel C, Spigelman M. (2016) TB Alliance regimen development for multidrug-resistant tuberculosis. *Int. J. Tuberc. Lung Dis.* 20(12):S38-41

Nakane S, Nakagawa N, Kuramitsu S, Masui R. (2009) Characterization of DNA polymerase X from Thermus thermophilus HB8 reveals the POLXc and PHP domains are both required for 3′-5′ exonuclease activity. *Nucleic Acids Res.* 37:2037-2052

Napolitano R, Janel-Bintz R, Wagner J, Fuchs RPP. (2000) All three SOS-inducible DNA polymerases (Pol II, Pol IV and Pol V) are involved in induced mutagenesis. *EMBO J.* 19(22):6259-6265

Nathan C, Shiloh MU. (2000) Reactive oxygen and nitrogen intermediates in the relationship between mammalian hosts and microbial pathogens. *Proc. Natl. Acad. Sci. USA* 97:8841–8848

Nohmi T, Battista JR, Dodson LA, Walker GC. (1988) RecA-mediated cleavage activates UmuD for mutagenesis: Mechanistic relationship between transcriptional derepression and posttranslational activation. *Proc. Natl. Acad. Sci. USA* 85:1816-1820

Nuermberger EL, Yoshimatsu T, Tyagi S, O'Brien RJ, Vernon AN, Chaisson RE, Bishai WR, Grosset JH. (2004) Moxifloxacin-containing regimen greatly reduces time to culture conversion in murine tuberculosis. *Am. J. Respir. Crit. Care Med.* 169(3):421-6

Nuermberger EL, Yoshimatsu T, Tyagi S, Williams K, Rosenthal I, O'Brien RJ, Vernon AA, Chaisson RE, Bishai WR, Grosset JH. (2004) Moxifloxacin-containing regimens of reduced duration produce a stable cure in murine tuberculosis. *Am. J. Respir. Crit. Care Med.* 170(10):1131-4

O'Sullivan DM, Hinds J, Butcher PD, Gillespie SH, McHugh TD. (2008) Mycobacterium tuberculosis DNA repair in response to subinhibitory concentrations of ciprofloxacin. *J. Antimicrob. Chemother.* 62(6):1199-202

Ochman H, Lawrence JG, Groisman EA. (2000) Lateral gene transfer and the nature of bacterial innovation. *Nature* 405(6784):299-304

Okamoto S, Tamaru A, Nakajima C, Nishimura K, Tanaka Y, Tokuyama S, Suzuki Y, Ochi K. (2007) Loss of a conserved 7-methylguanosine modification in 16S rRNA confers low-level streptomycin resistance in bacteria. *Mol. Microbiol.* 63(4):1096-1106

Ormerod LP. (2005) Multidrug-resistant tuberculosis (MDR-TB): epidemiology, prevention and treatment. *Br. Med. Bull.* 73(1):17-24

Painter RE, Adam GC, Arocho M, DiNunzio E, Donald RGK, Dorso K, Genilloud O, Gill C, Goetz M, Hairston NN, Murgolo N, Nare B, Olsen DB, Powles M, Racine F, Su J, Vicente F, Wisniewski D, Xiao L, Hammond M, Young K. (2015) Elucidation of DnaE as the Antibacterial Target of the Natural Product, Nargenicin. *Chem. Biol.* 22:1-12

Palomino JC, Martin A. (2014) Drug Resistance Mechanisms in Mycobacterium tuberculosis. *Antibiotics* 3:317-340

Papavinasasundaram KG, Anderson C, Brooks PC, Thomasa NA, Movahedzadehb F, Jenner PJ, Colston MJ, Davis EO. (2001) Slow induction of RecA by DNA damage in Mycobacterium tuberculosis. *Micorbiology* 147:3271–3279

Parsons LM, Jankowski CS, Derbyshire KM. (1998) Conjugal transfer of chromosomal DNA in Mycobacterium smegmatis. *Mol. Microbiol.* 28(3):571-82

Perry KL, Elledge SJ, Mitchell BB, Marsh L, Walker GC. (1985) umuDC and mucAB operons whose produce are required for UV light- and chemical-induced mutagenesis: UmuD, MucA, and LexA proteins share homology. *Proc. Natl. Acad. Sci. USA* 82:4331-4335

Pham P, Bertram JG, O'Donnell M, Woodgate R, Goodman MF. (2001) A model for SOS-lesion-targeted mutations in Escherichia coli. *Nature* 409:366–370

Pillon MC, Babu VMP, Randall JR, Cai J, Simmons LA, Sutton MD, Guarné A. (2015) The sliding clamp tethers the endonuclease domain of MutL to DNA. *Nucleic Acids Res.* 43(22):10746-10759

Pomerantz RT, O'Donnell M. (2007) Replisome mechanics: insights into a twin DNA polymerase machine. *Trends Microbiol.* 15(4):156-164

Radman M, Matic I, Taddei F. (1999) Evolution of Evolvability. *Ann. N. Y. Acad. Sci.* 870:146-155

Ramakrishnan L. (2012) Revisiting the role of the granuloma in tuberculosis. *Nat. Rev. Immunol.* 12:352-366

Ramaswamy S, Musser JM. (1998) Molecular genetic basis of antimicrobial agent resistance in Mycobacterium tuberculosis: 1998 update. *Tuber. Lung Dis.* 79(1):3-29

Ramaswamy SV, Reich R, Dou S-J, Jasperse L, Pan X, Wanger A, Quitungua T, Graviss EA. (2003) Single Nucleotide Polymorphisms in Genes Associated with Isoniazid Resistance in Mycobacterium tuberculosis. *Antimicrob. Agents Chemother.* 47(4):1241-1250

Rand L, Hinds J, Springer B, Sander P, Buxton RS, Davis EO. (2003) The majority of inducible DNA repair genes in Mycobacterium tuberculosis are induced independently of RecA. *Mol. Microbiol.* 50(3):1031-1042

Reece RJ, Maxwell A. (1991) DNA Gyrase: Structure and Function. *Crit. Rev. Biochem. Mol. Biol.* 26(3&4):335-375

Reiche MA, Warner DF, Mizrahi V. (2017) Targeting DNA Replication and Repair for the Development of Novel Therapeutics against Tuberculosis. *Front. Mol. Biosci.* 4:75

Rengarajan J, Sassetti CM, Naroditskaya V, Sloutsky A, Bloom BR, Rubin EJ. (2004) The folate pathway is a target for resistance to the drug para-aminosalicylic acid (PAS) in mycobacteria. *Mol. Microbiol.* 53(1):275-282

Reyes-Lamothe R, Possoz C, Danilova O, Sherratt DJ. (2008) Independent Positioning and Action of Escherichia coli Replisomes in Live Cells. *Cell* 133:90-102

Reyes-Lamothe R, Sherratt DJ, Leake MC. (2010) Stoichiometry and Architecture of Active DNA Replication Machinery in Escherichia coli. *Science* 328(5977):498-501

Robinson A, McDonald JP, Caldas VE, Patel M, Wood EA, Punter CM, Ghodke H, Cox MM, Woodgate R, Goodman MF, van Oijen AM. (2015) Regulation of mutagenic DNA polymerase V activation in space and time. *PLOS Genet.* 11(8):e1005482

Russell DG. (2001) Mycobacterium tuberculosis: here today, and here tomorrow. *Nat. Rev. Mol. Cell Biol.* 2:569–577

Russell DG. (2007) Who puts the tubercle in tuberculosis? *Nat. Rev. Microbiol.* 4:39-47

Safi H, Sayers B, Hazbón MH, Alland D. (2008) Transfer of embB Codon 306 Mutations into Clinical Mycobacterium tuberculosis Strains Alters Susceptibility to Ethambutol, Isoniazid, and Rifampin. *Antimicrob. Agents Chemother.* 52(6):2027-2034

Sandgren A, Strong M, Muthukrishnan P, Weiner BK, Church GM, Murray MB. (2009) Tuberculosis Drug Resistance Mutation Database. *PLOS Med.* 6(2):e1000002

Santi I, Dhar N, Bousbaine D, Wakamoto Y, McKinney JD. (2013) Single-cell dynamics of the chromosome replication and cell division cycles in mycobacteria. *Nat. Commun.* 4:2470

Santi I, McKinney JD. (2015) Chromosome Organization and Replisome Dynamics in Mycobacterium smegmatis. *MBio* 6(1):e01999-14

Schnarr M, Oertel-Buchheit P, Kazmaier M, Granger-Schnarr M. (1991) DNA binding properties of the LexA repressor. *Biochimie* 73:423-431

Scorpio A, Zhang Y. (1996) Mutations in pncA, a gene encoding pyrazinamidase/nicotinamidase, cause resistance to the antituberculous drug pyrazinamide in tubercle bacillus. *Nat. Med.* 2:662–7

Seifert M, Catanzaro D, Catanzaro A, Rodwell TC. (2015) Genetic mutations associated with isoniazid resistance in Mycobacterium tuberculosis: a systematic review. *PLOS One* 10(3):e0119628

Serres MH, Kerr AR, McCormack TJ, Riley M. (2009) Evolution by leaps: gene duplication in bacteria. *Biol. Direct* 4(1):46

Shehzad A, Rehman G, Ul-Islam M, Khattak WA, Lee YS. (2013) Challenges in the development of drugs for the treatment of tuberculosis. *Braz. J. Infect. Dis.* 17(1):74–81

Sherman DR, Mdluli K, Hickey MJ, Arain TM, Morris SL, Barry CE III, Stover KC. (1996) Compensatory ahpC gene expression in isoniazidresistant Mycobacterium tuberculosis. *Science* 272:1641-1643

Shinagawa H, Iwasaki H, Kato T, Nakata A. (1988) RecA protein-dependent cleavage of UmuD protein and SOS mutagenesis. *Proc. Natl. Acad. Sci. USA* 85(6):1806-1810

Shinagawa H, Kato T, Ise T, Makino K, Nakata A. (1983) Cloning and characterization of the umu operon responsible for inducible mutagenesis in Escherichia coli. *Gene* 23:167-174

Simmons LA, Davies BW, Grossman AD, Walker GC. (2008a) β Clamp Directs Localization of Mismatch Repair in Bacillus subtilis. *Mol. Cell* 29:291-301

Simmons LA, Foti JJ, Cohen SE, Walker GC. (2008b) The SOS regulatory network. *EcoSal Plus* 10.1128/ecosalplus.5.4.3

Siu GK, Zhang Y, Lau TC, Lau RW, Ho PL, Yew WW, Tsui SK, Cheng VC, Yuen KY, Yam WC. (2011) Mutations outside the rifampicin resistance-determining region associated with rifampicin resistance in Mycobacterium tuberculosis. *J. Antimicrob. Chemother.* 66(4):730-733

Smollett KL, Smith KM, Kahramanoglou C, Arnvig KB, Buxton RS, Davis EO. (2012) Global Analysis of the Regulon of the Transcriptional Repressor LexA, a Key Component of SOS Response in Mycobacterium tuberculosis. *J. Biol. Chem.* 287:22004-22014

Sogo JM, Lopes M, Foiani M. (2002) Fork Reversal and ssDNA Accumulation at Stalled Replication Forks Owing to Checkpoint Defects. *Science* 297(5581):599-602

Sreevatsan S, Pan X, Stockbauer KE, Williams DL, Kreiswirth BN, Musser JM. (1996) Characterization of rpsL and rrs mutations in streptomycin-resistant Mycobacterium tuberculosis isolates from diverse geographic localities. *Antimicrob. Agents Chemother.* 40(4):1024–1026

Sreevatsan S, Stockbauer KE, Pan X, Kreiswirth BN, Moghazeh SL, Jacobs WR Jr, Telenti A, Musser JM. (1997) Ethambutol Resistance in Mycobacterium tuberculosis: Critical Role of embB Mutations. *Antimicrob. Agents Chemother.* 41(8):1677-1681

Stanley RE, Blaha G, Grodzicki RL, Strickler MD, Steitz TA. (2010) The structures of the anti-tuberculosis antibiotics viomycin and capreomycin bound to the 70S ribosome. *Nat. Struct. Mol. Biol.* 17:289-293

Stass H, Dalhoff A, Kubitza D, Schühly U. (1998) Pharmacokinetics, Safety, and Tolerability of Ascending Single Doses of Moxifloxacin, a New 8-Methoxy Quinolone, Administered to Healthy Subjects. *Antimicrob. Agents Chemother.* 42(8):2060-2065

Storz G, Hennge R, Storz G. (2011) Bacterial stress responses (2nd ed.) *American Society for Microbiology Press* Washington DC

Suzuki Y, Katsukawa C, Tamaru A, Abe C, Makino M, Mizuguchi Y, Taniguchi H. (1998) Detection of Kanamycin-Resistant Mycobacterium tuberculosis by Identifying Mutations in the 16S rRNA Gene. *J. Clin. Microbiol.* 36(5):1220-1225

Taddei F, Radman M, Maynard-Smith J, Toupance B, Gouyon PH, Godelle B. (1997) Role of mutator alleles in adaptive evolution. *Nature* 387:700-702

Takeiri A, Wada NA, Motoyama S, Matsuzaki K, Tateishi H, Matsumoto K, Niimi N, Sassa A, Grúz P, Masumura K, Yamada M. (2014) In vivo evidence that DNA polymerase kappa is responsible for error-free bypass across DNA cross-links induced by mitomycin C. *DNA Repair* 24:113-21

Takiff HE, Salazar L, Guerrero C, Philipp W, Huang WM, Kreiswirth B, Cole ST, Jacobs WR Jr, Telenti A. (1997) Cloning and nucleotide sequence of Mycobacterium tuberculosis gyrA and gyrB genes and detection of quinolone resistance mutations. *Antimicrob. Agents Chemother.* 38(4):773-780

Tang M, Pham P, Shen X, Taylor J-S, O'Donnell M, Woodgate R, Goodman MF. (2000) Roles of E. coli DNA polymerases IV and V in lesion-targeted and untargeted SOS mutagenesis. *Nature* 404:1014-1018

Tang T, Bruck I, Eritja R, Turner J, Frank EG, Woodgate R, O'Donnell M, Goodman MF. (1998) Biochemical basis of SOS-induced mutagenesis in Escherichia coli: Reconstitution of in vitro lesion bypass dependent on the UmuD′2C mutagenic complex and RecA protein. *Proc. Natl. Acad. Sci. USA* 95:9755–9760

Telenti A, Philipp WJ, Sreevatsan S, Bernasconi C, Stockbauer KE, Wieles B, Musser JM, Jacobs WR Jr. (1997) The emb operon, a gene cluster of Mycobacterium tuberculosis involved in resistance to ethambutol. *Nat. Med.* 3:567-570

Terlain B, Thomas JP. (1971) Structure of griselimycin, polypeptide antibiotic extracted from streptomyces cultures [Article in French]. *Bull. Soc. Chim. Fr.* 6:2357-2362

Tessema B, Nabeta P, Valli E, Albertini A, Collantes J, Lan NH, Romancenco E, Tukavdze N, Denkinger CM, Dolinger DL. (2017) FIND tuberculosis strain bank: a resource for researchers and developers working on tests to detect Mycobacterium tuberculosis and related drug resistance. *J. Clin. Microbiol.* 55(4):1066-73

Timinskas K, Balvočiūtė M, Timinskas A, Venclovas Č. (2013) Comprehensive analysis of DNA polymerase III α subunits and their homologs in bacterial genomes. *Nucleic Acids. Res.* 42(3):1393-413

Tippin B, Pham P, Goodman MF. (2004) Error-prone replication for better or worse. *Trends Microbiol.* 12:289–295

Tomasz M, Chawla AK, Lipman R. (1988) Mechanism of monofunctional and bifunctional alkylation of DNA by mitomycin C. *Biochemistry* 27(9):3182-7

Torrey HL, Keren I, Via LE, Lee JS, Lewis K. (2016) High persister mutants in Mycobacterium tuberculosis. *PLOS One* 11(5):e0155127

Trindade S, Sousa A, Xavier KB, Dionisio F, Ferreira MG, Gordo I. (2009) Positive Epistasis Drives the Acquisition of Multidrug Resistance. *PLOS Genet.* 5(7):e1000578

Trojanowski D, Ginda K, Pióor M, Hołowka J, Skut P, Jakimowicz D, Zakrzewska-Czerwińska J. (2015) Choreography of the Mycobacterium Replication Machinery during the Cell Cycle. *Mbio* 6(1):e02125-14

Trojanowski D, Hołówka J, Ginda K, Jakimowicz D, Zakrzewska-Czerwińska J. (2017) Multifork chromosome replication in slow-growing bacteria. *Sci. Rep.* 7:43836

Udwadia ZF, Amale RA, Mullerpattan JB. (2014) Initial experience of bedaquiline use in a series of drug-resistant tuberculosis patients from India. *Int. J. Tuberc. Lung Dis.* 18(11):1315-8

van den Bergh B, Michiels JE, Wenseleers T, Windels EM, Boer PV, Kestemont D, De Meester L, Verstrepen KJ, Verstraeten N, Fauvart M, Michiels J. (2016) Frequency of antibiotic application drives rapid evolutionary adaptation of Escherichia coli persistence. *Nat. Microbiol.* 1:16020

van Oijen AM, Loparo JJ. (2010) Single-Molecule Studies of the Replisome. *Annu. Rev. Biophys.* 39:429-448

Venkatesan K, Rual JF, Vazquez A, Stelzl U, Lemmens I, Hirozane-Kishikawa T, Hao T, Zenkner M, Xin X, Goh KI, Yildirim MA. (2009) An empirical framework for binary interactome mapping. *Nat. Methods* 6(1):83-90

Vidal M, Fields S. (2014) The yeast two-hybrid assay: still finding connections after 25 years. *Nat. Methods* 11(12):1203-6

Vilchèze C, Av-Gay Y, Attarian R, Liu Z, Hazbón MH, Colangeli R, Chen B, Liu W, Alland D, Sacchettini JC, Jacobs WR Jr. (2008) Mycothiol biosynthesis is essential for ethionamide susceptibility in Mycobacterium tuberculosis. *Mol. Microbiol.* 69(5):1316-1329

Volmink J, Garner P. (2007) Directly observed therapy for treating tuberculosis. *Cochrane Database Syst. Rev.* 4

Wang F, Yang W. (2009) Structural insight into translesion synthesis by DNA Pol II. *Cell* 139(7):1279-89

Wang Y, Huang Y, Xue C, He Y, He ZG. (2011) ClpR protein-like regulator specifically recognizes RecA protein-independent promoter motif and broadly regulates expression of DNA damage-inducible genes in mycobacteria. *J. Biol. Chem.* 286(36):31159-67

Wang Z. (2001) Translesion synthesis by the UmuC family of DNA polymerases. *Mutat. Res.* 486:59–70

Warner DF, Mizrahi V. (2006) Tuberculosis chemotherapy: the influence of bacillary stress and damage response pathways on drug efficacy. *Clin. Microbiol. Rev.* 19(3):558-70

Warner DF, Ndwandwe DE, Abrahams GL, Kana BD, Machowski EE, Venclovas C, Mizrahi V. (2010) Essential roles for imuA′- and imuB-encoded accessory factors in DnaE2-dependent mutagenesis in Mycobacterium tuberculosis. *Proc. Natl. Acad. Sci. USA* 107:13093–13098

Wehrli W. (1983) Rifampin: Mechanisms of Action and Resistance. *Rev. Infect. Dis.* 5(3):407-411

Wieczorek A, McHenry CS. (2006) The NH2-terminal php Domain of the α Subunit of the Escherichia coli Replicase Binds the ϵ Proofreading Subunit. *J. Biol. Chem.* 281:12561-12567

Wolfson LJ, Walker A, Hettle R, Lu X, Kambili C, Murungi A, Knerer G. (2015) Cost-effectiveness of adding bedaquiline to drug regimens for the treatment of multidrug-resistant tuberculosis in the UK. *PLOS One* 10(3):e0120763

World Health Organisation. (2014) Antimicrobial Resistance: Global Report on Surveillance. *WHO Library Cataloguing-in-Publication Data* ISBN 978 92 4 156474 8

World Health Organisation. (2016) Global tuberculosis report 2016. *WHO Library Cataloguing-in-Publication Data* ISBN 978 92 4 156539 4

World Health Organization. (2017) Global tuberculosis report 2017. *WHO Library Cataloguing-in-Publication Data* ISBN 978 92 4 156551 6

World Health Organization. (2013) The use of bedaquiline in the treatment of multidrug-resistant tuberculosis: interim policy guidance. *WHO Library Cataloguing-in-Publication Data* ISBN 978 92 4 150548 2

Wu WJ, Yang W, Tsai MD. (2017) How DNA polymerases catalyse replication and repair with contrasting fidelity. *Nat. Rev. Chem.* 1(9):s41570-017

Xu P, Chen H, Xu J, Wu M, Zhu X, Wang F, Chen S, Xu J. (2017) Moxifloxacin is an effective and safe candidate agent for tuberculosis treatment: a meta-analysis. *Int. J. Infect. Dis.* 60:35-41

Yadon AN, Maharaj K, Adamson JH, Lai YP, Sacchettini JC, Ioerger TR, Rubin EJ, Pym AS. (2017) A comprehensive characterization of PncA polymorphisms that confer resistance to pyrazinamide. *Nat. Commun.* 8(1):588

Yang W, Woodgate R. (2007) What a difference a decade makes: insights into translesion DNA synthesis. *Proc. Natl. Acad. Sci. USA* 104(40):15591-8

Yanling J, Xin L, Zhiyuan L. (2006) Drug Discovery; Chapter 10: The antibacterial drug discovery. In El-Shemy, HA (ed),

Yee D, Valiquette C, Pelletier M, Parisien I, Rocher I, Menzies D. (2003) ncidence of serious side effects from first-line antituberculosis drugs among patients treated for active tuberculosis. *Am. J. Respir. Crit. Care Med.* 167(11):1472-7

Yew WW, Leung CC. (2006) Antituberculosis drugs and hepatotoxicity. *Respirology* 11(6):699-707

Young K, Olsen DB, Singh SB, Wilkening RR, Apgar JM, Meng D, Parker D, Mandal M., Yang L, Painter RE, Dang Q, Suzuki, T. (2016) Nargenicin compounds and uses thereof as antibacterial agents. WO2016064982 A1

Zaunbrecher MA, Sikes DR Jr, Metchock B, Shinnick TM, Posey JE. (2009) Overexpression of the chromosomally encoded aminoglycoside acetyltransferase eis confers kanamycin resistance in Mycobacterium tuberculosis. *Proc. Natl. Acad. Sci. USA* 106(47):20004-20009

Zhang J. (2003) Evolution by gene duplication: an update. *Trends Ecol. Evol.* 18(6):292-8

Zhang Y, Heym B, Allen B, Young D, Cole S. (1992) The catalase—peroxidase gene and isoniazid resistance of Mycobacterium tuberculosis. *Nature* 358:591-593

Zhao F, Wang X-D, Erber LN, Luo M, Guo A-z, Yang S-s, Gu J, Turman BJ, Gao Y-r, Li D-f, Cui Z-q, Zhang Z-p, Bi L-j, Baughn AD, Zhang X-E, Denga J-Y. (2014) Binding Pocket Alterations in Dihydrofolate Synthase Confer Resistance to para-Aminosalicylic Acid in Clinical Isolates of Mycobacterium tuberculosis. *Antimicrob. Agents Chemother.* 58(3):1479-1487

Zhao X, Hong Y, Drlica K. (2014) Moving forward with reactive oxygen species involvement in antimicrobial lethality. *J. Antimicrob. Chemother.* 70(3):639-42

Zheng X, Av-Gay Y. (2016) New Era of TB Drug Discovery and Its Impact on Disease Management. *Curr. Treat. Options Infect. Dis.* 8(4):299-310

CHAPTER II: METHODS

Table of Contents: **Page**

List of Figures: **Page**

List of Tables: **Page**

1. *In Silico* Techniques

1.1. Genes

The coding sequences for genes of interest were obtained from a selection of resources such as *TubercuList* (Lew, *et al.*, 2011), *SmegmaList* (Kapopoulou, *et al.*, 2011), *TuBerculosis DataBase* (Reddy, *et al.*, 2008), and the *National Center for Biotechnology Information* (NCBI) (NCBI RC, 2017) unless otherwise indicated. All sequences were obtained in, or converted to, standard '.FASTA' format before each sequence was loaded into *CLC Main Workbench* (v7.6) (QIAGEN Aarhus A/S, Denmark). Genes consisting of both open reading frames (ORFs) and regulatory sequences were annotated with available information obtained from the literature on *imuA'* (*MSMEG_1620*), *imuB* (*MSMEG_1622*), and *dnaE2* (*MSMEG_1633*) (as described in **Section 8.1**).

1.2. Construct Design

Parental plasmid maps for pTTP1B::1633, pMCAINT::1619/20, and pAINT::1619compPCR (pTTP1B::*dnaE2*, pMCAINT::*imuB*, and pAINT::*imuA'*, respectively), were obtained directly from the author, Warner *et al*. (2010). The plasmids were annotated with available sequence data from the literature. Restriction endonuclease (RE) restriction sites, that when used to digest the plasmid, would grant access to the 5'-end of each ORF (cleavage sites located above and below the first codon of each coding sequence), were identified. The intervening sequences between the identified RE sites were modified *in silico* to include the encoding region of the fluorescent reporter (either enhanced green fluorescent protein, *egfp,* or *meos4a*) directly upstream and in-frame of the native start codon of the gene of interest. *In silico* cloning experiments were subsequently performed in *CLC Main Workbench* (v7.6) (QIAGEN Aarhus A/S,

Denmark) to ensure feasibility of the cloning method using the identified RE sites. The resultant full-length gene sequences were subsequently translated in all six frames using the *ExPASy* online translation tool (http://web.expasy.org/translate/). The corresponding translated sequence of the protein fusions were identified. The full-length protein sequences were then validated by performing a sequence alignment search using *NCBI Basic Local Alignment Search Tool* (BLAST) (Altshcul, *et al.*, 1990) to ensure that the encoded protein sequences had been maintained without anomalous changes. Confirmed sequences were subsequently synthesized and cloned into pUC57 plasmid backgrounds by GeneWiz (China).

1.3. Oligonucleotide Design

1.3.1. Screening Primers

Primers were designed *in silico* using either *NCBI Primer-Blast* (Ye, *et al.*, 2012) or manually by identifying primer regions within target regions. Manual primers within the sequence of interest that were 16 to 22 bp in length were identified. Primer sequences with a guanine-cytosine (GC) content of between 45 and 60 %, and with a G or C at the 3′ position, were preferentially selected. Furthermore, primer sequences that contained potentially self-complementary sequences capable of forming hairpin loops were excluded. Primer sequences were sent to the *Department of Chemistry* (University of Cape Town, ZA) where they were synthesised.

1.3.2. Sequencing Primers

Sequencing primers were designed manually for both forward and reverse (complementary strand) reactions (**Figure 2-1**). Target sequences that extended at least 100 bp beyond the gene of interest in both directions were identified.

Thereafter, primer sequences that would allow for the entire target sequence to be sequenced were selected. Primer sequences were all between 18 to 22 bp in length, had a guanine:cytosine (GC) content of 55 to 62 %, and contained a 3′ guanine (G) or cytosine (C) where possible. The primer sequences were selected if approximately 400 bp separated adjacent primers. In addition, adjacent forward and reverse primers were selected to be approximately 200 bp apart. Primer sequences were sent to the *Department of Chemistry* (University of Cape Town, ZA) where they were synthesised.

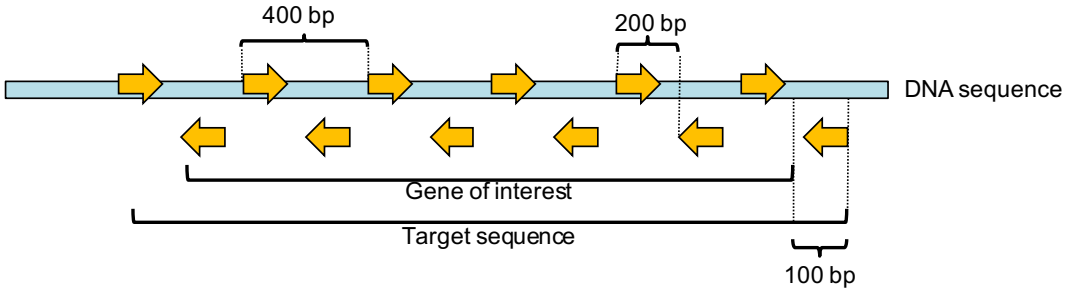

Figure 2-1 | Schematic diagram representing the distribution of designed sequencing primers
Forward primers (right arrow) were separated by approximately 400 bp and covered the entire target sequence; reverse primers (left arrows) were designed in a similar manner but complementary to the opposing strand of DNA and such that adjacent forward and reverse primers were ±200 bp apart. The first primer in each direction was designed to start 100 bp before the gene of interest in order to increase sequencing data accuracy over the gene of interest. Not drawn to scale.

1.4. Sequence Analysis

Sequencing reads obtained from the *Central Analytical Facility* (Stellenbosch University, ZA) were aligned to the respective parental plasmid. Thereafter, the sequence data were curated in *CLC Main Workbench* (v7.6) (QIAGEN Aarhus A/S, Denmark). Base calling was confirmed by visual assessment and regions of poor read quality were excluded (**Figure 2-2**). Sequence conflicts were addressed on an individual basis.

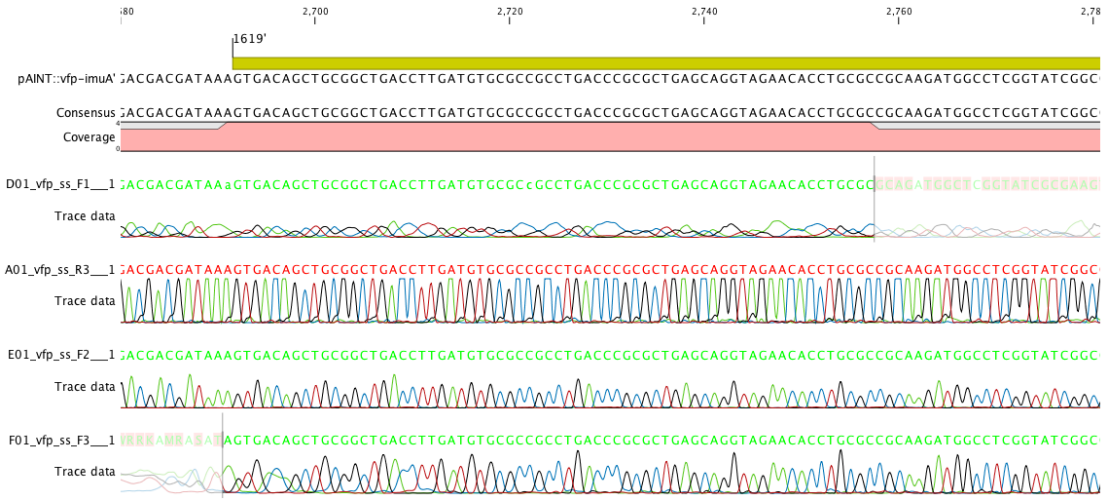

Figure 2-2 | Example of the manual curation of sequencing results
CLC Main Workbench was used to analyze sequence data and exclude poor-quality reads often found at the beginning and end of individual sequencing runs. The window illustrates a screenshot of the program window. In this example, poor-quality reads were excluded at the beginning and end of sequencing runs, which resulted in a read coverage of 3.8 times.

2. Bacterial Growth Conditions

A number of bacterial strains were utilized in this work (**Table 2-1**). Both *Escherichia coli* (*E. coli*) and *Mycobacterium smegmatis* (*Msm*) strains were grown in controlled media containing selection antibiotics if required.

Table 2-1 | List of strains used in this work

Strain	Description	Source
***E. coli* (plasmid)**		
pMCAINT	*E. coli*–mycobacterium integrating shuttle vector; Km^R Am^R	Boshoff and Mizrahi, 2000.
pAINT::*imuA'*	*Msm imuA'* complementation vector: pAINT carrying full-length *Msm imuA'* (MSMEG_1620); Km^R (pAMSIMUA)	Warner, *et al.*, 2010.
pUC57::PSOS(*imuA'*)-*egfp*	Episomal cloning vector pUC57 containing the designed PSOS(*imuA'*)-*egfp* construct; Km^R	GeneWiz (China)
pMCAINT::PSOS(*imuA'*)-*egfp*	pMCAINT plasmid carrying the PSOS(*imuA'*)-*egfp* construct at the *Hin*dIII RE site within the MCS; Km^R	This study

pUC57::*vfp-imuA''*	Episomal cloning vector pUC57 containing 5'- region of designed PSOS-*vfp-FLAG-imuA'* construct; Km^R	GeneWiz (China)
pAINT::*vfp-imuA'*	Resulting *BstB*I and *SexA*I ligation product of pAINT::*imuA'* and pUC57::*vfp-imuA''* carrying full-length *vfp-imuA'* recombinant gene; Km^R	Reiche, *et al.*, unpublished
pMCAINT::*imuB*	*Msm imuA'-imuB* complementation vector – pMC1r carrying full-length *Msm imuA'-imuB (MSMEG_1622)*; Km^R (PAMSIMUAB)	Warner, *et al.*, 2010.
pUC57::PSOS(*imuA'*)-*egfp-imuB'*	Episomal cloning vector pUC57 containing 5'- region of designed PSOS-*egfp-FLAG-imuB* construct; Km^R	GeneWiz (China)
pAINT::PSOS(*imuA'*)-*egfp-imuB*	Resulting *Blp*I and *Cla*I ligation product of pAINT::*imuB* and pUC57::PSOS(*imuA'*)-*egfp-imuB'* carrying only full-length PSOS(*imuA*)-*egfp-imuB* recombinant gene; Km^R	This study
pTTP1B::*dnaE2*	*Msm dnaE2* complementation vector: PTTP1B (Pham, *et al.*, 2007) carrying full-length *Msm dnaE2* (MSMEG_1633); Gm^R	Boshoff, *et al.*, 2003.
pUC57::*egfp-dnaE2'*	Episomal cloning vector pUC57 containing 5'- region of designed *egfp-FLAG-dnaE2* construct; Km^R	GeneWiz (China)
pTTP1B::*egfp-dnaE2*	Resulting *Kpn*I ligation product of pTTP1B::*dnaE2* and pUC57::*egfp-dnaE2'* carrying only full-length *egfp-dnaE2* recombinant gene; Gm^R	This study
pUC57::PSOS(*imuA'*)-*mEos4a-imuB'*	Episomal cloning vector pUC57 containing 5'- region of designed PSOS-*mEos4a-FLAG-imuB* construct; Km^R	GeneWiz (China)
pAINT::PSOS(*imuA'*)-*mEos4a-imuB*	Resulting *Blp*I and *Cla*I ligation product of pAINT::*imuB* and pUC57::PSOS(*imuA'*)-*mEos4a-imuB'* carrying only full-length PSOS(*imuA*)-*mEos4a-imuB* recombinant gene; Km^R	This study
pMCAINT::$imuB^{AAAAG}$	pMCAINT::*imuB* containing mutant *Msm ImuB*^{AAAAG} allele; Km^R (pAMSIMUAB^{AAAAGG})	Warner, *et al.*, 2010.
pMCAINT::PSOS(*imuA'*)-*egfp-imuB*^{AAAAG}	Resulting *Mau*BI ligation product of pAINT::*imuB*^{AAAAG} and pUC57::PSOS(*imuA'*)-*egfp-imuB'* carrying full-length PSOS(*imuA*)-*egfp-imuB*^{AAAAG} recombinant, mutant gene; Km^R	This study

Msm

mc^{2}155; wild-type (WT)	High-frequency transformation mutant of *Msm* mc^{2}6; ATCC 706	Snapper, *et al.*, 1990.
Δ*imuA'*	*imuA'* truncation-deletion mutant of mc^{2}155	Warner, *et al.*, 2010.
Δ*imuB*	*imuB* truncation-deletion mutant of mc^{2}155	Warner, *et al.*, 2010.
Δ*dnaE2*	*dnaE2* truncation-deletion mutant of mc^{2}155	Boshoff, *et al.*, 2003.
dnaE2^{AIA}	mc^{2}155 mutant containing mutant ^{441}AIA^{443} substitution in *dnaE2*	Warner, *et al.*, 2010.
WT::PSOS(*imuA'*)-*egfp*	mc^{2}155 carrying pMCAINT::PSOS(*imuA'*)-*egfp* integrated at the genomic *attB* site; *imuA'* transcriptional reporter	This study
Δ*imuA'*::*vfp-imuA'*	Δ*imuA'* carrying pAINT::*vfp-imuA'* at the *attB* integration site; Km^R	Reiche, *et al.*, unpublished
Δ*dnaE2*::*egfp-dnaE2*	Δ*dnaE2* carrying pTTP1B::*egfp-dnaE2* at the genomic *attP* integration; Gm^R	This study
Δ*imuB*::PSOS(*imuA'*)-*egfp-imuB*	Δ*imuB* carrying pAINT::PSOS(*imuA'*)-*egfp-imuB* at the *attB* integration site; Km^R	This study
Δ*imuA'*::PSOS(*imuA'*)-*egfp-imuB*	Δ*imuA'* carrying pAINT::PSOS(*imuA'*)-*egfp-imuB* at the *attB* integration site; Km^R	This study
Δ*dnaE2*::PSOS(*imuA'*)-*egfp-imuB*	Δ*dnaE2* carrying pAINT::PSOS(*imuA'*)-*egfp-imuB* at the *attB* integration site; Km^R	This study
dnaE2^{AIA}::PSOS(*imuA'*)-*egfp-imuB*	dnaE2^{AIA} carrying pAINT::PSOS(*imuA'*)-*egfp-imuB* at the *attB* integration site; Km^R	This study
Δ*imuB*::PSOS(*imuA'*)-*mEos4a-imuB*	Δ*imuB* carrying pAINT::PSOS(*imuA'*)-*mEos4a-imuB* at the *attB* integration site; Km^R	This study
Δ*imuB*::PSOS(*imuA'*)-*egfp-imuB*^{AAAAG}	Δ*imuB* carrying pMCAINT::PSOS(*imuA'*)-*egfp-imuB*^{AAAAG} at the *attB* integration site; Km^R	This study
dnaN-mCherry	mc^{2}155 with wildtype *Msm dnaN* (*MSMEG_0001*) replaced by recombinant *mCherry-dnaN* by homologous recombination of plasmid pIS225	Santi, *et al.*, 2013.
dnaN-mCherry:: PSOS(*imuA'*)-*egfp-imuB*	*dnaN-mCherry* carrying pAINT::PSOS(*imuA'*)-*egfp-imuB* at the *attB* integration site; Km^R	This study

Km^R=Carrying a kanamycin resistance gene; Am^R=Carrying an ampicillin resistance gene; Gm^R=Carrying a gentamycin resistance gene.

2.1. Liquid Cultures

E. coli liquid cultures were grown in Luria-Bertani (LB) broth (with the addition of appropriate antibiotics where suitable) in Erlenmeyer flasks or culture tubes dependent on the volume of culture required. Growth conditions consisted of incubation at 37 °C with mixing at approximately 100 rpm. Growth was assessed by measuring the optical density of 1 ml of culture by spectrophotometry using 600 nm wavelength light (OD_{600}).

Msm strains were grown in Middlebrook 7H9 broth (BD Science, USA) liquid media supplemented with 10 % (v/v) Middlebrook oxidase-albumin-dextrose-catalase (OADC) (BD Science, USA) and 0.05 % (v/v) *Tween-80* (Sigma, USA). Antibiotic selection by means of kanamycin (KAN) or gentamycin (GENT) supplementation was used where appropriate for strains containing the corresponding resistance genes. Cultures were incubated in Erlenmeyer flasks at 37 °C with mixing at 100 rpm. Growth was assessed by OD_{600} measurements.

2.2. Bacterial Growth on Solid Media

When isolated colonies were required, *E. coli* cultures of freezer stocks were streaked onto LB agar solid media in Petri dishes and incubated at 37 °C. Where antibiotic selection was required, molten media was supplemented with the appropriate amount of antibiotic.

Msm colonies were grown on Middlebrook 7H10 agar (BD Science, USA) supplemented with 10 % (v/v) Middlebrook OADC (BD Science, USA) in Petri dishes and incubated at 37 °C to allow bacterial growth and replication. Where

antibiotic selection was required, molten media was supplemented with the appropriate amount of antibiotic.

2.3. Antibiotic Selection

Different concentrations of various antibiotics were employed to select for the correct bacterial strain as per **Table 2-2**.

Table 2-2 | Antibiotics and concentrations used in this work

	E. coli (µg/ml)	*Msm* (µg/ml)
Solid media		
Kanamycin	50	20
Gentamycin	20	2.5
Liquid media		
Kanamycin	50	20
Gentamycin	20	5.0

3. Molecular Techniques

3.1. DNA Extractions

3.1.1. Large-scale Plasmid Extraction

A positively screened *E. coli* culture was used to inoculate a 40 ml culture which was subsequently cultured overnight at 37 °C. The culture was added to a 50 ml centrifuge tube and centrifuged at 3,901 relative centrifugal force (rcf) for 10 min at 4 °C. The supernatant was poured off and the remaining cell pellet was resuspended in 1.0 ml of Solution I by repipetting. Thereafter, 2.0 ml of Solution II was added to the solution and inverted to mix. The solution was incubated at room temperature (25 °C) for 5 min, after which 1.5 ml of Solution III was added. The solution was inverted to mix and kept on ice for 5 min. The lysed cell solution was centrifuged at 3,901 rcf for 10 min at 4 °C. Subsequently, 700 µl of the resulting supernatant was added to each of five 1.5 ml microfuge

tubes and 10 µl of 10 mg/ml RNAse A was added. The solutions were incubated at 42 °C for 30 min to remove contaminant RNA. Thereafter, 700 µl of isopropanol was added to each sample and the solutions were incubated at room temperature (25 °C) for 10 min with periodic inversion for mixing. Afterwards, the solutions were centrifuged at 16,100 rcf for 10 min. The resulting supernatant was poured off and 200 µl of 70 % ethanol was added to each DNA pellet. The solutions were centrifuged for a further 10 min at 16,100 rcf and the supernatant was removed. The microfuge tube was gently dabbed on paper towel to remove residual ethanol. Subsequently, 100 µl of nuclease-free dH_2O was added to each microfuge tube sample and the DNA was completely resuspended by heating to 42°C by using a heating block and flicking periodically to mix. All five samples were pooled together in a single microfuge tube and 700 µl of 24:25 phenol-chloroform was added to the sample. The solution was mixed extensively by vortex until the solution became milky-white in colour. The sample was centrifuged at 16,100 rcf for 10 min. The resulting aqueous phase was transferred to a new microfuge tube where 50 µl of 3 M sodium acetate was added to the solution. DNA precipitation was performed by adding 1.0 ml ice-cold absolute ethanol to the sample, whereby it was subsequently kept at -20 °C overnight. The sample was then centrifuged at 16,100 rcf for 10 min and resulting supernatant was poured off to remove contaminating proteins, polysaccharides, and lipids. Thereafter, 200 µl of 70 % ethanol was added and the sample was centrifuged at 16,100 rcf for 10 min. The supernatant was poured off and the microfuge tube was dabbed on paper towel and vacuum centrifuged at 42 °C for 10 min to remove residual ethanol. The DNA pellet was resuspended in 50–100 µl of nuclease-free dH_2O by heating to 42 °C and mixing. The DNA concentration was measured using

a spectrophotometer. Working stocks were prepared by dilution with dH_2O to a final concentration of 1,000 ng/ml. The final DNA plasmid solutions were stored at 4 °C for short time periods or -20 °C for extended periods of time.

3.1.2. Small-scale Plasmid Extraction

A single, isolated *E. coli* colony was picked from solid media using a sterile micropipette tip and used to inoculate 4 ml of LB liquid media containing appropriate concentrations of antibiotics. The culture was subsequently incubated at 37 °C overnight. After incubation, 1 ml of culture containing the desired plasmid was spun down at 16,100 rcf for 60 s in a centrifuge. The supernatant is poured off and the remaining cell pellet was resuspended in 100 µl of Solution I and 200 µl of Solution II was added before the solution was mixed by inversion. Thereafter, 150 µl of Solution III was added and the solution was mixed by shaking. The solution was centrifuged at 16,100 rcf for 5 min. The clear supernatant was transferred to a new microfuge tube. Contaminant RNA was degraded by adding 1 µl of 10 mg/ml RNAse A to the solution before incubation at 37 °C for 10 min. Then 350 µl of isopropanol was added and the solution was kept at room temperature (25 °C) for 10 min with periodic inversions to mix. The solution was centrifuged at 16,100 rcf for 10 min and the supernatant was discarded appropriately. 200 µl of 70 % ethanol was added to the pellet within the microfuge tube and was subsequently spun down for a further 10 min at 16,100 rcf. Residual ethanol was removed by dabbing gently on paper towel and by evaporation in a vacuum centrifuge for 10 min. Thereafter, purified DNA pellet was completely resuspended in 20 µl of nuclease-free dH_2O by mixing and heating to 42 °C. DNA concentration was determined by measurement with a spectrophotometer. The final DNA

plasmid solution was stored at 4 °C for short time periods or -20 °C for extended periods of time.

3.1.3. Crude *Msm* DNA Extraction by Colony Boil

Isolated *Msm* colonies were picked and resuspended in 20 µl of sterile dH_2O, from which 10 µl was used to inoculate 7H9-OADC liquid culture or solid 7H10-OADC media and incubated at 37 °C overnight for continuation of the culture. The remaining aliquot of cell suspension was added to 10 µl of chloroform (Sigma, USA) in a microfuge tube and heated to 90 °C for 20 min to denature the cells. After denaturation, the cells were centrifuged at 13,400 rcf for 1 min and 5 µl of supernatant was used as template for a polymerase chain reaction (PCR).

3.2. Polymerase Chain Reactions

3.2.1. List of Oligonucleotides

PCR primers were used to amplify specific sequences of DNA. Oligonucleotides were used for this function (**Table 2-3**).

Table 2-3 | Oligonucleotides used in this study

Oligonucleotide	Sequence (5'-to-3')
Screening of WT::PSOS(*imuA'*)-*egfp*	
GFP_Compl_Forward	GTGAACGGCCACAAGTTCTC
GFP_Compl_Reverse	GGGTCGACAGGTAGTGGTTG
Screening of PSOS(*imuA'*)-*egfp*-*imuB* construct within *Msm*	
FP_for	GGAGCGCACCATCTTCTTCA
FP_rev	TGTCGCCCTCGAACTTCAC

3.2.2. PCR Amplification

PCR for primer pair testing and screening were conducted as follows in **Table 2-4** (reaction mixture) and **Table 2-5** (cycle reaction conditions):

Table 2-4 | Reaction Mixture

Reagent	Volume
Template DNA	2.0 µl*#
10× FastStart™ taq polymerase buffer	2.0 µl
FastStart™ taq polymerase (20 U/µl)	0.5 µl
dNTPs (2 mM)	1.0 µl
Forward primer (10 µM)	2.0 µl
Reverse primer (10 µM)	2.0 µl
dH_2O	10.5 µl
Total for master mix	*18.0 µl*
TOTAL per reaction	*20.0 µl*

* 200 to 1,000 ng/µl of DNA sample.
# 5.0 µl of colony boil supernatant is used for *Msm* screening; in this case the amount of dH_2O is decreased to 7.5 µl and the master mix volume is similarly decreased to 15.0 µl.

Table 2-5 | PCR Cycle Conditions

	Step	Temperature	Time	Cycles
1.	Initial denaturation	95.0 °C	5 min	1
2.1.	Denaturation	95.0 °C	30 s	35 to 40
2.2.	Primer annealing	T_A OPT	30 s	35 to 40
2.3.	Elongation	72.0 °C	30 s per 500 bp	35 to 40
3.	Final elongation	72.0 °C	5 min	1
4.	Hold	12.0 °C	Indefinitely	1

T_A OPT represents the optimal annealing temperature as determined by temperature-gradient PCR.

3.2.3. PCR Temperature Gradient Optimization

PCR annealing temperature optimizations were conducted by setting up replicate PCR reactions as per **Section 3.2.2**. The reactions were performed as prior with the exception of the annealing temperature. For this, gradient thermocyclers were used to produce a gradient of differing temperatures at the

primer-annealing step (T_A) for the replicate reaction mixtures. The resulting amplicons were then separated through an agarose gel and visualized using a *Wealtec Keta*™ under ultraviolet (UV) light illumination and *Ketagalan M* software (Wealtech Company, USA) to determine the annealing temperature that resulted in the greatest yield with minimal non-specific amplification (T_AOPT) specific to a particular primer pair. The corresponding annealing temperature was used in subsequent reactions for each primer pair.

3.3. DNA Digestion by RE Enzymes

Plasmid DNA was digested with either New England Biolabs or Thermo Fisher Scientific RE enzymes as per the manufacturer's instructions. Briefly, 1,000 to 4,000 ng of plasmid sample was digested with 0.2 to 2 U of RE in the presence of 1× reaction buffer, and BSA if required, at a final volume of either 20 or 50 μl at the optimal temperature for a minimum of the recommended digestion time. After digestion, RE enzymes were inactivated where possible as per the instructions of the manufacturers.

3.3.1. Plasmid Screening by RE Digestion

Small-scale plasmid DNA extraction products were screened by RE digestion using a minimum of four separate REs in order to validate the correct restriction map of the putative plasmid. All RE reactions were performed as per the instructions of the manufacturer.

3.4. Gel Electrophoresis

Gel electrophoresis was used to separate DNA fragments and amplicons based on size. To this end, agarose gels were made to a concentration between 0.8 and

4.0 % dependent on the anticipated size of the fragments being separated. Small fragments of 50 to 200 bp were separated using 4 % agarose gels, whereas DNA fragments approximately 16,000 to 800 bp were separated with 1 % agarose gels. Gels were made by dissolving agarose in heated 1× TAE buffer before ethidium bromide (EtBr) (Sigma, USA) was added to a final concentration of 0.25 μg/ml before pouring into molds to allow the gels to set. Thereafter, gels were placed in electrophoresis tanks (BioRad, USA) and submerged in 1× TAE buffer. DNA samples with volumes of 20 or 50 μl were mixed with 5 or 10 μl of loading dye, respectively, before being loaded into wells. *Molecular Weight Markers III*, *IV*, *V*, or *VI* (Roche, Switzerland) were loaded in individual lanes where appropriate and used as molecular standards to determine the size of each DNA fragment within the gel. An electric current of 80 to 100 V and 200 ampere was applied across the gel using a *PowerPac™ Basic 75W* (BioRad, USA) until DNA fragments had separated sufficiently. Subsequent DNA migration was visualized using *Wealtec Keta™* under UV light illumination and *Ketagalan M* software (Wealtech Company, USA) or inspected manually with a blue light transilluminator.

3.5. Cloning of Constructs

Plasmid DNA was digested with appropriate RE enzymes to yield fragments with compatible ends that were to be ligated to yield the desired product. After RE digestion, DNA fragments were separated using gel electrophoresis and unambiguously separated fragments with the correct size were cut out the gel using a scalpel while viewing the gel using a blue light transilluminator. DNA fragments were extracted using the *NucleoSpin® Gel and PCR Clean-up* kit (Macherey-Nagel GmbH & Co. KG, Germany).

3.5.1. Gel Extraction

DNA was excised from agarose gels as per the instructions of the manufacturer. Specifically, each excised block of agarose gel was dissolved in a 1.5 ml microfuge tube by adding 2 µl of *Buffer NT1* for each milligram of gel and heated to 50 °C in a shaking (400 rpm) heating block until the gel had completely dissolved. Solutions containing the same DNA digest were pooled and placed into a silica membrane extraction column. The column was centrifuged at 11,000 rcf for 30 s. The flow-through was discarded and the sample was centrifuged for a second time at 11,000 rcf for 30 s. The flow-through was disposed of appropriately, and 700 µl of *Buffer NT3* (with ethanol) was added to the column. The column and collection tube was centrifuged at 11,000 rcf for 30 s to wash the DNA. The flow-through was discarded and the sample was centrifuged for a second time at 11,000 rcf for 90 s. The column was placed into a new 1.5 ml microfuge tube and heated to 65 °C to evaporate residual ethanol. Thereafter, 20 µl of nuclease-free dH_2O heated to 65 °C was added to the filter of the column. The sample was left at room temperature (25 °C) for 4 min to allow the DNA to elute. The column was subsequently centrifuged at 11,000 rcf for 2 min to collect the DNA fragment solution in the microfuge tube. To maximize DNA yield, the DNA solution was used to elute the DNA a second time before elution was completed with a final step using 20 µl of fresh nuclease-free dH_2O.

3.5.2. Vector Dephosphorylation

To dephosphorylate linear DNA, 5 U of *Antarctic Phosphatase* (New England Biolabs, USA) was used to digest 20 µl of purified, linear vector DNA in the presence of 1× *Antarctic Phosphatase Buffer* (New England Biolabs, USA). The

reaction solution was incubated for 30 min at 37 °C to remove the 5′ phosphate groups from vector DNA.

3.5.3. Plasmid Clean-up

Inactivated phosphatase reactions were cleaned up using the *NucleoSpin® Gel and PCR Clean-up* (Macherey-Nagel GmbH & Co. KG, Germany). Namely, 200 µl of *Buffer NT1* was added to each reaction mixture and heated to 50 °C in a shaking (400 rpm) heating block for 5 min. The solutions were placed into a silica membrane extraction column, which was subsequently centrifuged at 11,000 rcf for 30 s. The flow-through was discarded and the sample was centrifuged for a second time at 11,000 rcf for 30 s. The flow-through was disposed of appropriately, and 700 µl of *Buffer NT3* (with ethanol) was added to the column. The column and collection tube was centrifuged at 11,000 rcf for 30 s to wash the DNA. The flow-through was discarded and the sample was centrifuged for a second time at 11,000 rcf for 90 s. The column was placed into a new 1.5 ml microfuge tube and heated to 65 °C to evaporate residual ethanol. After evaporation, 20 µl of nuclease-free dH_2O heated to 65°C was added to the filter of the column. The sample was left at room temperature (25 °C) for 4 min to allow the DNA to elute. The column was subsequently centrifuged at 11,000 rcf for 2 min to collect the DNA fragment solution in the microfuge tube. To maximize DNA yield, the DNA solution was used to elute the DNA a second time before elution was completed with a final step using 20 µl of fresh nuclease-free dH_2O.

3.5.4. Ligation

Ligations to combine inserts into linearized vectors were performed as per the instructions of the manufacturer. Extracted vector and insert fragments with compatible ends were mixed in 1:1; 1:3; and 1:5 molar ratios in addition to a no insert control. Thereafter, 10 U of *T4 DNA ligase* (Roche, Switzerland) and *T4 DNA ligase buffer* (Roche, Switzerland) was added to the solution to a final concentration of 1× and a final volume of 20 µl. Ligation reactions were carried out at 4 °C overnight for both 'sticky-end' and 'blunt-end' ligations. Prior to bacterial transformation, the ligase was inactivated by heating the sample to 65 °C for 10 min.

3.6. DNA Sequencing

High-fidelity PCR reactions were conducted to amplify the region of interest from either genomic DNA or plasmid DNA using 'sequence space' primers to amplify the sequence of interest. The PCR products were separated using gel electrophoresis to validate the amplification of the target region based on the size of the fragment. Subsequently, the PCR product was purified and cleaned up as described in **Section 3.5.1**. Purified amplicons were sequenced by the Sanger sequencing method by *Central Analytical Facility* (Stellenbosch University, ZA).

3.7. Nucleic Acid Concentration Determination

DNA samples were quantified by measuring the concentration of 1.0 µl of sample using a *NanoDrop™ 2000c* spectrophotometer (Thermo Fisher Scientific, USA).

4. Microbiology Techniques

4.1. Glycerol Stocks

All liquid bacterial cultures were stored long term in 33 % (v/v) glycerol by combining 500 µl of cell culture with 500 µl of 66 % (v/v) glycerol in dH_2O. Thereafter, the glycerol stocks were stored at -80 °C indefinitely.

4.2. E. coli

4.2.1. Rubidium Chloride-competent Cells

DH5α or *dam*$^-$ strains of *E. coli* with an OD_{600} of 0.48 were chilled on ice for 15 min and pelleted in a 50 ml centrifuge tube by centrifugation at 3,901 rcf for 5 min at 4 °C. The supernatant was discarded and the pellet was resuspened in 40 % volume TFB I. The cell suspension was kept on ice for 15 min before the cells were pelleted once more by centrifugation at 3,000 rcf for 5 min. The supernatant was discarded and the pellet was resuspended in 4 % volume of TFB II. The cell suspension was kept on ice for 15 min before immediate use or stored at -80 °C indefinitely, whereby the cells were thawed prior to transformation experiments.

4.2.2. Heat-shock Transformation

100 µl of DH5α or *dam*$^-$ rubidium chloride-competent *E. coli* cell culture was added to a 1.5 ml microfuge tube containing 1.0 µl of plasmid suspension containing 100 ng of plasmid DNA or 40 µl of purified ligation product. The cell solution was kept on ice for 30 min. Thereafter, the cell solution was heat shocked at 42 °C for 90 s; after which it was cooled by placing onto ice for 60 s. After cooling, 750µl of two yeast tryptone (2YT) broth was immediately added and the culture was incubated at 37 °C for 1 h to allow transformed cells to

express resistance-associated proteins. Thereafter, cells were pelleted at 16,100 rcf for 1 min. The resulting cell pellet was resuspended in 100 µl of supernatant and was plated on appropriate selective solid media. Viable controls (untransformed competent cells) were plated onto standard LB agar plates to ensure competent cell viability. Non-plasmid, negative controls were also carried out by plating untransformed cells onto selective LB agar plates to ensure the absence of contamination and the efficacy of antibiotic selection. The plates were incubated at 37 °C overnight to reveal antibiotic resistant colonies.

4.3. *Msm*

4.3.1. Electroporation

Freezer stocks of *Msm* were used to inoculate 100 ml cultures of 7H9-OADC which were grown at 37 °C until an OD_{600} of 0.6 to 0.8. After growth of liquid cultures, a total of 90 ml of culture was centrifuged at 3,901 rcf for 10 min at 4 °C in two separate 50 ml centrifuge tubes. The resulting supernatant was poured off and each cell pellet was resuspended in 40 ml of 10 % (v/v) glycerol while keeping the cells on ice. The solutions were centrifuged again at 3,901 rcf for 10 min at 4 °C. The resulting supernatant was poured off and each cell pellet was again resuspended in 30 ml of 10 % (v/v) glycerol while keeping the cells on ice. The cell solution was again centrifuged at 3,901 rcf for 10 min at 4 °C. Again, the resulting supernatant was poured off and the cell pellet was resuspended in 20 ml of 10 % (v/v) glycerol while keeping the cells on ice. The two cell-glycerol solutions were pooled into a single 50 ml centrifuge tube. Thereafter, the cells were centrifuged again at 3,901 rcf for 10 min at 4 °C. The resultant cell pellet was resuspended in 4 ml of 10 % (v/v) glycerol for the final time.

Electroporation was then carried out with a *BioRad GenePulser Xcell*™ electroporation unit (BioRad, USA) utilizing the exponential protocol using the following parameters: 2,500 V of electric potential difference, 25 μF of capacitance, 1,000 Ω of resistance and a cuvette size of 2 mm. To this end, 10 μl of solution containing 0 to 4,000 ng of plasmid was placed in an electroporation cuvette with a chamber width of 2 mm (BioRad, USA) and kept on ice. Subsequently, 400 μl of cell-glycerol suspension was added to the cuvette, which was wiped to remove liquid on the outside of the cuvette. The cuvette was placed in the electroporation unit and pulsed with electricity. Immediately after electroporation, the cell suspension was rescued with 750 μl of 7H9-OADC broth and subsequently incubated at 37 °C for 4 h. Thereafter, the cell culture was centrifuged at 16,100 rcf for 1 min and the cell pellet was resuspended in 100 μl of supernatant prior to streaking onto antibiotic-selecting 7H10 solid media. Antibiotic-resistant transformants were allowed to grow into colonies by incubating the cultures at 37 °C for 3 to 5 days.

4.3.2. Mutagenesis Assays

Mutagenesis assays were performed as previously described (Boshoff, *et al.*, 2003; Warner, *et al.*, 2010). Briefly, liquid cultures of *Msm* were grown to an OD_{600} of 0.6 to 0.8 in 60 ml of 7H9-OADC after inoculation with a glycerol stock. Cell density was increased ten-fold by centrifugation of 50 ml of culture at 3,901 rcf for 10 min before resuspending the resultant pellet in 5 ml of fresh 7H9-OADC. The concentrated cell solution was pipetted into a Petri dish and spread across the entire surface of the dish before being exposed to 25 mJ/cm^2 of UV irradiation (254 nm) using a *StrataGene UV Stratalinker 1800* (StrataGene, USA). After irradiation, the concentrated cells were diluted back to 1× by adding 45

ml of fresh 7H9-OADC media to the cells in a culture flask. The cells were then allowed to recover at 37 °C in a shaking incubator for 4 h. In addition, 5 ml of unexposed culture was also cultured this way. In order to quantify the extent of DNA damage induced, six repeats of 250 µl of UV-exposed cells were plated onto 200 mg/ml rifampicin (RIF)-containing 7H10-OADC solid media. In parallel, unexposed cells were diluted by serial, ten-fold dilution seven times to yield cell dilutions factors of 10^{0} to 10^{-7}. Thereafter, 100 µl the final three dilutions were plated onto standard 7H10-OADC in duplicate in order to determine the number of cells in each culture, yielding 10^{-6}, 10^{-7}, and 10^{-8} dilutions. The cell enumeration (RIF-deficient) plates were incubated 37 °C for 2 days before colony counting was performed. The RIF-containing culture plates were incubated at 37 °C for 5 to 7 days to allow RIF-resistant mutants to grow. After incubation and successful growth, the number of colonies formed was counted for each strain and using the dilution series, the total number of cells in 1 ml of culture prior to plating out was determined. From this, the mutation frequency can be determined by dividing the number of RIF-resistant colonies by the number of cells present in the liquid culture prior to UV irradiation.

4.3.3. DNA Damage Tolerance Assays

In parallel to **Section 4.3.2** above, following ten-fold serial dilution of unexposed cells, 5.0 µl of each of the eight dilutions were spotted onto standard, 0.04, and 0.02 mg/ml mitomycin C (MMC)-containing 7H10-OADC solid media. These plates were incubated at 37 °C for 5 to 7 days to allow colonies to develop.

4.3.4. Induction Assays

For all experiments that required exposure of *Msm* to a genotoxin, bacterial cells were grown in 5 ml 7H9-OADC liquid media supplemented with the appropriate genotoxic agent. MMC (Sigma, USA) was dissolved in dH_2O to a concentration of 0.5 mg/ml. Novobiocin (NVB) (Sigma, USA) was dissolved in dH_2O to a working concentration of 10 mg/ml. Moxifloxacin (MOX) (Sigma, USA) was dissolved in dH_2O to a working concentration of 3.2 mg/ml. 4-Nitroquinoline 1-oxide (NQO) (Sigma, USA) was dissolved in acetone to a working concentration of 3.8 mg/ml. Methyl methanesulfonate (MMS) (Sigma, USA) was used neat due to the rapid loss of activity in aqueous solution. Ciprofloxacin (CIP) (Sigma, USA) was dissolved in 1 M HCl to a working concentration of 1.71 mg/ml. EtBr (Sigma, USA) was diluted in dH_2O 100-fold. Griselimycin (GRS) (Müller Lab, Germany) was dissolved in dimethyl sulfoxide (DMSO) (Sigma, USA) to a working concentration of 20 mg/ml prior to addition to the culture media. Specifically, a single culture of *Msm* was grown at 37 °C to an OD_{600} of between 0.2 and 0.4, representing mid log-phase growth. Thereafter, the culture was split into numerous 5 ml cultures and the genotoxic compound was added to experimental cultures to a final concentration relative to the minimum inhibitory concentration (MIC). The exposed cultures were further incubated at 37 °C on orbital shakers for varying periods of time before further sampling was performed.

4.3.5. Combination Exposure Experiments

In order to test the effect of GRS- or MOX-mediated DnaN inhibition on EGFP-ImuB recruitment, a liquid culture of *dnaN-mCherry*::PSOS(*imuA'*)-*egfp-imuB* with an optical density of 0.38 was split into nine separate 10 ml cultures as per

Figure 2-3. GRS or MOX and MMC were added in combination to each culture in various concentrations to produce a combination array of sub- and supra-inhibitory concentrations of each genotoxin. Thereafter, cultures were incubated at 37 °C for 4 h in a shaking incubator prior to visualisation by fluorescence microscopy.

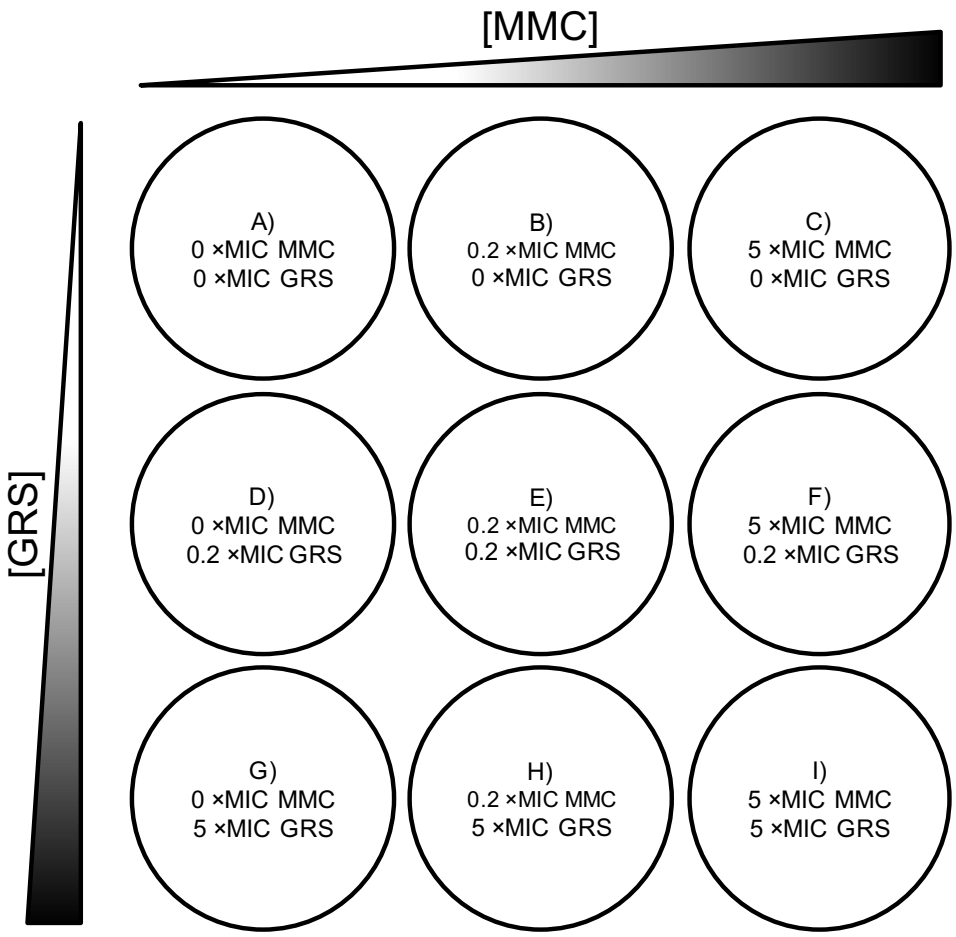

Figure 2-3 | A graphical representation of a combination exposure experiment set-up
Culture flasks with equal volumes of cell culture were exposed to an array of either MMC and GRS (shown here) or MMC and MOX. The set-up was designed such that there is a combination of 0×, 0.2×, and 5× of each of the two test compounds in every combination.

4.3.6. GRS Kill Kinetics

A liquid culture of mc²155 was grown from a single colony to an OD_{600} of 0.65 in 7H9-OADC. Subsequently, 1 ml of culture was diluted 100× by adding it to 99 ml of fresh 7H9-OADC. The resulting diluted culture was divided into three

separate 30 ml cultures: one culture flask contained no GRS; one culture flask had GRS added to a final concentration of 4.5 μg/ml; and GRS was added to the final culture flask to a final concentration of 22.5 μg/ml. Each culture was incubated in a shaking incubator at 37 °C. Thereafter, at 0, 3, 6, 9, 12, 24, 36, and 48 h, each culture was sampled for cell enumeration. Specifically, 1 ml of culture was centrifuged in a microfuge tube at 16,400 rcf for 5 min. The resulting cell pellet was resuspended in 1 ml of fresh 7H9-OADC media by re-pipetting and represented a non-diluted sample with a dilution factor of 10^{0}. Sequentially, 100 μl of each serial dilution was diluted in 900 μl of fresh media and shaken by vortex until a final dilution factor of 10^{-5}. Finally, 100 μl of the 10^{-3}, 10^{-4}, and 10^{-5} dilutions of each sample were spread onto 7H10-OADC solid media, resulting in a final dilution factor of 10^{4}, 10^{5}, and 10^{6}, respectively. Each sample was repeated in duplicate at each time point. Following 2 days of incubation, the number of colonies present on each plate was counted and the corresponding cell density was calculated by multiplying the colony forming units (CFU) of each plate by the corresponding dilution factor.

5. Analytical Experimentation

5.1. Flow Cytometry

Cultures of *Msm* were induced with MMC (as indicated in **Section 4.3.4**) before the cells were fixed in preparation for flow cytometry. To this end, 1 ml of culture was centrifuged at 14,600 rcf for 5 min. The resultant cell pellet was resuspended in 200 μl of 4 % (v/v) formaldehyde and left to fix in the dark for 30 min. After fixation, 800 μl of 0.05 % (v/v) *Tween-80*-phosphate-buffered saline (PBS) solution was added to the cell solution. Once more, the solution was centrifuged at 14,600 rcf for 5 min and the pellet was resuspended in 200

μl of 0.05 % (v/v) *Tween-80*-PBS solution. Prior to acquiring data with a flow cytometer, the cells were centrifuged a final time at 14,600 rcf for 5 min and the resultant pellet was resuspended in 200 μl of PBS. Immediately before acquisition, the cell solution was filtered through the 30 μm cell strainer lid of a 5 ml test tube (Corning, USA) and the tube was mixed by vortex for 5 s. Flow cytometry was performed using a *Fortessa*™ flow cytometer (BD Science, USA) using *FACSDiva*™ software (BD Science, USA). A FITC filter set (530/30 nm filter with 505 nm long-pass mirror) was used to detect the fluorescence of EGFP and had a voltage of 557 V. Forward- (FSC) and side-scatter (SSC) had voltages of 400 and 310 V, respectively. A laser window-extension period of 5.00 ms was used to acquire data. One million events were recorded for each acquisition run. Data was analyzed using *FlowJo*® (v9) (FlowJo, LLC, USA).

5.2. Microscopy and Imaging

In general, all microscopy images were generated by repeated, manual, random sampling of non-filtered liquid cultures by focusing on areas containing cells using non-fluorescent methods where possible before imaging by fluorescence microscopy in an attempt to avoid bias during sampling. In all cases, a minimum of five separate fields of view were imaged for each replicate of each strain under each condition. Detailed descriptions of the imaging techniques are presented below.

5.2.1. Confocal Fluorescence Microscopy

Confocal microscopy was performed on a *Zeiss LSM 510 Meta Confocal Microscope* and *AxioObserver* platform (Carl Zeiss AG, Germany). Samples were visualized by pipetting 2 μl of sample culture onto a glass microscope slide

(Lasec, ZA) before a #1.5 glass cover slip (Lasec, ZA; Sigma, USA) was placed over the sample. Samples were viewed using a 63× oil-immersion, plan-apochromat objective lens with a numerical aperture (NA) of 1.42 (Carl Zeiss AG, Germany). The oil immersion had a refractive index of 1.518 (*Immersol*™ *518 F*) (Carl Zeiss AG, Germany). Samples were located using either transmitted light and phase contrast or epifluorescent methods. Thereafter, confocal imaging was performed on focused field of views. Fields were changed according to the rate of photobleaching observed. Filter set properties are listed in **Table 2-6**. Images were captured using *ZEN Blue Microscope and Imaging Software* (Carl Zeiss AG, Germany) and further processed using the same software or *Fiji* (Schindelin, *et al.*, 2012).

Table 2-6 | Confocal fluorescence parameters

Green fluorescence	
Excitation laser λ	488 nm
Emission filter λ	525 nm
Yellow fluorescence	
Excitation laser λ	514 nm
Emission filter λ	538 nm
Red fluorescence	
Excitation laser λ	561 nm
Emission filter λ	603 nm

5.2.2. Wide-field Epifluorescence Microscopy

To visualize the *Msm* strain using an *Axio.Scope A1* microscope (Carl Zeiss AG, Germany), 2 to 5 µl of culture was placed between a glass microscope slide (Lasec, SA, or Sigma-Aldrich, USA) and a #1.5 coverslip (Sigma-Aldrich, USA). A transmitted mercury lamp light was used together with filter cubes to detect fluorescence with a 100× 1.4 NA plan apochromatic oil immersion objective

lens; to this end, *Immersol™ 518 F* (Carl Zeiss AG, Germany) was used. Images were captured with a *Zeiss 1 MP* monochrome camera (Carl Zeiss AG, Germany). Comparable samples were exposed to the same exposure settings for respective channels for image acquisition. Green fluorescence was detected using a 488 nm excitation filter and a 510 nm emission filter set; while the red fluorescence was detected using a 590 nm excitation laser filter and 700 nm long-pass emission filter (Carl Zeiss AG, Germany). In addition, brightfield imaging was used to detect the position of the bacteria.

5.2.3. Light Microscopy Cell Imaging

In addition to wide-field epifluorescence microscopy, bacilli were also imaged using a *ZOE™ Fluorescent Cell Imager* (BioRad, USA). The instrument was used as per the manufacturer's default hardware and acquisition settings while samples were prepared as previously described.

5.2.4. Superresolution, Interferometric Photo-Activated Light Microscopy

Superresolution samples were prepared as follows: A gold fiducial coverslip (Shtengel, *et al.*, 2009, supplementary information) was cleaned with 1 M KOH and coated with 1 % poly-L-lysine for 60 min at 37.0 °C before submerging the coverslip twice in fresh dH_2O for 5 min. At this point prepared coverslips were stored in dH_2O at 4 °C until use. Subsequently, 3.0 ml of bacterial sample was added to the fiducial-coated surface of the coverslip and centrifuged onto the coverslip at 3,200 rcf for 30 min. Unbound bacterial sample was washed off the coverslip by two sequential submersions in *Dulbecco's Phosphate-Buffered Saline* (Thermo Scientific, USA) for 5 min. The sample was fixed with 0.5 %

paraformaldehyde for 2 min before immediately being washed with PBS. After washing, the gold fiducial coverslip was mounted face-down to a standard #1.5 glass coverslip with PBS. The coverslips were immobilized together with epoxy resin and sealed with petroleum jelly to prevent evaporation.

A custom-built, interferometric photo-activated light microscope (iPALM), developed at the *Howard Hughes Medical Institute*, was used to image fluorescent-labelled ImuB foci at a sub-diffraction limited resolution in three-dimension (3D). The instrument set-up was used as previously reported (Shtengel, *et al.*, 2009). The previously prepared sample slide was mounted between two opposing 60× 1.4 NA oil immersion lenses to record the data of each sample and fluorescence-grade immersion oil (refractive index of 1.518) was added to both objective lenses. Bacterial cells were located by differential interference contrast (DIC) visualization before imaging each field of view. The opposing objectives were focused approximately 200 nm in the *Z*-axis above the gold fiducials present on the surface of the coverslip, a distance empirically determined to contain the bacterial sample. Set-up and focus of the objectives and beam splitter was performed as previously reported (Shtengel, *et al.*, 2009). Briefly, objectives were focused by adjusting the *Z*-plane of each lens and the beam splitter in accordance with the gold fiducial fluorescent signal intensity such that all three camera signals resembled Gaussian curves with oscillating *Z*-axis position. Furthermore, the beam splitter was adjusted such that the Gaussian fit of each detector was separated by 120° (360°÷3). Thereafter, a calibration image of 100 cycles was taken of the gold fiducials using a pulsating 488 nm laser prior to imaging of the bacteria for 25,000 cycles using alternating 400 nm and 561 nm laser cycles per frame with an acquisition rate of

approximately 20 frames per second (exposure time of 0.05 s for 590 nm light only). Each frame was recorded sequentially by an electron multiplying charge coupled device (EMCCD) monochrome camera (an EM gain of 200× was employed).

Prior to image generation, each file was processed within *PeakSelector*™ (v9.5) (Howard Hughes Medical Institute, USA) as follows: Calibration files were curated such that only the middle 30 frames (frame 35 to 65), corresponding to the most in-focus frames, were used to calibrate the position of the fiducial-coated coverslip. Furthermore, an upper bound of 60 nm was applied to the total change of *X*- and *Y*-axis positions for each calibration fiducial to reduce pixel uncertainty. A minimum of four fiducials was used as reference positions for the calibration of each sample image file. Thereafter, the generated 3D sample image was corrected for *XYZ*-axis tilt by transformation of all *Z*-axis positions by the plane of the coverslip/fiducials. Outlying signals were eliminated by restriction of the unwrapped *Z*-axis error to a symmetrical Gaussian curve. Furthermore, ghosting was reduced by removing incorrectly localized signal originating from below the coverslip by enforcing a lower bound limit on the unwrapped *Z*-axis position equal to the position of the fiducial plane. Each field of view was inspected individually to ensure that no biological data was filtered out.

5.3. Cell Measurement

Micrographs were analyzed using *Fiji* (v1.50b) (Schindelin, *et al.*, 2012). The distances (in pixels) between the poles of clearly defined, unambiguous bacilli were measured. Straight bacilli were measured using a single line between the

two poles of each cell. Bent or curved cells were measured by taking multiple line measures along the center of the bacilli. Thereafter, the pixel distance was converted to physical distance (μm) using the scale ratio specific to each image. Every undistorted cell in each micrograph was measured.

6. Statistical Methods

Statistics were determined using *GraphPad Prism* (GraphPad Software, USA) and *R Statistics* (R Foundation for Statistical Computing, Austria).

7. Routine Instruments

Spectrophotometry to determine the cell density of liquid cultures was measured using a *Biochrom WPA CO8000 Cell Density Meter* (Biochrom Ltd, USA).

Mixing of samples by vortex was performed using a *Vortex Mixer* (Stuart, UK).

PCR was performed using a *C1000*™ *Thermal Cycler* (BioRad, USA) or *T100*™ *Thermal Cycler* (BioRad, USA), with the latter also being used for temperature-gradient PCR.

Vacuum centrifugation was performed using a *miVac DNA concentrator* (Genevac Ltd and SP Industries, USA).

Centrifugation was performed using an *Allegra*™ *X-22R Centrifuge* (Beckman Coulter™, USA) for large samples at low rcf and a *Centrifuge 5415 D* (Eppendorf, Germany) for small, microfuge samples at high rcf.

Techne Dri-Block® DB-2D (Cole-Parmer, UK) heating blocks were used to heat liquid samples within microfuge tubes.

8. Detailed Strain and Plasmid Development

8.1. Design of Constructs

All mutasome constructs (containing either *imuA'*, *imuB*, or *dnaE2*) were designed with the following promoter features specific to the genes of the mutasome maintained in each respective case (**Table 2-7**). The sequence of each promoter element such as ribosome binding site (RBS), SOS box, -35, -10 sites, and transcription start site was identified in the mc²155 genome using comparable information from *Mtb* H37Rv (Davis, *et al*., 2002; Newton-Foot and van Pittius, 2013); and *Msm* gene information from the *J. Craig Venter Institute Comprehensive Microbial Resource* (Peterson, *et al*., 2001). All designed constructs were synthesized in pUC57 backgrounds by Genewiz (China).

Table 2-7 | The regulatory sequences of mc²155 mutasome components

Promoter	Feature	Identifiable Sequence (5'-to-3')	Location in mc²155 genome*
P(*imuA'-imuB*)#			
	-35	TTGACG	1710760..1710765
	-10	TGTTTACT	1710781..1710788
	PSOS(*imuA'*)	TCGAACATACATTCGA	1710796..1710811
	+1	A	1710814
P(*imuA'*)			
	RBS	CGGGAGG	1710834..1710840
	Start/Met codon	GTG	1710848..1710850
	Stop codon	TAG	1711553..1711555
P(*imuB*)			
	RBS	AGGGG	1711514..1711518
	Start/Met codon	ATG	1711558..1711560
	Stop codon	TGA	1713133..1713135
P(*dnaE2*)			
	-35	*Not identified*	-
	-10	*Not identified*	-
	PSOS(*dnaE2*)	TCGAACACGTGTTCGA	1723911..1723926

	+1	*Not identified*	-
	RBS	TCGGA	1723969..1723973
	Start/Met codon	ATG	1723975..1723977
	Stop codon	TGA	1727224..1727226

* Reference to the genome sequence published by Cole, *et al*. (1998)
[#] Promoter elements that regulate both *imuA* and *imuB* as part of the *imuA'-imuB* operon

8.1.1. PSOS(*imuA'*)-*egfp*

The construct PSOS(*imuA'*)-*egfp* was designed with the aim of developing a fluorescence-based transcriptional reporter in *Msm* to investigate DNA damage-induced gene expression in a bacillus following DNA damage. In addition to providing preliminary data in support of the construction of mutasome protein-specific translational fusions, the reporter construct would itself be used to study the expression dynamics of the *imuA'* promoter in the mycobacterial SOS response, allowing use of the same promoter for use in future constructs if proven successful. The construct consisted of the 267 bp upstream promoter region of *MSMEG_1620* (mc^{2}155 genomic region 1710581..1710847) (**Figure 2-4**), which included all *imuA'*-specific promoter elements such as the RBS and transcription factor-binding sites listed in **Table 2-7**. The native, relatively uncommon mycobacterial GTG start codon present in *MSMEG_1620* was not maintained in this construct and was changed to the standard ATG start codon. The remaining coding sequence for *egfp* (Cormack, *et al*., 1996), which was not codon optimized for expression in *Msm*, immediately followed the start codon. The construct was designed with *Hin*dIII restriction sites on either end to allow cloning into the multiple cloning site (MCS) of pMCAINT for stable integration into the mycobacterial genome (Warner, *et al*., 2010).

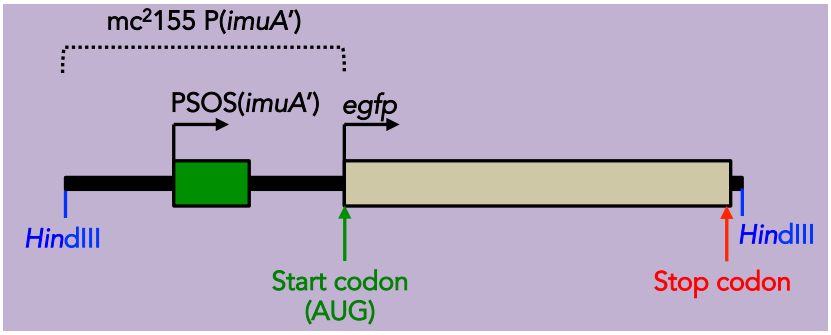

Figure 2-4 | Design of PSOS(*imuA'*)-*egfp*
The transcriptional reporter construct, PSOS(*imuA'*)-*egfp*, is represented in this schematic. The P(*imuA'*) promoter, containing PSOS(*imuA'*), was designed to drive expression of *egfp*. The construct was flanked by two *Hin*dIII RE sites to allow easy cloning of the construct into plasmids, in particular pMCAINT.

8.1.2. PSOS(*imuA'*)-*egfp-imuB'*

Owing to the fact that *imuB* is the second gene in a predicted bi-cistronic operon comprising *imuA'-imuB*, the promoter region of *gfp-imuB* was untested and it was likely that the inefficient gene expression by this promotor was the reason GFP-ImuB fluorescence was not detected in the previously developed Δ*imuB*::*gfp-imuB* strain. The failure of this strain, together with the subsequent success of the PSOS(*imuA'*)-*egfp* reporter gene, led to two changes in the design of a fluorescently tagged ImuB-expressing construct (illustrated in **Figure 2-5**). Instead of maintaining the operon controlling expression of *MSMEG_1622* (*imuB*), the tagged-*imuB* ORF in this construct was preceded by the native *imuA'* promoter region (as described in **Section 8.1.1**), which included PSOS(*imuA'*). The second change incorporated in the design of PSOS(*imuA'*)-*egfp-imuB'* was to utilize EGFP as opposed to the previously used GFP. This change was decided due to the more reliable and brighter fluorescence of EGFP (Cormack, *et al.*, 1996). The truncated construct PSOS(*imuA'*)-*egfp-imuB'* was designed to be synthesized and cloned into pMCAINT::*imuB* using the *Blp*I and *Cla*I cloning sites located 1,165 bp downstream of the *imuB* start and 1,501 bp upstream of *imuB*, respectively (**Figure 2-5**). This would allow restoration of the

full upstream promotor sequence of *imuA'* as well as the *imuB* ORF present in the pMCAINT::*imuB* plasmid. Furthermore, a FLAG tag-encoding sequence (with the translated sequence of DYKDDDDK) was used as a linker between the two components of the fusion gene to prevent steric collision in the translated protein and allow native folding of each protein (Gokhale and Khosla, 2000) as well as for downstream protein purification purposes (Einhauer and Jungbauer, 2001). This construct design was tested by performing cloning *in silico* using *CLC Main Workbench* (v7.6) (QIAGEN Aarhus A/S, Denmark), after which the resulting full-length, translated amino acid sequence was validated by *NCBI BLASTp* (Altshcul, *et al.*, 1990) and the *Conserved Domain Database* (**Figure 2-6**) (Marchler-Bauer, *et al.*, 2014).

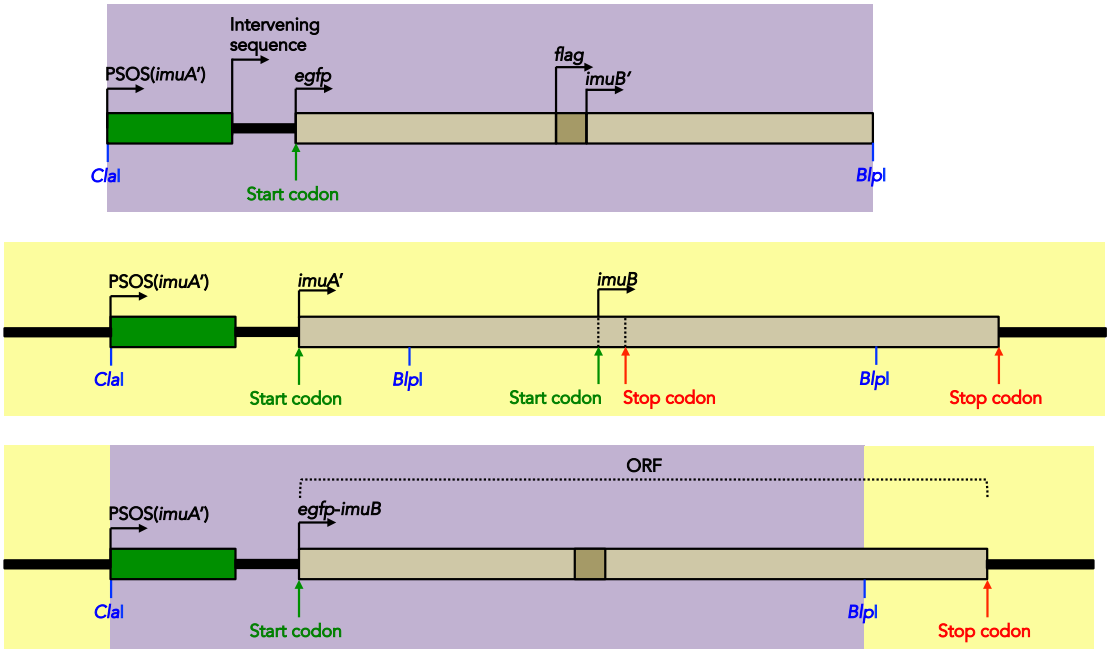

Figure 2-5 | Schematic design of EGFP-ImuB encoding gene
Top: Schematic layout of PSOS(*imuA*)'-*egfp*-*imuB*' sequence designed to be synthesized. The sequence consists of the region immediately upstream of *imuA*' (which includes the *imuA*' promoter). The start codon starts the sequence of *egfp*. The reading frame is maintained uninterrupted to include the linking *flag* sequence and the 5'-end of *imuB*. The construct is flanked by a 5' *Cla*I site and a 3' *Blp*I site. Middle: Schematic representation of the *imuA*'-*imuB* operon. Bottom: Schematic of the final PSOS(*imuA*)'-*egfp*-*imuB* gene after insertion of the construct at the *Cla*I and *Blp*I sites within the *imuA*'-*imuB* operon.

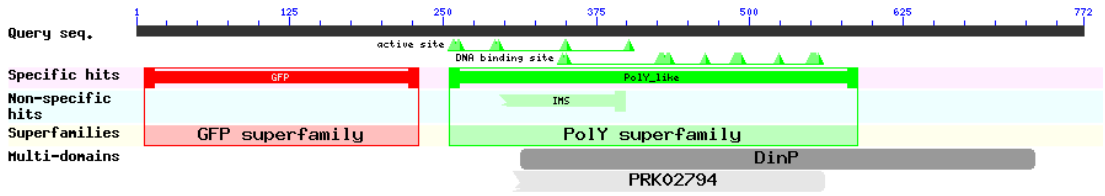

Figure 2-6 | EGFP-ImuB contained conserved domains
The translated PSOS(*imuA'*)-*egfp-imuB* gene was analysed using the *NCBI Conserved Domain Database*. The summary result of the predicted conserved domains of the translated *egfp-imuB* sequence indicated that both EGFP and ImuB were conserved, linked by the FLAG tag.

8.1.3. PSOS(*imuA'*)-*mEos4a-imuB'*

It was necessary to tag ImuB with an additional fluorescent protein (FP) in order to confirm that any observations were a result of the biological function of ImuB and not spurious anomalies associated with EGFP. To this end, MEos4a was identified as a suitable FP for a number of reasons. Firstly, it is derived from the Eos FP isolated from *Lobophyllia hemprichii* coral making it sufficiently different from GFP (*Aequorea victoria*)-derived FPs (Wiedenmann, *et al.*, 2004). MEos4a is also a photoswitchable FP, which is suitable for superresolution imaging techniques such as PALM/STORM. In addition, MEos4a was selected above similar photoswitchable proteins such as Kaede due to the limited impact it has on cell function (Betzig, *et al.*, 2006). Finally, MEos4a is also fixation resistant which improves the utility of tagged proteins for methods such as flow cytometry and imaging (Paez-Segala, *et al.*, 2015). The PSOS(*imuA'*)-*mEos4a-imuB* construct was designed by replacing the *egfp* sequence in PSOS(*imuA'*)-*egfp-imuB'* with the *Mycobacterium tuberculosis* (*Mtb*) codon-optimized sequence of *mEos4a* (Paez-Segala, *et al.*, 2015).

8.1.4. *egfp-dnaE2'*

As a result of the failure to observe fluorescence from the previously constructed *cfp-dnaE2* gene despite it providing functional restoration of the

mutasome (Reiche, *et al.*, unpublished), it was necessary to design a construct that utilized EGFP, which had already been used successfully to tag ImuB. Therefore, *egfp-dnaE2'* was designed by inserting *egfp* directly upstream of, and in frame with, the native *dnaE2* ORF. Once more, the two proteins were linked via a FLAG tag-encoding sequence (Einhauer and Jungbauer, 2001). Thereafter, the construct sequence was truncated to allow cloning of *egfp-dnaE2'* into pTTP1B::*dnaE2* at the *Kpn*I sites located -353 and +421 relative to the *MSMEG_1633* ORF. This allowed for the 5' portion of the native *dnaE2* gene to be 'swapped out' for the modified *egfp-dnaE2'* construct. The construct could then be complemented by the remaining upstream portion of the gene containing the PSOS(*dnaE2*) promoter and downstream '*dnaE2* in PTTP1B::*dnaE2* to yield a single *egfp-dnaE2* ORF (**Figure 2-7**). The construct design was tested by performing the intended cloning strategy *in silico* using *CLC Main Workbench* (v7.6) (QIAGEN Aarhus A/S, Denmark). The resultant full-length, translated amino acid sequence was verified by *NCBI BLASTp* (Altshcul, *et al.*, 1990) and a *Conserved Domain Database* query (**Figure 2-8**) (Marchler-Bauer, *et al.*, 2014). Both the EGFP and DnaE2 domains of the resultant protein were present in both *in silico* validations.

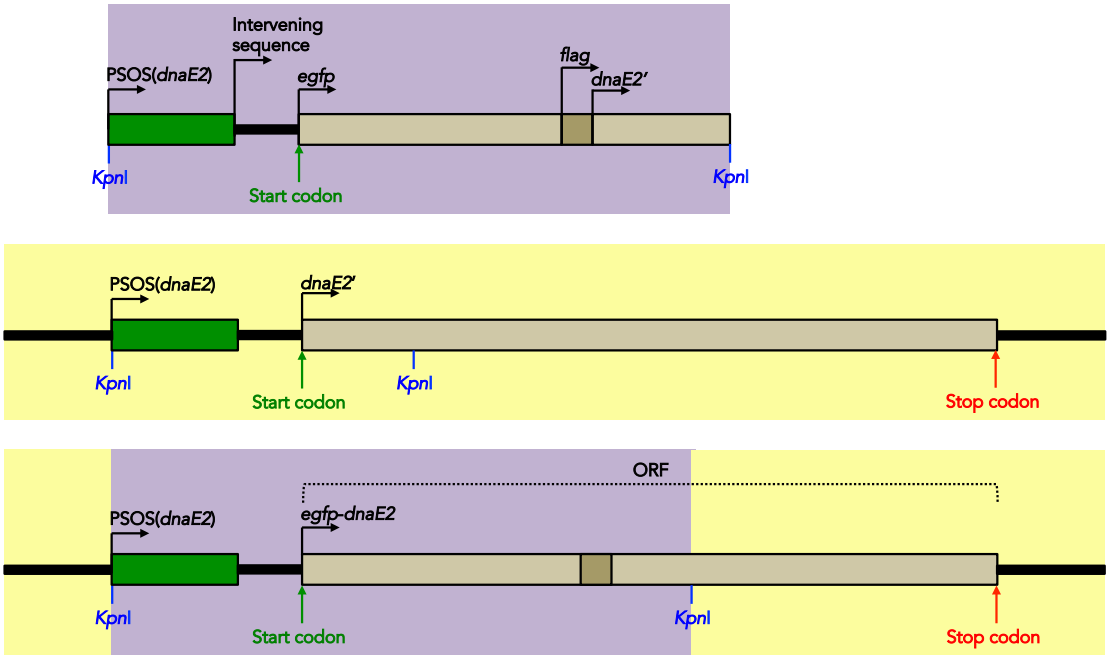

Figure 2-7 | Schematic design of *egfp-dnaE2'*
Top: Schematic layout of the *egfp-dnaE2'* construct. The sequence consists of the region immediately upstream of *dnaE2* (which includes the *dnaE2* promoter). The start codon starts the sequence of *egfp*. The reading frame is maintained uninterrupted through the linking *flag* sequence and the 5'-end of *dnaE2*. The construct is flanked at both ends by *Kpn*I recognition sites. Middle: Schematic representation of the *dnaE2* in the *Msm* genome. Bottom: Schematic of the final *egfp-dnaE2* gene after insertion of the construct at the *Kpn*I sites found within the *dnaE2* gene. Full-length *dnaE2* is restored as part of the *egfp-dnaE2* gene.

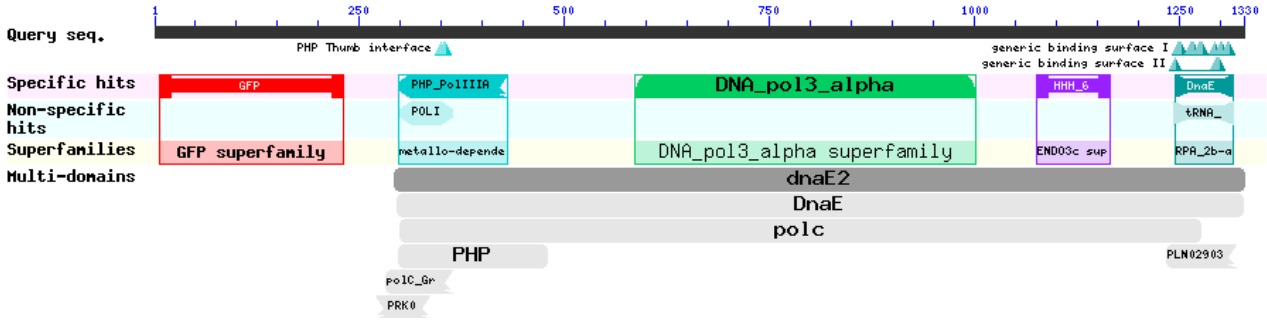

Figure 2-8 | EGFP-DnaE2 contained conserved domains
The translated *egfp-dnaE2* gene was analysed using the *NCBI Conserved Domain Database*. The summary result of the predicted conserved domains of the translated *egfp-dnaE2* sequence indicated that both EGFP and DnaE2 were conserved, linked by the FLAG tag, and contained no sequence deviations from the intended sequences.

8.1.5. PSOS(*imuA'*)-*egfp-imuB*^{AAAAG}

In order to validate the co-localization observed between EGFP-ImuB and MCherry-DnaN, it was necessary to show that this observation could be

prevented genetically. To this end, PSOS(*imuA'*)-*egfp*-*imuB*^{AAAAG} was designed to encode a version of EGFP-ImuB that lacked the previously predicted β clamp-binding domain within the coding sequence of ImuB (Warner, *et al.*, 2010). In order to maintain all other characteristics similar to the previously tested, non-mutated PSOS(*imuA'*)-*egfp*-*imuB*, the pMCAINT::PSOS(*imuA'*)-*egfp*-*imuB* plasmid was the backbone for the cloning of pMCAINT::PSOS(*imuA'*)-*egfp*-*imuB*^{AAAAG}. The final construct was designed such that the locus encoding the predicted QLPLWG β clamp-binding domain within *imuB* (position 1712234..1713043 in the mc^{2}155 genome) could be excised from pMCAINT::PSOS(*imuA'*)-*egfp*-*imuB* by digestion with *Mau*BI. Similarly, the corresponding locus within pMCAINT::*imuB*^{AAAAG} (Warner, *et al.*, 2010) could be isolated similarly by digestion with *Mau*BI. Thereafter, the linear, truncated pMCAINT::PSOS(*imuA'*)-*egfp*-*imuB* molecule could be ligated with the DNA fragment containing the mutant AAAAGG allele from *imuB*^{AAAAG} to form a single ORF encoding *egfp*-*imuB*^{AAAAG}. The designed construct was validated by alignment and comparison of the WT sequence against that of the mutant β clamp-binding domain using *Clustal Omega* (Sievers and Higgins, 2014).

8.2. Generation of an *imuA'* Transcriptional Reporter Strain of *Msm*

The construct pMCAINT::PSOS(*imuA'*)-*egfp* was generated by ligating the 996 bp fragment of *Hin*dIII-digested pUC57::PSOS(*imuA'*)-*egfp* with the dephosphorylated 3,995 bp *Hin*dIII-linearized pMCAINT vector (**Figure 2-9**). The cloning strategy is indicated in **Figure 2-10**.

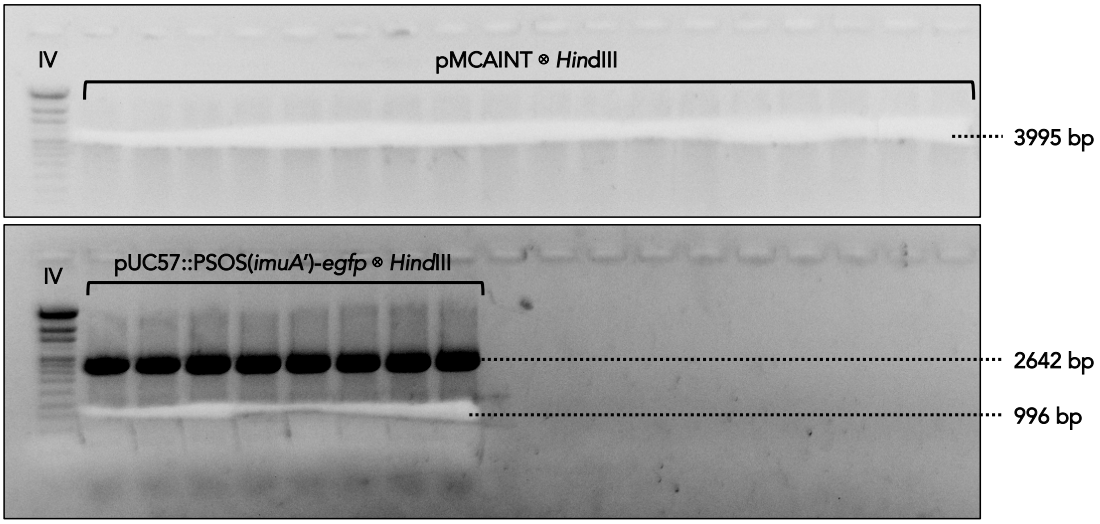

Figure 2-9 | Cloning of pMCAINT::PSOS(*imuA'*)-*egfp*
The portion of the gel extracted (clear) indicates the corresponding sizes of the bands used during cloning. Reaction products were separated on a 1 % (w/v) agarose TAE gel supplemented with 0.01 % (w/v) EtBr by electroporation under a 100 V electric field in TAE buffer. Gel picture was recorded and imaged using UV light illumination. The sizes of the product fragments (both excised and visible bands) are indicated. The symbol '⊗' indicates that the plasmid was digested by the indicated RE.

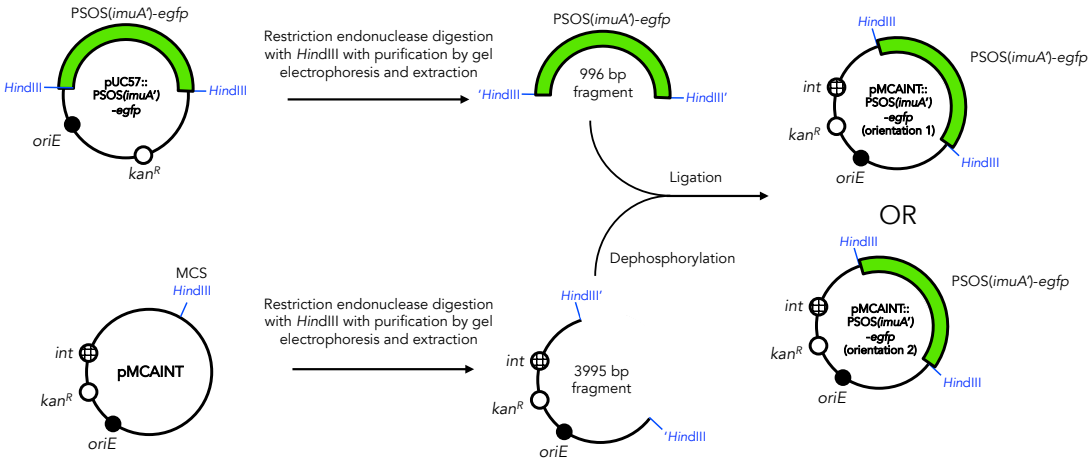

Figure 2-10 | Cloning strategy of pMCAINT::PSOS(*imuA'*)-*egfp*
The schematic represents that steps under taken to clone pMCAINT::PSOS(*imuA'*)-*egfp* from pMCAINT and pUC57::PSOS(*imuA'*)-*egfp*. The final product could yield plasmids with the insert ligated in either direction.

Ligation product was used to heat-shock transform competent DH5α cells and small-scale plasmid extractions were conducted on the resulting colonies. The RE enzyme *Xho*I was used as a preliminary screen of pMCAINT::PSOS(*imuA'*)-*egfp* (**Figure 2-11**). Positive clones are differentiated from self-ligated vector by the presence of two restriction sites – one in the insert and one in the vector.

This maps to fragments of 2,286 and 2,713 bp for orientation 1 (green) and 2141 and 2,858 bp for orientation 2 (blue), in comparison to the 3,995 bp digestion of self-ligated vector (red). After large-scale plasmid extractions, additional screening of pMCAINT::PSOS(*imuA'*)-*egfp* was performed by digestion with *Bst*BI and *Sma*I which yielded inconclusive results (**Figure 2-12**). For further clarification and to rule out the presence of concatamer inserts, both plasmids were screened with *Bgl*II, *Bam*HI, and *Pvu*I (**Figure 2-13**); and rescreened with *Xho*I (**Figure 2-14**).

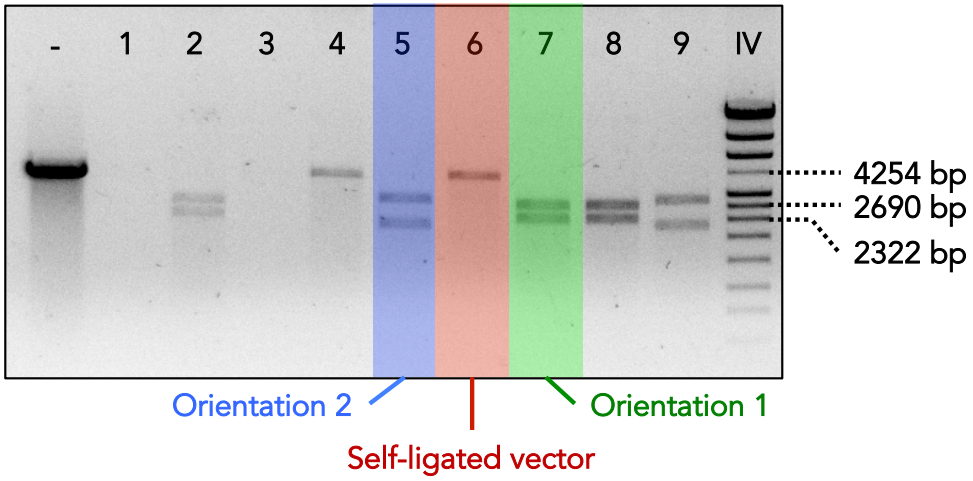

Figure 2-11 | *Xho*I screen of pMCAINT::PSOS(*imuA'*)-*egfp*
Reaction products were separated on a 1 % (w/v) agarose TAE gel supplemented with 0.01 % (w/v) EtBr by electroporation under a 100 V electric field in TAE buffer. Gel picture was recorded and imaged using UV light illumination. The sizes of selected *Roche molecular weight marker IV* fragments are indicated.

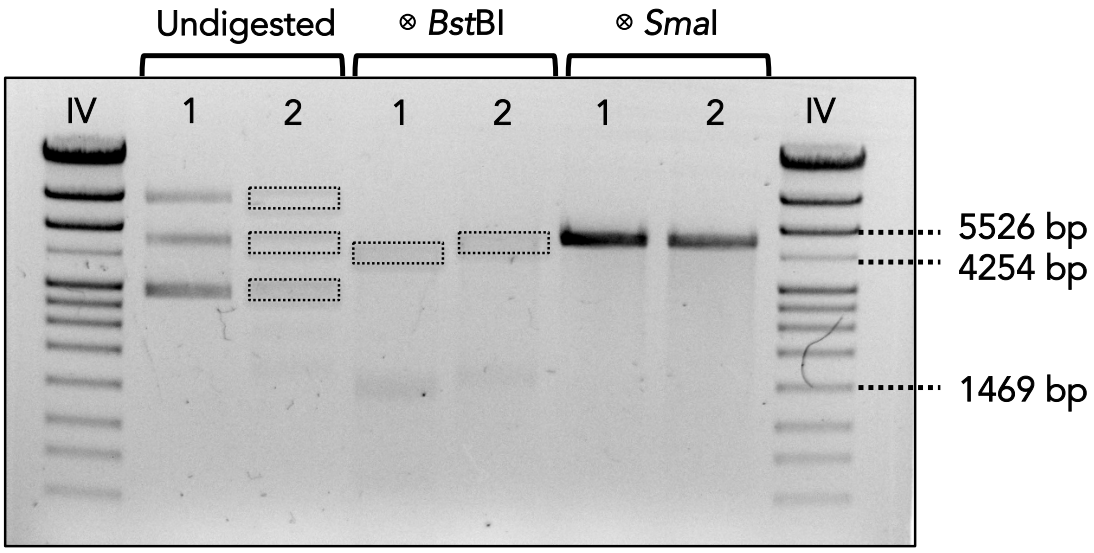

Figure 2-12 | pMCAINT::PSOS(*imuA'*)-*egfp* screened with *Bst*BI and *Sma*I
Gel image indicating the resulting fragment pattern of both orientation 1 (1) and orientation 2 (2) of pMCAINT::PSOS(*imuA'*)-*egfp* following digestion with either *Bst*BI or *Sma*I. Positive result for *Bst*BI digestion for orientation 1 is 770 and 4,225 bp; and 238 and 4,757 bp for orientation 2. SmaI is predicted to linearize (4,991 bp) the plasmid of both orientations. Reaction products were separated on a 1 % (w/v) agarose TAE gel supplemented with 0.01 % (w/v) EtBr by electroporation under a 100 V electric field in TAE buffer. Gel picture was recorded and imaged using UV light illumination. The sizes of selected *Roche molecular weight marker IV* fragments are indicated. Dotted rectangles indicate the position of bands clearly visible with altered contrast settings. The symbol '⊗' indicates that the plasmid was digested by the indicated RE.

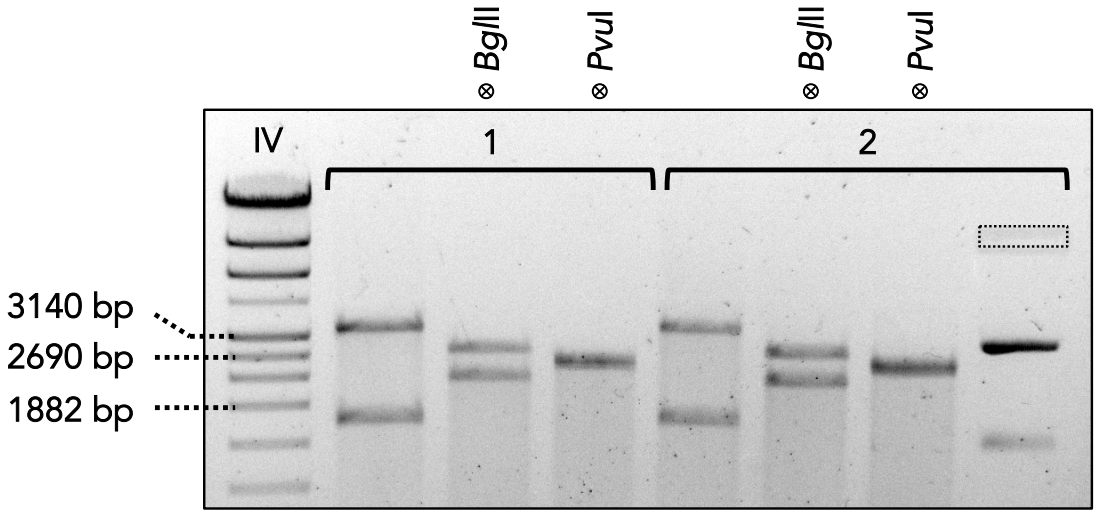

Figure 2-13 | pMCAINT::PSOS(*imuA'*)-*egfp* screened with *Bam*HI, *Bgl*II and *Pvu*I
Gel image indicating the resulting fragment pattern of both orientation 1 (1) and orientation 2 (2) of pMCAINT::PSOS(*imuA'*)-*egfp* following digestion with either *Bam*HI, *Bgl*II or *Pvu*I. Both plasmid orientations should fragment into 1,711 and 3,288 bp after digestion with *Bam*HI; 2,248 and 2,751 bp following digestion with *Bgl*II; and 2,437 and 2,558 bp (indistinguishable) after digestion with *Pvu*I. Reaction products were separated on a 1 % (w/v) agarose TAE gel supplemented with 0.01 % (w/v) EtBr by electroporation under a 100 V electric field in TAE buffer. Gel picture was recorded and imaged using UV light illumination. The sizes of selected *Roche molecular weight marker IV* fragments are indicated.

The dotted rectangle indicates the position of a band clearly visible with altered contrast settings. The symbol '⊗' indicates that the plasmid was digested by the indicated RE.

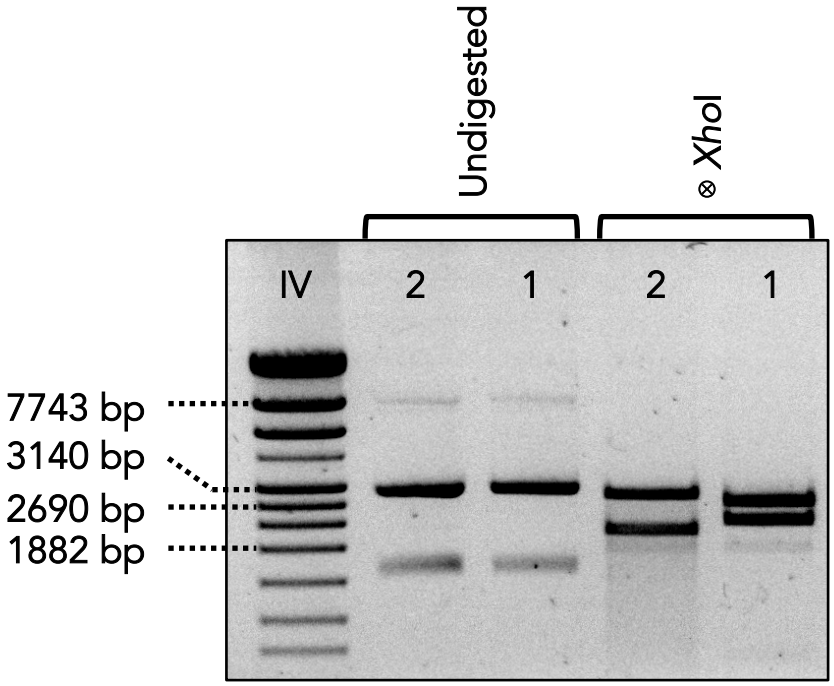

Figure 2-14 | Rescreen of pMCAINT::PSOS(*imuA'*)-*egfp* by digestion with *Xho*I
Orientation 1 and 2 products of the pMCAINT::PSOS(*imuA'*)-*egfp* were digested with *Xho*I. Reaction products were separated on a 1 % (w/v) agarose TAE gel supplemented with 0.01 % (w/v) EtBr by electroporation under a 100 V electric field in TAE buffer. Gel picture was recorded and imaged using UV light illumination. The sizes of selected *Roche molecular weight marker IV* fragments are indicated. The symbol '⊗' indicates that the plasmid was digested by the indicated RE.

Verified plasmids were subsequently electroporated into WT *Msm* to allow plasmid integration into the genome (see time constants presented in **Table 2-8**). Of the resultant transformed *Msm* colonies, two of each insert orientation were screened by PCR following genome release by colony boil. Primers *FP_for* and *FP_rev* were used to amplify the 71 bp region specific to the EGFP-encoding sequence of *egfp* (**Figure 2-15**) and the amplicons were visualized following separation by gel electrophoresis on a 4 % (w/v) agarose gel (**Figure 2-16**). Positive strains were identified, and future experimentation was conducted only with positively identified clones containing the PSOS(*imuA'*)-*egfp* insert in orientation 1.

Table 2-8 | Time constants generated during the development of WT::PSOS(*imuA'*)-*egfp*

PSOS(*imuA'*)-*egfp* insert orientation	pMCAINT::PSOS(*imuA'*)-*egfp* amount (ng)	Time constant, μ
Orientation 1	0.0	24.3
Orientation 1	1000	24.4
Orientation 1	2000	24.2
Orientation 1	4000	24.0
Orientation 2	0.0	24.1
Orientation 2	1000	23.8
Orientation 2	2000	23.8
Orientation 2	4000	23.8

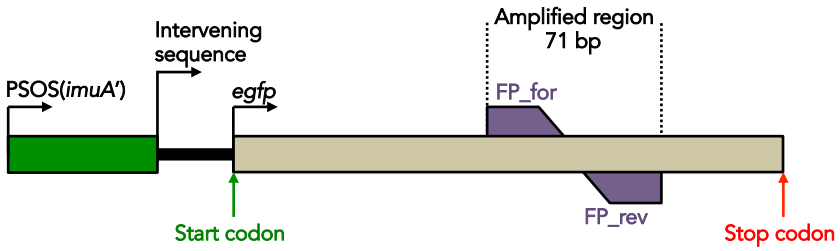

Figure 2-15 | Rationale of WT::PSOS(*imuA'*)-*egfp* PCR screen
Schematic representation of the PCR screening strategy used to screen WT::PSOS(*imuA'*)-*egfp*. The primers FP_for and FP_rev were used to amplify a 71 bp region specific to *egfp*.

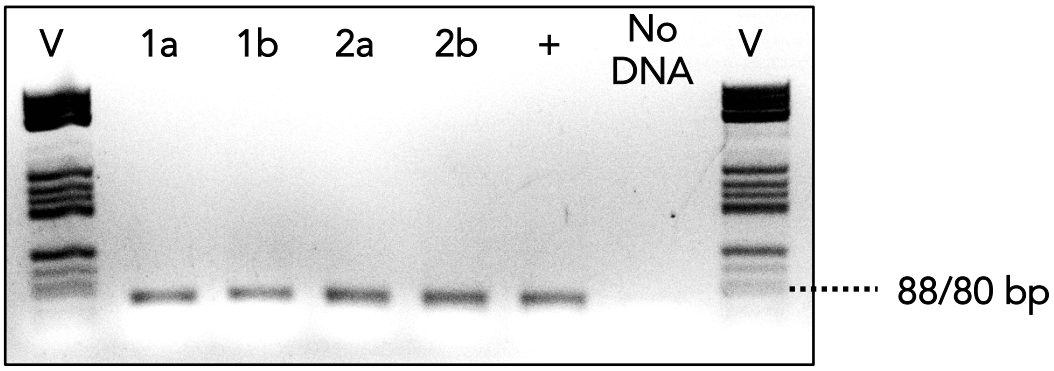

Figure 2-16 | PCR screen of putative WT::PSOS(*imuA'*)-*egfp*
PCR was conducted using primer FP_for and FP_rev to screen for the presence of a 71 bp region specific to *egfp* in putative *Msm* transformants. Two colonies (a or b) with either orientation 1 or 2 insert were screened. Positive control (+) was conducted on 200 ng of pUC57::PSOS(*imuA'*)-*egfp* plasmid. PCR products were separated on a 4 % (w/v) agarose TAE gel supplemented with 0.01 % (w/v) EtBr by electroporation under a 70 V electric field in TAE buffer. Gel picture was recorded and imaged using UV light illumination. The sizes of selected *Roche molecular weight marker V* fragments are indicated.

8.3. Fluorescent Fusion Proteins of Mutasome Components Expressed in *Msm*

8.3.1. Tagged Variants of ImuB

8.3.1.1. GFP-ImuB

pUC57::*gfp-imuB'* was digested with *Dra*I, *Cla*I and *Blp*I. The resultant fragments were separated in a 1 % (w/v) agarose gel (**Figure 2-17**) before the band corresponding to the fragment of interest (1,991 bp) was excised from the gel and purified. Simultaneously, pMCAINT::*imuB* was digested with the RE enzymes *Cla*I and *Blp*I. Following separation of the fragments on a 1 % (w/v) agarose gel, the 4,994 bp band corresponding to the complementary vector region of the plasmid was purified from the gel. The cloning strategy implemented in the development of pMCAINT::*gfp-imuB* is indicated in **Figure 2-18**. It was necessary to digest pUC57::*gfp-imuB'* with an additional, non-cloning RE enzyme (*Dra*I) in order to resolve the desired *gfp-imuB'* fragment from the remaining plasmid fragment of similar size after separation by gel electrophoresis.

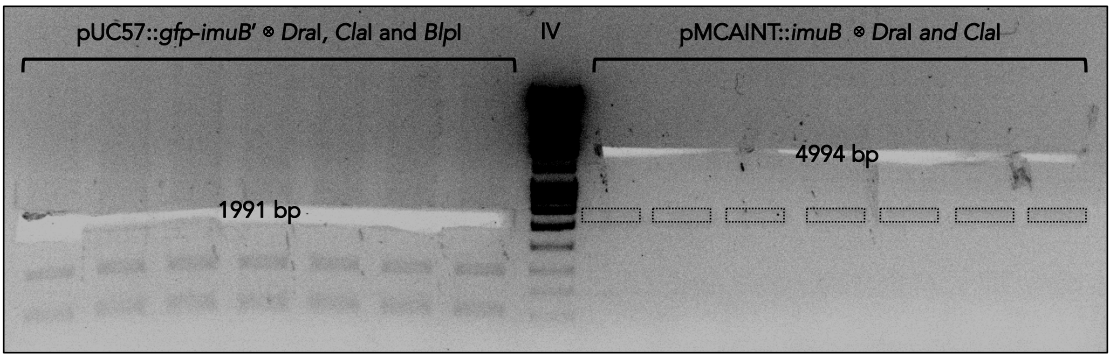

Figure 2-17 | Cloning of pMCAINT::*gfp-imuB*
The portion of the gel extracted (clear) indicates the corresponding sizes of the bands used during cloning. Reaction products were separated on a 1 % (w/v) agarose TAE gel supplemented with 0.01 % (w/v) EtBr by electroporation under a 100 V electric field in TAE buffer. Gel picture was recorded and imaged using UV light illumination. The sizes of the excised fragments are indicated. Dotted rectangles indicate the position of bands clearly visible with altered contrast settings. The symbol '⊗' indicates that the plasmid was digested by the indicated REs.

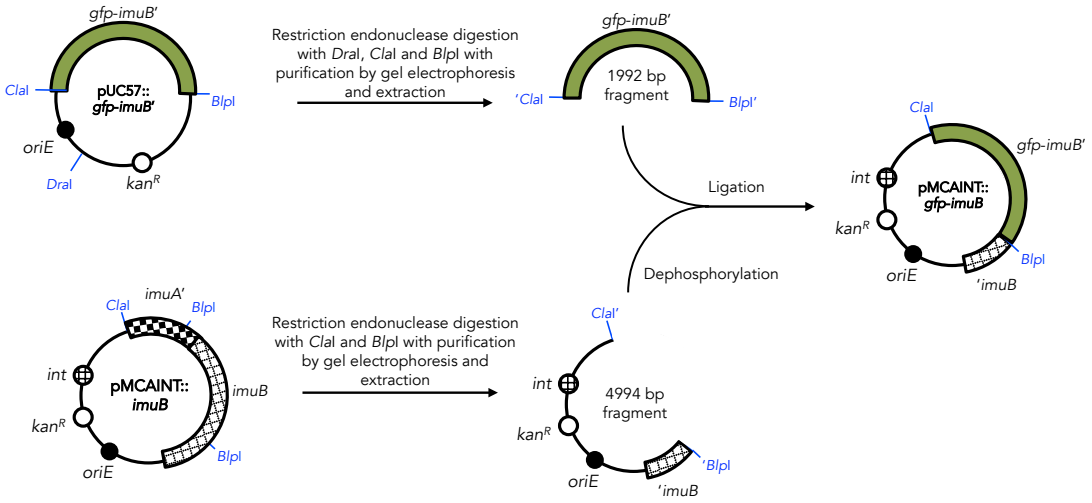

Figure 2-18 | Cloning strategy of pAINT::*gfp-imuB*
The schematic represents that steps under taken to clone pAINT::*gfp-imuB* from pMCAINT::*imuB* and pUC57::*gfp-imuB*.

The two extracted fragments were ligated using T4 DNA ligase and the resultant reaction product was used to transform DH5α cells. Small-scale plasmid extractions were performed on the resultant KAN-resistant colonies, containing the putative pMCAINT::*gfp-imuB* plasmid. Thirty-two colonies were preliminary screened by RE digestion with *Bam*HI (**Figure 2-19**), of which six clones yielded the positive, visible bands corresponding to 3,284, 1,734, 1,103, and 738 bp (green lanes).

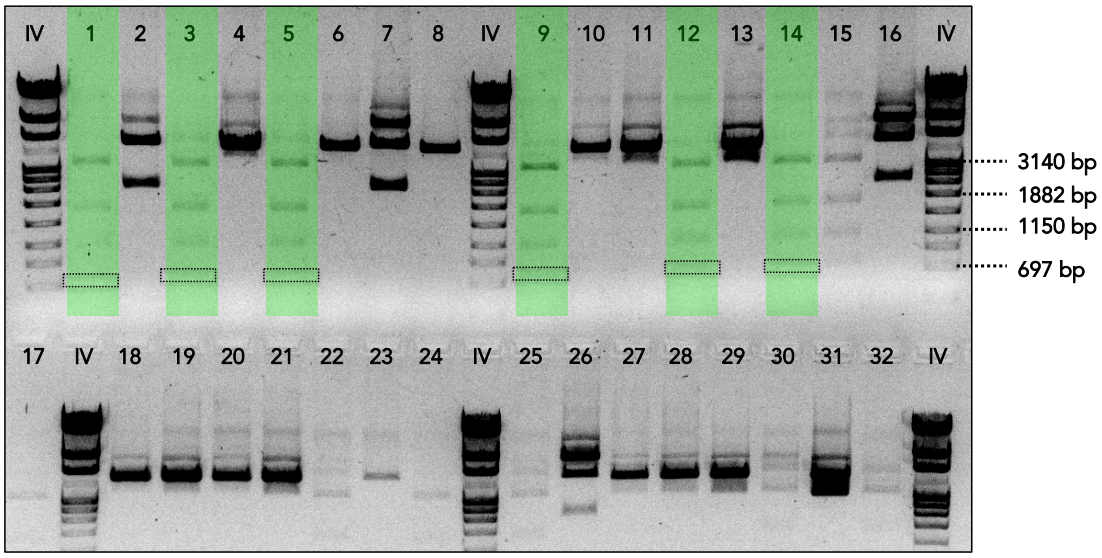

Figure 2-19 | *Bam*HI screen of putative pMCAINT::*gfp-imuB* plasmids
Green lanes indicated positively identified clones and were selected for further screening. Reaction products were separated on a 1 % (w/v) agarose TAE gel supplemented with 0.01 % (w/v) EtBr by electroporation under a 100 V electric field in TAE buffer. Gel picture was recorded and imaged using UV light illumination. The sizes of selected *Roche molecular weight marker IV* fragments are indicated. Dotted rectangles indicate the position of bands clearly visible with altered contrast settings.

The positively identified cultures (green lanes in **Figure 2-19**) were screened by digestion with *Blp*I and separated by electrophoresis on a 1 % (w/v) agarose gel (**Figure 2-20**). After a large-scale plasmid extraction, the putative plasmid was further characterized and validated by RE digestion with *Dra*III, *Nsp*I, *Pvu*II, and *Pst*I (**Figure 2-21**). The positively identified pMCAINT::*gfp-imuB* plasmid was subsequently electroporated into the Δ*imuB* mutant (Warner, *et al.*, 2010) (**Table 2-9**).

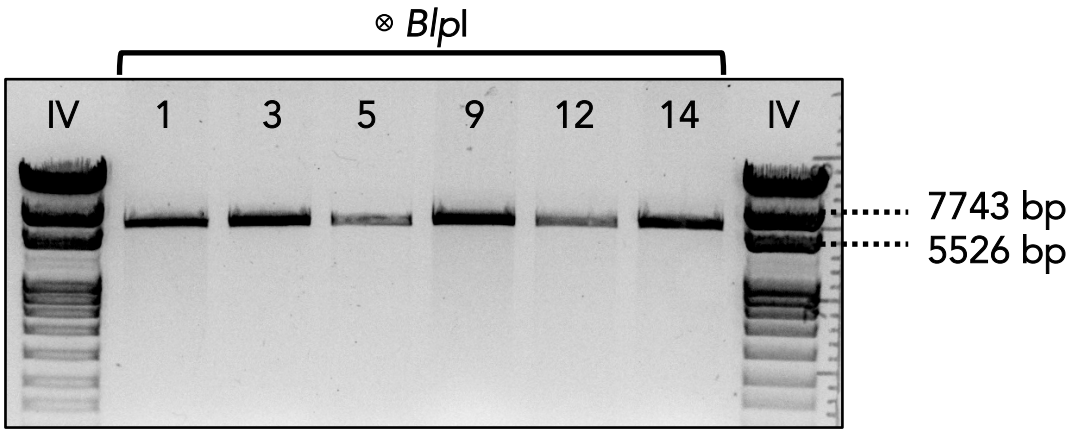

Figure 2-20 | *Blp*I screen of selected putative clones of pMCAINT::*gfp-imuB*
Positive pMCAINT::*gfp-imuB* plasmids would be linearized by *Blp*I, yielding a single fragment of 6,986 bp. Reaction products were separated on a 1 % (w/v) agarose TAE gel supplemented with 0.01 % (w/v) EtBr by electroporation under a 100 V electric field in TAE buffer. Gel picture was recorded and imaged using UV light illumination. The sizes of selected *Roche molecular weight marker IV* fragments are indicated.

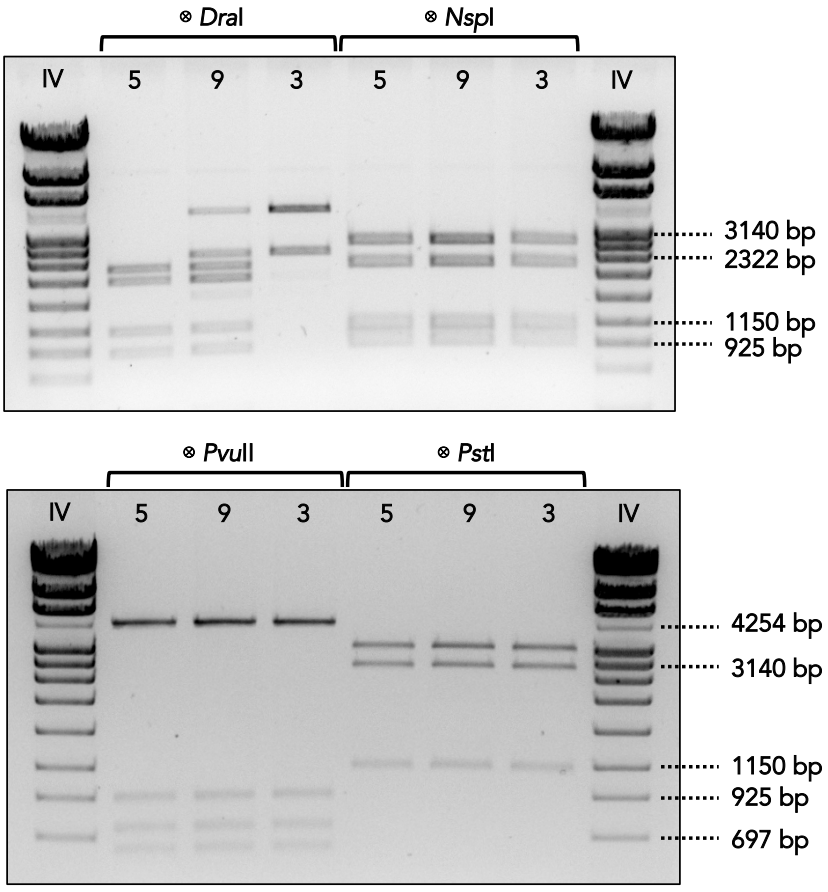

Figure 2-21 | Additional RE screening of pMCAINT::*gfp-imuB*
Top: Selected putative pMCAINT::*gfp-imuB* clones screened with either *Dra*I or *Nsp*I. Positive *Dra*I digestion would yield a linearized plasmid of 6,986 bp; while positive *Nsp*I digestion would yield 947, 1,144, 2,130, and 2,781 bp. The *Dra*I digest exhibited a degree of star-activity. Bottom: Selected putative pMCAINT::*gfp-imuB* clones screened with either *Pvu*II or *Pst*I. Positive *Pvu*II

digestion would yield fragments of 90, 636, 741, 924, and 4,595 bp; while positive *Pst*I digestion would yield 1,132, 2,620, and 3,246 bp.
Reaction products were separated on a 1 % (w/v) agarose TAE gel supplemented with 0.01 % (w/v) EtBr by electroporation under a 100 V electric field in TAE buffer. Gel picture was recorded and imaged using UV light illumination. The sizes of selected *Roche molecular weight marker IV* fragments are indicated.

Table 2-9 | Record of time constants generated during the electroporation of pMCAINT::*gfp-imuB* into Δ*imuB*

pMCAINT::*gfp-imuB* amount (ng)	Time constant, μ
0.0	22.9
1000	*Not recorded*
1000	22.5
2000	22.7
2000	22.5
4000	22.3
4000	22.5

The electroporation yielded more than 50 individual, KAN-resistant colonies (colonies were absent from the negative control in which no plasmid DNA was included in electroporation mixture), of which 13 colonies were randomly selected for screening by PCR after colony boil (**Figure 2-22**). Primers *GFP_Comlp_Forward* and *GFP_Compl_Reverse* were designed to amplify a 547 bp region specific to the *gfp* gene (**Figure 2-23**). Selected PCR-positive colonies of Δ*imuB*::*gfp-imuB* were cultured and used for further characterization.

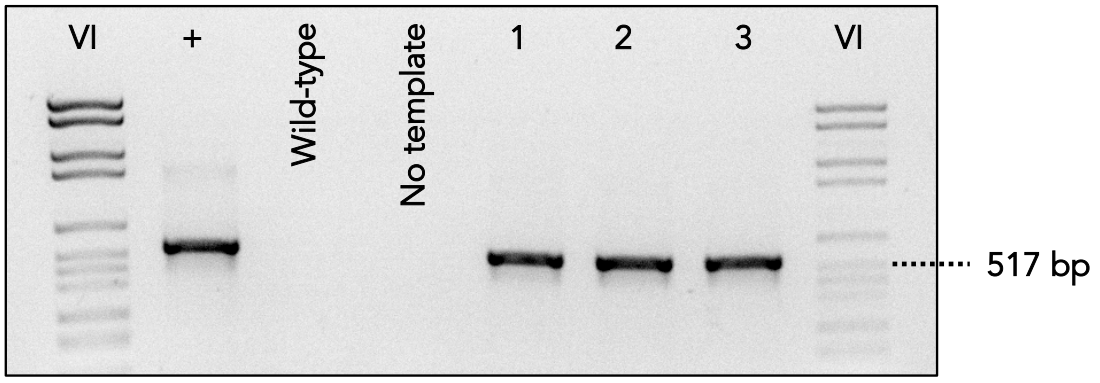

Figure 2-22 | Colony boil PCR screen of putative Δ*imuB*::*gfp-imuB* colonies
PCR was conducted using primers GFP_Comlp_Forward and GFP_Compl_Reverse to screen for the presence of a 547 bp region specific to *gfp-imuB* in putative *Msm* transformants. Positive control (+) was conducted on 200 ng of pUC57::*gfp-imuB*' plasmid. PCR products were separated on a 2 % (w/v) agarose TAE gel supplemented with 0.01 % (w/v) EtBr by electroporation under a 100 V electric field in TAE buffer. Gel picture was recorded and imaged using UV light illumination. The sizes of selected *Roche molecular weight marker VI* fragments are indicated.

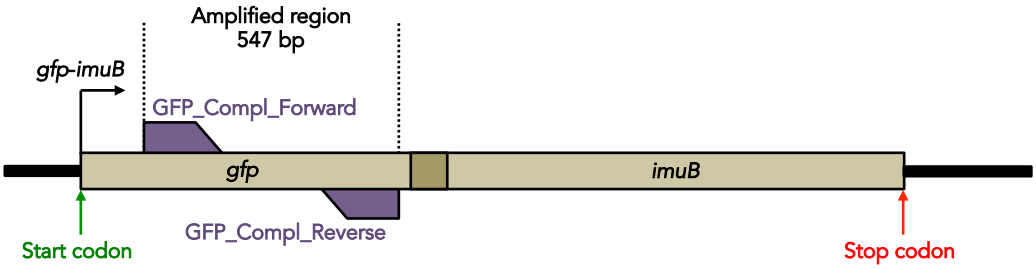

Figure 2-23 | Rational behind PCR screening of Δ*imuB*::*gfp-imuB*
Schematic of the strategy used for screening of Δ*imuB*::*gfp-imuB* by PCR amplification. The primers GFP_Compl_Forward and GFP_Compl_Reverse were used to amplify a 547 bp region specific to *gfp*.

8.3.1.2. EGFP-ImuB

pUC57::PSOS(*imuA'*)-*egfp-imuB'* was digested with *Dra*I, *Cla*I and *Blp*I and the resulting 2,401 bp band was extracted and ligated with the 4,994 bp fragment extracted after the digestion of pMCAINT::*imuB* with *Cla*I and *Blp*I (**Figure 2-24**). The cloning strategy implemented is presented in **Figure 2-25**. After heat-shock transformation of competent DH5α cells with the ligation product, twenty-four isolated colonies were preliminarily screened for the presence of pMCAINT::PSOS(*imuA'*)-*egfp-imuB* by digestion of small-scale plasmid extracts with *Pvu*I (**Figure 2-26**). Owing to an ambiguity in the *Pvu*I screen,

large-scale plasmid extractions were performed on putative positively identified candidates and the samples were further screened with *Hin*dIII (**Figure 2-27**) and *Nae*I (**Figure 2-28**). Clone 12 was selected for final confirmation by digestion with *Sma*I (**Figure 2-29**).

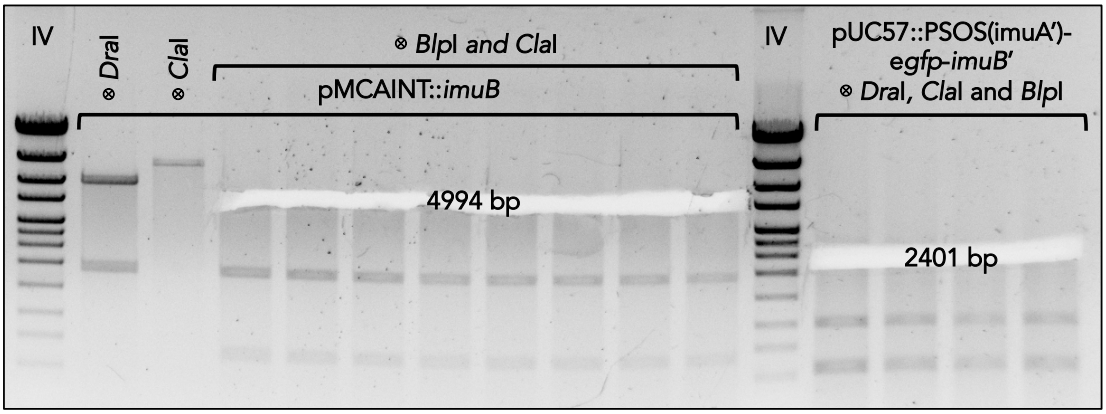

Figure 2-24 | Cloning of pMCAINT::PSOS(*imuA'*)-*egfp-imuB*
The portion of the gel extracted (clear) indicates the corresponding sizes of the bands used during cloning. Reaction products were separated on a 1 % (w/v) agarose TAE gel supplemented with 0.01 % (w/v) EtBr by electroporation under a 100 V electric field in TAE buffer. Gel picture was recorded and imaged using UV light illumination. The sizes of excised bands are indicated.

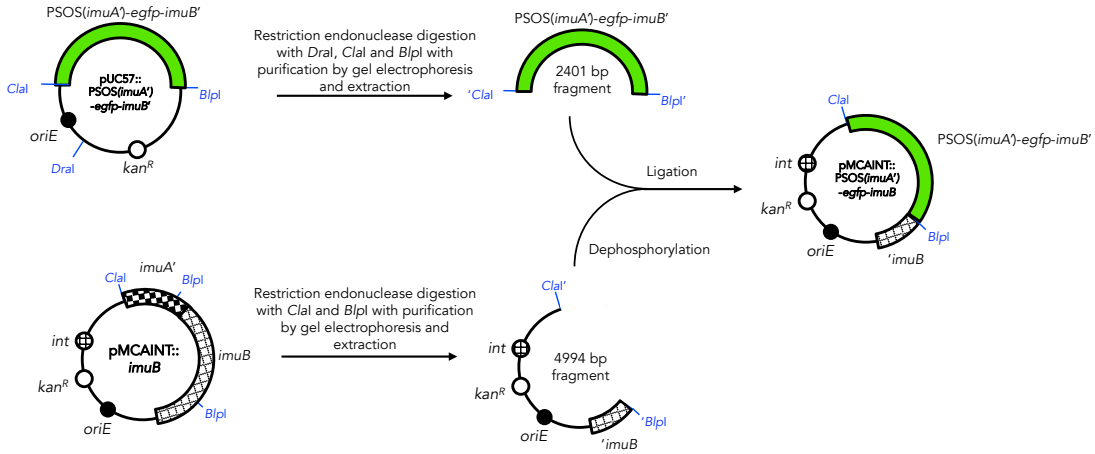

Figure 2-25 | Cloning strategy of pMCAINT::PSOS(*imuA'*)-*egfp-imuB*
The schematic represents that steps under taken to clone pMCAINT::PSOS(*imuA'*)-*egfp-imuB* from pMCAINT::*imuB* and pUC57::PSOS(*imuA'*)-*egfp-imuB'*.

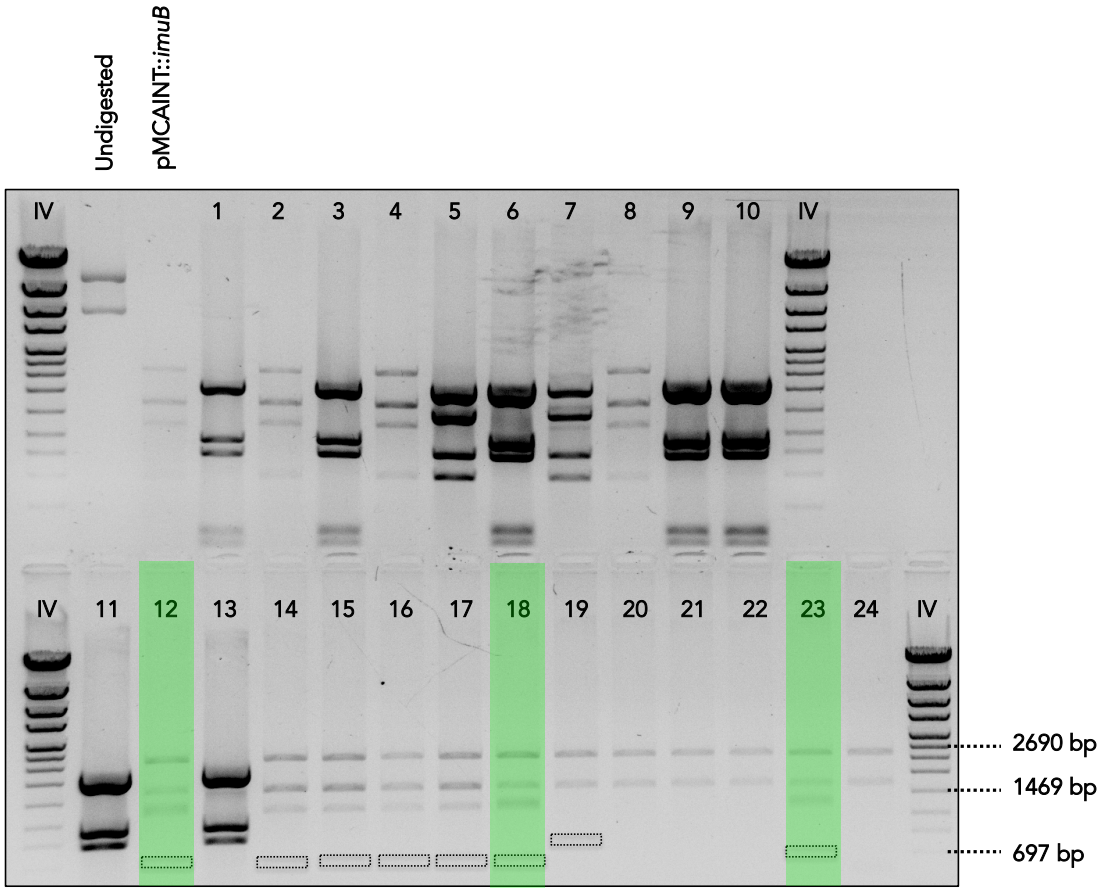

Figure 2-26 | *Pvu*I screen of putative pMCAINT::PSOS(*imuA'*)-*egfp*-*imuB* clones
Positive screen of the pMCAINT::PSOS(*imuA'*)-*egfp*-*imuB* plasmid would generate fragments with sizes 665, indistinguishable 1,274 and 1,355, 1,668, and 2,437 bp. The unambiguous, differential band is 1,355 bp. Green lanes indicate clones that were deemed positive due to a thick band at approximately 1,300 bp (third band from top of lane), representing the two indistinguishable bands. Reaction products were separated on a 1 % (w/v) agarose TAE gel supplemented with 0.01 % (w/v) EtBr by electroporation under a 100 V electric field in TAE buffer. Gel picture was recorded and imaged using UV light illumination. The sizes of selected *Roche molecular weight marker IV* fragments are indicated. Dotted rectangles indicate the position of bands clearly visible with altered contrast settings.

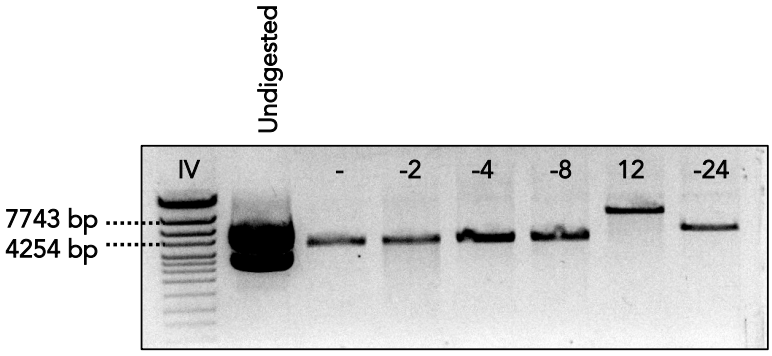

Figure 2-27 | *Hin*dIII screen of putative pMCAINT::PSOS(*imuA'*)-*egfp*-*imuB* clones
Negative (-) samples were included to verify the previous *Pvu*I digestion result. Owing to the presence of the PSOS(*imuA'*)-*egfp* portion of the construct (*Hin*dIII site absent), which replaced the *imuA'* gene upstream of *imuB* (*Hin*dIII present), a positive screen would result in a single, linearized fragment with a size of 7,389 bp, while a negative result (pMCAINT::*imuB*) would be digested at two positions on the plasmid, yielding two indistinguishable bands of 3,669 and 3,999 bp. Reaction products were separated on a 1 % (w/v) agarose TAE gel supplemented with 0.01 % (w/v) EtBr by electroporation under a 120 V electric field in TAE buffer. Gel picture was recorded and imaged using UV light illumination. The sizes of selected *Roche molecular weight marker IV* fragments are indicated.

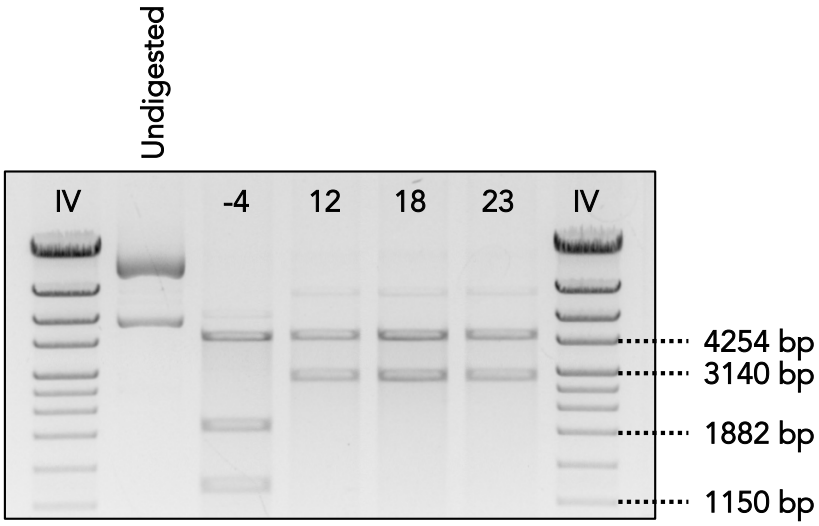

Figure 2-28 | *Nae*I screen of selected pMCAINT::PSOS(*imuA'*)-*egfp*-*imuB* clones
Negatively identified clone number 4 was included as a negative reference. A positive *Nae*I screen yielded a 4,424 bp band and a distinguishable 2,965 bp band. In contrast, pMCAINT::*imuB* yielded 1,280, 1,956, and 4,424 bp sized fragments when digested with *Nae*I. Reaction products were separated on a 1 % (w/v) agarose TAE gel supplemented with 0.01 % (w/v) EtBr by electroporation under a 100 V electric field in TAE buffer. Gel picture was recorded and imaged using UV light illumination. The sizes of selected *Roche molecular weight marker IV* fragments are indicated.

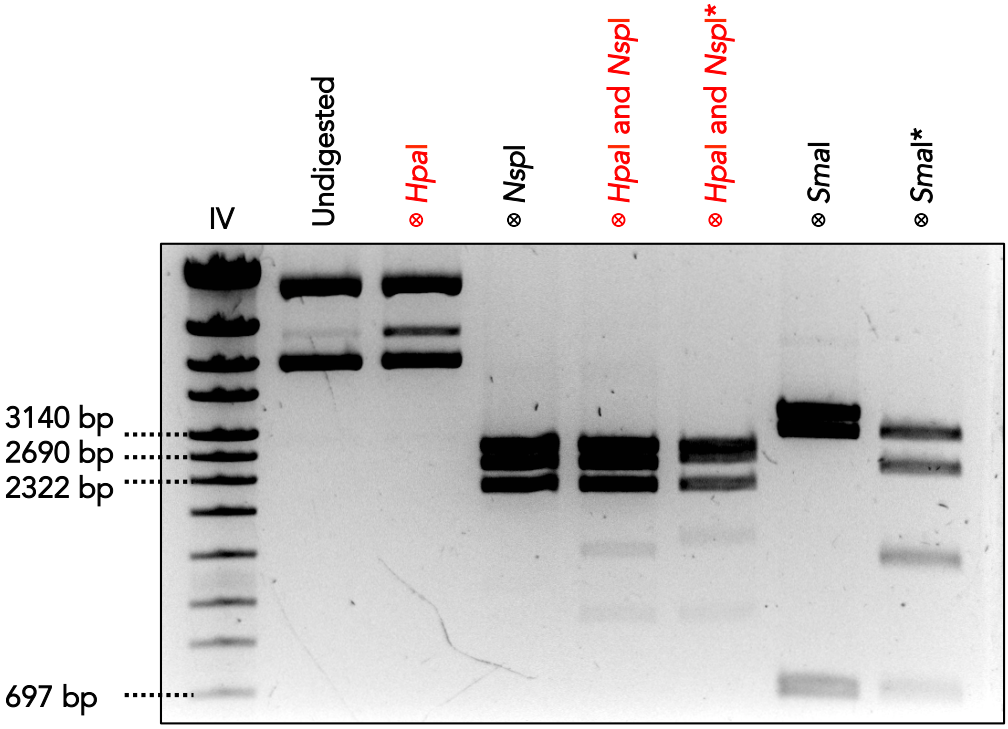

Figure 2-29 | Confirmation of pMCAINT::PSOS(*imuA'*)-*egfp*-*imuB* (clone 12) by *Nsp*I and *Sma*I digest
Positive *Nsp*I screen of pMCAINT::PSOS(*imuA'*)-*egfp*-*imuB* yields 2,130, distinguishable 2,490, and 2,781 bp fragments. A positive SmaI screen yielded 678, 3,126, and distinguishable 3,585 bp fragments. *Hpa*I was also included in this screen; however, it did not digest completely but still proved useful in confirming clone number 12 (compare lane 5 to lane 6). For comparison purposes, a negative control plasmid was also digested and is indicated by an asterisk. Reaction products were separated on a 1 % (w/v) agarose TAE gel supplemented with 0.01 % (w/v) EtBr by electroporation under a 100 V electric field in TAE buffer. Gel picture was recorded and imaged using UV light illumination. The sizes of selected *Roche molecular weight marker IV* fragments are indicated.

pMCAINT::PSOS(*imuA'*)-*egfp*-*imuB* was electroporated into multiple strains of *Msm* (time constants presented in **Table 2-10**) and, following 4 days of incubation at 37 °C, over 1,000 colonies formed, of which 20 were screened by PCR. However, genotypic confirmation of successful transformation by PCR proved problematic due to a persistent failure of the negative control. Positive bands were consistently amplified in controls containing no DNA (data not shown), likely due to contamination of laboratory equipment with DNA. Therefore, screening was performed by direct observation of green fluorescence under a confocal fluorescent microscope following exposure of selected 5 ml KAN-resistant *Msm* liquid cultures to 1× MIC MMC for 4 h. This

method of screening could only confirm positive results and negative results would need to be further screened by genotype to confirm. Due to subsequent results and time constraints, this was not performed.

Table 2-10 | Record of time constants generated during the electroporation of pMCAINT::PSOS(*imuA'*)-*egfp-imuB* into various *Msm* backgrounds

Msm strain	pMCAINT::PSOS(*imuA'*)-*egfp-imuB* amount (ng)	Time constant, μ
Δ*imuB*	0.0	23.6
Δ*imuB*	1000	23.9
Δ*imuB*	2000	23.8
Δ*imuB*	4000	23.5
Δ*dnaE2*	2000	23.2
dnaE2^{AIA}	0.0	24.3
dnaE2^{AIA}	1000	24.4
dnaE2^{AIA}	4000	24.0
Δ*imuA'*	0.0	21.5
Δ*imuA'*	1000	22.0
Δ*imuA'*	2000	22.1
Δ*imuA'*	4000	22.0

8.3.1.3. MEos4a-ImuB

pUC57::PSOS(*imuA'*)-*mEos4a-imuB'* was digested with *Dra*I, *Cla*I and *Blp*I and the resultant 2,354 bp fragment was extracted following separation by gel electrophoresis. Additionally, pMCAINT::*imuB* was digested with *Cla*I and *Blp*I to yield a 4,995 bp fragment that was similarly purified after separation of digestion products through a 1 % agarose gel (**Figure 2-30**). Ligation reactions were conducted with 50 ng of the digested pMCAINT::'*imuB* vector and either 23.6, 70.8 or 118.0 ng of PSOS(*imuA'*)-*mEos4a-imuB'* fragment insert for 1:1, 1:3, and 1:5 vector-to-insert ratios. The cloning strategy adopted is illustrated in **Figure 2-31**. The ligation product was transformed into competent DH5α by

the heat-shock method. After 24 h of incubation, 600 isolated colonies formed on 2 plates, while 50 colonies formed on the negative control (no insert) plate. Subsequently, 10 colonies were selected for screening and small-scale plasmid samples of each clone were digested with *Nsp*I (**Figure 2-32**). Clone number 5, with a putative pMCAINT::PSOS(*imuA'*)-*mEos4a-imuB* plasmid, was further confirmed by digestion with *Nco*I (**Figure 2-33**).

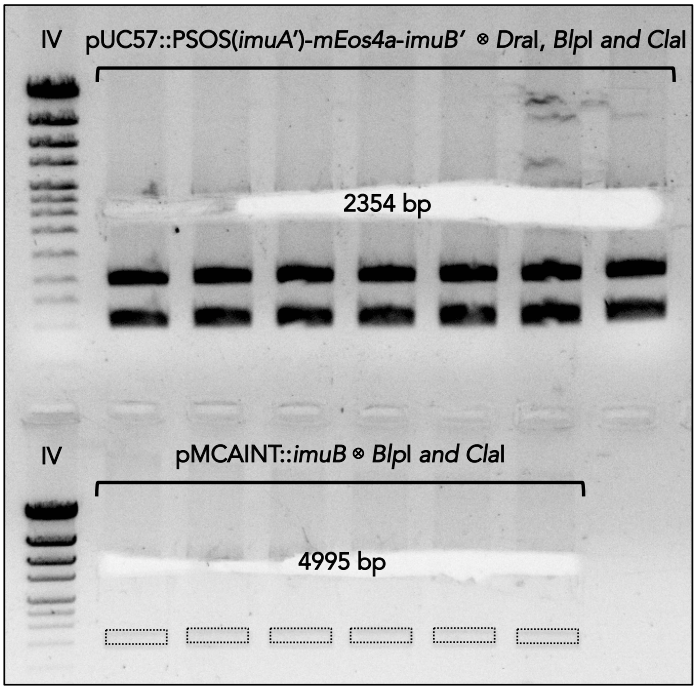

Figure 2-30 | Gel extraction performed during the cloning of pMCAINT::PSOS(*imuA'*)-*mEos4a-imuB*
The portion of the gel extracted (clear) indicates the corresponding sizes of the bands used during cloning. Reaction products were separated on a 1 % (w/v) agarose TAE gel supplemented with 0.01 % (w/v) EtBr by electroporation under a 100 V electric field in TAE buffer. Gel picture was recorded and imaged using UV light illumination. The sizes of excised bands are indicated. Dotted rectangles indicate the position of bands clearly visible with altered contrast settings.

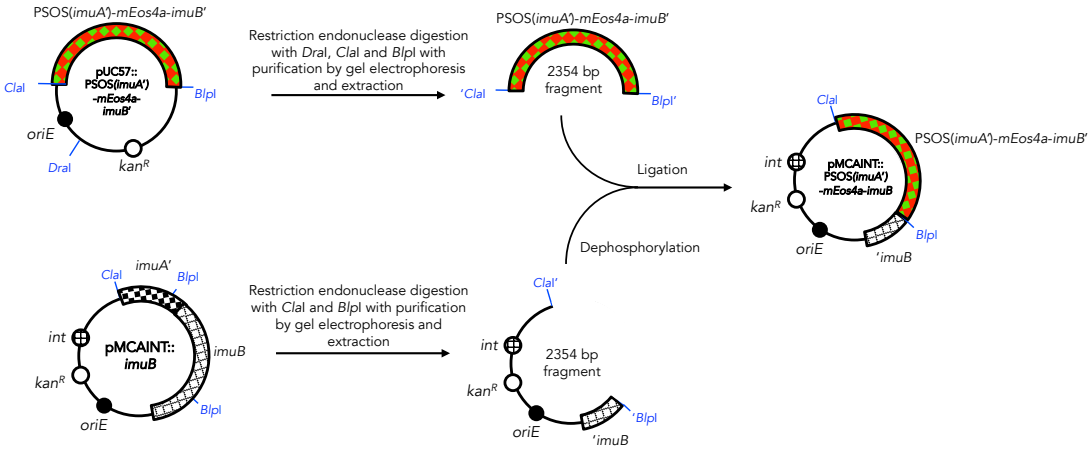

Figure 2-31 | Cloning strategy of pMCAINT::PSOS(*imuA'*)-*mEos4a-imuB*
The schematic represents that steps under taken to clone pMCAINT::PSOS(*imuA'*)-*mEos4a-imuB* from pMCAINT::*imuB* and pUC57::PSOS(*imuA'*)-*mEos4a-imuB'*.

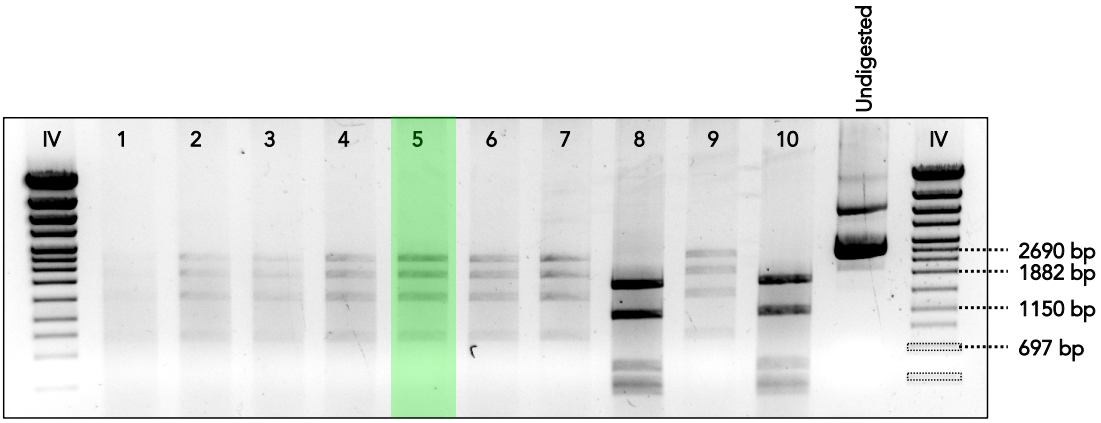

Figure 2-32 | Preliminary NspI screen of putative pMCAINT::PSOS(*imuA'*)-*mEos4a-imuB* transformants
Clone number Lane 5 was selected for further screening due to the positively identifiable restriction fragment products of 890, a distinct 1,568, 2,130, and 2,781 bp in size. Reaction products were separated on a 1 % (w/v) agarose TAE gel supplemented with 0.01 % (w/v) EtBr by electroporation under a 100 V electric field in TAE buffer. Gel picture was recorded and imaged using UV light illumination. The sizes of selected *Roche molecular weight marker IV* fragments are indicated. Dotted rectangles indicate the position of bands clearly visible with altered contrast settings.

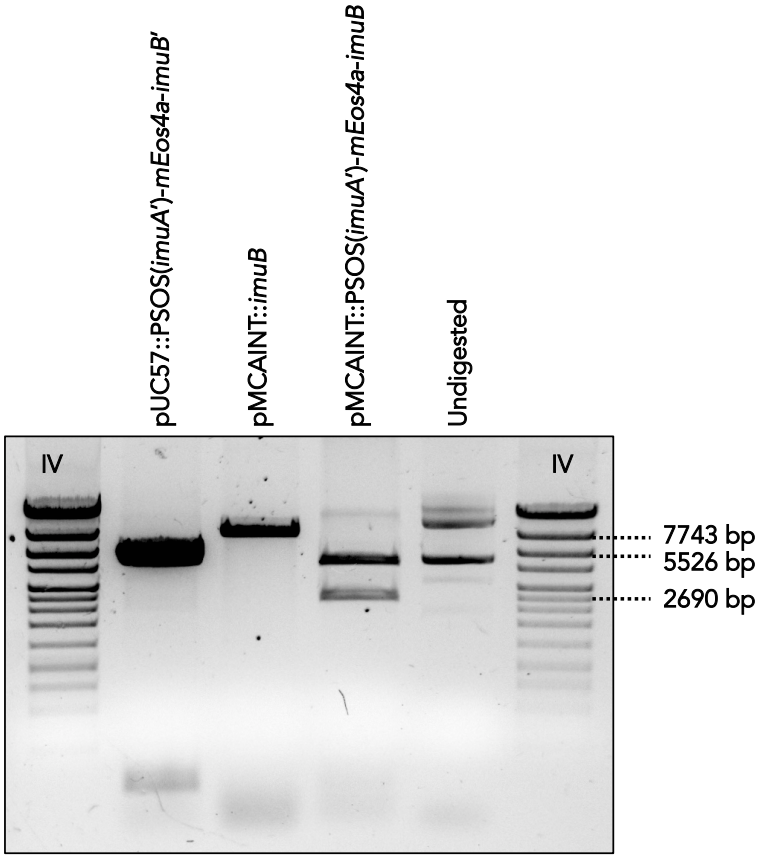

Figure 2-33 | Final confirmation of pMCAINT::PSOS(*imuA'*)-*mEos4a-imuB* by *Nco*I digestion
The two NcoI restriction sites of pMCAINT::PSOS(*imuA'*)-*mEos4a-imuB* would result in three fragments with sizes 211, 2,574, and 4,580 bp. The parental pMCAINT::*imuB* is only linearized by this RE. Reaction products were separated on a 1 % (w/v) agarose TAE gel supplemented with 0.01 % (w/v) EtBr by electroporation under a 100 V electric field in TAE buffer. Gel picture was recorded and imaged using UV light illumination. The sizes of selected *Roche molecular weight marker IV* fragments are indicated.

Thereafter, the confirmed plasmid was electroporated into Δ*imuB* (time constants presented in **Table 2-11**) and, after growth of colonies, two were selected to be screened by direct observation of photoswitchable MEos4a fluorescence following exposure of resultant KAN-resistant liquid cultures to 1× MIC MMC for 4 h.

Table 2-11 | Time constants during the electroporation of pMCAINT::PSOS(*imuA'*)-*mEos4a-imuB* into Δ*imuB*

pMCAINT::PSOS(*imuA'*)-*mEos4a-imuB* amount (ng)	Time constant, μ
0.0	23.2
1000	23.8
2000	23.6
4000	23.6

8.3.1.4. EGFP-ImuB^{AAAAG}

With the aim of introducing the ^{352}AAAAGG^{357} mutated beta clamp binding site of ImuB (Warner, *et al.*, 2010) into the EGFP-ImuB protein, the corresponding encoding nucleotide sequence from pMCAINT::*imuB*^{AAAAG} containing the mutant sequence was designed as previously described. Vector construction and screening was performed by a third-party. Briefly, the mutant AAAAG-encoding sequence of pMCAINT::*imuB*^{AAAAG} (Warner, *et al.*, 2010) was swapped into the corresponding position of PSOS(*imuA'*)-*egfp-imuB* by digestion of both plasmids with *Mau*BI (**Figure 2-34**). The 810 bp fragment derived from pMCAINT::*imuB*^{AAAAG} was ligated with the 6,587 bp product derived from PSOS(*imuA'*)-*egfp-imuB* to produce a single ORF encoding EGFP-FLAG-ImuB^{AAAAG} contained within the mycobacterial integrative shuttle vector, pMCAINT, which was cloned in DH5α *E. coli* with KAN 50 mg/ml selection. The isolated pMCAINT::PSOS(*imuA'*)-*egfp-imuB*^{AAAAG} plasmid was screened by RE digestion verification (data not shown). Electroporation of the pMCAINT::PSOS(*imuA'*)-*egfp-imuB*^{AAAAG} plasmid into *Msm* was performed by a third-party (data not shown).

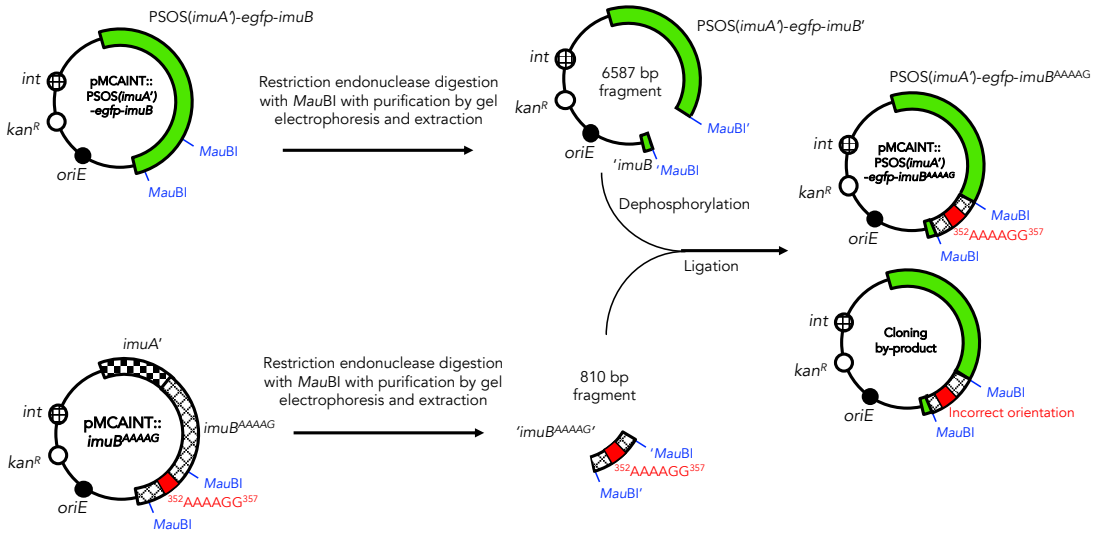

Figure 2-34 | Cloning strategy of pMCAINT::PSOS(*imuA'*)-*egfp-imuB*^{AAAAG}
The schematic represents that steps under taken to clone pMCAINT::PSOS(*imuA'*)-*egfp-imuB*^{AAAAG} from pMCAINT::*imuB*^{AAAAG} and pMCAINT::PSOS(*imuA'*)-*egfp-imuB*. The final ligation step yields two potential plasmids with opposite insert orientations.

8.3.2. Tagged variants of DnaE2

8.3.2.1. EGFP-DnaE2

To generate the construct pTTP1B::*egfp-dnaE2*, both the parental plasmids pTTP1B::*dnaE2* and pUC57::*egfp-dnaE2'* were digested with *Kpn*I. The digested vector with a size of 10,749 bp (derived from pTTP1B::*dnaE2*) and the insert fragment with a size of 1,525 bp (derived from pUC57::*egfp-dnaE2'*) were purified after separation by gel electrophoresis (**Figure 2-35**). The two extracted DNA fragments were non-directionally ligated together before the ligation (**Figure 2-35**) product was used to transform competent DH5*α* cells. Zero colonies formed on the no insert control plate (data not shown), and the plasmids of 21 isolated colonies were extracted by small-scale extraction in preparation of screening. The extracted plasmids were screened by digestion with *Blp*I (**Figure 2-37**). Thereafter, large-scale plasmid extractions of putatively correct clones were performed, and the plasmids were screened with *Bst*BI and *Aat*II (**Figure 2-38**).

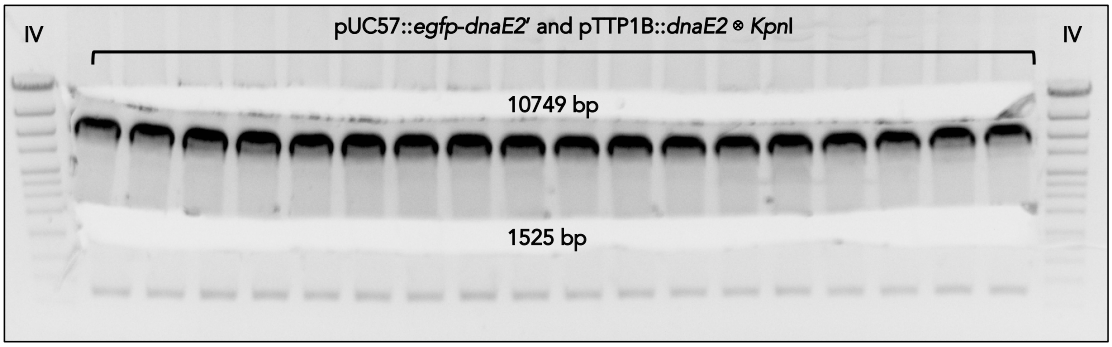

Figure 2-35 | Cloning of pTTP1B::*egfp-dnaE2*

Both plasmids were digested in the same reaction before being unambiguously separated by gel electrophoresis. The portion of the gel extracted (clear) indicates the corresponding sizes of the bands used during cloning. Reaction products were separated on a 1 % (w/v) agarose TAE gel supplemented with 0.01 % (w/v) EtBr by electroporation under a 100 V electric field in TAE buffer. Gel picture was recorded and imaged using UV light illumination. The sizes of excised bands are indicated.

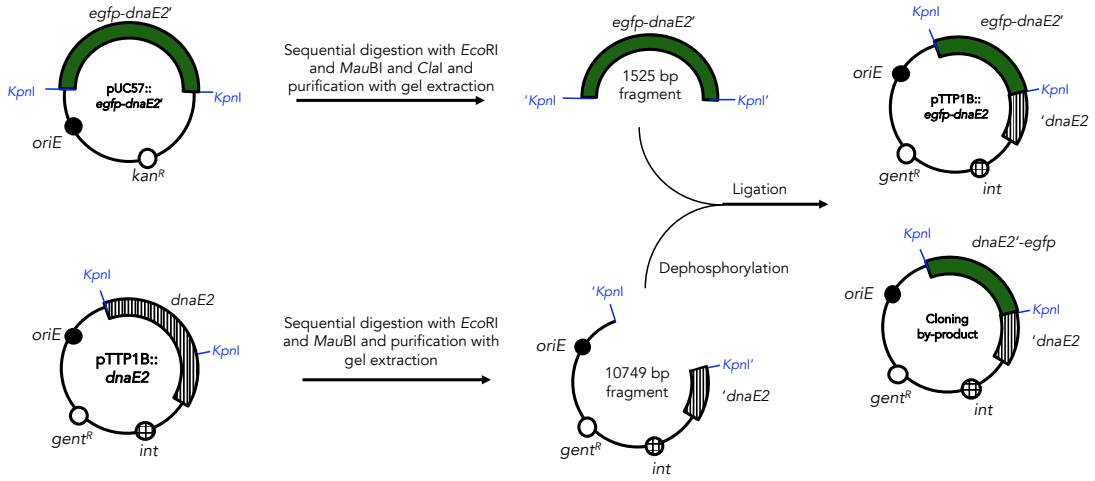

Figure 2-36 | Cloning strategy implemented for the development of pTTP1B::*egfp-dnaE2*

A schematic diagram representing the steps taken to clone pTTP1B::*egfp-dnaE2* from pTTP1B::dnaE2 and pUC57::egfp-dnaE2. The final ligation reaction results in two possible products owing to the non-directional cloning utilizing a single *Kpn*I restriction site.

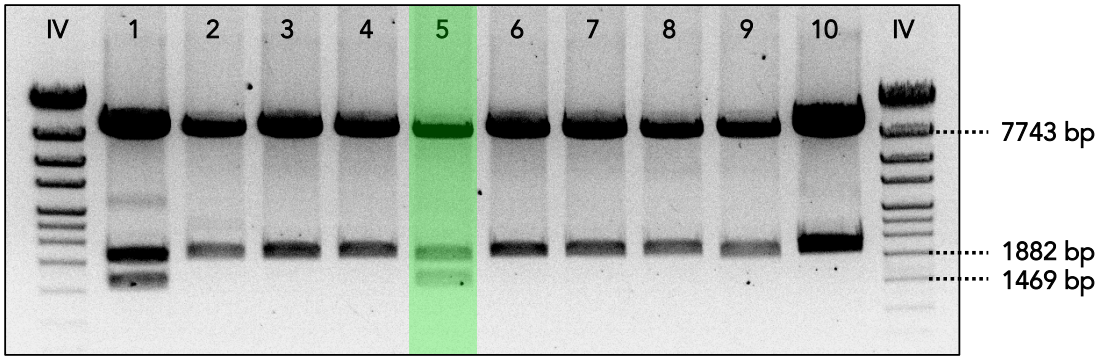

Figure 2-37 | Preliminary screen of pTTP1B::*egfp-dnaE2* with *Blp*I
Clone number 5 (lane 5) resulted in the predicted positive restriction pattern (1,587, distinct 2,004, and 8,684 bp) and was selected for further screening. Reaction products were separated on a 1 % (w/v) agarose TAE gel supplemented with 0.01 % (w/v) EtBr by electroporation under a 100 V electric field in TAE buffer. Gel picture was recorded and imaged using UV light illumination. The sizes of selected *Roche molecular weight marker IV* fragments are indicated.

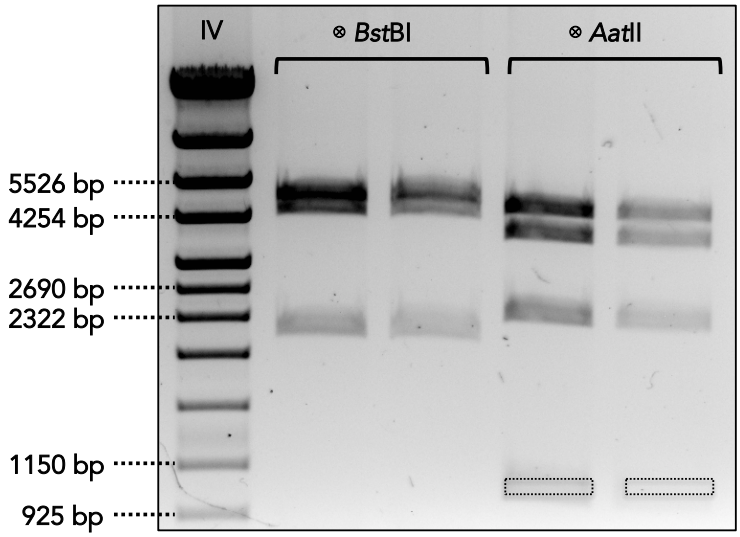

Figure 2-38 | Final screen of putative pTTP1B::*egfp-dnaE2* plasmid by digestion with *Bst*BI and *Aat*II
Positive result of *Bst*BI yielded fragments with sizes corresponding to 611 (unseen), 2,110, distinct 4,339, and 5,214 bp. Digestion of pTTP1B::*egfp-dnaE2* with AatII was expected to result in 331 (unseen), 2,342, distinct 3,796, and 5,813 bp bands. However, upon further inspection, it was identified that pTTP1B::*dnaE2* had not been fully sequenced. The sequence of a 2,284 bp region was unknown. If an *Aat*II recognition site were present in this unsequenced region, the predicted 3,796 bp fragment would be cleaved. This is evident by the unaccounted bands with approximate sizes of 2,600 and 1,100 bp which when added together produce the missing 3,796 bp band, thereby confirming the identity of pTTP1B::*egfp-dnaE2*. Reaction products were separated on a 1 % (w/v) agarose TAE gel supplemented with 0.01 % (w/v) EtBr by electroporation under a 100 V electric field in TAE buffer. Gel picture was recorded and imaged using UV light illumination. The sizes of selected *Roche molecular weight marker IV* fragments are indicated. Dotted rectangles indicate the position of bands clearly visible with altered contrast settings.

The confirmed plasmid was electroporated into the Δ*dnaE2* mutant (time constants presented in **Table 2-12**) and resulting GENT-resistant clones were

screened by direct observation of EGFP fluorescence following exposure of liquid cultures to MMC at MIC for 4 h. This method of screening did not identify positive results and negative results were not screened by genotype to confirm, due to changes in experimental aims of the project.

Table 2-12 | Record of time constants generated during the electroporation of pTTP1B::*egfp-dnaE2* into Δ*dnaE2*

pTTP1B::*egfp-dnaE2* amount (ng)	Time constant, μ
0.0	23.2
1000	23.4
2000	23.6
4000	23.2

9. Reagents, Preparations and Solutions

Agarose gel (1 %):

- 1× TAE buffer is used to dissolve 1 % w/v of agarose (Sigma, USA) by heating in a microwave
- Evaporated water is replaced by adding the required amount of dH_2O
- 0.5-1.0 μl of 10 mg/ml EtBr (*E1510-10ML*; Sigma, USA) is added per 40 ml of agarose
- Pour gel into gel cast (BioRad, USA) and is allowed to set

Agarose gel (4 %):

- 1× TAE buffer is used to dissolve 4 % w/v of agarose (Sigma, USA) by slow heating in a 60 °C water bath
- Evaporated water is replaced by adding the required amount of dH_2O
- Solution is heated in a 60 °C water bath again and slowly mixed
- 0.5-1.0 μl of 10 mg/ml EtBr (*E1510-10ML*; Sigma, USA) is added per 40 ml of agarose
- Solution is heated in a 60 °C water bath again and slowly mixed
- Pour gel into gel cast (BioRad, USA) and is allowed to set

DNA molecular weight markers:

- 10 μl marker (Roche, UK)
- 10 μl loading dye
- 40 μl dH_2O

dNTPs (200 μM):

- dATPs, dTTPs, dCTPs and dGTPs (New England Biolabs, USA) are made to a final total concentration of 200 μM by dilution with dH_2O.
- Stored at 4 °C

Ethanol (70 %):

- Dilute 7 parts absolute ethanol (Sigma, USA) with 3 parts dH_2O
- Store at room temperature

Ethylenediaminetetraacetic acid disodium salt dihydrate (EDTA, 0.5 M):

- 93.06 g of EDTA (Sigma, USA) dissolved in 400 ml dH_2O
- Adjust pH to 8.00 with NaOH (Sigma, USA)
- Make up to final volume of 500 ml
- Autoclave to sterilise
- Store at room temperature

Gentamycin (GENT):

- Dissolve gentamycin (Sigma, USA) in dH_2O to a final concentration of 50 mg/ml
- Filter sterilise with 0.22 μm filter (Merck Millipore, USA)
- Store in aliquots at –20 °C for long-term storage or 4 °C for frequent use

Glucose (0.5 M):

- 9.01 g of D-(+)-glucose (Sigma, USA) dissolved in 100 ml of dH_2O
- Sterilise through 0.22 μm filter

Glucose salt solution (100×):

- 20 g D-(+)-glucose (Sigma, USA)
- 8.5 g NaCl (Sigma, USA)
- Dissolve in 10 ml dH_2O
- Sterilise through 0.22 μm filter (Merck Millipore, USA)

Glycerol (10 %):

- 10 ml glycerol (Sigma, USA)
- Dissolve in 70 ml dH_2O
- Mix
- Make up to final volume of 100 ml with dH_2O
- Filter sterilise with 0.22 μm filter syringe (Merck Millipore, USA)
- Store at room temperature

Glycerol (66 %):

- 66 ml glycerol (Sigma, USA)
- Make up to final volume of 100 ml with dH_2O
- Mix
- Filter sterilise with 0.22 μm filter syringe (Merck Millipore, USA)
- Store at room temperature

Isopropanol:

- Procured from Sigma (USA)
- Store at room temperature

Kanamycin sulphate (Kanamycin, KAN):

- Dissolve Kanamycin sulphate (Sigma, USA) in dH_2O to a final concentration of 50 mg/ml
- Filter sterilise with 0.22 μm filter (Merck Millipore, USA)
- Store in aliquots at –20 °C for long-term storage or 4 °C for frequent use

Loading Dye:
- 4.5 ml glycerol (Sigma, USA)
- 10.5 ml dH_2O
- 0.04 g bromophenol blue (Sigma, USA)
- Mix well
- Filter sterilise (0.22 μm filter) (Merck Millipore, USA)
- Store at 4 °C

Luria-Bertani (LB) Agar:
- 10 g *Bacto™ Tryptone* (BD Biosciences, USA), 10 g sodium chloride (Sigma, USA), 5 g *Difco™ Yeast Extract* (BD Biosciences, USA) and 15 g *Bacto™ Agar* (BD Biosciences, USA) is dissolved in 1,000 ml of dH_2O
- Autoclave to sterilise
- Appropriate amount of antibiotic after the media has cooled sufficiently
- Pour 20 ml into Petri dish
- Allow to solidify

Luria-Bertani (LB) Broth:
- 10 g *Bacto™ Tryptone* (BD Biosciences, USA), 10 g sodium chloride (Sigma, USA) and 5 g *Difco™ Yeast Extract* (BD Biosciences, USA) is dissolved in 1,000 ml of dH_2O
- Autoclave to sterilise
- Appropriate amount of antibiotic after the media has cooled sufficiently
- Filter through a 0.02 μm filter to sterilize (Merck Millipore, USA)
- Store at 37 °C

Mitomycin C (MMC):
- Dissolve mitomycin C from *Streptomyces caespitosus* (Sigma, USA) in dH_2O to a final concentration of 0.04 μg/ml
- Filter sterilise with 0.22 μm filter (Merck Millipore, USA)
- Store in aliquots at –20 °C for long-term storage or 4 °C for frequent use
- Light sensitive

NaCl (5 M):
- Dissolve 292.2 g sodium chloride (Sigma, USA) in 800 ml dH_2O
- Adjust final volume to 1,000 ml with dH_2O
- Autoclave
- Store at room temperature

NaOH (10 M):
- 40 g sodium hydroxide (Sigma, USA) dissolved in 100 ml dH_2O
- Autoclave to sterilise

Phenol-chloroform (24:25):

- Mix 120 ml of phenol (Sigma, USA) with 125 ml of chloroform (Sigma, USA)
- Filter sterilise with 0.02 μm filter (Seperations, ZA)
- Store at 4 °C

Potassium acetate (5 M):

- 49.075 g of potassium acetate (Sigma, USA) is dissolved in 100 ml dH_2O
- Autoclave to sterilise

Rifampicin (RIF):

- Dilute RIF (Sigma, USA) to a final stock concentration of 100 μg/ml
- Filter sterilise with 0.22 μm filter (Merck Millipore, USA)
- Store in aliquots at 4 °C for frequent use
- Light sensitive

RNAse A:

- Dilute stock 100 mg/ml RNAse A (Sigma, USA) to 10 mg/ml with dH_2O
- Boil for 10 min at 100 °C
- Store at -20 °C

Sodium acetate (3 M, pH 5.20):

- Dissolve 408.24 g sodium acetate trihydrate (Sigma, USA) in 800 ml dH_2O
- Adjust the pH to 5.20 with acetate (Sigma, USA)
- Make up to final volume of 1,000 ml with dH_2O
- Autoclave and store at room temperature

Sodium dodecyl sulfate (SDS, 10 %):

- 10 g of SDS (Sigma, USA) is dissolved in 100 ml of dH_2O on heat
- Store at room temperature

Solution I (Lysis buffer):

- 10 ml of 0.5 M glucose, 2.5 ml Tris·HCl (1 M; pH 8.00) and 2.0 ml EDTA (0.5M; pH 8.00) is dissolved in 85.5 ml dH_2O
- Filter sterilise with 0.22 μm filter syringe
- Store at 4 °C

Solution II (Neutralisation buffer):

- 4 ml 10 M NaOH and 20 ml 10% (w/v) SDS is dissolved in 176 ml dH_2O
- Autoclave to sterilise
- Store at room temperature

Solution III (Precipitation buffer):

- 60 ml of 5 M potassium acetate and 11.5 ml of glacial acetic acid (Sigma, USA) is dissolved in 28.5 ml dH_2O
- Autoclave to sterilise

- Store at 4 °C

Standard Transformation Buffer I (TFB I):

- 0.588 g of potassium acetate (Sigma, USA), 2.42 g of rubidium chloride (Sigma-Aldrich), 0.294g of calcium chloride dihydrate (Sigma, USA), 2.0 g of manganese chloride (Sigma, USA) and 30 ml of glycerol (Sigma, USA) is dissolved in 100 ml of dH_2O.
- The pH is adjusted to 5.80 with dilute acetic acid (Sigma, USA)
- Make up to final volume of 200 ml
- Filter sterilise with 0.22 μm filter (Seperations, ZA)
- Store at room temperature
- Bring to 4 °C before use

Standard Transformation Buffer II (TFB II):

- 0.21 g of 3-(N-morpholino)propanesulfonic acid (MOPS; Sigma, USA), 1.1 g of calcium chloride dihydrate (Sigma, USA), 0.121 g of rubidium chloride (Sigma, USA) and 15 ml of glycerol (Sigma, USA) is dissolved in 50 ml of dH_2O
- The pH is adjusted to 6.50 with dilute NaOH (Sigma, USA)
- Filter sterilise with 0.22 μm filter (Merck Millipore, USA)
- Store at room temperature
- Bring to 4 °C before use

Tris-acetic-EDTA buffer (TAE buffer, 50×):

- Dissolve 242 g of Tris(hydroxymethyl)aminomethane (Sigma, USA) in 500 ml distilled water
- Add 100 ml 0.5M EDTA (pH 8.00) and 57.1 ml glacial acetic acid (Sigma, USA)
- Adjust volume to 1,000 ml with distilled water
- Store at room temperature
- Make up 1× working solution for gel electrophoresis by mixing 1 part with 49 parts dH_2O

Tris-EDTA buffer (TE buffer, 10×):

- 20 ml 1 M, pH 8.00 Tris·HCl
- 4 ml 0.5 M EDTA
- Dissolve in 150 ml dH_2O
- Make to final volume of 200 ml with dH_2O
- Adjust pH to 7.50 sodium hydroxide (Sigma, USA)
- Autoclave to sterilise
- Store at room temperature

Tris·HCl (1 M, pH 8.00):

- 60.56 g Tris·HCl (Sigma, USA) dissolved in 400 ml dH_2O
- Adjust pH to 8.00 with HCl (Sigma, USA)
- Make up final volume of 500 ml
- Autoclave to sterilise

Tween® 80 (25 %):

- 25 ml *Tween® 80* (Sigma, USA)
- Make up to final volume of 100 ml with dH_2O
- Mix thoroughly
- Filter sterilise with 0.22 μm filter syringe (Merck Millipore, USA)
- Store at room temperature

7H10 Agar (OADC):

- 5.7 g *Difco™ Middlebrook 7H10 Agar* (BD Biosciences, USA) and 1ml of glycerol (Sigma, USA) is dissolved in 270 ml of dH_2O
- Autoclave
- Add 30 ml *BBL™ Middlebrook OADC Enrichment* (BD Biosciences, USA)
- Add appropriate amount of antibiotic if required
- Pour 20 ml into Petri dish
- Allow to solidify

7H9 Broth (OADC):

- 2.35 g *Difco™ Middlebrook 7H9 Broth* (BD Biosciences, USA), 1 ml glycerol (Sigma, USA) and 1 ml 25 % (v/v) *Tween® 80* dissolved in 450 ml dH_2O
- Autoclave to sterilise
- Add 50 ml *BBL™ Middlebrook OADC Enrichment* (BD Biosciences, USA)
- Add required amount of antibiotic
- Mix
- Filter sterilise with 0.22 μm filter
- Store at 37 °C

10. References

Altschul SF, Gish W, Miller W, Myers EW, Lipman DJ. (1990) Basic local alignment search tool. *J. Mol. Biol.* 215:403-410

Betzig E, Patterson GH, Sougrat R, Lindwasser OW, Olenych S, Bonifacino JS, Davidson MW, Lippincott-Schwartz J, Hess HF. (2006) Imaging Intracellular Fluorescent Proteins at Nanometer Resolution. *Science* 313:1642-1645

Boshoff HIM, Mizrahi V. (2000) Widespread distribution of a lexA-regulated DNA damage- inducible multiple gene cassette in the Proteobacteria phylum. *J. Bacteriol.* 182:5479-5485

Boshoff HIM, Reed BR, Barry III CE, Mizrahi V. (2003) DnaE2 polymerase contributes to in vivo survival and the emergence of drug resistance in Mycobacterium tuberculosis. *Cell* 113:183–193

Cole ST, Brosch R, Parkhill J, Garnier T, Churcher C, Harris D, Gordon SV, Eiglmeier K, Gas S, Barry III CE, Tekaia F, Badcock K, Basham D, Brown D, Chillingworth T, Connor R, Davies R, Devlin K, Feltwell T, Gentles S, Hamlin N, Holroyd S, Hornsby T, Jagels K, Krogh A, McLean J, Moule S, Murphy L, Oliver K, Osborne J, Quail MA, Rajandream M-A, Rogers J, Rutter S, Seeger K, Skelton J, Squares R, Squares S, Sulston JE, Taylor K,

Whitehead S, Barrell BG. (1998) Deciphering the biology of Mycobacterium tuberculosis from the complete genome sequence. *Nature* 393:537-544

Cormack BP, Valdivia RH, Falkow S. (1996) FACS-optimized mutants of the green fluorescent protein (GFP). *Gene* 173(1):33-8

Davis EO, Dullaghan EM, Rand L. (2002) Definition of the Mycobacterial SOS box and use to identify LexA-regulated genes in Mycobacterium tuberculosis. *J. Bacteriol.* 184:3287–3295

Einhauer A, Jungbauer A. (2001) The FLAG™ peptide, a versatile fusion tag for the purification of recombinant proteins. J. *Biochem. Biophys. Methods* 49(1):455-65

Gokhale RS, Khosla C. (2000) Role of linkers in communication between protein modules. *Curr. Opin. Chem. Biol.* 4(1):22-7

Kapopoulou A, Lew JM, Cole ST. (2011) The MycoBrowser portal: a comprehensive and manually annotated resource for mycobacterial genomes. *Tuberculosis* 91(1):8-13

Kling A, Lukat P, Almeida DV, Bauer A, Fontaine E, Sordello S, Zaburannyi N, Herrmann J, Wenzel SC, König C, Ammerman NC, Barrio MB, Borchers K, Bordon-Pallier F, Brönstrup M, Courtemanche G, Gerlitz M, Geslin M, Hammann P, Heinz DW, Hoffmann H, Klieber S, Kohlmann M, Kurz M, Lair C, Matter H, Nuermberger E, Tyagi S, Fraisse L, Grosset JH, Lagrange S, Müller R. (2015) Targeting DnaN for tuberculosis therapy using novel griselimycins. *Science* 348(6239):1106-1112

Lew JM, Kapopoulou A, Jones LM, Cole ST. (2011) TubercuList–10 years after. *Tuberculosis* 91(1):1-7.

Marchler-Bauer A, Derbyshire MK, Gonzales NR, Lu S, Chitsaz F, Geer LY, Geer RC, He J, Gwadz M, Hurwitz DI, Lanczycki CJ. (2014) CDD: NCBI's conserved domain database. *Nucleic Acids Res.* 43(D1):D222-6

NCBI, Resource Coordinators. (2017) Database Resources of the National Center for Biotechnology Information. *Nucleic Acids Res.* 45(D1):D12

Newton-Foot M, van Pittius NCG. (2013) The complex architecture of mycobacterial promoters. *Tuberculosis* 93(1):60-74

Paez-Segala MG, Sun MG, Shtengel G, Viswanathan S, Baird MA, Macklin JJ, Patel R, Allen JR, Howe ES, Piszczek G, Hess HF, Davidson MW, Wang Y, Looger LL. (2015) Fixation-resistant photoactivatable fluorescent proteins for CLEM. *Nat. Methods* 12:215-218

Papavinasasundaram KG, Anderson C, Brooks PC, Thomasa NA, Movahedzadehb F, Jenner PJ, Colston MJ, Davis EO. (2001) Slow induction of RecA by DNA damage in Mycobacterium tuberculosis. *Micorbiology* 147:3271–3279

Peterson JD, Umayam LA, Dickinson T, Hickey EK, White O. (2001) The comprehensive microbial resource. *Nucleic Acids Res.* 29(1):123-5

Pham TT, Jacobs-Sera D, Pedulla ML, Hendrix RW, Hatfull GF. (2007) Comparative genomic analysis of mycobacteriophage Tweety: evolutionary insights and construction of compatible site-specific integration vectors for mycobacteria. *Microbiol.* 53(8):2711-23

Reddy TB, Riley R, Wymore F, Montgomery P, DeCaprio D, Engels R, Gellesch M, Hubble J, Jen D, Jin H, Koehrsen M. (2008) TB database: an integrated platform for tuberculosis research. *Nucleic Acids Res.* 37(suppl_1):D499-508

Reiche MA, Gopinath K, Mizrahi V, Warner DF. (Unpublished) (2013) Mini-thesis project: Generation of Venus Fluorescent Protein-tagged ImuA′-expressing vector. *University of Cape Town*

Santi I, Dhar N, Bousbaine D, Wakamoto Y, McKinney JD. (2013) Single-cell dynamics of the chromosome replication and cell division cycles in mycobacteria. *Nat. Commun.* 4:2470

Schindelin J, Arganda-Carreras I, Frise E, Kaynig V, Longair M, Pietzsch T, Preibisch S, Rueden C, Saalfeld S, Schmid B, Tinevez JY. (2012) Fiji: an open-source platform for biological-image analysis. *Nat. Methods* 9(7):676-82

Shtengel G, Galbraith JA, Galbraith CG, Lippincott-Schwartz, Gillette JM, Manley S, Sougrat R, Waterman CM, Kanchanawong P, Davidson MW, Fetter RD, Hess HF (2009) Interferometric fluorescent super-resolution microscopy resolves 3D cellular ultrastructure. *Proc. Natl. Acad. Sci. USA* 106(9):3125-3130

Sievers F, Higgins DG. (2014) Clustal omega. *Curr. Protoc. Bioinformatics* 3-13

Snapper SB, Melton RE, Mustafa S, Kieser T, Jacobs WR Jr. (1990) Isolation and characterization of efficient plasmid transformation mutants of Mycobacterium smegmatis. *Mol. Microbiol.* 4:1911-1919

Warner DF, Ndwandwe DE, Abrahams GL, Kana BD, Machowski EE, Venclovas C, Mizrahi V. (2010) Essential roles for imuA′- and imuB-encoded accessory factors in DnaE2-dependent mutagenesis in Mycobacterium tuberculosis. *Proc. Natl. Acad. Sci. USA* 107:13093–13098

Wiedenmann J, Ivanchenko S, Oswald F, Schmitt F, Röcker C, Salih A, Spindler K-D, Nienhaus GU. (2004) EosFP, a fluorescent marker protein with UV-inducible green-to-red fluorescence conversion. *Proc. Natl. Acad. Sci. USA* 101(45):15905-15910

Ye J, Coulouris G, Zaretskaya I, Cutcutache I, Rozen S, Madden TL. (2012) Primer-BLAST: a tool to design target-specific primers for polymerase chain reaction. *BMC Bioinform.* 13:134

CHAPTER III: RESULTS

Table of Contents: **Page**

List of Figures: **Page**

List of Tables: **Page**

1. Analysis of *Mycobacterium smegmatis* SOS Response Regulation

In preliminary work conducted during my BSc(Med)(Hons) degree, a translational reporter construct comprising *Mycobacterium smegmatis* (*Msm*) ImuA' tagged at the N-terminus with Venus fluorescent protein (VFP) (Δ*imuA'*::*vfp*-*imuA'*) had been constructed but not extensively tested in live *Msm* cells (Reiche, *et al*., unpublished). Moreover, the tagging of ImuB with a fluorescent protein (FP) had not been attempted since it posed a greater design challenge given the location of *imuB* within a putative *imuA'*-*imuB* operon (Warner, *et al*., 2010) that was predicted to be regulated by a single SOS box located as part of the *imuA'* gene (Davis, *et al*., 2002). Therefore, prior to the development of a labelled ImuB-expressing construct, it was necessary to identify a suitable FP to be used to tag ImuB. To confirm that the selected FP was functional within *Msm*, a construct that did not include ImuB was developed as an experimental control. In addition, it was necessary to define a suitable promoter that would result in DNA damage-dependent expression of ImuB alone in future experiments. To this end, PSOS(*imuA'*)-*egfp* was designed and consisted of the *imuA'* promoter, P(*imuA'*), driving expression of the enhanced green fluorescent protein gene (*egfp*) alone. The upstream promoter sequence exclusively included *imuA'* regulatory sequence to prevent potential complications associated with employing the operonic *imuB* promoter in the absence of an upstream *imuA'* open reading frame (ORF) (**Chapter II**, **Section 8.1**). The use of the *imuA'* promoter was considered appropriate for the following reasons: (i) as noted above, the *imuA'*-*imuB* operon was predicted to be regulated by a single SOS box located within the *imuA'* gene (Davis, *et al*., 2002) (see **Chapter II**, **Table 2-7**); and (ii) the ORF of *imuB* overlaps with that of *imuA'*, therefore altering the 5' sequence of *imuB* would result in the alteration

the 3′-end of *imuA′*. Refer to **Figure 3-1** for a graphical depiction of the genomic context of *imuA′* and *imuB* within *Msm* and for a comparison of selected fluorescent constructs presented in this chapter.

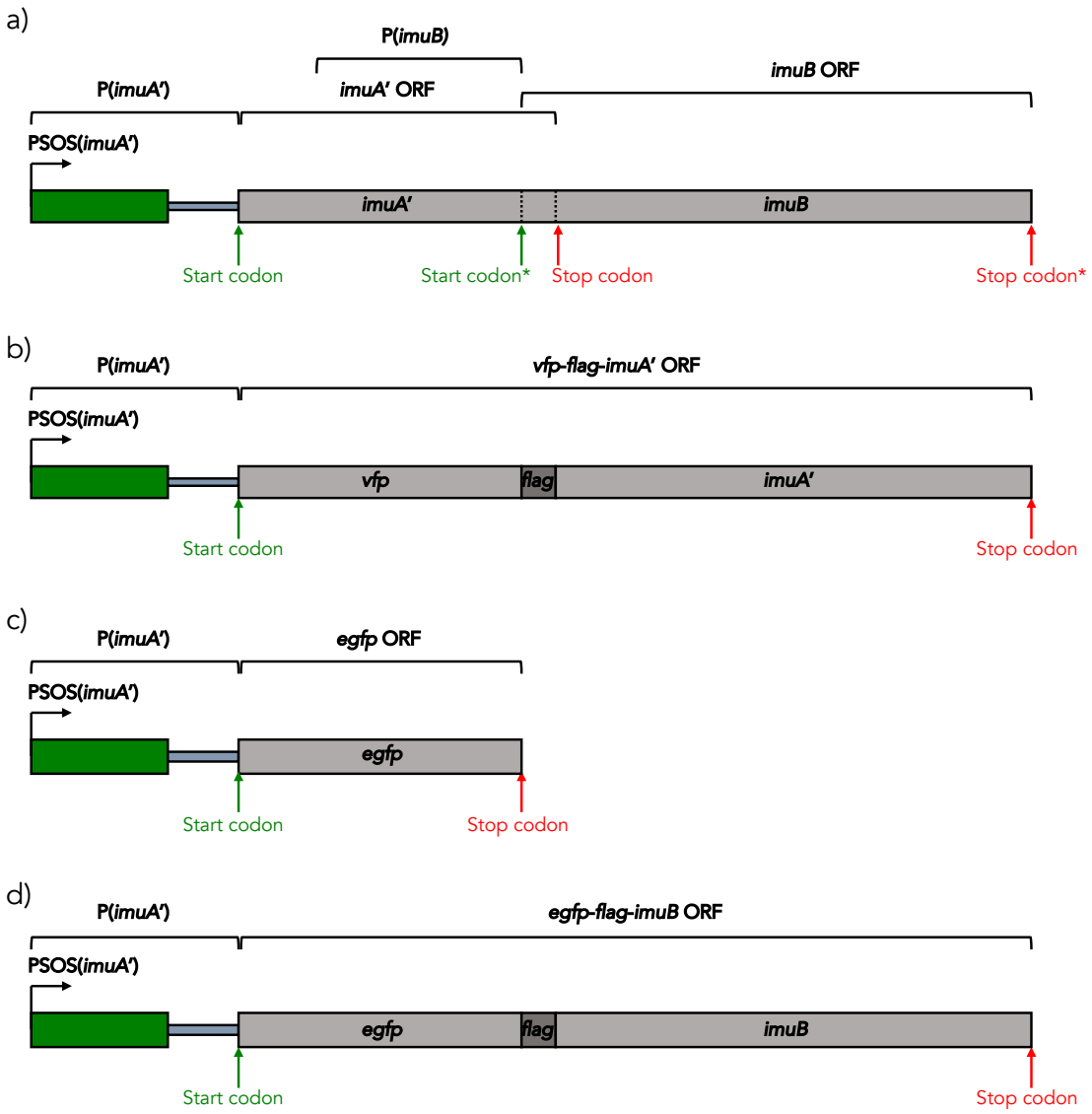

Figure 3-1 | Schematic representation of *Msm imuA′* and *imuB* genes and fluorescent constructs
a) The genomic context of wild-type *Msm imuA′* and *imuB*. The promoter elements as well as ORFs are presented. Here, the over-lapping *imuA′-imuB* ORFs are transcribed from two different frames (denoted by the asterisk). Undefined *imuB*-specific promoter elements are located within *imuA′*. (b) The design of *vfp-imuA′* utilizes the promoter of *Msm imuA′* and controls a single VFP-ImuA′-encoding ORF. (c) The *imuA′* promoter is again used to drive expression of *egfp* in the PSOS(*imuA′*)-*egfp* reporter construct and is the basis of (d) the PSOS(*imuA′*)-*egfp-imuB* construct that encodes EGFP-ImuB in the absence of *imuB*-specific promoter elements. Details of design are presented in Chapter II.

EGFP was selected and used to design the PSOS(*imuA'*) fluorescent reporter owing to its excellent fluorescent properties (Cormack, *et al.*, 1996) and consistent use in the literature. The purpose of the resultant PSOS(*imuA'*)-*egfp* construct was three-fold: (i) to identify whether the *imuA'* promoter could be used as a robust promoter to regulate expression of *egfp* in the presence of genotoxic stress, and so could be applied in the design of future constructs; (ii) to validate EGFP for use in hybrid constructs and as an experimental control in the event that fluorescence was lost following tagging of a specific mutasome protein such as ImuB; and (iii) to study the regulatory dynamics of P(*imuA'*) using flow cytometry to assess induction of the mutasome SOS response in individual bacilli.

1.1. Detection of *imuA'* Promoter-dependent EGFP Expression by Microscopy

Following the introduction of the PSOS(*imuA'*)-*egfp* transcriptional reporter construct into wild-type (WT) *Msm*, the first objective was to demonstrate DNA damage-inducible fluorescence of the resultant WT::PSOS(*imuA'*)-*egfp* strain, thus confirming both the function of EGFP and the use of P(*imuA'*) in future constructs. To this end, WT::PSOS(*imuA'*)-*egfp* and a WT (negative fluorescence) control were assessed by fluorescence confocal microscopy following exposure to mitomycin C (MMC) to induce genotoxic stress (1× minimum inhibitory concentration, MIC, for 2.5 h) (**Figure 3-2**). Both MMC-treated and untreated WT bacilli were indistinguishable, indicating that the presence of MMC in the media did not inherently induce auto-fluoresence of *Msm*. By comparison, when WT::PSOS(*imuA'*)-*egfp* was exposed to 1× MIC

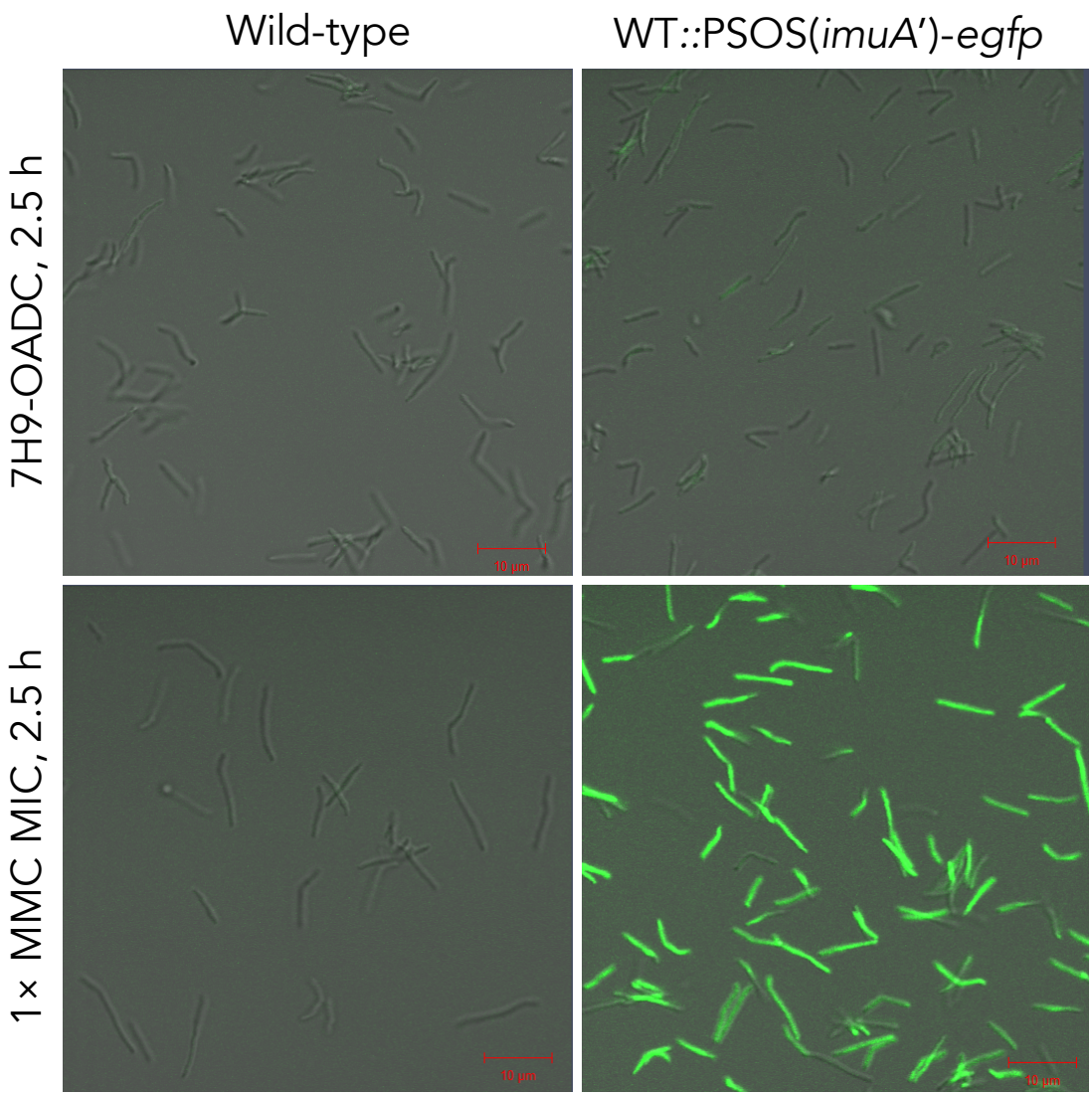

Figure 3-2 | Exposure of *Msm* to MMC induces expression from the *imuA'* promoter
Confocal fluorescent micrograph of the indicated *Msm* strains before and after exposure to genotoxic stress. Green fluorescence was detected by imaging WT (left) and WT::PSOS(*imuA'*)-*egfp* (right), both without (top) and with (bottom) exposure to 1× MIC MMC for 2.5 h. Images were captured at 100× magnification using a 1.4 NA oil objective lens. Overlaying fluorescent signal onto brightfield images generated micrographs. The scale bar in the bottom-right of each frame indicates 10 µm.

MMC for 2.5 h, sample-wide green fluorescent bacilli were observed. Previous transcriptional studies (Warner, *et al.*, 2010) demonstrated that *imuA'* was tightly regulated as part of the mycobacterial SOS response; therefore, the considerable increase in green fluorescence in WT::PSOS(*imuA'*)-*egfp* bacilli following exposure to MMC indicated that the promoter was functional. This result established that P(*imuA'*) was suitable for use in the development of

future constructs requiring the expression of mutasome components. In addition, it validated the use of EGFP as a fluorescent protein in *Msm* and suggested the potential utility of WT::PSOS(*imuA'*)-*egfp* as an SOS reporter mutant.

1.2. Using Flow Cytometry to Quantify the Level of Expression from the *imuA'* Promoter

Next, it was necessary to validate the use of WT::PSOS(*imuA'*)-*egfp* as an SOS reporter. To this end, flow cytometry was adopted in the expectation that it would allow rapid, population-wide investigation of changes in mutasome expression in *Msm* bacilli in response to varying conditions of genotoxic stress by detection of green fluorescence within individual bacilli. It would also enable insight into the level of induction of P(*imuA'*) and confirm the use of the PSOS(*imuA'*)-*egfp* construct for downstream analyses of mutasome expression, recruitment, and localization. Specifically, it was envisaged that flow cytometry would be used to quantify the level of expression from P(*imuA'*) and to test the hypothesis that different MMC concentrations and exposure periods would result in different levels of EGFP expression in *Msm* as a function of induction of the *imuA'* promoter (a proxy of mutasome expression) by the SOS response.

1.2.1. Flow Cytometry Can be Used to Detect Differences in Expression of EGFP

A pilot experiment was conducted to validate the use of flow cytometry as an analytical tool to measure EGFP expression levels. The secondary aim of this experiment was to determine if changes in the EGFP expression level of individual bacilli within an entire population could be detected by flow

cytometry. This would prove beneficial over other batch-culture methods such as real-time polymerase chain reaction (PCR) which provide average readings for a large number of cells. The pilot experiment was based on the premise that an increasing concentration of MMC would result in detectable changes in P(*imuA'*) induction, as suggested by previous transcriptional data (Warner, *et al.*, 2010). The underlying experimental hypothesis was that the population-wide green fluorescent signal in WT::PSOS(*imuA'*)-*egfp* bacilli would respond proportionally to the amount of MMC applied.

Bacilli were exposed to MMC at a concentration of 0, 0.5, 1.0, 2.0, or 10× MIC for 2.5 h before cells were fixed in 4 % formaldehyde and analysed by flow cytometry. **Figure 3-3a** presents the increase in EGFP signal measured in WT::PSOS(*imuA'*)-*egfp* cells in response to the increasing dose of MMC. Unexposed cells had a baseline geometric mean of 100 arbitrary fluorescence units (AFU), which was 20 AFU more than WT and indicated a low-level basal expression during normal growth conditions. In comparison, all cultures of WT::PSOS(*imuA'*)-*egfp* exposed to MMC exhibited elevated levels of green fluorescence signal. Cells exposed to 0.5, 1.0, 2.0, and 10× MMC yielded increasing geometric mean EGFP signal levels of 890, 1100, 1400, and 1800 AFU, respectively. A direct comparison of 0× and 10× MMC is presented in **Figure 3-3c**. As before, WT was included as a fluorescence negative control for comparison purposes (**Figure 3-3b** and **Figure 3-3d**). Regardless of the MMC dose, the detectable green fluorescence signal in WT cells did not vary: WT exposed to 0×, 1.0×, and 10× MIC MMC resulted in geometric mean EGFP signal levels of 64, 84, and 80 AFU, respectively. This pilot experiment therefore indicated that EGFP expressed following induction of P(*imuA'*) could be

detected at the individual cell level, reinforcing the utility of WT::PSOS(*imuA'*)-*egfp* as a fluorescence-based reporter.

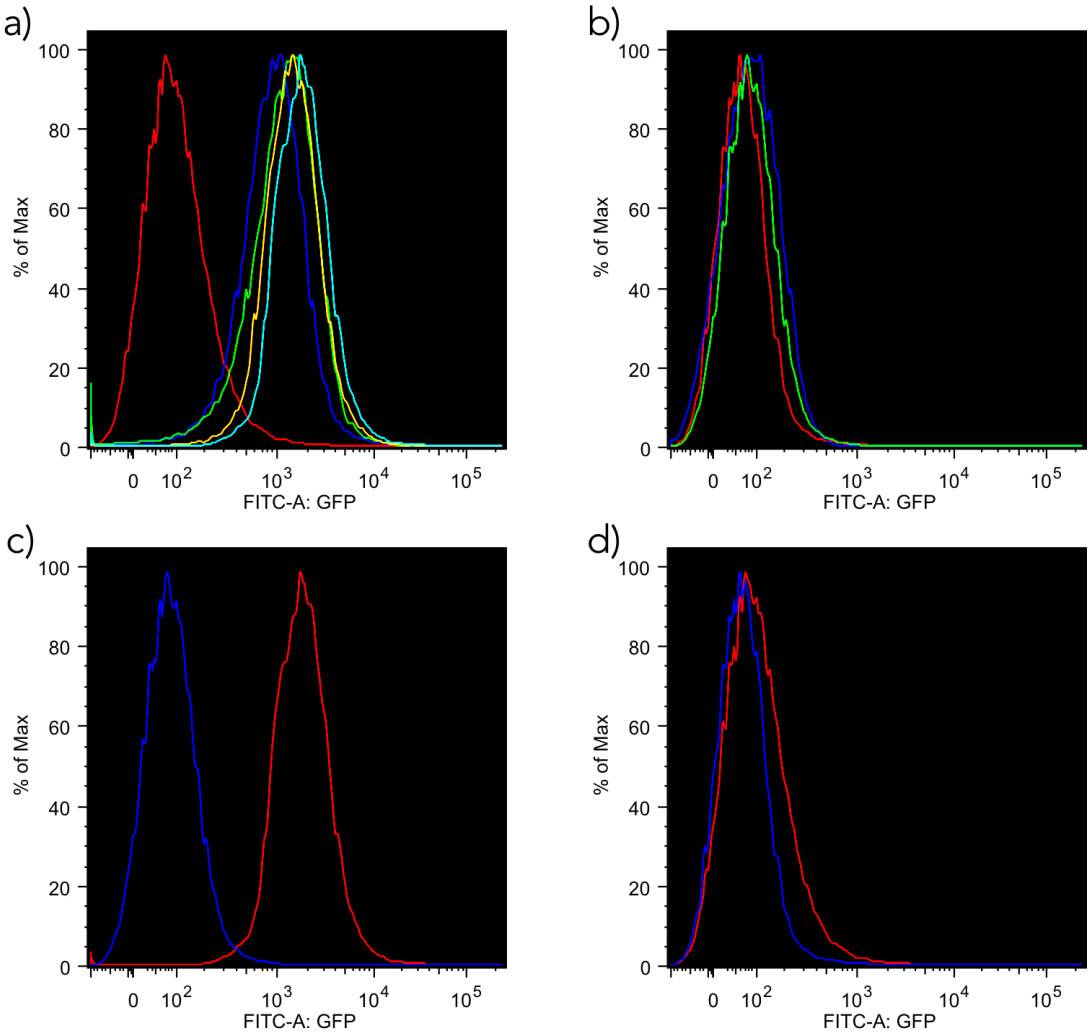

Figure 3-3 | Changes in EGFP expression level in the *imuA'* reporter strain can be detected using flow cytometry

The *x*-axis of each graph represents the relative intensity/magnitude of green fluorescence signal detected; the *y*-axis represents the histogram, indicating the percent of the maximum that falls into each category in the *x*-axis. (a) WT::PSOS(*imuA'*)-*egfp* treated with different concentrations of MMC. Red = 0×; navy blue = 0.5×; green = 1.0×; orange = 2.0×; and light blue = 10× MIC. (b) WT treated to 0× (red); 1.0× (navy blue); or 10× (green) MIC MMC. (c) Comparison of WT::PSOS(*imuA'*)-*egfp* (red) and WT (navy blue) exposed to 10× MIC. (d) Comparison of WT::PSOS(*imuA'*)-*egfp* (red) and WT (navy blue) without exposure to MMC. Events were detected by forward (400 V) and side scatter (310 V) correlation until 1,000,000 events had been recorded. EGFP signal was detected under the FITC parameters (excitation: 488 nm; emission: 507 nm; 557 V) with no compensation. The associated event rate was 15,000 events per second. Cells were fixed in 4 % formaldehyde prior to acquisition.

1.2.2. Expression Dynamics of *imuA'*

Having established the utility of flow cytometry in measuring the response of the WT::PSOS(*imuA'*)-*egfp* reporter strain to genotoxic stress, the next step was to perform more elaborate and accurate dose- and time-response experiments to determine whether *imuA'* was transcribed proportionally to the amount of DNA damage incurred. These experiments would also serve the purpose of identifying the optimal conditions (*i.e.*, MMC dose and exposure time) that yield detectable levels of fluorescent protein for future analyses.

1.2.2.1. Induction of *imuA'* Increases as a Function of Time During Genotoxic Stress

In the first of two large-scale experiments, the aim was to quantify the extent to which P(*imuA'*) was induced following exposure of bacilli to genotoxic stress for increasing periods of time. This was achieved by measuring the level of EGFP expressed by WT::PSOS(*imuA'*)-*egfp* as a proxy for ImuA' (and mutasome) expression. The hypothesis was that the magnitude of PSOS(*imuA'*)-*egfp* induction would be proportional to the duration of MMC exposure. To this end, cultures of WT::PSOS(*imuA'*)-*egfp* were treated with MMC at 1× MIC for varying periods of time (5, 15, and 30 min, and 1, 2, 4, 6, 12, and 24 h) before being fixed in 4 % formaldehyde for 30 min. Each sample was then filtered through a 30 μm cell strainer to remove objects that would obstruct the flow through the instrument or cause blockage, before analysis by flow cytometry. The green fluorescence (FITC-A:GFP) intensity of each acquisition was recorded and, after acquisition, the geometric means for FITC-A:GFP (green fluorescence) intensity were determined as the data acquired in a single run were log-normally distributed. The mean and 95 % confidence

interval (CI) calculated from all six geometric mean fluorescence intensities at each time point is plotted in the graph in **Figure 3-4** as a function of the treatment duration. The cells required approximately 30 min of exposure to MMC before increased expression of EGFP was detectable. Between 30 min and 6 h there was a positive linear correlation between the mean fluorescence of the population and the duration of exposure to MMC ($\Delta y / \Delta x$ = 356.48 AFU per hour, R^2 = 0.92). Maximal EGFP expression was detected after 6 h, which correlated with approximately two generation times in exponential growth-phase *Msm* (Aldridge, *et al.*, 2012; Santi, *et al.*, 2013). In addition, a decrease in fluorescence intensity of 25.78 % was observed between 6 and 12 h. Bacilli exposed to MMC for 24 h could not be analysed using flow cytometry as the cells could not be passed through a 30 µm cell strainer, suggesting the possible induction of a filamentous state (**Section 3**, below).

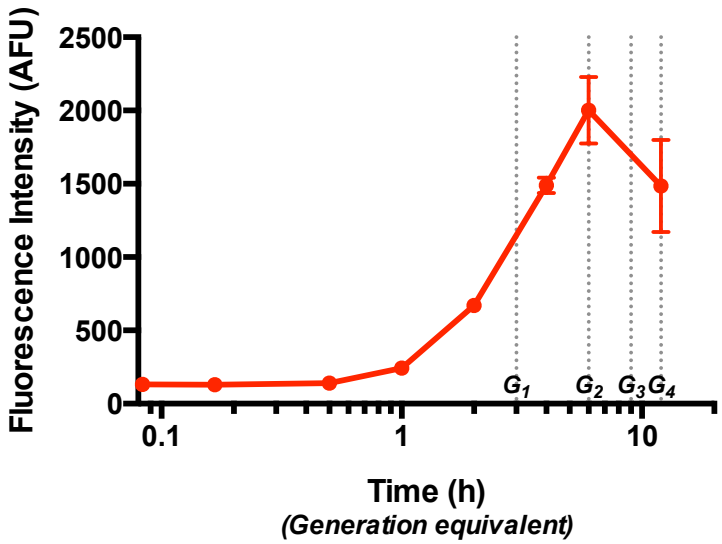

Figure 3-4 | Time response of the *imuA'* promoter to MMC
Level of EGFP expression from PSOS(*imuA'*) as a function of time following exposure to MMC. The time-response graph presents the results of flow cytometric analysis of the level of EGFP expressed by WT::PSOS(*imuA'*)-*egfp* following exposure to the MIC of MMC (*y*-axis) for various periods of time (*x*-axis, log scale). Each point represents the average geometric mean of 6 repeats. The error bars represent a 95 % CI. The estimated generation time of *Msm* (3 h) is indicated on the *x*-axis: G_x=generation time *x*.

1.2.2.2. The *imuA'* Promoter Responds Proportionally to the Dose of Genotoxic Stress

The second aspect of characterising the *imuA'* promoter required an assessment of the genotoxic dose response of P(*imuA'*). The aim of this experiment was to quantify the level of EGFP expression under control of P(*imuA'*) following exposure of WT::PSOS(*imuA'*)-*egfp* to different concentrations of MMC for a fixed period of time. It was expected that this would yield insight into the expression dynamics of the *imuA'* promoter and was based on the hypothesis that EGFP expression would increase in proportion to the amount of DNA damage incurred. Therefore, WT::PSOS(*imuA'*)-*egfp* cultures were treated to varying concentrations of MMC for 4 h before fixation and analysis by flow cytometry. An exposure duration of 4 h was selected to ensure sufficient time for the SOS response to be induced and for detectable levels of EGFP to be translated (see **Section 1.2.2.1**). As before, the FITC-A:GFP detection parameters were used to quantify the relative levels of EGFP expressed in individual cells. The geometric mean green fluorescence intensity of each acquisition for each sample was determined (**Figure 3-5**), with mean and 95 % CI of the geometric mean level of EGFP signal plotted as a function of MMC concentration. From these results, it was apparent that the dose response comprised three different phases: a positive linear relationship was evident between 0 and 0.1× MIC ($\Delta y / \Delta x$ = 5563.7.48 AFU per MIC factor, R^2 = 0.99); between 1 and 5× MIC, a static relationship existed whereby no statistically significant change in the level of EGFP expression in the population was detected (P = 0.095, Student's t-test); finally, at 10× MIC and greater, there was a rapid decrease in the mean green fluorescence intensity detected by flow

cytometry. This established that maximal expression of EGFP from the *imuA'* promoter corresponded with inhibitory but sub-lethal concentrations of MMC.

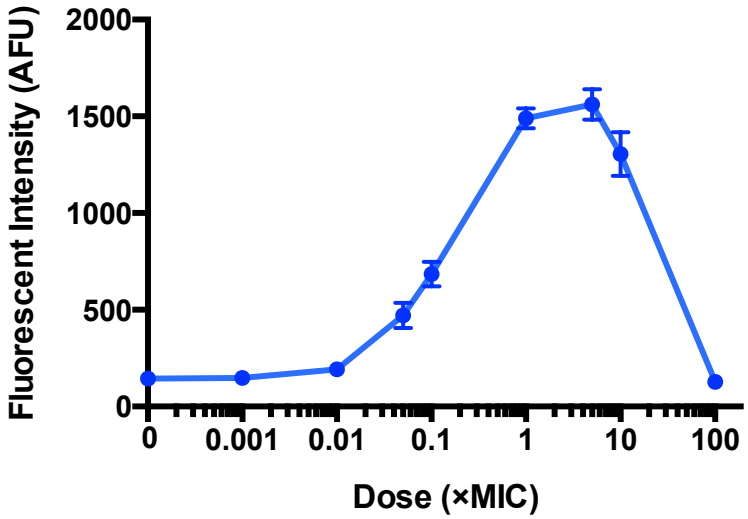

Figure 3-5 | Dose-response of the *imuA'* promoter to MMC
SOS-dependent fluorescence intensity correlates with genotoxin dose over sub-MIC range in *Msm*. This dose-response graph represents the results of the cytometric analysis of the level of EGFP expressed by WT::PSOS(*imuA'*)-*egfp* (*y*-axis) following exposure to various concentrations of MMC (*x*-axis, log scale) for 4 h. Each point represents the average geometric mean of 6 repeats. The error bars represent the 95 % CI.

2. A Modified Sequence Encoding EGFP-ImuB

The demonstrated utility of the PSOS(*imuA'*)-*egfp* construct supported the continuation of efforts to develop a fluorescently tagged ImuB translational reporter construct. In addition, the WT::PSOS(*imuA'*)-*egfp* transcriptional reporter (**Figure 3-2**) provided a useful control in evaluating any attempt to link a mutasome component such as ImuB to EGFP in constructing a translational reporter. To this end, a new construct was designed to express EGFP-tagged ImuB and was based on the PSOS(*imuA'*)-*egfp* construct (**Figure 3-1**). As before, the *imuA'* promoter was utilized to drive expression of the downstream ORF, which consisted of *egfp* – thus far identical to the PSOS(*imuA'*)-*egfp* construct – fused in-frame to the *imuB*-encoding sequence after a FLAG tag-encoding

spacer sequence. The full-length PSOS(*imuA'*)-*egfp-imuB* construct was inserted into a mycobacterium-specific integrative plasmid, pMCAINT (Warner, *et al.*, 2010), and the resulting construct was electroporated into *Msm* Δ*imuB* (Warner, *et al.*, 2010) in order to assess the function of the encoded EGFP-ImuB protein in the absence of the WT *imuB* allele. It was imperative to confirm that the respective hybrid proteins maintained biological function to ensure that any inferences from fluorescence localization experiments were representative of the biological response being assessed.

2.1. N-terminally Labelled ImuB Controlled by P(*imuA'*) Maintains Function in Inducible Mutagenic DNA Repair

Mutagenesis assays to assess the mutagenic capacity of experimental *Msm* strains were performed as previously described (Warner, *et al.*, 2010; Boshoff, *et al.*, 2003), and involved the determination of rifampicin (RIF)-resistance frequencies following exposure to genotoxic stress. In this assay, the ability of the mutasome to generate mutations following DNA damage is measured through the development of RIF-resistance (conferred as single nucleotide polymorphisms, SNPs, and insertion-deletion events, indels, in *rpoB*; Boshoff, *et al.*, 2003) after ultraviolet (UV) irradiation of bacilli. Experiments were conducted on Δ*imuA'*::*vfp-imuA'* (Reiche, *et al.*, unpublished) and Δ*imuB*::PSOS(*imuA'*)e*gfp-imuB*, as well as WT, and Δ*imuA'* and Δ*imuB* deletion mutants as experimental controls. The previously developed ImuA' reporter strain, Δ*imuA'*::*vfp-imuA'*, was included here to confirm function of VFP-ImuA'. The mean frequencies and associated standard deviations (SDs) of RIF-resistance are indicated in **Figure 3-6**. WT *Msm* exposed to 25 mJ.cm^{-2} exhibited

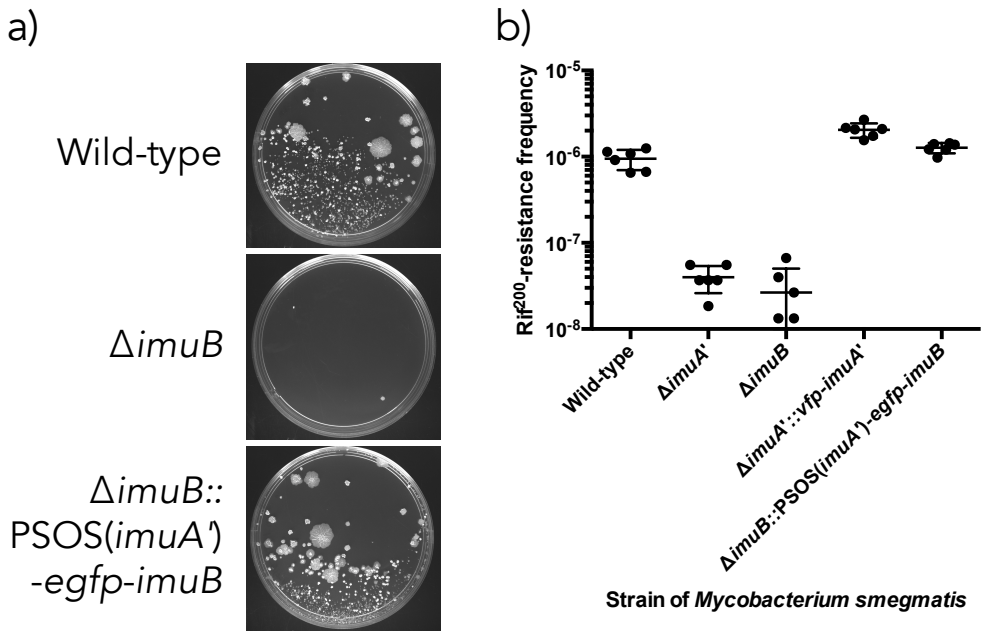

Figure 3-6 | Labelled mutasome components maintain mutagenic capacity
Inducible mutation frequencies of various fluorescent strains of *Msm*. (a) Representative photographs of the number of colonies grown on 200 µg/ml RIF-containing plates. The visible colonies represent the number of RIF-resistant mutants in 250 µl of UV-exposed culture after 5 days of growth. (b) The mutation frequency is represented by the frequency of RIF resistance (*y*-axis, log-scale) for each strain (*x*-axis). Each point represents the result of a single sample and the error bar represents the SD calculated for each strain. Zero-values are not presented on the log-scale.

a mean inducible mutation frequency (MIMF) of approximately 9.49×10^{-7} while Δ*imuA*′ and Δ*imuB* had MIMFs of 3.99×10^{-8} and 2.66×10^{-8}, respectively. Specifically, the MIMF for WT was 23.8-fold and 35.7-fold greater than Δ*imuA*′ and Δ*imuB*, respectively, consistent with previous observations (Warner, *et al*., 2010). The corresponding deletion mutants complemented with experimental FP-tagged alleles yielded MIMFs of 2.05×10^{-6} for Δ*imuA*′::*vfp-imuA*′ and 1.27×10^{-6} for Δ*imuB*::PSOS(*imuA*′)-*egfp-imuB*. The MIMF of Δ*imuA*′::*vfp-imuA*′ was 2.16-fold greater than WT and 51.3-fold greater than Δ*imuA*′. Similarly, the MIMF of Δ*imuB*::PSOS(*imuA*′)-*egfp-imuB* was 1.33-fold and 47.6-fold greater than those of WT and Δ*imuB*, respectively. Therefore, both complemented strains exhibited mutation frequencies that were comparable to WT, thus confirming function of the FP-tagged mutasome proteins. This was an important result as it demonstrated that the addition of an N-terminal

fluorescent tag did not appear to impede the function of either ImuA' or ImuB during mutasome-dependent mutagenesis and further established the potential utility of the FP-tagged proteins for downstream assays of expression dynamics and protein localization in live *Msm* cells.

2.2. N-terminal Labelling of ImuB Impacts DNA Damage Tolerance

A second functional role of the mutasome is to increase the tolerance of *Msm* bacilli to genotoxic stress. That is, prior work has demonstrated that deletion mutants lacking any one of the mutasome components (DnaE2, ImuB, or ImuA') are hypersusceptible to genotoxic stress (Warner, *et al.*, 2010; Boshoff, *et al.*, 2003). Therefore, it was necessary to test whether the EGFP tag had impacted this function of the ImuB protein in the Δ*imuB*::PSOS(*imuA'*)-*egfp-imuB* complemented strain. The DNA damage tolerance of the Δ*imuA'*::*vfp-imuA'* mutant had been characterized as part of previous work (**Section 6.1**, **Supplementary Figure S1**) (Reiche, *et al.*, unpublished); therefore, DNA damage tolerance assays were conducted on Δ*imuB*::PSOS(*imuA'*)-*egfp-imuB* (**Figure 3-7**). WT *Msm* exhibited growth at a maximum dilution factor of 10^3 (~2.7×10^7 colony forming units, CFU, per ml) on 0.04 μg/ml MMC and 10^5 on 0.02 μg/ml MMC. In comparison, Δ*imuB* was at least 10-fold more susceptible, failing to grow beyond a dilution of 10^1 and 10^3 on 0.04 μg/ml and 0.02 μg/ml MMC, respectively. Again, these results were consistent with prior observations (Warner, *et al.*, 2010). Unexpectedly, despite the ability of the PSOS(*imuA'*)-*egfp-imuB* allele to complement loss of mutagenic capacity (**Figure 3-6**), the same construct did not result in a detectable decrease in MMC susceptibility when compared to the Δ*imuB* parental strain. Instead, the Δ*imuB*::PSOS(*imuA'*)-*egfp-imuB* and Δ*imuB* strains had similar growth on

MMC-supplemented solid media: growth at a maximum dilution of 10^3 on 0.02 µg/ml and 10^1 on 0.04 µg/ml MMC. This was 2-$\log_{10}$ less than the growth of WT on 0.02 µg/ml MMC and 1-$\log_{10}$ less than the growth of WT *Msm* on 0.04 µg/ml MMC. This result was surprising and indicated that the modified *imuB* allele of PSOS(*imuA'*)-*egfp*-*imuB* did not maintain WT functionality with respect to tolerance of DNA damage. The reason for this was not clear and may have resulted from the EGFP tag partially disrupting function of the ImuB N-terminus or from a change in the regulation and expression of the fusion protein under sustained genotoxic stress on solid medium.

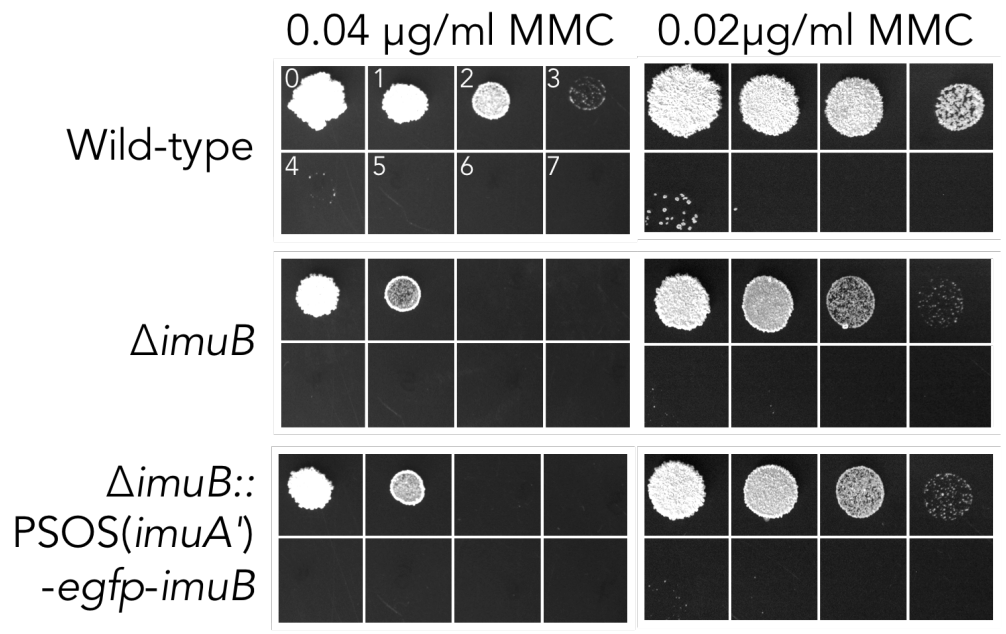

Figure 3-7 | DNA damage tolerance assay of Δ*imuB*::PSOS(*imuA'*)-*egfp*-*imuB*
The photographs indicate the growth of *Msm* colonies (white) on 0.02 µg/ml (top) and 0.04 µg/ml (bottom) MMC-containing media (black) after serial dilution. The spotting order of each dilution factor (10^0 to 10^7) is presented in the first block and is the same for each strain.

2.3. EGFP Linked to the N-terminus of ImuB Maintains Fluorescent Capacity

The restoration of mutagenic capacity in Δ*imuB*::PSOS(*imuA'*)-*egfp-imuB* indicated that the EGFP-ImuB fusion protein retained biological function in mutgenesis assays, but not damage tolerance. This result supported progression of this work to an evaluation of the fluorescence function of the EGFP tag. To this end, *Msm* strains were visualized under a fluorescent confocal microscope following induction of the SOS response by exposure to MMC for 4 h (equating approximately to one generation time and one round of chromosome replication; Aldridge, *et al*., 2012; Santi, *et al*., 2013). In this experiment, the hypothesis was that, upon exposure of Δ*imuB*::PSOS(*imuA'*)-*egfp-imuB* to MMC for 4 h, green fluorescent signal generated by EGFP-ImuB would be detected, indicating functional fluorescence of the hybrid reporter protein. In addition, the previously generated Δ*imuA'*::*vfp-imuA'* strain was assessed for yellow fluorescent signal the same way by growing 5 ml cultures in the presence of 2× MIC MMC for 4 h to incur DNA damage. Representative images of both untreated and MMC-exposed Δ*imuA'*::*vfp-imuA'* and Δ*imuB*::PSOS(*imuA'*)-*egfp-imuB* are presented in **Figure 3-8**. Following exposure of Δ*imuA'*::*vfp-imuA'* to MMC, a diffuse yellow fluorescent signal (514 nm excitation and 538 nm emission) was observed throughout each bacillus. This suggested that VFP-ImuA' signal was present throughout the cytoplasm of the cell. In contrast, visualisation of Δ*imuB*::PSOS(*imuA'*)-*egfp-imuB* after exposure to MMC revealed confinement of the green fluorescent signal to specific punctate foci within each bacillus. That is, cells with detectable levels of EGFP signal were characterized by clearly defined green fluorescence 'foci'.

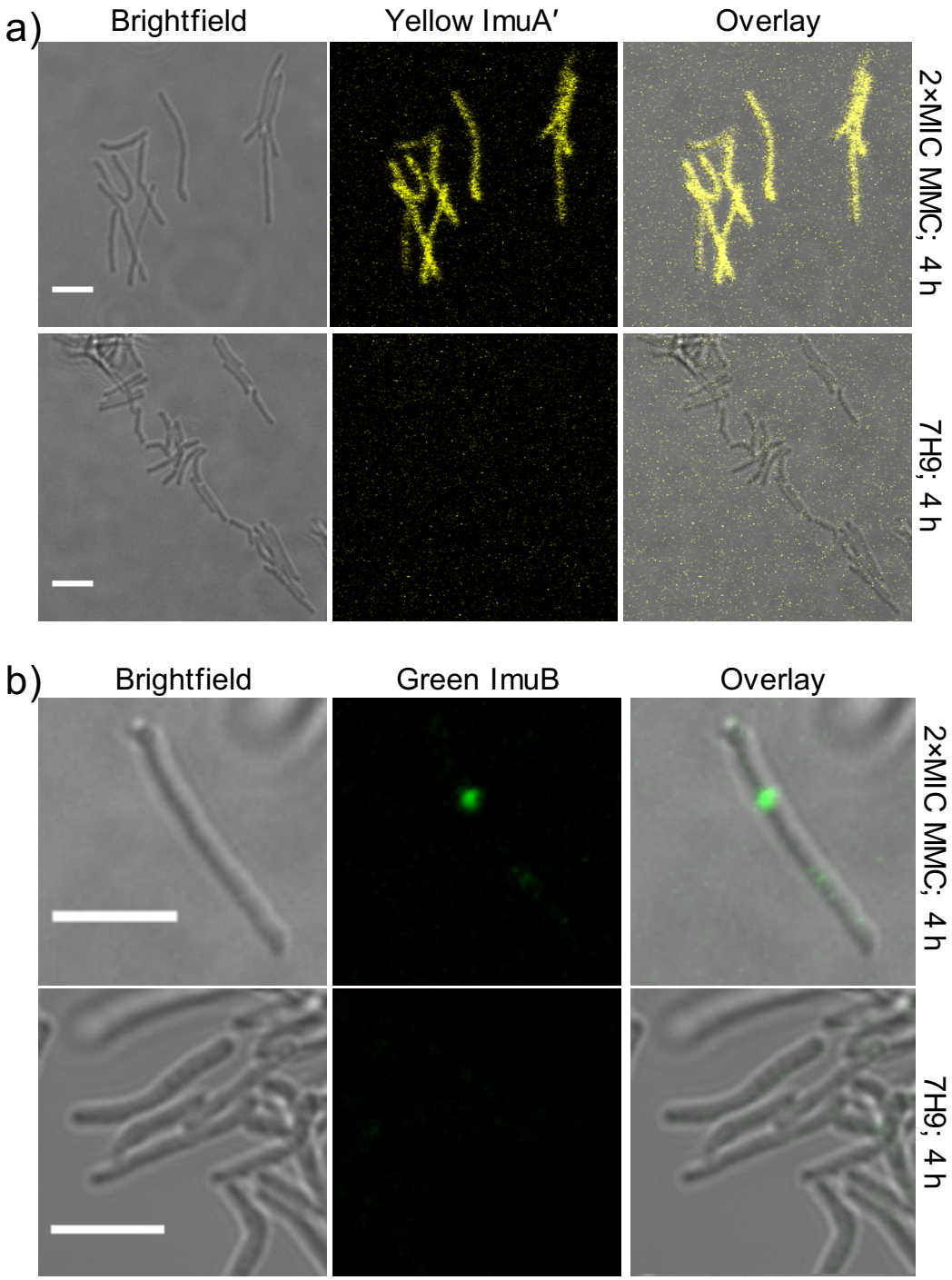

Figure 3-8 | Expression and location of fluorescently tagged mutasome components
Fluorescent micrographs of the ImuA′ and ImuB localization. The *in vivo* localization of the mutasome accessory proteins during mutagenic DNA repair. (a) VFP-ImuA′ fluorescence of Δ*imuA*′::*vfp-imuA*′ in the presence (top row) or absence of MMC (bottom row). Left pane illustrates brightfield micrographs of bacilli; middle pane shows detected yellow fluorescence; right pane is an overlay of yellow fluorescence signal and brightfield micrographs. (b) EGFP-ImuB fluorescence of Δ*imuB*::PSOS(*imuA*′)-*egfp-imuB* in the presence (top row) or absence of MMC (bottom row). Left pane illustrates brightfield micrographs of bacilli; middle pane shows detected green fluorescence; right pane is an overlay of green fluorescence signal and brightfield micrographs. Scale bars represent 5 µm.

In general, these foci appeared to be located within the interior of the bacilli as opposed to near the cell poles. A large majority of cells exposed to MMC contained at least one focus of EGFP-ImuB signal. Bacilli with cell lengths greater than the standard *Msm* size of ~4 μm (Gordon and Smith, 1953; Santi and McKinney, 2015) were associated with multiple, distinct foci. In these cases, it appeared that one focus was often larger than the others. The contrasting fluorescence profiles of Δ*imuB*::PSOS(*imuA'*)-*egfp*-*imuB* and Δ*imuA'*::*vfp*-*imuA'* indicated a difference in the location of each respective protein. Notably, the fact that the same focus formation was not observed with the PSOS(*imuA'*)-*egfp* reporter construct (which expressed EGFP without being linked to the ImuB protein; **Figure 3-2**) suggested that localization was due to the presence of ImuB, and not due to the formation of non-specific EGFP aggregations or inclusions. A third mutasome reporter strain, Δ*dnaE2*::*egfp*-*dnaE2* was also constructed, but this did not yield observable green fluorescence after multiple attempts (data not shown) and was abandoned in favor of a thorough investigation of ImuB, the predicted, central adapter protein of the mutasome (Warner, *et al*., 2010) (**Chapter I**, **Figure 1-5**).

2.4. ImuB Localizes to Specific Points within Bacilli During the DNA Damage Response

To confirm that the apparently specific localization of EGFP foci following exposure of Δ*imuB*::PSOS(*imuA'*)-*egfp*-*imuB* to MMC was a function of ImuB, it was necessary to generate an alternative reporter in which ImuB was tagged with a different FP. To this end, Δ*imuB*::PSOS(*imuA'*)-*mEos4a*-*imuB* was developed by replacing *egfp* with a gene encoding the photoconvertible FP, MEos4a. This FP was chosen as it is not derived from GFP, and thus does not

share significant sequence homology with EGFP. Consequently, the potential for non-physiological localization of the fusion protein as a consequence of fluorescence tagging with unrelated FPs was considered highly unlikely.

The hypothesis for this experiment was that fluorescent foci of MEos4a would be visible, replicating the foci observed previously during EGFP-ImuB expression. Confocal fluorescent micrographs of representative Δ*imuB*::PSOS(*imuA'*)-*mEos4a-imuB* cells in the absence or presence of MMC are presented in **Figure 3-9**. Similar to EGFP-ImuB, fluorescence foci were present following the exposure of Δ*imuB*::PSOS(*imuA'*)-*mEos4a-imuB* to 1× MIC MMC for 4 h (**Figure 3-9a**, middle panel). As a photoconvertible fluorescent protein, exposure of MEos4a to low levels of UV light converted the fluorophore into a 'converted' state (Paez-Segala, *et al*., 2015). Specifically, MEos4a is converted from a native, green fluorescent state to a red fluorescent state. This was achieved by exposing the field of view to low-intensity UV light (390 nm epifluorescent light) for 30 s (**Figure 3-9a**, right panel; and **Figure 3-9b**, bottom). It was evident that the green MEos4a-ImuB foci photoconverted to the red-fluorescent state (**Figure 3-9a**), resulting in congruent red fluorescent foci that exhibited an activation contrast of 10.16× (**Figure 3-9b** and **Figure 3-9c**), defined as the ratio of the signal intensity after UV-photoconversion to the signal intensity before conversion. The presence of MEos4a-ImuB foci following MMC treatment strongly suggested that the location of the fluorescent focus was a function of SOS-dependent ImuB expression and recruitment, and was not a spurious consequence of the FP tag. This observation was further supported by the previous demonstration that untagged EGFP protein

expressed from P(*imuA'*) during DNA damage did not localize into observable foci within the WT::PSOS(*imuA'*)-*egfp* bacilli.

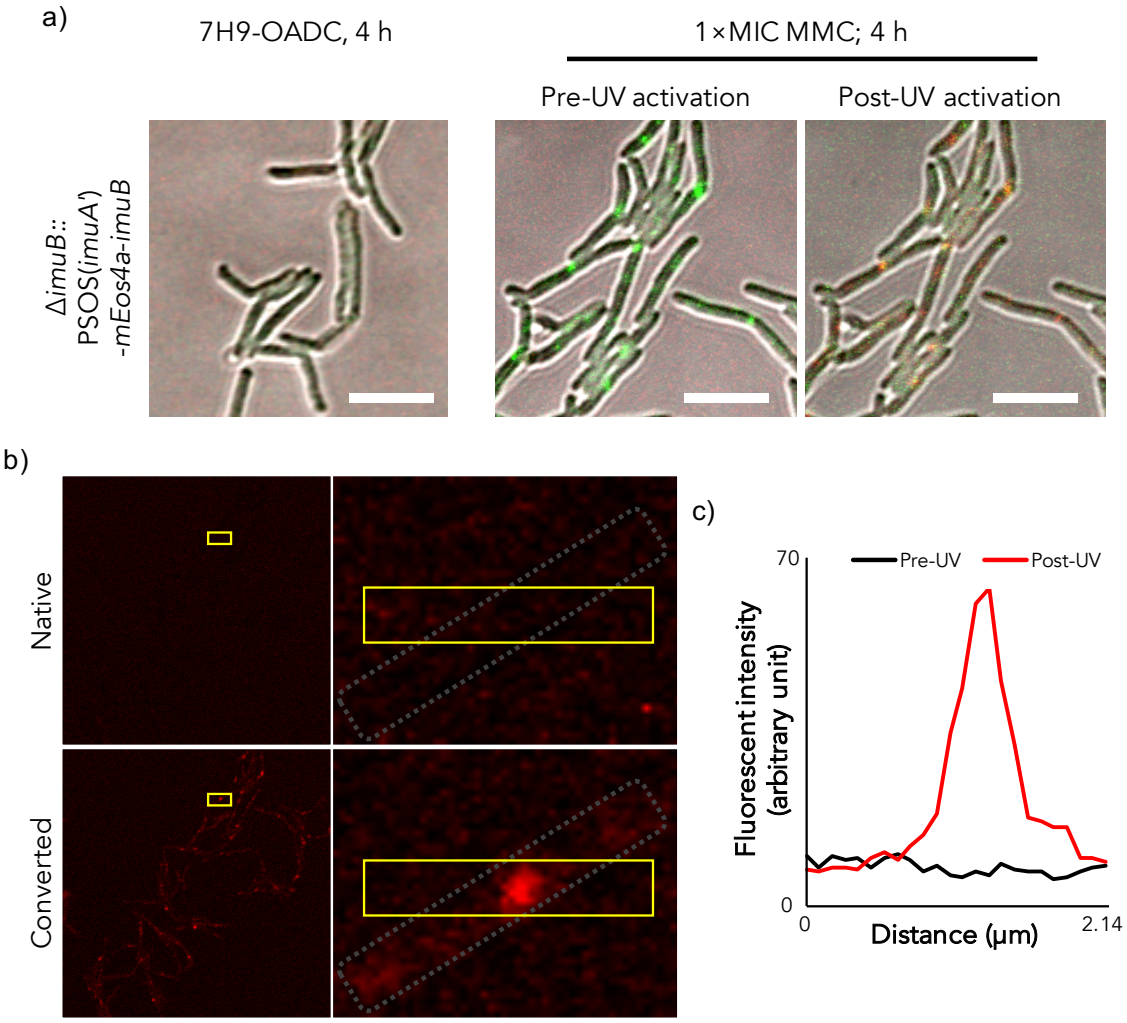

Figure 3-9 | Photoconverion of MEos4a tagged ImuB

(a) Micrographs of MEos4a-ImuB foci fluorescence conversion. Each micrograph consists of a brightfield image overlayed with both green and red fluorescent signal from Δ*imuB*::PSOS(*imuA'*)-*mEos4a-imuB*. The left-hand pane indicates the lack of fluorescence observed in the absence of MMC. The two panes on the right illustrate different fluorescent states of the MEos4a-ImuB protein before (center) and after (right) UV light photoconversion following exposure to 1× MIC MMC for 4 h. Scale bars represent 5 μm. (b) Red fluorescent micrographs of MEos4a-ImuB-expressing bacilli before (top row) and after (bottom row) conversion by UV light. The left pane illustrates a full field of view, while the right pane indicates a single bacillus (demarcated by the grey dotted line). The area marked by the yellow rectangle indicates the region of interest used to plot the fluorescent intensity profile represented in the graph in (c). In this graph, the red plotted line illustrates the red fluorescent intensity following UV light conversion of MEos4a; while the black plot illustrates the red fluorescent intensity before photoconversion. The peak of red fluorescence following UV conversion corresponds to the location of the fluorescent MEos4a-ImuB foci in the bacilli.

2.5. Superresolution Imaging Confirms Formation of ImuB Foci in SOS-active Mycobacterial Cells

The photoswitchable MEos4a tag provided the opportunity to visualize ImuB foci using superresolution three-dimensional interferometric photo-activated light microscopy (3D-iPALM) (Shtengel, *et al*., 2009). Indeed, because the large photoconversion activation contrast of MEos4a-ImuB was in excess of the requisite four-fold difference (Jesse Aaron, personal communication, 2015), Δ*imuB*::PSOS(*imuA'*)-*mEos4a-imuB* presented an ideal sample for iPALM imaging. Consequently, cultures of Δ*imuB*::PSOS(*imuA'*)-*mEos4a-imuB* were exposed to 5× MIC MMC for 8 h to induce maximal expression of the mutasome before cells were fixed in 0.5% paraformaldehyde and prepared for iPALM imaging.

Bacilli were imaged and fluorescent MEos4a-ImuB foci were resolved with a resolution near 20 nm (comparison presented in **Figure 3-10a**). Despite the increase in resolving power, an underlying macromolecular structure was not easily resolved in any cells imaged. Clearly separated foci were determined to be 287 ± 32.75 nm (mean ± SD) in size as measured by full-width, half maximum along the axis of the cell (data not shown). It was also evident that large foci observed under epifluorescence microscopy often consisted of two separate foci when resolved using iPALM localization (**Figure 3-10b**). An interesting observation was made during the imaging of *Msm* by this technique: that is, it consistently appeared that the bacilli were located ~200 nm above the coverslip, preventing the use of total internal reflection fluorescence (TIRF) imaging for data acquisition. Addressing this anomaly was not within the scope of this

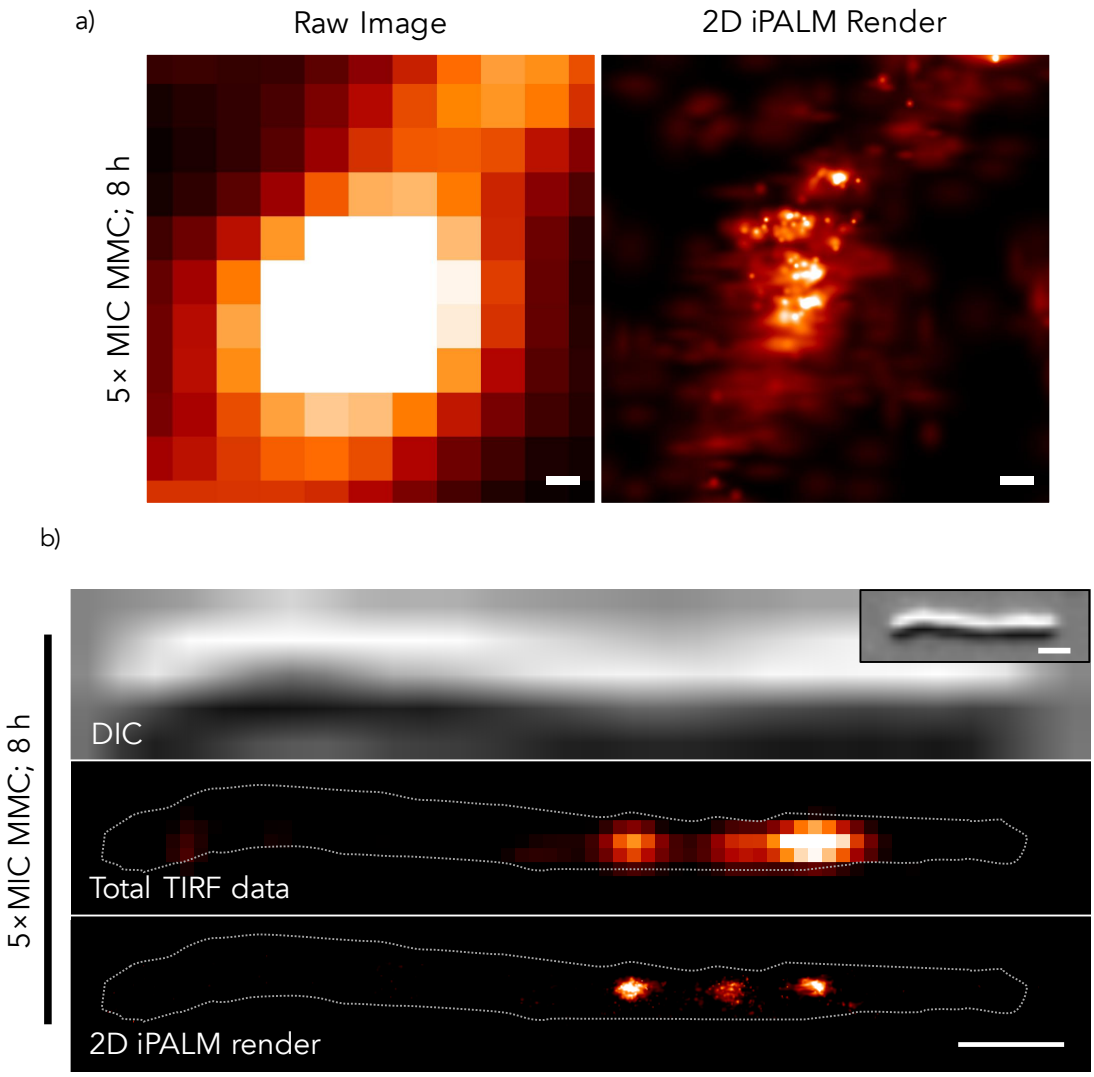

Figure 3-10 | Superresolution images of ImuB foci in *Msm*
3D-iPALM images of bacilli expressing MEos4a-ImuB. (a) The fluorescent signals imaged from MEos4a-ImuB foci were resolved to 20 nm, allowing detailed observation of foci (right) – marked increase over standard fluorescent microscopy (left). However, no underlying structure was observed. Scale bars represent 200 nm. Signal intensity of 2D iPALM render represents the Total Molecule Probability and ranges from minimum (black) to maximum (white) red fluorophore molecules/nm^2. (b) A single bacillus (demarcated by grey, dotted line) when imaged by 3D-iPALM illustrates that often large MEos4a-ImuB foci consisted of two smaller foci. Scale bars represent 1 µm.

work nor supportable given the limited time frame for accessing the iPALM system at the *Janelia Research Campus* of the *Howard Hughes Medical Institute*. As a result, the cause and potential solution were not investigated; however, it is important to note that this could represent a biologically significant observation or that the sample preparation affected the sample in an unknown manner. Regardless, iPALM imaging further illustrated specific recruitment of

ImuB within *Msm*; however, it was not possible to discern any clear pattern of distribution of foci, nor did the foci themselves permit any inference regarding mechanism of polymerization or aggregation. However, limited and time-restricted access to the iPALM instrument precluded further investigation, and future work into exploring a possible pattern of ImuB recruitment is recommended. Future iPALM experiments should utilise a second protein of interest, such as *dronpa-dnaN*, to view recruitment of ImuB to the β clamp in superresolution and resolve the association of the two proteins. Additionally, it would be worthwhile to consider statistical methods (*i.e.*, Rubin-Delanchy, *et al.*, 2015) to analyse and identify if there is any pattern that could indicate a mechanism of ImuB-DnaN assembly.

2.6. ImuB Co-localizes with the β clamp in *Msm* During Mutagenic DNA Repair

The observation that ImuB localized to specific locations within bacilli suggested that these foci might indicate sites of active mutagenic DNA repair. Previous work (Warner, *et al.*, 2010) provided compelling genetic evidence for a direct protein-protein interaction (PPI) between ImuB and the *dnaN*-encoded β clamp, and further suggested that this interaction was essential for mutasome-dependent mutagenesis. To investigate the inferred ImuB-β clamp interaction further, we utilized the *Msm mCherry-dnaN* strain expressing an MCherry-tagged variant of DnaN, which homodimerizes to form the β clamp processivity factor. The *mCherry-dnaN* reporter mutant has been used previously to visualize the location of the replicative machinery and active replication forks (Santi, *et al.*, 2013; Santi and McKinney, 2015). Both the pAINT::*vfp-imuA'* and pMCAINT::PSOS(*imuA'*)-*egfp-imuB* plasmids were

introduced into the *mCherry-dnaN* mutant, resulting in the generation of *mCherry-dnaN*::*vfp-imuA'* and *mCherry-dnaN*::PSOS(*imuA'*)-*egfp-imuB*, respectively. Please refer to **Table 3-1** for a clarification of strains used in this experiment.

Table 3-1 | Phenotypes of and alleles present within fluorescent mutants of *Msm*

Strain name	Genotype			Fluorescence phenotype
	imuA' allele	*imuB* allele	*dnaN* allele	
mc^2155	*wt*	*wt*	*wt*	ImuA' ImuB DnaN
Δ*imuA'*::*vfp-imuA'*	*vfp-imuA'*	*wt*	*wt*	ImuA' ImuB DnaN
Δ*imuB*::PSOS(*imuA'*)-*egfp-imuB*	*wt*	PSOS(*imuA'*)-*egfp-imuB*	*wt*	ImuA' ImuB DnaN
mCherry-dnaN	*wt*	*wt*	*mCherry-dnaN*	ImuA' ImuB DnaN
mCherry-dnaN::*vfp-imuA'*	*wt*, *vfp-imuA'*	*wt*	*mCherry-dnaN*	ImuA' ImuB DnaN
mCherry-dnaN::PSOS(*imuA'*)-*egfp-imuB*	*wt*	*wt*, PSOS(*imuA'*)-*egfp-imuB*	*mCherry-dnaN*	ImuA' ImuB DnaN

wt, wild-type allele of the corresponding gene found in mc^2155 (Cole, *et al.*, 1998)

As the *mCherry-dnaN* strain already contained a full complement of *Msm* genes, the resulting dual reporter mutants contain the WT alleles (*wt*) of both *imuA'* or *imuB* (at the native genomic location) as well as the hybrid gene *vfp-imuA'* or PSOS(*imuA'*)-*egfp-imuB* located at the *attB*-integrative site, respectively. Therefore, mutagenesis assays were conducted on both mutants to confirm that the merodiploids retained biological function, and to evaluate the potential impact of the MCherry-DnaN protein on inducible mutagenesis (**Figure 3-11a**). All three DnaN-tagged strains resulted in similar MIMFs after exposure to UV irradiation: the MIMF of *mCherry-dnaN* was 5.40×10^{-7}, while *mCherry-dnaN*::*vfp-imuA'* and *mCherry-dnaN*::PSOS(*imuA'*)-*egfp-imuB* had MIMFs of 7.32×10^{-7} and 4.75×10^{-7}, respectively. This result indicated that the merodiploids had similar inducible mutation frequencies to mutants that contained only one variant of

the mutasome genes, albeit with a $\log_{10}$ decrease of 0.431 when compared to WT mc²155.

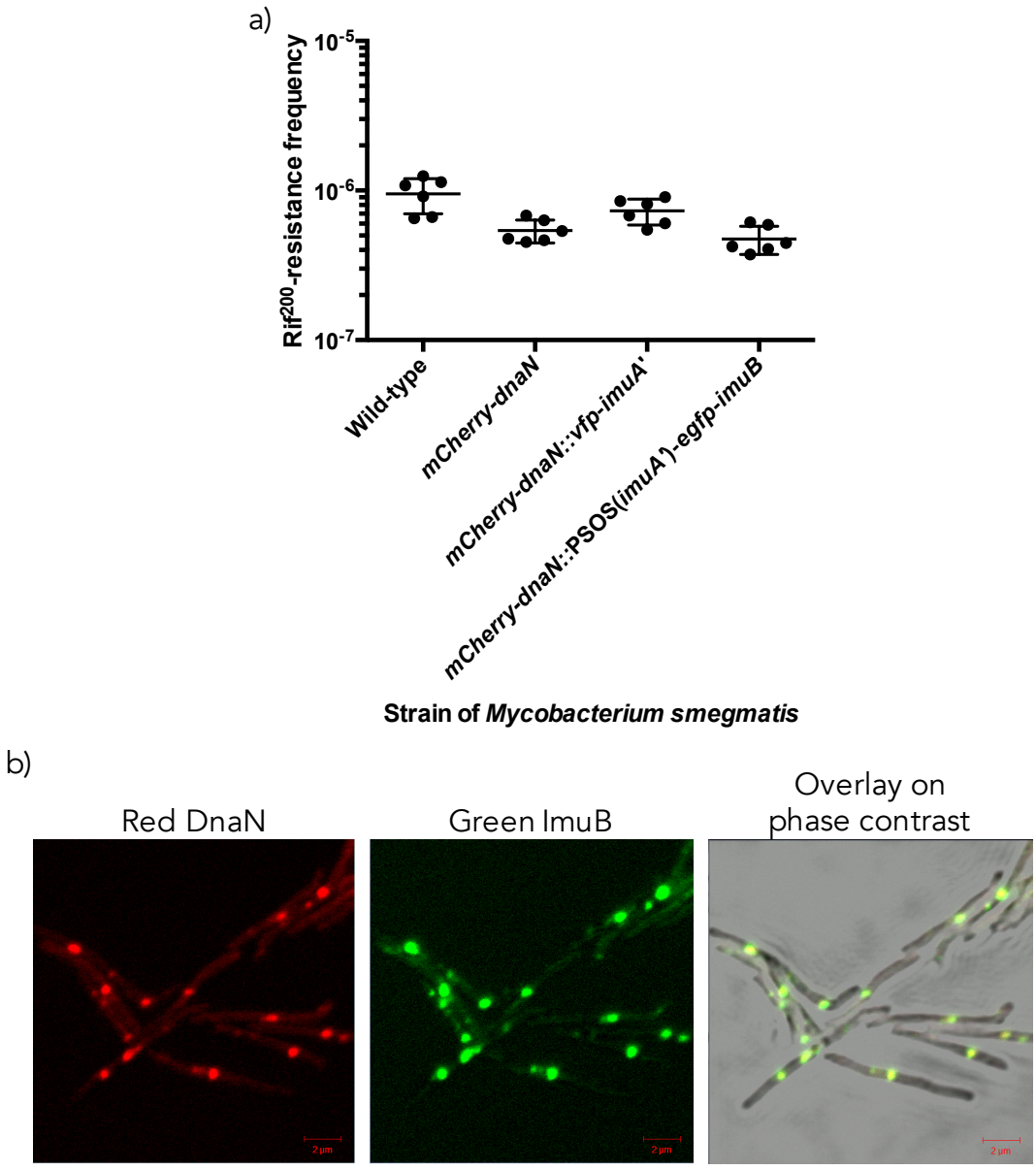

Figure 3-11 | DnaN-MCherry and EGFP-ImuB associate during genotoxic stress
(a) Validation of mCherry-dnaN by mutagenesis assay. The inducible mutation frequency is represented by the frequency of RIF-resistance (*y*-axis, log-scale) for each strain (*x*-axis). Each point represents the result of a single sample and the error bar represents the SD calculated for each strain. Zero-values are not presented on the log-scale. (b) Co-localization of EGFP-ImuB and MCherry-DnaN. Individual micrographs represent different light detection of the same field of view of *mCherry-dnaN*::PSOS(*imuA'*)-*egfp-imuB* bacilli exposed to the genotoxin MMC. Scale bar represents 2 µm.

After confirming the mutagenic capacities of the *mCherry-dnaN* mutants, the *mCherry-dnaN*::PSOS(*imuA'*)-*egfp-imuB* dual reporter was visualized by confocal microscopy following induction of the SOS response with 1× MIC MMC (**Figure 3-11b**). Green fluorescent foci were detected which indicated the location of EGFP-ImuB while red fluorescent foci were used to infer the location of the β clamp (MCherry-DnaN) and, by implication, the active replication fork. When combined, the red and green fluorescent signals are viewed as yellow foci (**Figure 3-11b**, third frame), strongly indicating that EGFP-ImuB and MCherry-DnaN were in close proximity within a single bacillus, consistent with the physical interaction inferred previously by yeast two-hybrid (Y2H) analysis (Warner, *et al.*, 2010). Notably, ImuB foci (green fluorescence) were always located where there was corresponding β clamp (red fluorescence) signal; from analysis of numerous fields of view, this requirement was never relaxed, suggesting the absolute dependency of ImuB on β for accurate recruitment. In turn, this observation supported the hypothesis that the location of EGFP-ImuB foci represent the sites of active mutagenic DNA repair.

2.7. The Development of an ImuB Foci is Independent of a Functional Mutasome

The use of recombinant fluorophore-protein fusions revealed the possibility that multiple mutasome complexes (inferred from EGFP-ImuB foci) could form in association with multiple replication forks (MCherry-DnaN) in a single bacillus during prolonged genotoxic stress. This prompted the hypothesis that, despite induction of the SOS response, genome replication continued – thereby explaining why multiple foci appeared to develop in a time-dependent manner. If this were the case, the only way the entire chromosome could be

replicated in the presence of extensive DNA damage would be if repair mechanisms allowed DNA synthesis to continue despite the presence of DNA lesions. In turn, this raised the intriguing possibility that a non-functional mutasome might result in stalled genome replication in the presence of severe DNA damage. That is, it might be plausibly predicted that multiple chromosomes would not form in a mutasome-deficient *Msm* strain during MMC treatment and multiple mutasome foci would not be visible. To test this hypothesis, Δ*imuA'*::PSOS(*imuA'*)-*egfp-imuB*, *dnaE2*^{AIA}::PSOS(*imuA'*)-*egfp-imuB*, and Δ*dnaE2*::PSOS(*imuA'*)-*egfp-imuB*, all of which lack a functional mutasome (Warner, *et al*., 2010), were exposed to inhibitory concentrations of MMC for 3 h and visualized using an epifluorescent light microscope (**Figure 3-12**). In contrast to the experimental hypothesis, more than one focus was evident in cells of all three mutasome-deficient strains (Δ*imuA'*, Δ*dnaE2*, and *dnaE2*^{AIA}) after only one generation. This result indicated that the formation of multiple

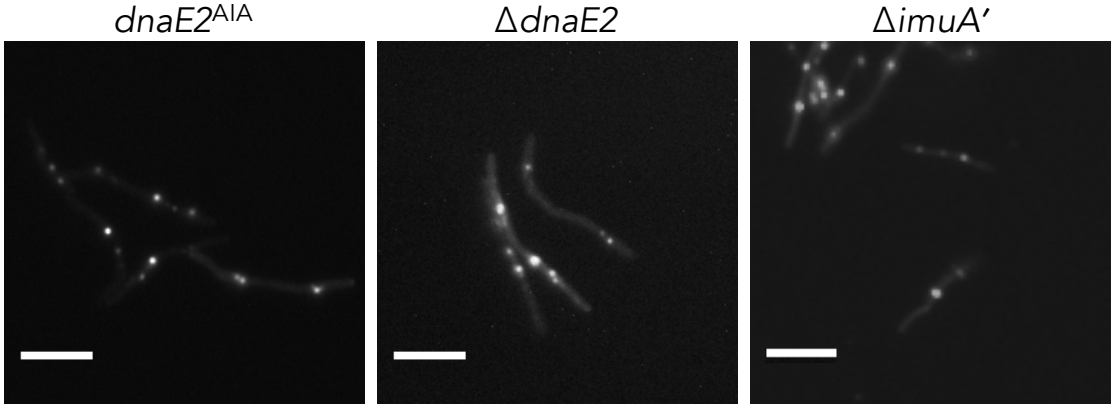

Figure 3-12 | DNA damage-induced formation of multiple ImuB foci is independent of ImuA' or DnaE2 during prolonged MMC exposure

Fluorescent EGFP-ImuB was imaged in different backgrounds of *Msm* following exposure to 1× MMC for 3 h. Left: Green fluorescence derived from Δ*dnaE2*::*dnaE2*^{AIA}::PSOS(*imuA'*)-*egfp-imuB* bacilli after induction of the SOS response. Middle: Green fluorescent micrograph of Δ*dnaE2*::PSOS(*imuA'*)-*egfp-imuB*. Right: Green fluoreacent signal detected from Δ*imuA'*::PSOS(*imuA'*)-*egfp-imuB* indicates the formation of multiple fluorescent foci in individual bacilli. Images were captured with a monochrome camera, with an 80× 1.2 NA objective lens. Scale bars represent 5 μm.

mutasome complexes was not dependent on the repair of the chromosome by a functional mutasome. Importantly, this result also indicated that the formation of ImuB foci was independent of functional DnaE2 and ImuA'.

2.8. ImuB Recruitment is Dependent on a Functional β Clamp-binding Domain

In order to validate the inferred association between EGFP-ImuB and MCherry-DnaN, it was necessary to confirm that the recruitment of ImuB to the β clamp could be prevented by a rational, genetic disruption. To this end, the putative β clamp-binding motif located within ImuB was mutated as described previously (Warner, *et al*., 2010), by alanine replacement of the essential QLPLWG residues (**Figure 3-13a**). The resulting mutant, denoted Δ*imuB*::PSOS(*imuA'*)-*egfp*-*imuB*^{AAAAG}, contained a nonfunctional β clamp-binding domain that would nevertheless allow visualisation of ImuB localization in the absence of the putative interaction with DnaN. Following induction of the SOS response in Δ*imuB*::PSOS(*imuA'*)-*egfp*-*imuB*^{AAAAG} by exposure of bacilli to 2× MIC MMC for 4 h (**Figure 3-13b**, right panel), diffuse green fluorescence was observed throughout the cells and there was a clear absence of defined foci. When the level of fluorescence throughout randomly selected individual bacilli was quantified (**Figure 3-13c**), it was evident that there was increased fluorescence in the EGFP-ImuB^{AAAAG} mutant, confirming induction of the *egfp*-*imuB*^{AAAAG} allele, but that the mutant had lost the capacity to form clearly-defined foci.

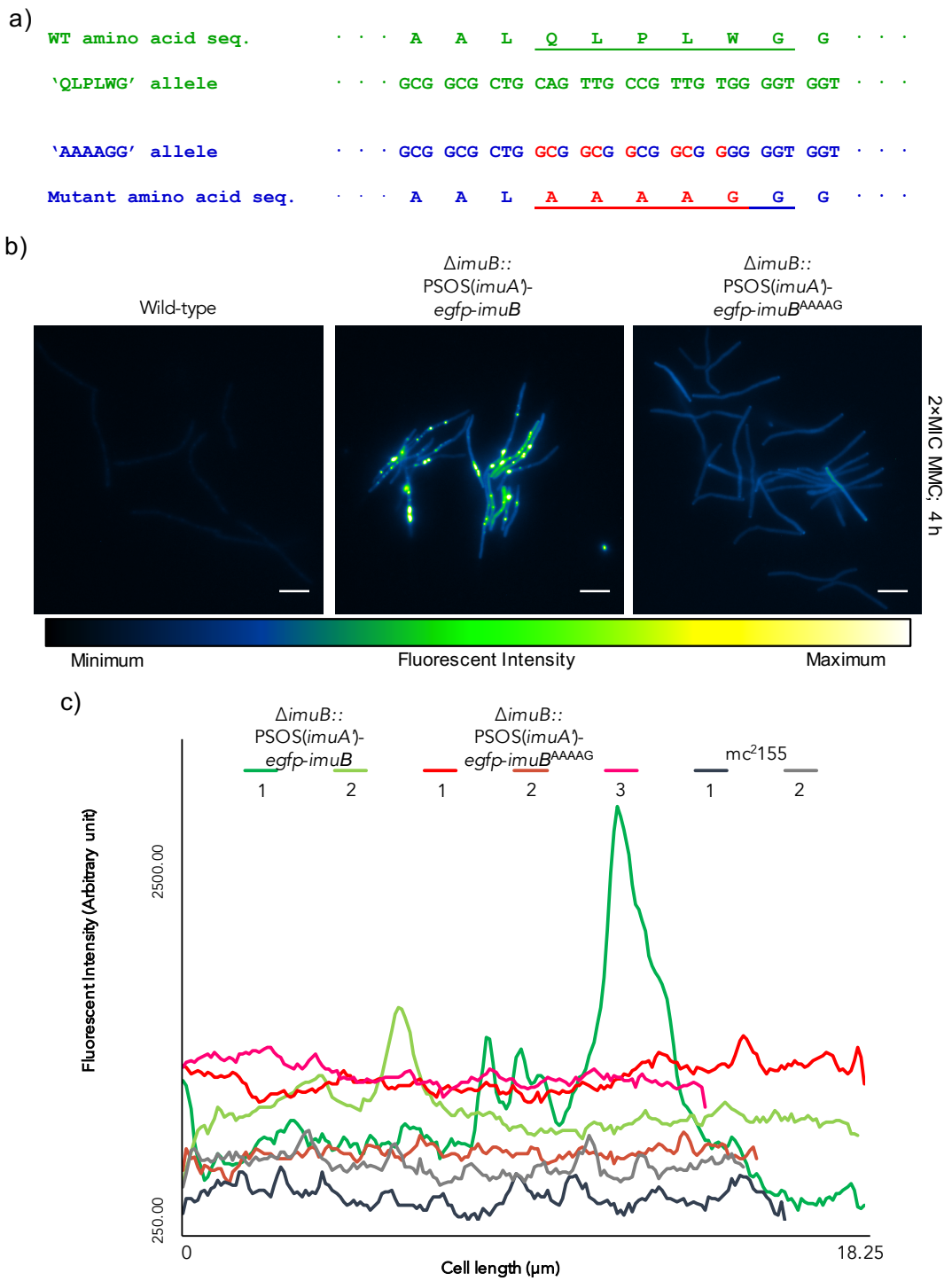

Figure 3-13 | Disruption of ImuB-β clamp interaction eliminated EGFP-ImuB focus formation in *Msm*
(a) Illustration of the mutated β clamp binding domain (AAAAG) in *Msm*. Red letters represent altered nucleotides and amino acids different from the WT (QLPLW) sequence. (b) The fluorescent reporter strain containing a mutated β clamp binding site within the *imuB* gene was exposed to MMC and imaged using an epifluorecscent microscope. Although Δ*imuB*::PSOS(*imuA'*)-*egfp-imuB*^{AAAAG} exhibited green fluorescence, the bacilli did not produce observable foci following exposure to MMC and induction of the SOS response. Scale bars represent 5 μm. (c) Green fluorescent intensity profiles of randomly selected bacilli illustrating the lack of fluorescent foci and increased cell-wide fluorescence observed in Δ*imuB*::PSOS(*imuA'*)-*egfp-imuB*^{AAAAG}. Light and dark green lines represent Δ*imuB*::PSOS(*imuA'*)-*egfp-imuB*; red, brown and pink lines represent Δ*imuB*::PSOS(*imuA'*)-*egfp-imuB*^{AAAAG}; and black and grey lines represent WT.

3. DNA Replication and Repair in Filamentous *Msm* Cells During Prolonged DNA Damage

While investigating the response of *Msm* to genotoxic stress as a function of time (**Section 1.2.2.1**), it became evident that *Msm* cells exposed to inhibitory concentrations of MMC for 24 h were not able to pass through a 30 µm cell strainer. This suggested that the cells might be clumping or may have grown longer than 30 µm. To investigate these possibilities, the cells that were prepared for cytometric analysis were visualized using a brightfield cell imaging microscope (**Figure 3-14**). It was immediately evident that prolonged exposure to the genotoxin had induced a cell elongation phenotype, with many cells characterized by lengths in excess of 25 µm; in contrast, cells not exposed to MMC exhibited normal cell lengths of ±4 µm (Gordon and Smith, 1953; Santi and McKinney, 2015). In turn, this observation prompted a more thorough investigation into the genotoxicity-mediated cell elongation phenotype in *Msm*.

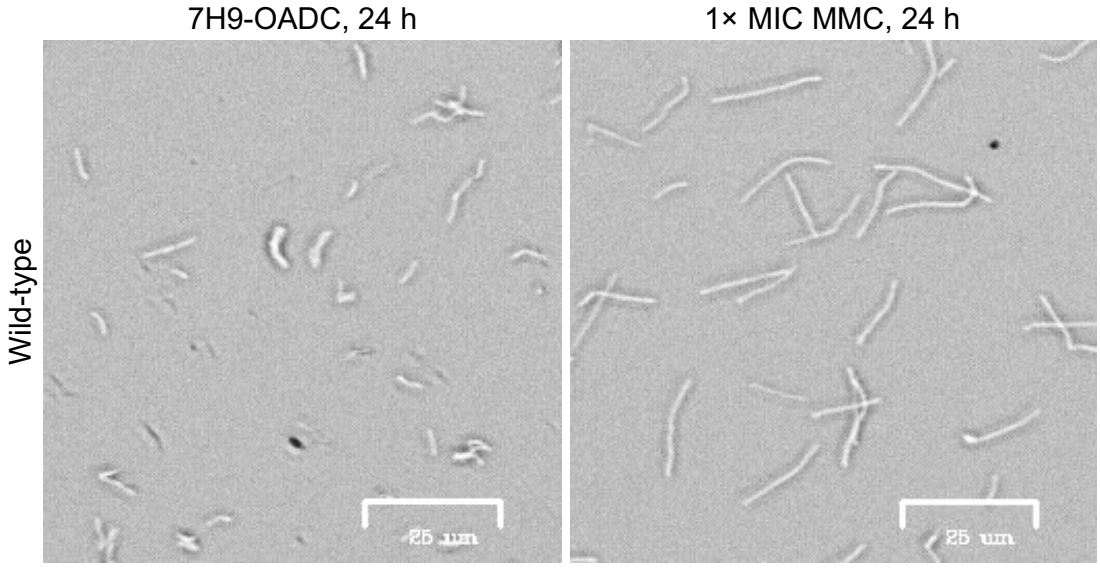

Figure 3-14 | Light micrograph of *Msm* cell elongation following prolonged MMC exposure
Brightfield images of WT::PSOS(*imuA'*)-*egfp* cells grown for 24 h either in the absence (left) or presence of 1× MIC MMC (right) as part of the time response experiment. Scale bars represent 25 µm.

3.1. Retrospective Analysis of Cell Length During MMC-exposure Experiments

To test the hypothesis that exposure of *Msm* to MMC for extended durations resulted in cell elongation, all previous micrograph images were analyzed retrospectively. To achieve this, the length of every undistorted and discernible *Msm* bacillus exposed to inhibitory concentrations of MMC was manually measured and stratified by exposure duration. **Figure 3-15a** illustrates the individual cell lengths for samples not exposed to MMC (untreated), as well as cultures exposed to inhibitory concentrations of MMC for differing time periods from 3 to 48 h. It is necessary to point out that these results reflected the cell lengths of all *Msm* strains imaged during the course of this work (with the exception of the mutasome deletion mutants Δ*imuA'*, Δ*imuB*, and Δ*dnaE2*). Owing to the retrospective nature of this analysis, compounding factors such as growth phase, cell viability, and cell density were not accounted for: the aim was to obtain a cumulative picture of the propensity for filamentation in MMC-treated bacilli. From this analysis, it was evident that cells grown in the absence of MMC had a median length of 4.7 μm and an interquartile range (IQR) of 1.8 μm. The morphology of these cells represented the expected size of rod-shaped *Msm* bacilli over all phases of growth in 7H9-oxidase-albumin-dextrose-catalase (OADC). When observing the lengths of cells exposed to inhibitory concentrations of MMC, it was clear that cell length increased with increasing duration of exposure. *Msm* exposed to MMC for 3 h exhibited a median cell length of 7.1 μm (IQR: 2.6 μm). The median cell length of bacilli exposed to MMC for 4 h was 1.71 times greater than that of unexposed cells (8.0 μm median; IQR of 2.6 μm). Exposure of *Msm* to MMC for 24 h was associated with

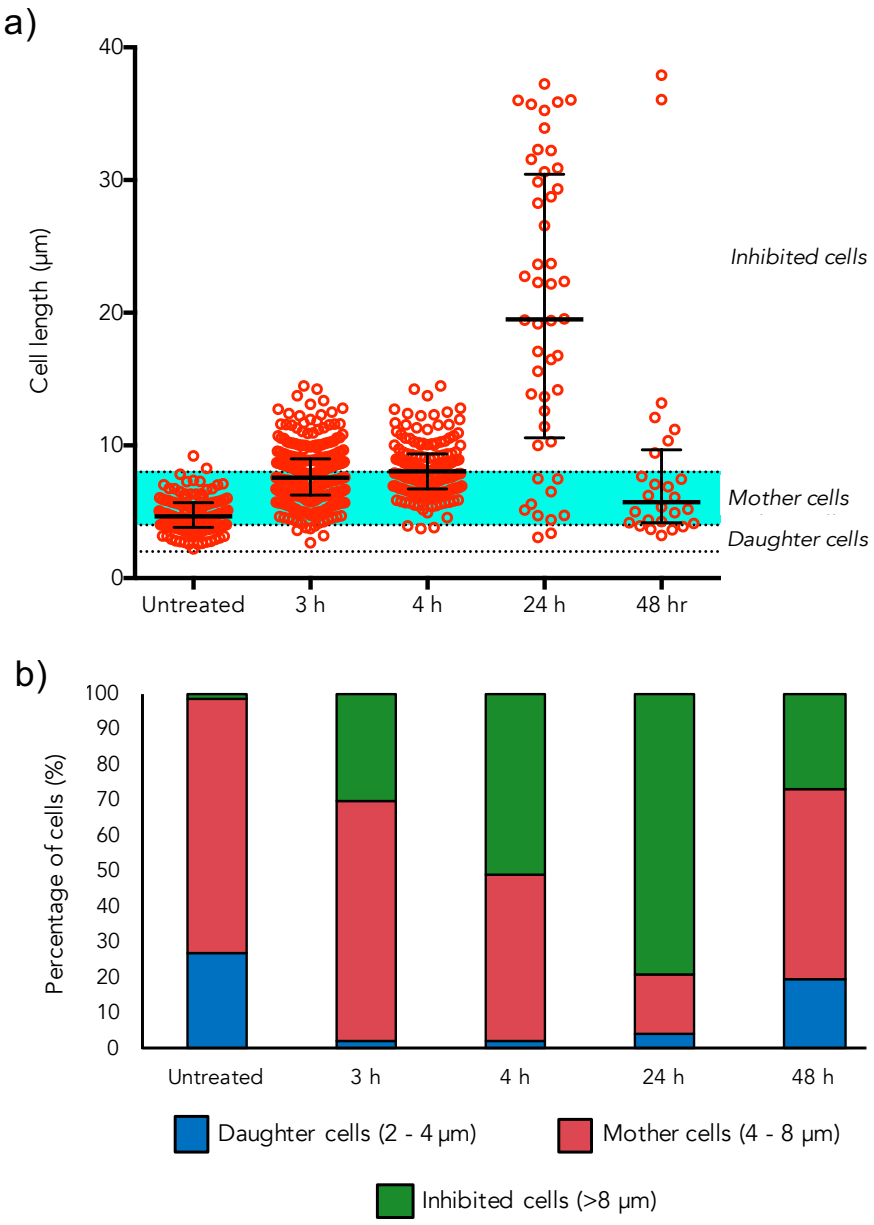

Figure 3-15 | Exposure of *Msm* to inhibitory concentrations of MMC increases the average cell length over time.

(a) The length of cells measured during MMC exposure experiments. The length of individual cells was measured for *Msm* grown in the absence of MMC (untreated) (n = 196) and cells exposed to inhibitory concentrations of MMC (1× or 5× MIC) for 3 h (n = 189); 4 h (n = 160); 24 h (n = 48); and 48 h (n = 26). The median and IQR are indicated by the error bars. The classification of cell length is indicated on the right of the graph. (b) Stacked-bar graph representing the proportional population composition of *Msm* following exposure to MMC for different periods of time. Differing supra-inhibitory concentrations (1× or 5× MIC) of MMC was deemed not to significantly affect the length of cells (presented in Supplementary Figure S2).

a considerable increase in median cell length (19.5 µm, 4.1 times greater than untreated cells) as well as distribution (IQR of 19.9 µm). Conversely, cells exposed to MMC at inhibitory concentrations for 48 h had decreased cell

lengths with a median of 5.7 μm but a comparatively large IQR of 5.5 μm. This discrepancy was likely due to the decreased stability of MMC in liquid growth media and, potentially, the death of bacilli owing to accumulated DNA damage. To investigate this, future experiments consisting of extended time points should include wash steps and resuspension of bacilli in media containing fresh MMC at regular intervals of 12 h. Furthermore, a dead-cell stain such as propidium iodide (Krämer, *et al.*, 2016) could be used to enumerate the number of cells killed during extended MMC exposure times to determine if this was the cause of the decreased cell lengths following 48 h exposure periods.

When comparing the frequency distribution of each subset of cells (**Figure 3-15a**), it was evident that, with increasing duration of MMC exposure, there was a corresponding shift in the distribution towards longer cell lengths. The composition of each population could be arbitrarily categorized into newly divided daughter cells (lengths between 2 and 4 μm); mother cells capable of cell division (4 to 8 μm); or division-inhibited cells (greater than 8 μm). The cell distribution of each population is presented in **Figure 3-15b**. Here, 27.04 % of untreated *Msm* represented newly divided bacilli, while 71.43 % of cells in the population were actively growing in preparation of cell division and only 1.53 % exhibited inhibition of cell division. In comparison, 2.12 % of the cells present after 3 h of MMC exposure represented newly divided cells, 67.20 % represented cells ready for cell division and 30.69 % presented with inhibited cell division. Of the cells exposed to MMC for 4 h, 1.88 % represented newly divided daughter cells, 46.88 % were ready for cell division and 51.25 % indicated a division arrest/elongation phenotype. Only 4.17 % of cells observed

after exposure to MMC for 24 h were newly formed daughter cells, while 16.67 % were ready for division and 79.17 % had inhibited cell division. In comparison, 19.23 % of cells visible after 48 h of MMC exposure were newly divided daughter cells, 53.85 % were mother cells capable of division, and 26.92 % had the cell division inhibition phenotype. The apparent loss of the MMC effect at 48 h is likely due to loss of potency of the drug over the time course of the experiment. This is illustrated by the frequency distribution of cells exposed to MMC for 48 h, which more closely resembled that of normal *Msm* populations or those exposed to MMC for a short period of time, suggesting the commencement of cell division between 24 and 48 h. This is also supported by the sample of cells exposed to MMC for 48 h which had a higher proportion of 'daughter cells', mimicking that of untreated cells. Overall, the decrease in frequency of newly divided cells in the presence of MMC indicated inhibition of cell division. This was associated with an increase in the number of abnormally long cells, suggesting that genotoxic stress resulted in inhibition of cell division which, over prolonged periods of time, resulted in filamentous bacilli.

3.2. Individual Cell Elongation as a Response to Prolonged Genotoxic Stress

It was evident that prolonged exposure to genotoxic stress had induced a cell elongation phenotype, with many cells characterized by lengths in excess of 25 μm. In turn, this observation suggested the possibility that cell elongation as a result of DNA damage in *Msm* may additionally result in the development of multiple mutated (mutasome-associated) genomes within individual cells, potentially allowing for the rapid emergence and selection of resistant mutants

by providing an environment suitable for DNA recombination between differentially-mutated chromosomes. For this to be a plausible hypothesis, it was necessary first to test whether the observed elongated cell phenotype was a consequence of the continued growth of bacilli in the absence of cell division (*i.e.*, elongated cells that lacked division septa), or whether multiple, distinct daughter cells of normal lengths were forming concatenated structures owing to a failure to separate physically after normal cytokinesis. To this end, the *wag31-gfp* strain of *Msm* was utilized, which expressed a recombinant GFP-tagged Wag31 protein. This protein has been identified to localize to the cell poles during cell growth as part of peptidoglycan synthesis (Santi, *et al.*, 2013; Santi and McKinney, 2015); therefore, localization of a green fluorescence signal to the cell poles in this strain can be used to delineate individual cells. The *wag31-gfp* reporter strain was exposed to 1× or 5× MIC MMC for 24 h before visualisation under a confocal fluorescent microscope (**Figure 3-16**). Once more, the cell elongation phenotype was evident in cells exposed to MMC, with the length of single cells exceeding 35 μm in some cases. Importantly, green fluorescence was detected at the cell poles of each elongated structure. In addition, most elongated cells also exhibited small green fluorescent foci at positions internal to the cell poles, perhaps indicating failed or inhibited septation. There was no difference between cells exposed to 1× or 5× MIC MMC. In combination, these observations supported the hypothesis that elongated filaments represented individual mother cells which, despite remaining metabolically active and retaining the capacity for chromosomal replication, were incapable of completing cell division through several cycles of growth and DNA replication.

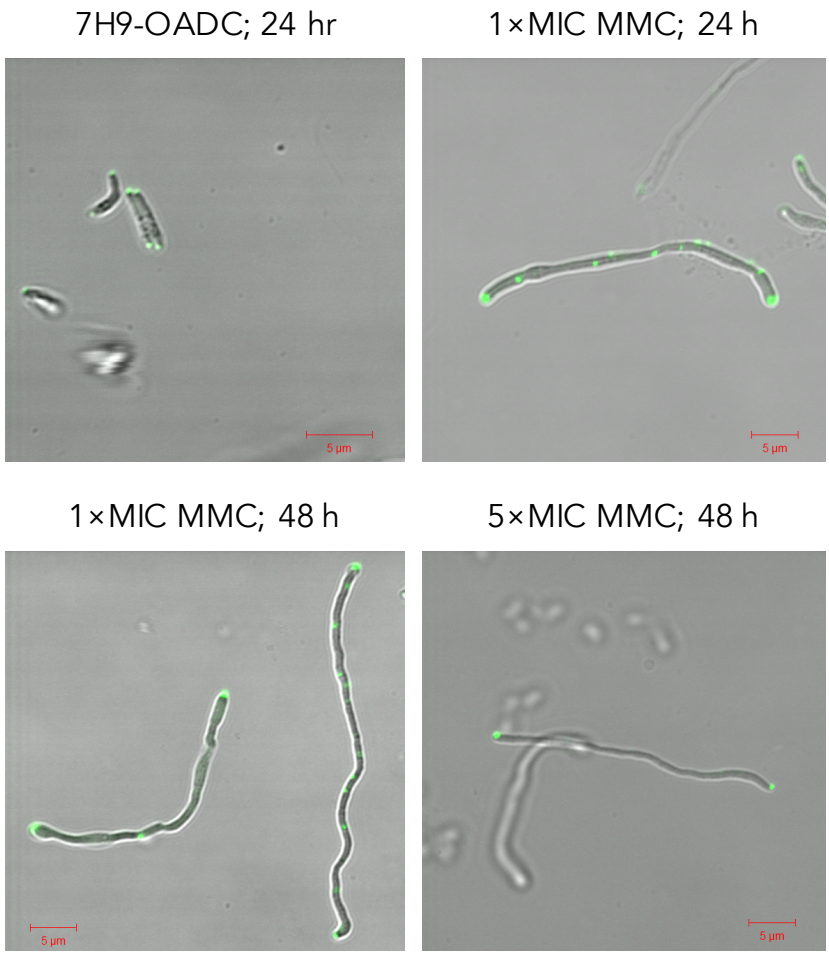

Figure 3-16 | Cell elongation phenotype of individual bacilli expressing *wag31-gfp*
Visualization of *wag31-gfp* after growth for 24 or 48 h in the absence and presence of 1× and 5× MIC MMC. Micrographs represent green fluorescence overlayed onto phase contrast images. Scale bars represent 5 µm.

3.3. Multiple ImuB Foci Form During Prolonged Genotoxic Stress in Elongated Bacilli

The observation that individual cells could elongate in excess of 10 times their normal lengths during genotoxic stress raised the possibility that this filamentous state might be associated with the development of multiple mutasome foci – in turn, suggesting the opportunity for recombination between differentially mutated genomes during periods of genotoxic stress. For this purpose, *mCherry-dnaN*::PSOS(*imuA'*)-*egfp-imuB* was exposed to inhibitory concentrations of MMC (1× and 5× MIC) for 24 h before being

visualised using a confocal fluorescent microscope (**Figure 3-17**). As before, it was evident that the bacilli grew in length but failed to divide under applied genotoxic stress. In addition, it was evident that all elongated cells contained multiple foci comprising overlapping EGFP-ImuB and MCherry-DnaN signals. Additionally, when exposed to sub-inhibitory concentrations (0.25× MIC) of MMC for 6 h, *mCherry-dnaN*::PSOS(*imuA'*)-*egfp-imuB* bacilli exhibited multiple foci as well (data not shown). This result indicated that the mutasome assembled during exposure to sub-inhibitory and inhibitory concentrations of MMC. Therefore, it is possible that the function of the mutasome contributes to the survival of the cell when exposed to sub-inhibitory levels of genotoxic

Figure 3-17 | Multiple mutasome foci develop in response to prolonged genotoxic stress in *Msm*
Visualization of a *mCherry-dnaN*::PSOS(*imuA'*)-*egfp-imuB* bacillus after growth for 24 h in the presence of 1× MIC MMC. Micrograph represents green (EGFP-ImuB) and red (MCherry-DnaN) fluorescence overlayed onto phase contrast. Scale bar represents 5 µm.

stresses, and aids in preserving cell viability when exposed to inhibitory concentrations by maintaining chromosome integrity. However, it was evident that the dynamics of the mutasome and replication machinery in *Msm* needed to be studied in more detail over the course of smaller time intervals to determine if there was a correlation between foci number and cell length or treatment duration. Nonetheless, multiple replication fork-associated ImuB foci appeared to develop within individual, elongated bacilli when exposed to genotoxic compounds for extended periods of time.

4. The Effect of Different Genotoxic Stressors on ImuB Recruitment

The antibiotic effect of MMC is mediated by inter-strand cross-linking of genomic DNA caused by the formation of covalent bonds between the compound and the component nucleotides (Papavinasasundaram, *et al*., 2001). To test whether the observed EGFP-ImuB foci formed exclusively as a response to this specific type of DNA lesion, or if ImuB was commonly recruited to other types of DNA damage, *mCherry-dnaN*::PSOS(*imuA'*)-*egfp-imuB* was treated with the MIC of various compounds that have been reported to impact bacterial DNA metabolism in different ways. The specific focus was on mutagenic compounds or antibiotics known to inhibit DNA replication (**Table 3-2**). These included:

(i) 4-nitroquinoline 1-oxide (NQO), which has been shown to cause transversions in *Escherichia coli* (*E. coli*) (Fronza, *et al*., 1992). Although the associated hydroxydeoxyguanosine nucleotides have been reported to be repaired by nucleotide excision repair (NER) mechanisms, NQO was included to evaluate if the mycobacterial mutasome was involved in the response to this type of damage.

Table 3-2 | Expression of EGFP-ImuB foci following exposure of *Msm* to various genotoxins

Compound	MIC equivalent in *Msm*	Reference	ImuB foci	Foci with MMC
NQO	20 mM	Warner, *et al*. (2010)	Yes	Yes
MMS	0.1 %	Stephanou, *et al*. (2007)	Yes	Yes
CIP	1.25 µg/ml	Naran, unpublished	Yes	Yes
EtBr	6.25 µg/ml	Rodrigues, *et al*. (2011)	No	No
NVB	8.0 µg/ml	Naran, unpublished	No	Yes
GRS	4.5 µg/ml	Jungmann, unpublished	No	No

NQO, 4-nitroquinoline 1-oxide; MMS, methyl methanesulfonate; CIP, ciprofloxacin; EtBr, ethidium bromide; NVB, novobiocin; GRS, griselimycin.

(ii) Methyl methanesulfonate (MMS) methylates specific nitrogen atoms in purine bases, thereby inhibiting DNA replication by alkylation and was included in this experiment (Beranek, 1990; Lundin, *et al*., 2005).

(iii) Ciprofloxacin (CIP) is a second-generation quinolone that was included in this experiment as the compound functions by inhibiting DNA gyrase and topoisomerase IV, which consequently inhibits DNA replication (Drlica and Zhao, 1997; Pommier, *et al*., 2010).

(iv) Ethidium bromide (EtBr) is an intercalating agent that is thought to cause DNA deformations and cause mutations in *Salmonella enterica* serovar Typhimurium (*S. typhimurium*) following the breakdown of the compound into various metabolites (Waring, 1965; McCann, *et al*., 1975; Rodrigues, *et al*., 2011).

(v) Novobiocin (NVB) is a coumarin class antibiotic that inhibits GyrB function without triggering the classic fluoroquinolone (FLQ)-induced SOS response in *Staphylococcus aureus* (*S. aureus*) (Schröder, *et al*., 2012) and mycobacteria (Chatterji, *et al*., 2001; Chopra, *et al*., 2012).

(vi) The recently described DnaN (β clamp) inhibitor, griselimycin (GRS) (Kling, *et al*., 2015), was also included to test the effect of β clamp inhibition on the recruitment of ImuB to the replication fork.

For ease of comparison, all agents were exposed to *mCherry-dnaN*::PSOS(*imuA'*)-*egfp-imuB* at 1× MIC for 4 h before the cells were imaged using an epifluorescent microscope (data not shown). Foci were detected following treatment with NQO, MMS, and CIP while GRS induced expression of EGFP-ImuB and MCherry-DnaN without foci formation, indicating that these four compounds were capable of inducing the mutagenic DNA repair pathway in *Msm*; however, GRS exposure did not induce clearly defined foci formation while NQO and CIP did not induce foci as abundant as previous MMC experiments. As a control to prevent false-negatives, cultures were exposed to 1× MIC MMC in addition to the compound of interest to determine if exposure of the cells to any of the test compounds prevented expression and recruitment of EGFP-ImuB. It was notable that GRS treatment prevented EGFP-ImuB foci formation during MMC co-treatment. Of the compounds that did not result in EGFP-ImuB foci formation, NVB did not prevent mutasome formation as a function of MMC co-treatment. Conversely, only EtBr prevented the formation of foci in the presence of MMC. This result may indicate that EtBr is extremely toxic to *Msm*, as highly toxic antibiotic levels have been associated with little or no transcriptional remodeling in *Saccharomyces cerevisiae* (Fry, *et al*., 2005). Thus, in this case, the bacilli may have been rapidly killed by the effect of EtBr prior to expression of EGFP-ImuB. It should be noted, though, that these results were tentative, but did suggest the potential value in investigation GRS further.

4.1. Investigation into the Effect of GRS on ImuB Recruitment

As GRS was the only compound tested to show induction of the SOS response and failure to form EGFP-ImuB foci in the presence of MMC, it was decided to

investigate this novel antibiotic further. The GRS compound and its pharmacologically more stable analog, cyclohexyl-griselimycin, were reported to be bactericidal in *Mtb* (Kling, *et al.*, 2015). Therefore, to validate that GRS had a similar effect on *Msm*, a kill-kinetic assay was conducted on WT mc^2155 (**Figure 3-18a**). Following enumeration of surviving cells following exposure to 1× or 5× MIC GRS over time, it was evident that, after 48 h of exposure, there was a 2-$\log_{10}$ reduction in cell viability, indicating that GRS was in fact weakly bactericidal to *Msm* (Kaur, *et al.*, 2009). Having illustrated similar effects of GRS on *Msm*, and due to the demonstrated inhibition of the replicative DnaN by GRS (Kling, *et al.*, 2015), the effect of this drug on the recruitment of ImuB in *Msm* was evaluated. To achieve this, Δ*imuB*::PSOS(*imuA'*)-*egfp-imuB* was exposed to 2× MIC GRS for 4 h and imaged by epifluorescence microscopy to visualise EGFP-ImuB expression and recruitment. The micrograph of Δ*imuB*::PSOS(*imuA'*)-*egfp-imuB* exposed to GRS (**Figure 3-18b**, right panel) indicated expression of EGFP-ImuB (as observed by the increased green fluorescence detected within bacilli). Furthermore, GRS appeared to prevent EGFP-ImuB focus formation as seen during MMC exposure (**Figure 3-18b**, middle panel). This result was further validated in Δ*imuB*::PSOS(*imuA'*)-*mEos4a-imuB* exposed to 5× MIC GRS for 8 h and imaged by superresolution 3D-iPALM (**Figure 3-18c**). Here, the lack of high-density fluorophore signal and the presence of evenly distributed, cell-wide signal indicated that MEos4a-ImuB was not recruited to DnaN during exposure to GRS. These results established that GRS exposure appears to prevent recruitment of ImuB to the β clamp despite induction of P(*imuA'*).

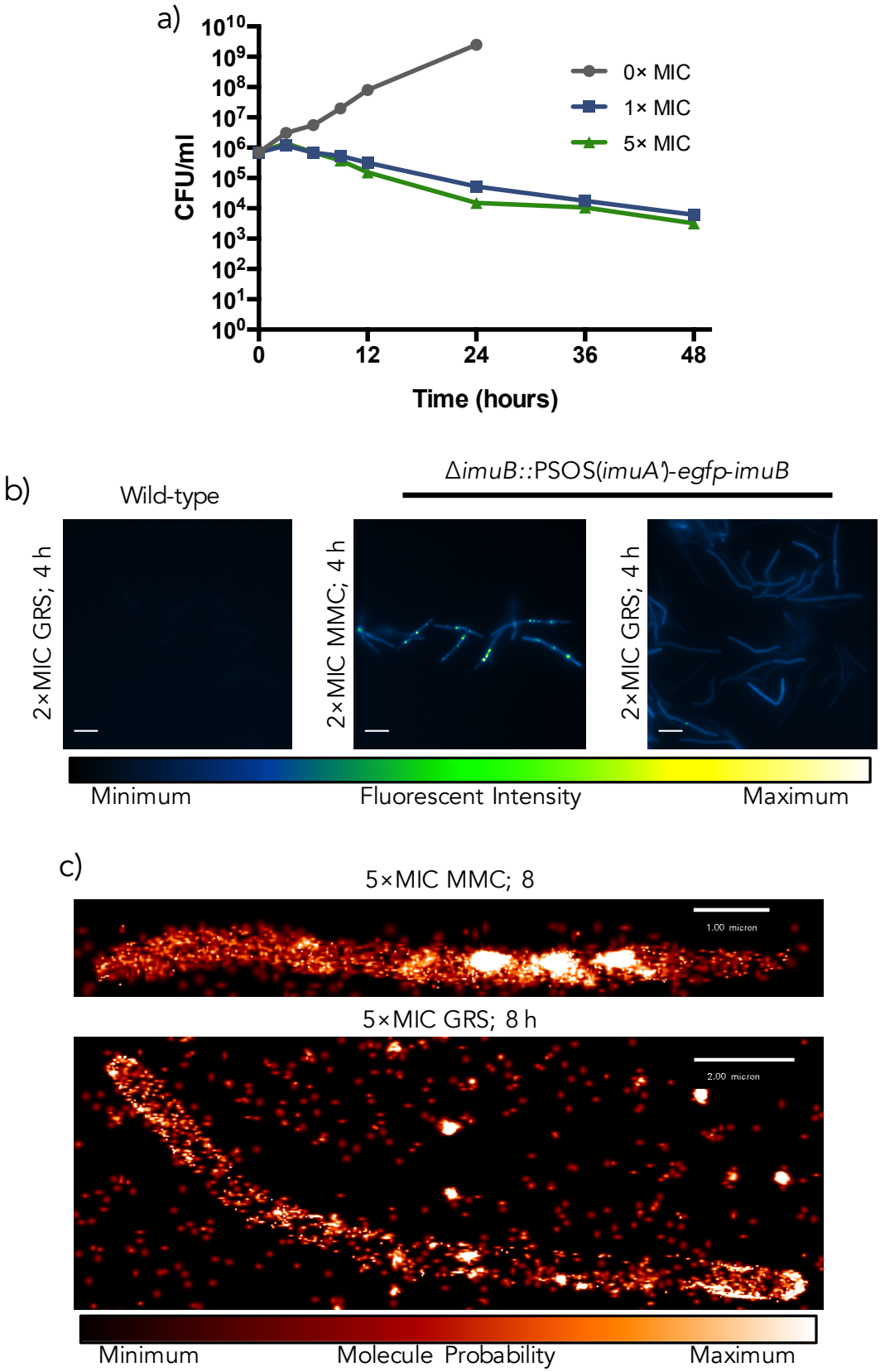

Figure 3-18 | GRS inhibits EGFP-ImuB foci formation
(a) Kill kinetics of GRS in *Msm*. Cell viability of WT growin in the presence of 0× (grey), 1× (blue), and 5× (green) MIC GRS over time was determined. GRS was determined to be slightly bactericidal in *Msm* as

Figure 3-18 | Continued
cultures exposed to inhibitory concentrations of GRS had reduced numbers of viable cells over time. (b) GRS does not induce EGFP-ImuB foci formation. Cultures of *Msm* were imaged using fluorescence microscopy. WT exposed to GRS (left) exhibited no fluorescence. The experimental Δ*imuB*::PSOS(*imuA'*)-*egfp-imuB* strain exhibited green fluorescent foci when exposed to 2× MIC MMC (middle) but failed to produce a similar phenotype when exposed to 2× MIC GRS (right). Scale bar represents 5 μm. (c) 3D-iPALM imaging identified that, despite formation of MEos4a-ImuB foci following exposure of Δ*imuB*::PSOS(*imuA'*)-*mEos4a-imuB* to 5× MIC MMC (top), the same strain did not produce high-density fluorophore signal that could be interpreted as MEos4a-ImuB foci when exposed to 5× MIC GRS for 8 h (bottom). Intensity bar represents the Total Molecule Probability and ranges from minimum (black) to maximum (white) red fluorophore molecules/nm^2.

4.2. Co-treatment with GRS and MMC or Moxifloxacin

As GRS was shown not to be inherently mutagenic while also indicating a capacity to prevent ImuB foci formation in *Msm* during MMC co-exposure, it was hypothesized that GRS may be able to prevent ImuB recruitment and interaction with DnaN. In order to test this hypothesis, a combination assay was developed such that two DNA damaging agents – MMC and the clinically relevant antibiotic, moxifloxacin (MOX) – were co-administered with GRS. The assay was constructed such that each compound could be administered to *mCherry-dnaN*::PSOS(*imuA'*)-*egfp-imuB* in two-dimensional combination at sub- (0.2× MIC) and supra- (5× MIC) inhibitory concentrations. This experimental set-up allowed for direct visual observation of the effect different concentrations of the genotoxic agent had on EGFP-ImuB foci formation in the presence of different concentrations of GRS. Following exposure of bacilli to the drug combinations for 4 h, green and red epifluorescent images were acquired for each experimental condition (**Figure 3-19**). The bacilli exposed to no compound exhibited no expression of EGFP-ImuB, as previously observed. As expected, bacilli exposed only to MMC (at either concentration) exhibited the development of green fluorescent EGFP-ImuB foci indicating recruitment of ImuB to DnaN.

Notably, MOX exposure alone also induced the formation of EGFP-ImuB foci at both concentrations, consistent with the result of CIP and the known capacity of FLQ drugs to induce an SOS response (Cirz, *et al.*, 2007; O'Sullivan, *et al.*, 2008). Furthermore, increased cell-wide red fluorescence was also detected in these cells – potentially as a result of increased expression of *mCherry-dnaN* due to collapsed replication forks. When imaging cells exposed solely to 0.2× MIC GRS, EGFP-ImuB foci were observed in the majority of cells. Similarly, bacilli exposed to either concentration of MMC or MOX in addition to 0.2× MIC GRS exhibited a similar phenotype of EGFP-ImuB foci formation in greater than 50 % of cells. In contrast, all bacteria exposed to inhibitory concentrations (5× MIC) of GRS exhibited cell-wide green fluorescence and the absence of clearly defined EGFP-ImuB foci, regardless of the type or concentration of the co-exposed genotoxic compound. Furthermore, MCherry-DnaN foci were also absent in all cells exposed to 5× MIC of GRS. As above, it was notable that all cells exposed to MOX (regardless of concentration) showed increased levels of whole-cell, red fluorescent signal, suggesting highly induced expression of *dnaN* under FLQ treatment.

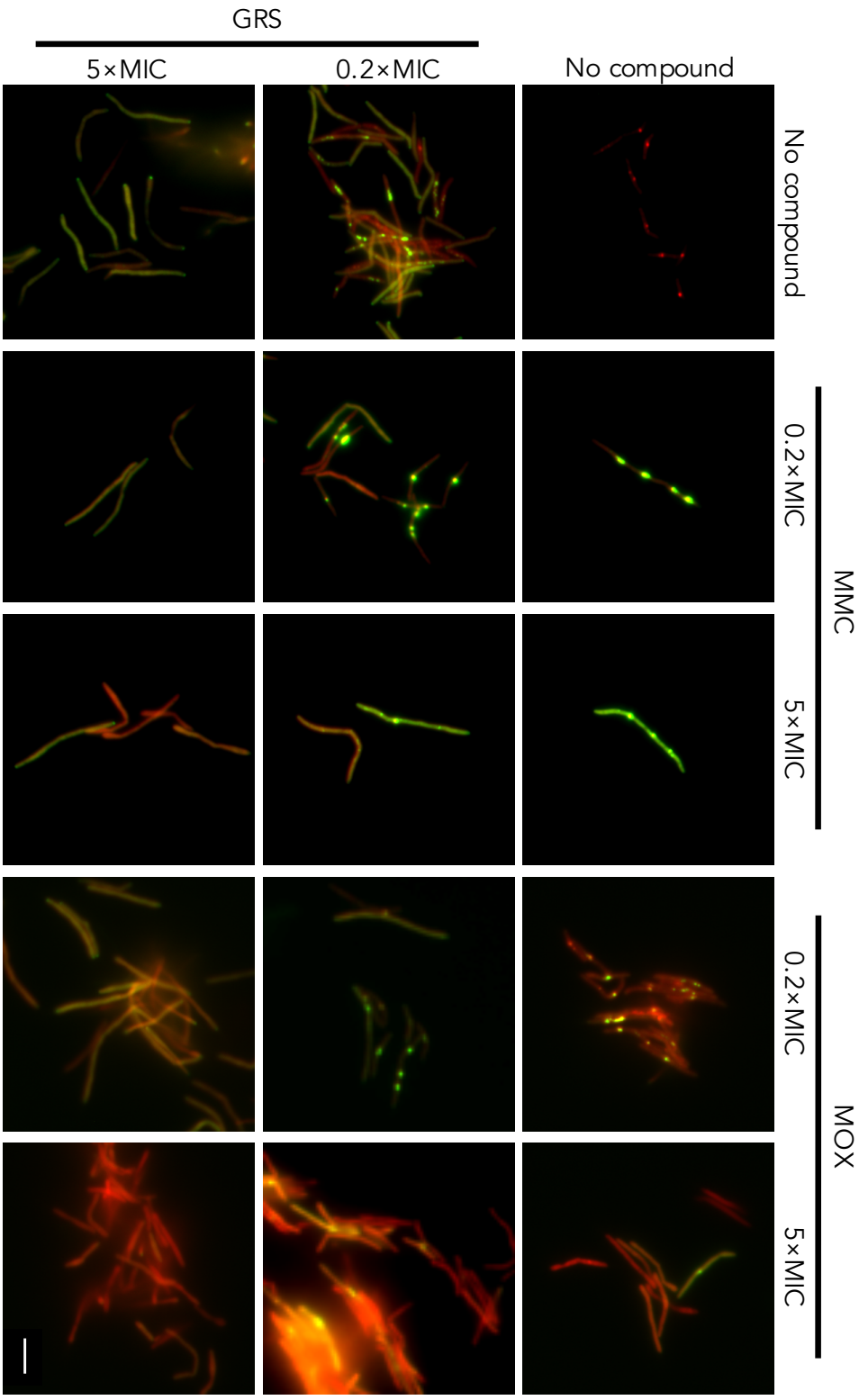

Figure 3-19 | Combination assay microscopy
Different concentrations of MMC or MOX and GRS were administered to *mCherry-dnaN*::PSOS(*imuA'*)-*egfp-imuB* cells prior to imaging with fluorescence microscopy. Green EGFP-ImuB and red DnaN-MCherry fluorescent foci are not evident in cells exposed to inhibitory concentrations (5× MIC) of GRS – regardless of the presence of a secondary compound. Furthermore, cells exposed solely to MOX (0.2× and 5× MIC) induced formation of EGFP-ImuB foci, indicating potential mutasome-mediated mutagenesis as a result of MOX exposure. Scale bar represents 5 μm.

5. References

Aldridge BB, Fernandez-Suarez M, Heller D, Ambravaneswaran V, Irimia D, Toner M, Fortune SM. (2012) Asymmetry and aging of mycobacterial cells lead to variable growth and antibiotic susceptibility. *Science* 335(6064):100-4

Beranek DT. (1990) Distribution of methyl and ethyl adducts following alkylation with monofunctional alkylating agents. *Mutat. Res.* 231, 11–30

Boshoff HIM, Mizrahi V. (2000) Expression of Mycobacterium smegmatis Pyrazinamidase in Mycobacterium tuberculosis Confers Hypersensitivity to Pyrazinamide and Related Amides. *J. Bacteriol*. 182(19):5479-85

Boshoff HIM, Reed BR, Barry III CE, Mizrahi V. (2003) DnaE2 polymerase contributes to in vivo survival and the emergence of drug resistance in Mycobacterium tuberculosis. *Cell* 113:183–193

Chatterji M, Unniraman S, Mahadevan S, Nagaraja V. (2001) Effect of different classes of inhibitors on DNA gyrase from Mycobacterium smegmatis. *J. Antimicrob. Chemother.* 48(8):479-485

Chopra S, Matsuyama K, Tran T, Malerich JP, Wan B, Franzblau SG, Lun S, Guo H, Maiga MC, Bishai WR, Madrid PB. (2012) Evaluation of gyrase B as a drug target in Mycobacterium tuberculosis. *J. Antimicrob. Chemother.* 67(2):415-421

Cirz RT, Jones MB, Gingles NA, Minogue TD, Jarrahi B, Peterson SN, Romesberg FE. (2007) Complete and SOS-mediated response of Staphylococcus aureus to the antibiotic ciprofloxacin. *J. Bacteriol.* 189(2):531-9

Cole ST, Brosch R, Parkhill J, Garnier T, Churcher C, Harris D, Gordon SV, Eiglmeier K, Gas S, Barry III CE, Tekaia F, Badcock K, Basham D, Brown D, Chillingworth T, Connor R, Davies R, Devlin K, Feltwell T, Gentles S, Hamlin N, Holroyd S, Hornsby T, Jagels K, Krogh A, McLean J, Moule S, Murphy L, Oliver K, Osborne J, Quail MA, Rajandream M-A, Rogers J, Rutter S, Seeger K, Skelton J, Squares R, Squares S, Sulston JE, Taylor K, Whitehead S, Barrell BG. (1998) Deciphering the biology of Mycobacterium tuberculosis from the complete genome sequence. *Nature* 393:537-544

Cormack BP, Valdivia RH, Falkow S. (1996) FACS-optimized mutants of the green fluorescent protein (GFP). *Gene* 173:33-38

Davis EO, Dullaghan EM, Rand L. (2002) Definition of the Mycobacterial SOS box and use to identify LexA-regulated genes in Mycobacterium tuberculosis. *J. Bacteriol.* 184:3287–3295

Drlica K, Zhao X. (1997) DNA Gyrase, Topoisomerase IV, and the 4-Quinolones. *Microbiol. Mol. Biol. Rev.* 61(30:377-392)

Fronza G, Campomenosi P, lannone R, Abbondandolo A. (1992) The 4-nitroquinoline 1-oxide mutational spectrum in single stranded DNA is characterized by guanine to pyrimidine transversions. *Nucleic Acids Res*. 20(6):1283-7

Fry RC, Begley TJ, Samson LD. (2005) Genome-Wide Responses to DNA-Damaging Agents. *Annu. Rev. Microbiol.* 59:357–77

Gordon RE, Smith MM. (1953) RAPIDLY GROWING, ACID FAST BACTERIA I.: Species' Descriptions of Mycobacterium phlei Lehmann and Neumann and

Mycobacterium smegmatis (Trevisan) Lehmann and Neumann. *J. Bacteriol*. 66(1):41

Jungmann K, Naran K, Mizrahi V, Müller R, Warner DF. (Unpublished) (2016) The effect of griselimycin on DNA metabolism. *University of Cape Town*

Kaur P, Ghosh A, Krishnamurthy RV, Bhattacharjee DG, Achar V, Datta S, Narayanan S, Anbarasu A, Ramaiah S. (2015) A high-throughput cidality screen for Mycobacterium tuberculosis. *PLOS One* 10(2):e0117577

Kling A, Lukat P, Almeida DV, Bauer A, Fontaine E, Sordello S, Zaburannyi N, Herrmann J, Wenzel SC, König C, Ammerman NC, Barrio MB, Borchers K, Bordon-Pallier F, Brönstrup M, Courtemanche G, Gerlitz M, Geslin M, Hammann P, Heinz DW, Hoffmann H, Klieber S, Kohlmann M, Kurz M, Lair C, Matter H, Nuermberger E, Tyagi S, Fraisse L, Grosset JH, Lagrange S, Müller R. (2015) Targeting DnaN for tuberculosis therapy using novel griselimycins. *Science* 348(6239):1106-1112

Krämer CE, Wiechert W, Kohlheyer D. (2016) Time-resolved, single-cell analysis of induced and programmed cell death via non-invasive propidium iodide and counterstain perfusion. *Sci. Rep*. 6:32104

Lundin C, North M, Erixon K, Walters K, Jenssen D, Goldman ASH, Helleday T. (2005) Methyl methanesulfonate (MMS) produces heat-labile DNA damage but no detectable in vivo DNA double-strand breaks. *Nucleic Acids Res.* 33(12):3799-3811

McCann J, Choi E, Yamasaki E, Ames BN. (1975) Detection of carcinogens as mutagens in the Salmonella/microsome test: assay of 300 chemicals *Proc. Natl. Acad. Sci. USA* 72(12):5135-5139

Naran K, Mizrahi V, Warner DF. (Unpublished) (2015) Minimum inhibitory concentrations of genotoxic agents. *University of Cape Town*

O'Sullivan DM, Hinds J, Butcher PD, Gillespie SH, McHugh TD. (2008) Mycobacterium tuberculosis DNA repair in response to subinhibitory concentrations of ciprofloxacin. *J. Antimicrob. Chemother.* 62(6):1199-202

Paez-Segala MG, Sun MG, Shtengel G, Viswanathan S, Baird MA, Macklin JJ, Patel R, Allen JR, Howe ES, Piszczek G, Hess HF, Davidson MW, Wang Y, Looger LL. (2015) Fixation-resistant photoactivatable fluorescent proteins for CLEM. *Nat. Methods* 12:215-218

Papavinasasundaram KG, Anderson C, Brooks PC, Thomasa NA, Movahedzadehb F, Jenner PJ, Colston MJ, Davis EO. (2001) Slow induction of RecA by DNA damage in Mycobacterium tuberculosis. *Micorbiology* 147:3271–3279

Pommier Y, Leo E, Zhang H, Marchand C. (2010) DNA Topoisomerases and Their Poisoning by Anticancer and Antibacterial Drugs. *Chem. Biol.* doi:10.1016/j.chembiol.2010.04.012

Reiche MA, Gopinath K, Mizrahi V, Warner DF. (Unpublished) (2013) Mini-thesis project: Generation of Venus Fluorescent Protein-tagged ImuA'-expressing vector. *University of Cape Town*

Rodrigues L, Ramos J, Couto I, Amaral L, Viveiros M. (2011) Ethidium bromide transport across Mycobacterium smegmatis cell-wall: correlation with antibiotic resistance. *BMC Microbiol.* 11:35

Rubin-Delanchy P, Burn GL, Griffié J, Williamson DJ, Heard NA, Cope AP, Owen DM. (2015) Bayesian cluster identification in single-molecule localization microscopy data. *Nat. Methods* 12(11):1072

Santi I, Dhar N, Bousbaine D, Wakamoto Y, McKinney JD. (2013) Single-cell dynamics of the chromosome replication and cell division cycles in mycobacteria. *Nat. Commun.* 4:2470

Santi I, McKinney JD. (2015) Chromosome Organization and Replisome Dynamics in Mycobacterium smegmatis. *MBio* 6(1):e01999-14

Schröder W, Goerke C, Wolz C. (2012) Opposing effects of aminocoumarins and fluoroquinolones on the SOS response and adaptability in Staphylococcus aureus. *J. Antimicrob. Chemother.* 68(30):529-538

Shtengel G, Galbraith JA, Galbraith CG, Lippincott-Schwartz, Gillette JM, Manley S, Sougrat R, Waterman CM, Kanchanawong P, Davidson MW, Fetter RD, Hess HF. (2009) Interferometric fluorescent super-resolution microscopy resolves 3D cellular ultrastructure. *Proc. Natl. Acad. Sci. USA* 106(9):3125-3130

Stephanou NC, Gao F, Bongiorno P, Ehrt S, Schnappinger D, Shuman S, Glickman MS. (2007) Mycobacterial Nonhomologous End Joining Mediates Mutagenic Repair of Chromosomal Double-Strand DNA Breaks. *J. Bacteriol.* 189(14):5237-5246

Waring MJ. (1965) Complex formation between ethidium bromide and nucleic acids. *J. Mol. Biol.* 13(1):269-282

Warner DF, Ndwandwe DE, Abrahams GL, Kana BD, Machowski EE, Venclovas C, Mizrahi V. (2010) Essential roles for imuA′- and imuB-encoded accessory factors in DnaE2-dependent mutagenesis in Mycobacterium tuberculosis. *Proc. Natl. Acad. Sci. USA* 107:13093–13098

6. Supplementary Results

6.1. Previous Validation of VFP-ImuA′ Function

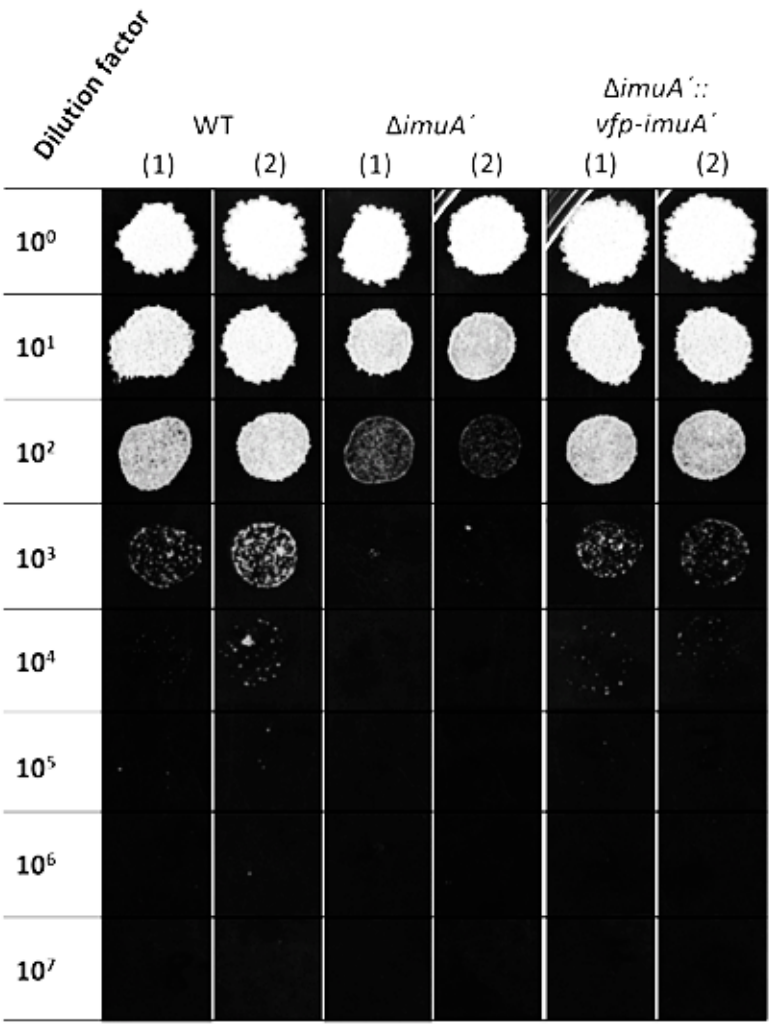

Supplementary Figure S1 | DNA damage tolerance of Δ*imuA*′::*vfp-imuA*′
The photographs indicate the growth of *Msm* colonies (white) on 0.02 and 0.04 µg/ml MMC-containing media (black) after serial dilution. The spotting order of each dilution factor is 10^0 to 10^7 from top to bottom. Figure is replicated from Reiche, *et al*. (unpublished).

6.2. Effect of Increased Inhibitory Concentrations of MMC on *Msm* Cell Length

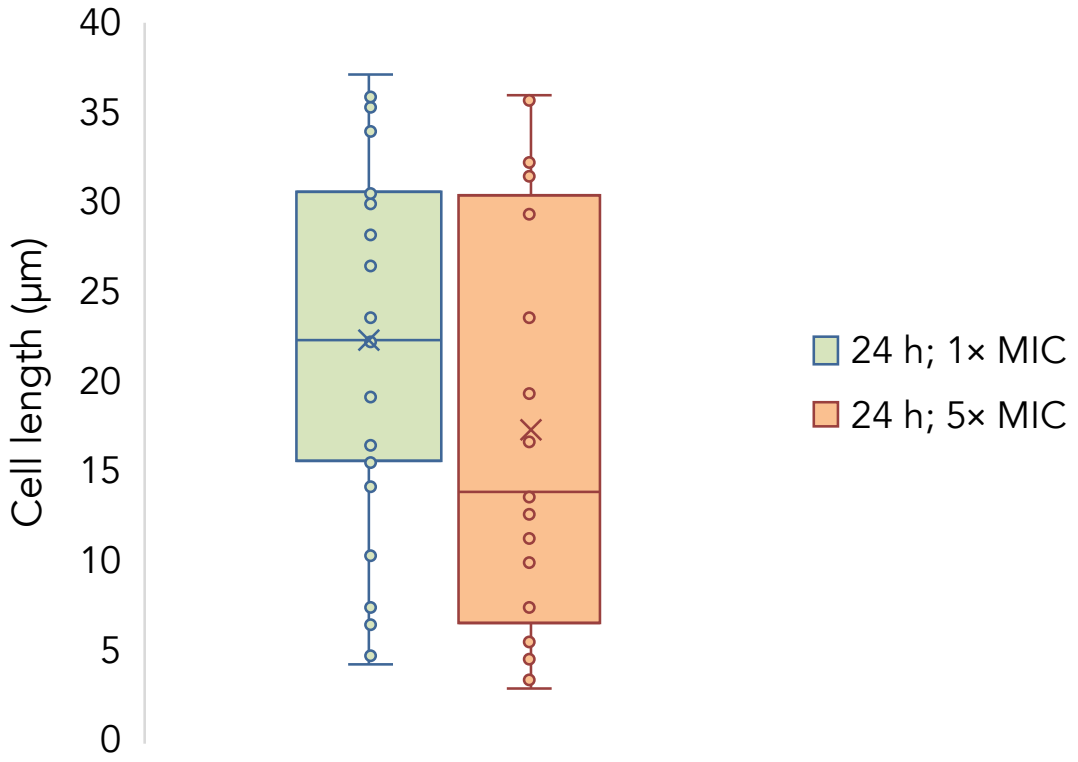

Supplementary Figure S2 | Comparison of the effect of supra-inhibitory concentrations of MMC on cell length following 24 h of exposure
The two-tailed *P*-value equals 0.1138; therefore, the difference between 1× and 5× is not statistically significant.

6.3. Statistical Data of P(*imuA'*) Flow Cytometric Analyses

Supplementary Table S1 | Stats and data from time response flow cytometry

Time	5 min	15 min	30 min	1 h	2 h	4 h	6 h	12 h
n	6	6	6	6	6	6	6	6
Minimum	126	120	129	231	626	1400	1770	1129
Lower Quartile	127.5	125.3	132.8	236.3	652.3	1441	1837	1275
Median	129.5	129.5	140.5	241.5	668.5	1516	1917	1435
Upper Quartile	135.3	134.3	146.8	248.3	690.8	1527	2231	1668
Maximum	142	135	155	258	705	1532	2364	2056
Mean	131.3	129.2	140.5	242.5	669.2	1490	2002	1486
SD	5.715	5.636	8.961	9.006	26.45	52.32	226.6	315
SEM	2.333	2.301	3.658	3.677	10.8	21.36	92.5	128.6
Lower 95% CI of mean	125.3	123.3	131.1	233	641.4	1435	1764	1155
Upper 95% CI of mean	137.3	135.1	149.9	252	696.9	1545	2240	1817

Supplementary Table S2 | Stats and data from dose response flow cytometry

Dose (× MIC)	0.0001	0.001	0.01	0.05	0.1	1	5	10	100
n	6	6	6	6	6	6	6	6	6
Minimum	140	135	179	369	594	1400	1482	1163	118
Lower Quartile	142.3	141.8	179	425.3	637.5	1441	1482	1174	120.3
Median	144	147.5	194	470.5	680.5	1516	1561	1338	127.5
Upper Quartile	145.3	154.3	200.3	516.3	740.3	1527	1617	1383	133
Maximum	146	161	216	568	768	1532	1694	1455	136
Mean	143.7	147.8	192.8	470.2	684.3	1490	1562	1305	127
SD	2.16	8.612	13.63	65.34	63.3	52.32	79.01	113.1	7.043
SEM	0.8819	3.516	5.564	26.68	25.84	21.36	32.26	46.19	2.875
Lower 95% CI of mean	141.4	138.8	178.5	401.6	617.9	1435	1479	1186	119.6
Upper 95% CI of mean	145.9	156.9	207.1	538.7	750.8	1545	1645	1424	134.4

CHAPTER IV: DISCUSSION

Table of Contents: **Page**

List of Figures: **Page**

1. Overview

Previous work based predominantly on genetic approaches had established that inducible mutagenesis in mycobacteria is mediated by the ImuA', ImuB, and DnaE2 proteins (Boshoff, *et al.*, 2003; Warner, *et al.*, 2010). Together, it is thought that these proteins function as part of a single pathway, with yeast two-hybrid (Y2H) interaction data suggesting the potential for protein-protein interactions (PPIs) between the components (**Figure 1-3**). The working model, therefore, predicted ImuB as central adapter protein, which facilitates access of ImuA' and DnaE2 to the chromosome via its essential interaction with the β clamp (**Figure 1-5**). Although suggesting some similarities in component complexity with *Escherichia coli* (*E. coli*) Pol V (Jiang, *et al.*, 2009), this model remained skeptical, with multiple unanswered questions when compared to that of the model organism system. For example, it was unknown if the mutasome proteins co-localized or interacted within mycobacterial bacilli. Furthermore, the regulatory dynamics dictating stoichiometry, timing, and activity of the putative mutasome complex are not understood. While DnaE2 is postulated to perform nucleotide polymerization, the functional role of the accessory proteins ImuA' and ImuB remained unexplored. Overall, the understanding of the mycobacterial mutasome has previously been limited to genetic observations and required new insight to support the mycobacterial mutasome model.

While the aim of this study was to investigate the PPIs predicted between each component of the mycobacterial mutasome, many aspects of the mycobacterial mutasome model have been reinforced including the predicted DnaN-ImuB PPI, which was directly observed by the co-recruitment of ImuB and DnaN foci

(**Figure 3-11**). This identified ImuB as the central adapter component of the mutasome in *Mycobacterium smegmatis* (*Msm*) and highlighted the necessity to further investigate the protein at the center of the mycobacterial mutasome and the potential to inhibit similar PPI in an effort to restrict the mutagenic capacity of mycobacteria. Indeed, it was observed that the novel antitubercular drug griselimycin (GRS) was able to prevent recruitment of ImuB to DnaN (**Figure 3-18**), paralleling genetic inhibition of the DnaN-ImuB binding interface (**Figure 3-13**; and Warner, *et al.*, 2010). Furthermore, the insights into the molecular dynamics of the mutasome supported a hypothesis for the swapping of replicative and mutagenic DNA polymerase systems at the site of the replication fork; while other evidence presented in this work raises the intriguing possibility of a highly adaption-mediating environment during genotoxic stress as a result of the interplay between mutagenic DNA repair and cell division inhibition in mycobacteria (**Figure 3-17**).

2. Regulatory Dynamics of the *imuA'* Promoter During Genotoxic Stress

The genes encoding *imuA'* and *imuB* constitute a predicted two-gene operon under the regulation of a single SOS box (Davis, *et al.*, 2002). The *imuA'* promoter, P(*imuA'*), was used to drive expression of enhanced green fluorescent protein (EGFP) with the aim of establishing if it was suitable for use in constructing fluorescently labelled variants of ImuB in addition to providing an EGFP-only control to compare to EGFP-ImuB. Quantification by flow cytometry of the green fluorescence generated by EGFP proved useful for determining the regulatory dynamics of P(*imuA'*). Here, the response of *Msm* to mitomycin C (MMC) was robust with the majority of cells exposed to inhibitory conditions of MMC exhibiting levels of green fluorescence above

that of untreated bacilli. Moreover, it was observed that EGFP expression (as determined by fluorescence intensity) corresponded to both the duration (**Figure 3-4**) and concentration (**Figure 3-5**) of MMC exposure. Notably, maximal expression of EGFP was attained at MMC concentrations corresponding to cell growth inhibition. It appeared, therefore, that inhibition of growth by genotoxins such as MMC occurred subsequent to maximal induction of the responding repair mechanisms (*i.e.*, the SOS response, which includes the mutasome). Expression in this scenario may be limited by factors such as the rate of RecA activation, formation of a steady state between LexA repressor degradation and synthesis, or saturation of DNA damage. Regardless, the result of the PSOS(*imuA'*)-*egfp* transcriptional reporter suggested that the inhibitory effect of MMC occurred as a consequence of a failure to repair extensive DNA damage, which resonates with observations in *E. coli* that identified a correlation between DNA damage and activity of SOS gene promoters (Friedman, *et al.*, 2005).

The response of *Msm* to genotoxic stress was rapid, with induction of *imuA'* gene expression detected within the first hour following exposure to MMC. Although the initial response at 1 h was only 12.1 % of the maximal expression (at 6 h), it indicated that an initial response to inhibitory concentrations of DNA damage occurred within one generation time (~3 h) (Aldridge, *et al*., 2012; Santi, *et al*., 2013). As the rate of diffusion or uptake of MMC across the mycobacterial cell membrane is not known, it is possible that this delayed maximal induction of *imuA'* (occurring at 2 generation times) represented an accumulation of MMC over time, resulting in increased DNA damage over time (Friedman, *et al.*, 2005), in addition to a potential delay caused by RecA/LexA regulation

dynamics which delayed induction of PSOS(*imuA'*)-*egfp* (Kamenšek, *et al.*, 2010; Schnarr, *et al.*, 1991). The decrease in fluorescence signal observed after cells were exposed to 1× minimum inhibitory concentration (MIC) MMC for longer than 6 h might be the result of two factors: (i) MMC is known to be relatively unstable and precipitate in culture media over time (Beijne, *et al.*, 1990), therefore the decrease in PSOS(*imuA'*) induction may represent degradation of MMC beyond 6 h; or (ii) during extended experimental time periods, cell division is more likely to occur stochastically, resulting in a decrease in total fluorescence signal per measured cytometric event as two daughter cells effectively inherit half the total fluorescence signal of the mother cell. This second possibility is supported by the increased variation within each sample as the standard deviation (SD) increased from 8.96 arbitrary fluorescence units (AFU) at 30 min to 315.0 AFU at 12 h (**Chapter III**, **Supplementary Table S1**) indicating a large variation in the EGFP levels of each cell at 12 h. The increase in event variation is likely dependent to a greater extent on time than signal magnitude, as the maximal variation observed in the dose-dependent study was not as large, with a SD of 113.1 AFU (**Chapter III**, **Supplementary Table S2**).

An important caveat to acknowledge here, however, is that these results only represent induction and expression of *imuA'*. The other component genes of the mutasome, *imuB* and *dnaE2*, may be controlled by additional transcriptional and post-translational regulatory processes, one of which may be mediated by ImuA' itself. At the transcript level, there is already a disparity between the level of induction for *Mycobacterium tuberculosis* (*Mtb*) *imuA'* and *imuB*, which exhibited a 32-times and 80-times increase in transcript level, respectively, 6 h

post ultraviolet (UV) irradiation (Warner, *et al.*, 2010). This suggests the existence of unknown, differential regulatory systems controlling the transcription of each open reading frame (ORF) of the *imuA'-imuB* operon, further contributing to the complexity of the mycobacterial mutasome. Moreover, there exists the possibility of post-translational regulation of any mutasome component – as seen with the sub-cellular sequestration of Pol V within *E. coli* (Robinson, *et al.*, 2015), the requirement of ATP as a co-factor for Pol V function (Jiang, *et al.*, 2008), and post-translational processing of UmuD (Nohmi, *et al.*, 1988) – which may further contribute to the complexity surrounding function and regulation of the mutasome. The total extent of regulatory mechanisms controlling expression of the mutasome and how this regulation affects the function of the complex and mutational load remains unknown and warrants further investigation.

3. Visualising the Mutasome in Live Bacilli: the Role of ImuB and ImuA'

Overall, the fluorescent tagging of individual mutasome components was successful. The addition of the fluorescent tag to ImuA' in the Δ*imuA'*::*vfp-imuA'* mutant appeared not to interfere with mutasome function, phenocopying wild-type (WT) mc^{2}155 in both induced mutagenesis (**Figure 3-6**) and DNA damage tolerance assays (**Chapter III**, **Supplementary Figure S1**). In contrast, Δ*imuB*::PSOS(*imuA'*)-*egfp-imuB* exhibited an 'uncoupled' phenotype: the inducible mutagenesis capacity of the strain was retained whereas damage survival (as measured by growth on solid medium containing MMC) was impaired (**Figure 3-7**). The reason for the apparent uncoupling of inducible mutagenesis and DNA damage repair is unclear but may be explained by the respective assays employed. The former is tested by

challenging bacilli with a single dose of UV irradiation to induce DNA damage; while the latter is assayed by exposing *Msm* to MMC for the duration of the experiment. This means that during periods of extended DNA damage (such as 3 to 5 days), the Δ*imuB*::PSOS(*imuA'*)-*egfp*-*imuB* bacilli were not able to consistently and repeatedly repair the lesions caused by MMC. Although it is possible that the EGFP domain of the complementing hybrid protein may have restricted the function of the mutasome, the observed restoration of mutagenic capacity suggested that this uncoupling resulted from dysregulation of *egfp*-*imuB* in contrast to the native *imuB* gene, which is the second ORF of the *imuA'*-*imuB* operon (Warner, *et al.*, 2010). As noted above, the promoter of PSOS(*imuA'*)-*egfp*-*imuB* consisted solely of *imuA'* upstream elements and did not include all potential promoter elements of *MSMEG_1622* (*imuB*) found within *MSMEG_1620* (*imuA'*) (**Figure 3-1**). This may render the bacterium unable to consistently express the appropriate levels of (EGFP-)ImuB required to endure the extended presence of MMC. In addition to this, the stability of EGFP-ImuB relative to ImuB might be a factor contributing to the decreased DNA damage tolerance of Δ*imuB*::PSOS(*imuA'*)-*egfp*-*imuB*, though this requires further investigation. Quantitative, reverse transcription (qRT-)PCR is warranted for future investigations to determine if *egfp*-*imuB* transcript levels are comparable to WT *imuB* transcript levels during a time-course experiment following exposure of bacilli to MMC. This approach will also enable an evaluation of the potential impact of the additional EGFP-encoding sequence on the stability of the transcript or if promoter sequences were inadvertently disrupted during the design of the construct, therefore accounting for the susceptibility of Δ*imuB*::PSOS(*imuA'*)-*egfp*-*imuB* to MMC in solid media over prolonged periods. Furthermore, an alternative method should be considered

when evaluating MMC-sensitivity in future experiments: MIC determinations of different reporter strains of *Msm* could be used to highlight more accurately the difference in sensitivities to MMC in both solid and liquid media.

The observed inducible mutagenesis of Δ*imuB*::PSOS(*imuA'*)-*egfp*-*imuB* nevertheless suggested that EGFP-ImuB retained sufficient functional activity to warrant microscopic visualization and analysis of the protein within live cells. These analyses revealed that EGFP-ImuB localized to specific regions or 'foci' within each bacillus (**Figure 3-8**). In contrast, the VFP-ImuA' protein was seen to disperse throughout the mycobacterial cell. The differential localization patterns of VFP-ImuA' and EGFP-ImuB during inducible mutagenesis may indicate differing functions: ImuB was previously predicted to serve as an adapter protein, providing structural support to enable access of ImuA' and DnaE2 to the replication fork through its own β clamp binding capacity, while the weak homology of ImuA' to RecA implied the potential for an analogous DNA scanning function to identify specific markers of DNA damage. It may also reveal a difference in binding time of each respective protein within the mutasome complex. If the binding time of VFP-ImuA' with the mutasome complex is lower than the exposure time of the microscope camera, the protein will be observed to disperse throughout the cell. Furthermore, as ImuB is predicted to function as a 'hub protein' within the mutasome complex (Warner, *et al.*, 2010), it is likely that it would have a greater binding time and be detected as 'foci' – as observed in this study. However, there is the possibility that the discrepancy of ImuA'-ImuB localization is indicative of differing functions. In this regard, the evidence presented in this study suggested that ImuB maintained a central role within the mutasome. In contrast, the location of VFP-

ImuA′ suggested that the protein contributed to mutagenic DNA repair by means of a more transient function – potentially requiring only short-lived interactions with other proteins or DNA. The cell-wide dispersal of ImuA′ may indicate that the protein functions as part of a mutasome regulation mechanism and operates in multiple regions of a bacillus: either sensing DNA damage or performing post-translational regulation of the system. Both of these regulatory possibilities are supported by the homology shared between the mycobacterial ImuA′ and RecA (Warner, *et al.*, 2010; Galhardo, *et al.*, 2005). However, it must be pointed out that ImuA′ was not required for localization of EGFP-ImuB (**Figure 3-12**), indicating that ImuA′ is not required for post-translational processing of ImuB. Again, the caveat exists that, in this study, EGFP-ImuB was expressed under control of a non-native promoter and perhaps ImuA′ is capable of regulating the genetically linked *imuB* gene. This hypothesis is supported by the differential increase in transcript levels of *imuA′* and *imuB* in *Mtb* mentioned previously (Warner, *et al.*, 2010). In a final scenario, ImuA′ may function as a cell architecture regulator, similar in function to the more distant homologue SulA (Galhardo, *et al.*, 2005), which inhibits cell division as part of the SOS response; however, all speculation into the function of ImuA′ requires future investigation. These latter possibilities suggest that ImuA′ is potentially not a component of the mutasome. Indeed, the data presented in this thesis do not support any inference of specific sub-cellular localization of ImuA′. However, it is not possible to rule out definitely the possibility that ImuA′ is incorporated into the mutasome. Further work is required to determine the exact composition of the mutasome and, moreover, whether it does comprise multiple proteins in addition to ImuB and DnaE2.

In contrast to ImuA', this study did afford new insight into the function of ImuB. When visualized together with the labelled β clamp (**Figure 3-11**), it was evident that both EGFP-ImuB and MCherry-DnaN were recruited to the same location within *Msm*. Previous Y2H evidence suggested an interaction between ImuB and DnaN (Warner, *et al.*, 2010), and the microscopy data presented here appeared to support the inferred PPI. This conclusion is reinforced by the observation that alteration of the putative β clamp binding domain within ImuB in EGFP-ImuB^{AAAAG} prevented foci formation via association with DnaN (**Figure 3-13**). In turn, this suggests that ImuB enables access of the other mutasome components (particularly DnaE2) to the replication fork, explaining its essentiality for mutagenic DNA repair. Again, this is supported by observations that DnaE2, which possesses DNA polymerase function, does not contain a β clamp binding domain (Warner, *et al.*, 2010). Therefore, the function of ImuB has been identified as contributing to the structural formation of the mutasome complex through the interaction with DnaN and a putative interaction with the DnaE2 polymerase (**Figure 4-1**). However, the exact reason ImuB fulfills this role, as well as the evolutionary consequence thereof, is not known and requires further study. It is intriguing to postulate that the primary role of ImuB is to out-compete other polymerases for access to the β clamp at stalled replication forks. This can further explain the greatly increased transcript levels of *imuB* in *Mtb* observed following UV damage (Warner, *et al.*, 2010), which may be required to out-compete other polymerases such as DnaE1 and DinB during genotoxic stress. This notion is further supported by the recent observation that different polymerases 'share' access to the replication fork through the rapidly successive binding of replicative and mutagenic polymerases in *E. coli* (Zhao, *et al.*, 2017; Beattie, *et al.*, 2017). In this vein, a high

concentration of ImuB proteins might be required to ensure temporal out-competition of (stalled) polymerases and overall function of the mutasome during periods of genotoxic stress (**Figure 4-1**).

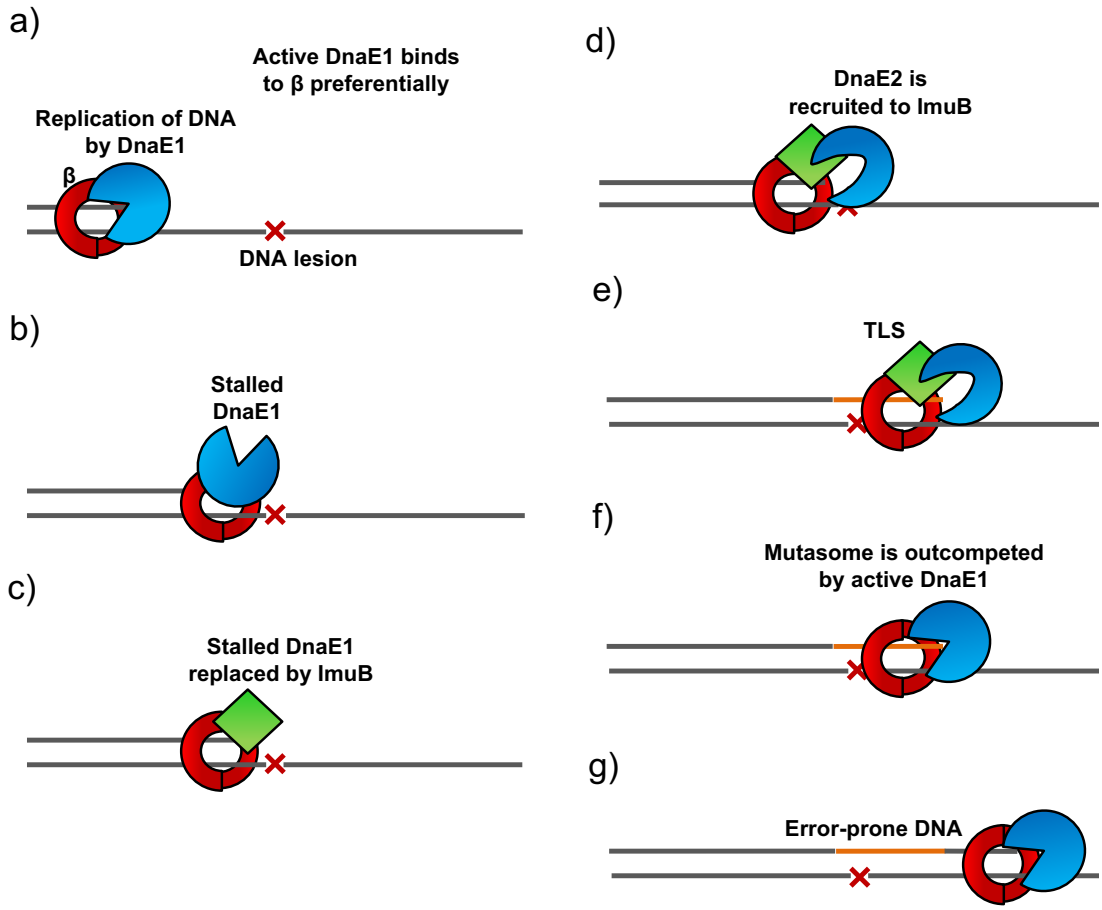

Figure 4-1 | Model for recruitment of the mycobacterial mutasome
The schematic representation of the predicted mutasome model illustrates how the mycobacterial mutasome might assemble and function. (a) DnaE1 preferentially binds to the β-clamp and polymerizes DNA under normal circumstances. (b) DnaE1 is unable to synthesize DNA opposite DNA lesions and the replication fork stalls. (c) The stalled replicative DnaE1 is unstable and replaced by the more abundant ImuB. (d) Once ImuB has bound to the β-clamp, DnaE2 is able to bind to ImuB. (e) The fully formed mutasome complex is able to perform translesion DNA synthesis (TLS) across the DNA lesion, producing error-prone DNA. (f) The actively progressing mutasome is outcompeted by DnaE1. (g) The replicative DnaE1 resumes chromosome replication. This model is supported by observations in the recent publication Zhao, *et al.* (2017).

Furthermore, the theorized scaffold (or adapter) function of ImuB can be compared to another Y family polymerase found in eukaryotes, Rev1, which is also postulated to perform an essential, non-catalytic, structural role during TLS across 6-4 thymine photodimers (Nelson, *et al.*, 2000; Haracska, *et al.*, 2001; Otsuka, *et al.*, 2005; Kuang, *et al.*, 2013). Although Rev1 has catalytic activity and functions by inserting cytosine nucleotides opposite abasic sites during DNA repair (Nelson, *et al.*, 1996), this activity is not required for TLS function of Rev3/7 (Pol ζ). Instead, Rev1 is thought to interact with other catalytic polymerases (such as Pol ζ) through the BRCA1 C-terminal (BRTC) and C-terminal domains of Rev1 (Acharya, *et al.*, 2005; D'souza and Walker, 2006; Kikuchi, *et al.*, 2012), thereby enabling effective TLS strand extension (Budzowska, *et al.*, 2015). If a comparable situation indeed occurs between ImuB and DnaE2 during mutagenic DNA repair in actinobacteria, this may indicate a propensity for polymerase swapping – a phenomenon that itself warrants investigation at the molecular level. The evidence for the Rev1-essentiality in TLS sets a molecular and evolutionary precedent for the theory of the mycobacterial mutasome, whereby ImuB provides the 'landing pad' required for the recruitment of the catalytically active DnaE2 polymerase. Furthermore, the Rev1- and ImuB-adapter models, although comprised of non-related proteins, may provide insight into the evolution of DNA metabolism pathways (specifically those involved in TLS), in turn, helping identify potential PPIs to guide rational drug design.

Although moxifloxacin (MOX) is known to cause double-stranded DNA breaks by the inhibition of DNA gyrase (Mduli and Ma, 2007; Reece and Maxwell, 1991), evidence presented in this work has identified that ImuB (and potentially

the whole mutasome) is recruited during MOX exposure (**Figure 3-19**). This result suggests that the DNA lesion associated with MOX might also be repaired by the TLS mechanism of the mycobacterial mutasome, which contradicts the model proposed in this thesis. However, the exact reason for induction of PSOS(*imuA'*)-*egfp-imuB* and recruitment of EGFP-ImuB is unknown and may be a result of either direct repair of the MOX-induced double-stranded break by the mutasome or subsequent correction of previously repaired intermediate DNA adducts formed by other repair processes. To investigate this further, qRT-PCR experiments are required to confirm that all three component genes of the mutasome are up-regulated in WT *Msm* during MOX exposure. Furthermore, it is necessary to determine if the frequency of EGFP-ImuB foci following MOX exposure is comparable to that following MMC exposure. In this regard, it is possible that the contribution to overall DNA repair of double-stranded breaks is less than that of DNA cross-linked lesions or occurs with different timing.

4. Genotoxic Stress Induces Dysregulated Bacterial Cell Fission and Growth

In addition to inducing repair mechanisms, the *E. coli* SOS response is also known to include cell division inhibitors such as MinC and SulA (Justice, *et al.*, 2000). Indeed, when *Msm* was exposed to MMC for prolonged periods of time, a cell filamentation phenotype was observed (**Figure 3-14** and **Figure 3-15**). After 4 h of exposure to MMC, approximately 50 % of *Msm* bacilli exhibited cell lengths greater than 98 % of cells grown in standard 7H9 liquid broth. Similarly, after 24 hours, 79 % of cells exhibited inhibited cell division with a population mean length of 19.5 μm. This indicated that, although cell division

was inhibited during MMC-exposure, cell growth continued uninterrupted at a linear rate of approximately 2.4 μm per generation time. Additionally, this growth appeared to be accompanied by completion of genome replication – as suggested by the formation of multiple ImuB-DnaN foci in single filamentous bacilli (**Figure 3-16** and **Figure 3-17**) – potentially providing an opportunity for accelerated micro-evolution. Avenues exploring bacilli filamentation are well merited as *Mtb* has been observed to exhibit a filamentous phenotype during infection of macrophages (Chauhan, *et al.*, 2006; Caire-Brändli, *et al.*, 2014), indicating that this is an infection-relevant phenotype and that cell division-inhibiting conditions do occur *in vivo*. Future experiments may benefit from using membrane stains such as Nile Red (Strahl, *et al.*, 2014), 4-*N*,*N*-dimethylamino-1,8-naphthalimide-trehalose conjugates (Kamariza, *et al.*, 2017), or fluorescent D-alanine analogs (Botella, *et al.*, 2017); these would prove very useful for discerning septa formation in elongated cells – providing the clarity to identify filamented cells by the absence of labelled septa.

Genotoxic stress results in an increased number of mutations in *Msm* through the induction of the mycobacterial mutasome (Boshoff, *et al.*, 2003; Warner, *et al.*, 2010). In addition to this, MMC exposure resulted in the dysregulation of cell division, possibly leading to the presence of multiple, differentially-mutated chromosomes within individual bacilli (**Figure 3-17**). This scenario may result in accelerated evolution through the recombination of genes and chromosomal regions, resulting in the duplication (or deletion) of DNA previously repaired by the error-prone mutasome (**Figure 4-2**). Notably, multiple chromosomes within filamentous bacilli will be differentially (and randomly) mutated, allowing for recombination events to result in unique

combinations of mutations. The possibility of such events occurring as a response to genotoxic stress has been alluded to previously in *E. coli* (Bos, *et al.*, 2015).

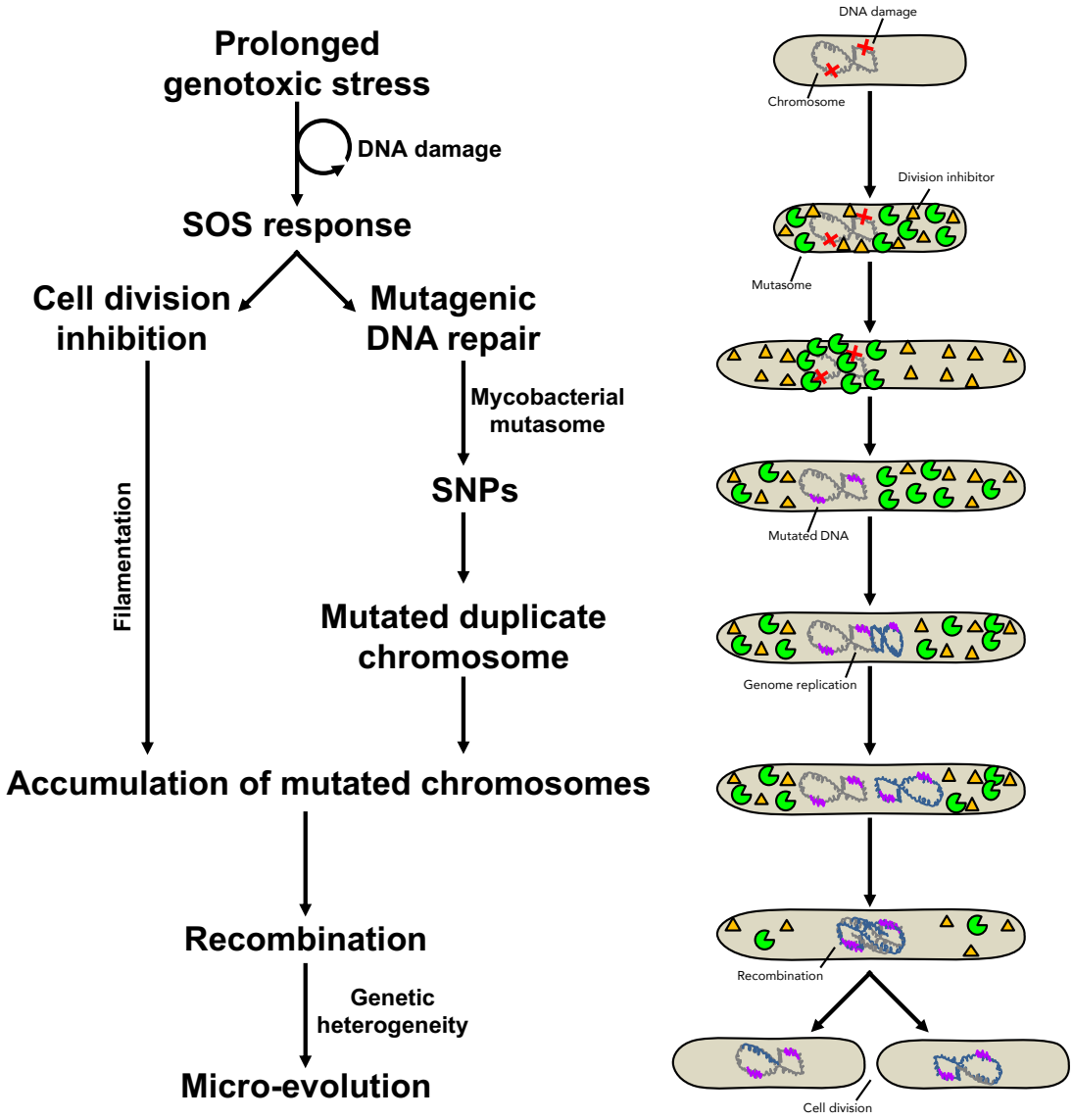

Figure 4-2 | The pathway to genotoxic stress-induced micro-evolution in bacteria
The flow diagram on the left represents the series of events that may contribute to the micro-evolution of mycobacteria during prolonged genotoxic stress. The flow diagram on the right illulstrates the processes that occur during this time in mycobacterial bacilli as part of chromosome replication and cell division. The two primary contributors to genetic diversity are the introduction of SNPs as a funtion of the mutasome as well as the potential recombination of accumulated chromosomes as a function of cell division inhibition.

Filamentation may represent an important survival response in pathogenic bacteria (reviewed by Justice, *et al.*, 2008, 2014). In this work, it is hypothesized that this phenotype has the potential to generate polyploidy, which is a commonly observed occurrence amongst bacteria (Soppa, 2017). The phenomenon of polyploidy is thought to facilitate evolution during cell division inhibition in bacteria (Van der Peer, *et al.*, 2017) and has been observed to facilitate adaptation in yeast (Selmecki, *et al.*, 2015). In addition to this, a recent study by Sun and colleagues has identified that in *E. coli,* multi-fork chromosome replication (which results in polyploidy) causes phenotypic delay whereby the presence of multiple different, mutant alleles of the same gene contribute to the success of the mutant phenotype by minimising the deleterious effect of the mutation – thereby reducing mutational load of the mutation in the short-term (Sun, *et al.*, 2018). Notably, multi-fork replication has been recently observed in mycobacteria (Trojanowski, *et al.*, 2017). Additionally, polyploidy may contribute to the survival of bacteria by acting as a phosphorus storage mechanism (Zerulla, *et al.*, 2014).

The exact contribution of polyploidy to the evolution of bacteria remains to be further elucidated; however, this phenomenon is likely able to contribute to the evolution of drug resistance (Bos, *et al.*, 2015). Therefore, it remains an unanswered question as to whether the development of transient polyploidy during filamentation (and the resolution of multiple chromosomes) in *Mtb* contributes to evolution of the genome and development of drug resistance during infection. At a basic level, it is not known how filamentation affects viability of the resultant daughter cells, nor how effectively these daughter cells are resolved during division of the filamented mother cell. Furthermore, the

potential for polyploidy occurring highlights an important risk associated with chemotherapeutics that cause DNA damage, such as the fluoroquinolones (FLQs), whereby the rate of drug resistance development increases as a result of the mechanism of action (Malik, *et al.*, 2012; Mo, *et al.*, 2016) – likely as a result of the induction of the SOS response as seen in *E. coli* (Cirz, *et al.*, 2005). Therefore, it is of great interest to investigate new anti-tuberculosis (TB) agents that are capable of restricting micro-evolution-promoting mechanisms during chemotherapy treatment (Reiche, *et al.*, 2017).

5. GRS-mediated Inhibition of DnaN Prevented Functional Interaction with ImuB

The natural product compound GRS is reported to be bactericidal in *Mtb* (Kling, *et al.*, 2015). In line with this observation, the compound was also found to be bactericidal in *Msm*, resulting in a 2-$\log_{10}$ reduction in culturable bacilli in 48 h. GRS inhibits DNA replication by blocking the hydrophobic pocket located between DnaN subdomains II and III (Kling, *et al.*, 2015) responsible for polymerase binding and recruitment (denoted "sub-site 1" by Burnouf, *et al.*, 2004, and "hydrophobic channel on the surface of the β-clamp," by Bunting, *et al.*, 2003). In particular, this hydrophobic cleft is noted as being important for the recruitment of TLS polymerases in *E. coli*, making GRS an attractive compound to investigate. Indeed, when Δ*imuB*::PSOS(*imuA'*)-*egfp-imuB* bacilli were exposed to GRS, it was notable that EGFP-ImuB did not form clearly defined foci as produced during MMC exposure (**Figure 3-18**), indicating that the protein was not recruited as previously observed. Importantly, the diffuse, cell-wide fluorescence observed in GRS-exposed ImuB-EGFP-expressing cells was indistinguishable from the phenotype of the mutant Δ*imuB*::PSOS(*imuA'*)-

egfp-imuB^{AAAAG} strain following MMC exposure (**Figure 3-13**). This suggested that chemical inhibition of the PPI between DnaN and ImuB had a similar effect on the recruitment of ImuB to the genetic disruption of the ImuB β clamp binding site. Given that the WT QLPLWG motif of ImuB was reported as essential for the function of the mutasome (Warner, *et al.*, 2010), it can be reasoned that GRS-mediated inhibition of ImuB recruitment to DnaN will result in the similar abrogation of mutasome function and inducible mutagenesis in mycobacteria; although, similar results need to be reproduced in other species of mycobacteria – particularly *Mtb*.

Although the mechanism of action that prevented ImuB recruitment to DnaN can only be postulated at this point, it is likely that this occurred as a result of competitive binding of GRS to the binding domain located on the surface of DnaN. This could potentially result in the steric occlusion of ImuB and interference of the mutasome-essential interaction. It seems very likely that this renders the mutasome unable to function and results in the absence of inducible mutagenesis in the presence of inhibitory concentrations of GRS; however, demonstrating this effect was extremely challenging. GRS is bactericidal (**Figure 3-18a**; and Kling, *et al.*, 2015), therefore it proved problematic to determine whether a decrease in mutation frequency in the presence of the compound (as measured by the survival of rifampicin (RIF)-resistant mutants following UV irradiation) was a result of mutasome inhibition or simply cell death caused by GRS. As a result of this complexity, GRS-mediated inhibition of mutasome function remains purely theoretical and requires further investigation to validate. It is important to highlight that, at sub-inhibitory concentrations, GRS did not prevent recruitment of EGFP-ImuB

in the presence of MMC but, conversely, on its own induced mutasome recruitment at 0.2× MIC. Therefore, it is possible that GRS may induce mutagenic DNA repair at non-inhibitory concentrations. Future investigations need to establish if low concentrations of GRS can cause mutagenesis in the presence or absence of other genotoxic agents. Furthermore, how GRS prevents ImuB recruitment is unknown and requires attention. This work demonstrates that high (inhibitory) concentrations of GRS prevented the functional association between DnaN and ImuB and resulted in the dissociation of ImuB from DnaN – either directly by sterically occluding ImuB by competitive binding to DnaN or indirectly through other, unknown mechanisms.

This work further identified the utility of novel compounds that target the DNA replication and repair machinery and validated the continued study of GRS as an anti-TB therapeutic. With respect to the inhibition of the mycobacterial mutasome, the concept of "anti-evolution" adjuvants has been proposed and investigated before (reviewed by Culyba, *et al.*, 2015; Mo, *et al.*, 2016); however, GRS has a subtle deviation from the standard concept. Although it is hypothesized here that GRS may be able to prevent the function of the mycobacterial mutasome, this is a secondary effect resulting from the inhibition of the essential function of the β clamp. This suggests that resistance mechanisms against the anti-evolution effect of GRS may be different to purely non-lethal adjuvant therapies. Therefore, this sets GRS apart from other proposed non-lethal anti-evolution drugs such as suramin (Nautiyal, *et al.*, 2014), iron(III) phthalocyanine-4,4′,4′′,4′′′-tetrasulfonic acid (Alam, *et al.*, 2016), natural compounds (Bellio, *et al.*, 2017), as well as others (Mo, *et al.*, 2017; Yakimov, *et al.*, 2017). In addition, these other anti-evolution adjuvants function

predominantly by targeting the induction of the SOS response by inhibiting RecA; whereas GRS has the unique potential to specifically prevent mutagenic DNA repair – which also co-incidentally reduces the risk of off-target effects within the human host of *Mtb*. Regardless, the potential reduction of mutational frequency through the disruption of the ImuB-DnaN PPI during GRS treatment warrants further investigation. Specifically, it is imperative to showcase the effect GRS co-treatment has on the development of RIF-resistance in a mouse infection model of TB (as previously performed by Boshoff, *et al.*, 2003) in order to confirm the anti-evolution capacity of the compound. More specifically, genetic disruption of the mycobacterial mutasome was associated with a decrease in both virulence and the development of RIF-resistance in this mouse infection model (Boshoff, *et al.*, 2003); therefore, given the similarities between the genetic disruption of the mutasome and the chemical inhibition of ImuB foci by GRS presented in this work, there is enticing evidence to indicate that GRS may result in a similar suppression of the development of drug resistance of *Mtb* during infection of mice.

6. Conclusion

DNA repair is an important survival mechanism in *Mtb* that may have contributed to the success of *Mtb* as one of the greatest pathogens in history (Hingley-Wilson, *et al.*, 2003). However, the substantial reliance of *Mtb* on DNA repair, often seen as an advantageous self-sufficiency mechanism, may also present a vulnerability. In this vein, there is potential to exploit the non-redundant DNA repair pathways such as the mycobacterial mutasome to prevent the micro-evolution of drug resistance and help maintain the efficacy of currently employed anti-TB chemotherapeutics. The possibility that the

novel antibiotic GRS is capable of restricting mutagenic DNA repair by preventing the assembly of the mutasome on the β clamp (by inhibition of the proven ImuB-DnaN PPI) illustrates vulnerability of the system and encourages further investigation into the inhibition of the mutasome and other DNA repair systems. Of additional interest is the impact of GRS on mutagenesis and short-term evolution of mycobacteria. Moreover, evidence in this work suggests that SOS-mediated cell elongation may contribute to the adaptation of mycobacteria through the recombination of multiple chromosomes during conditions of genotoxic stress. Therefore, GRS presents the unique potential to inhibit a downstream SOS effector response – specifically DNA damage-inducible mutagenic DNA repair – with a bactericidal compound. Investigation into the potential anti-evolutionary capacity of GRS is critical in limiting the development of drug-resistant TB in the future and ensuring the prolonged efficacy of current treatment options.

7. References

Acharya N, Haracska L, Johnson RE, Unk I, Prakash S, Prakash L. (2005) Complex formation of yeast Rev1 and Rev7 proteins: a novel role for the polymerase-associated domain. *Mol. Cell Biol.* 25(21):9734-40

Alam MK, Alhhazmi A, DeCoteau JF, Luo Y, Geyer CR. (2016) RecA inhibitors potentiate antibiotic activity and block evolution of antibiotic resistance. *Cell Chem. Biol.* 23(3):381-91

Aldridge BB, Fernandez-Suarez M, Heller D, Ambravaneswaran V, Irimia D, Toner M, Fortune SM. (2012) Asymmetry and aging of mycobacterial cells lead to variable growth and antibiotic susceptibility. *Science* 335(6064):100-4

Beattie TR, Kapadia N, Nicolas E, Uphoff S, Wollman AJM, Leake MC, Reyes-Lamothe R. (2017) Frequent exchange of the DNA polymerase during bacterial chromosome replication. *eLife* e21763

Beijne JH, Van Gijn R, Underberg WJ. (1990) Chemical stability of the antitumor drug mitomycin C in solutions for intravesical instillation. *PDA J. Pharm. Sci. Technol*. 44(6):332-5

Bellio P, Di Pietro L, Mancini A, Piovano M, Nicoletti M, Brisdelli F, Tondi D, Cendron L, Franceschini N, Amicosante G, Perilli M. (2017) SOS response in

bacteria: Inhibitory activity of lichen secondary metabolites against Escherichia coli RecA protein. *Phytomedicine* 29:11-8

Bos J, Zhang Q, Vyawahare S, Rogers E, Rosenberg SM, Austin RH. (2015) Emergence of antibiotic resistance from multinucleated bacterial filaments. *Proc. Natl. Acad. Sci. USA* 112(1):178-83

Boshoff HIM, Reed BR, Barry III CE, Mizrahi V. (2003) DnaE2 polymerase contributes to in vivo survival and the emergence of drug resistance in Mycobacterium tuberculosis. *Cell* 113:183–193

Botella H, Yang G, Ouerfelli O, Ehrt S, Nathan CF, Vaubourgeix J. (2017) Distinct Spatiotemporal Dynamics of Peptidoglycan Synthesis between Mycobacterium smegmatis and Mycobacterium tuberculosis. *mBio* 8(5):e01183-17

Bunting KA, Roe SM, Pearl LH. (2003) Structural basis for recruitment of translesion DNA polymerase Pol IV/DinB to the β-clamp. *EMBO J.* 22(21):5883-92

Budzowska M, Graham TG, Sobeck A, Waga S, Walter JC. (2015) Regulation of the Rev1–pol ζ complex during bypass of a DNA interstrand cross-link. *EMBO J.* 34(14):1971-85

Burnouf DY, Olieric V, Wagner J, Fujii S, Reinbolt J, Fuchs RP, Dumas P. (2004) Structural and biochemical analysis of sliding clamp/ligand interactions suggest a competition between replicative and translesion DNA polymerases. *J. Mol. Biol.* 335(5):1187-97

Caire-Brändli I, Papadopoulos A, Malaga W, Marais D, Canaan S, Thilo L, de Chastellier C. (2014) Reversible lipid accumulation and associated division arrest of Mycobacterium avium in lipoprotein-induced foamy macrophages may resemble key events during latency and reactivation of tuberculosis. *Infect. Immun.* 82(2):476-90

Chauhan A, Madiraju MV, Fol M, Lofton H, Maloney E, Reynolds R, Rajagopalan M. (2006) Mycobacterium tuberculosis cells growing in macrophages are filamentous and deficient in FtsZ rings. *J. Bacteriol*. 188(5):1856-65

Cirz RT, Chin JK, Andes DR, de Crécy-Lagard V, Craig WA, Romesberg FE. (2005) Inhibition of mutation and combating the evolution of antibiotic resistance. *PLOS Biol.* 3(6):e176

Culyba MJ, Mo CY, Kohli RM. (2015) Targets for combating the evolution of acquired antibiotic resistance. *Biochem*. 54(23):3573-82

D'Souza S, Walker GC. (2006) Novel role for the C terminus of Saccharomyces cerevisiae Rev1 in mediating protein-protein interactions. *Mol. Cell. Biol.* 26(21):8173-82

Davis EO, Dullaghan EM, Rand L. (2002) Definition of the Mycobacterial SOS box and use to identify LexA-regulated genes in Mycobacterium tuberculosis. *J. Bacteriol.* 184:3287–3295

Friedman N, Vardi S, Ronen M, Alon U, Stavans J. (2005) Precise temporal modulation in the response of the SOS DNA repair network in individual bacteria. *PLOS Biol.* 3(7):e238

Galhardo RS, Rocha RP, Marques MV, Menck CFM. (2005) An SOS-regulated operon involved in damage-inducible mutagenesis in Caulobacter crescentus. *Nucleic Acids Res.* 33:2603–2614

Haracska L, Unk I, Johnson RE, Johansson E, Burgers PM, Prakash S, Prakash L. (2001) Roles of yeast DNA polymerases δ and ζ and of Rev1 in the bypass of abasic sites. *Genes Dev.* 15(8):945-54

Hingley-Wilson SM, Sambandamurthy VK, Jacobs WR. (2003) Survival perspectives from the world's most successful pathogen, Mycobacterium tuberculosis. *Nat. Immunol.* 4(10):949-55

Jiang Q, Karata K, Woodgate R, Cox MM, Goodman MF. (2009) The active form of DNA polymerase V is UmuD′2C-RecA-ATP. *Nature* 460:359–363

Justice SS, García-Lara J, Rothfield LI. (2000) Cell division inhibitors SulA and MinC/MinD block septum formation at different steps in the assembly of the Escherichia coli division machinery. *Mol. Microbiol.* 37(2):410-23

Justice SS, Harrison A, Becknell B, Mason KM. (2014) Bacterial differentiation, development, and disease: mechanisms for survival. *FEMS Microbiol. Lett.* 360(1):1-8

Justice SS, Hunstad DA, Cegelski L, Hultgren SJ. (2008) Morphological plasticity as a bacterial survival strategy. *Nat. Rev. Microbiol.* 6(2):162-8

Kamariza M, Shieh P, Rodriguez-Rivera FP, Ealand CS, Chu B, Martinson N, Kana BD, Bertozzi CR. (2017) Detection of live mycobacteria with a solvatochromic trehalose probe for point-of-care tuberculosis diagnosis. *bioRxiv* 171553 [Currently not peer-reviewed]

Kamenšek S, Podlesek Z, Gillor O, Žgur-Bertok D. (2010) Genes regulated by the Escherichia coli SOS repressor LexA exhibit heterogenous expression. *BMC Microbiol.* 10:283

Kikuchi S, Hara K, Shimizu T, Sato M, Hashimoto H. (2012) Structural basis of recruitment of DNA polymerase ζ by interaction between REV1 and REV7 proteins. *J. Biol. Chem.* 287(40):33847-52

Kling A, Lukat P, Almeida DV, Bauer A, Fontaine E, Sordello S, Zaburannyi N, Herrmann J, Wenzel SC, König C, Ammerman NC, Barrio MB, Borchers K, Bordon-Pallier F, Brönstrup M, Courtemanche G, Gerlitz M, Geslin M, Hammann P, Heinz DW, Hoffmann H, Klieber S, Kohlmann M, Kurz M, Lair C, Matter H, Nuermberger E, Tyagi S, Fraisse L, Grosset JH, Lagrange S, Müller R. (2015) Targeting DnaN for tuberculosis therapy using novel griselimycins. *Science* 348(6239):1106-1112

Kuang L, Kou H, Xie Z, Zhou Y, Feng X, Wang L, Wang Z. (2013) A non-catalytic function of Rev1 in translesion DNA synthesis and mutagenesis is mediated by its stable interaction with Rad5. *DNA Repair* 12(1):27-37

Malik M, Chavda K, Zhao X, Shah N, Hussain S, Kurepina N, Kreiswirth BN, Kerns RJ, Drlica K. (2012) Induction of mycobacterial resistance to quinolone class antimicrobials. *Antimicrob. Agents Chemother.* 56(7):3879-87

Mduli K, Ma Z. (2007) Mycobacterium tuberculosis DNA Gyrase as a Target for Drug Discovery. *Infect. Disord. Drug Targets* 7(2):159-168

Mo CY, Culyba MJ, Selwood T, Kubiak JM, Hostetler ZM, Jurewicz AJ, Keller PM, Pope AJ, Quinn A, Schneck JL, Widdowson KL. Inhibitors of LexA autoproteolysis and the bacterial SOS response discovered by an academic-industry partnership. *ACS Infect. Dis.* [e-publication ahead of print] doi: 10.1021/acsinfecdis.7b00122

Mo CY, Manning SA, Roggiani M, Culyba MJ, Samuels AN, Sniegowski PD, Goulian M, Kohli RM. (2016) Systematically altering bacterial SOS activity under stress reveals therapeutic strategies for potentiating antibiotics. *mSphere* 1(4):e00163-16

Nautiyal A, Patil KN, Muniyappa K. (2014) Suramin is a potent and selective inhibitor of Mycobacterium tuberculosis RecA protein and the SOS response: RecA as a potential target for antibacterial drug discovery. *J. Antimicrob. Chemother.* 69(7):1834-43

Nelson JR, Gibbs PE, Nowicka AM, Hinkle DC, Lawrence CW. (2000) Evidence for a second function for Saccharomyces cerevisiae Rev1p. *Mol. Microbiol.* 37(3):549-54

Nelson JR, Lawrence CW, Hinkle DC. (1996) Deoxycytidyl transferase activity of yeast REV1 protein. *Nature* 382(6593):729

Nohmi T, Battista JR, Dodson LA, Walker GC. (1988) RecA-mediated cleavage activates UmuD for mutagenesis: Mechanistic relationship between transcriptional derepression and posttranslational activation. *Proc. Natl. Acad. Sci. USA* 85:1816-1820

Otsuka C, Kunitomi N, Iwai S, Loakes D, Negishi K. (2005) Roles of the polymerase and BRCT domains of Rev1 protein in translesion DNA synthesis in yeast in vivo. *Mutat. Res.-Fund. Mol. M.* 578(1):79-87

Reece RJ, Maxwell A. (1991) DNA Gyrase: Structure and Function. *Crit. Rev. Biochem. Mol. Biol.* 26(3&4):335-375

Reiche MA, Warner DF, Mizrahi V. (2017) Targeting DNA Replication and Repair for the Development of Novel Therapeutics against Tuberculosis. *Front. Mol. Biosci.* 4:75

Robinson A, McDonald JP, Caldas VE, Patel M, Wood EA, Punter CM, Ghodke H, Cox MM, Woodgate R, Goodman MF, van Oijen AM. (2015) Regulation of mutagenic DNA polymerase V activation in space and time. *PLOS Genet.* 11(8):e1005482

Santi I, Dhar N, Bousbaine D, Wakamoto Y, McKinney JD. (2013) Single-cell dynamics of the chromosome replication and cell division cycles in mycobacteria. *Nat. Commun.* 4:2470

Schnarr M, Oertel-Buchheit P, Kazmaier M, Granger-Schnarr M. (1991) DNA binding properties of the LexA repressor. *Biochimie* 73:423-431

Selmecki AM, Maruvka YE, Richmond PA, Guillet M, Shoresh N, Sorenson AL, De S, Kishony R, Michor F, Dowell R, Pellman D. (2015) Polyploidy can drive rapid adaptation in yeast. *Nature* 519(7543):349-52

Soppa J. (2017) Polyploidy and community structure. *Nat. Microbiol*. 2:16261

Strahl H, Bürmann F, Hamoen LW. (2014) The actin homologue MreB organizes the bacterial cell membrane. *Nat. Commun.* 5:3442

Sun L, Alexander HK, Bogos B, Kiviet DJ, Ackermann M, Bonhoeffer S. (2018) Effective polyploidy causes phenotypic delay and influences bacterial evolvability. *PLOS Biol.* 16(2):e2004644

Trojanowski D, Hołówka J, Ginda K, Jakimowicz D, Zakrzewska-Czerwińska J. (2017) Multifork chromosome replication in slow-growing bacteria. *Sci. Rep.* 7:43836

Van de Peer Y, Mizrachi E, Marchal K. (2017) The evolutionary significance of polyploidy. *Nat. Rev. Genet.* 18(7):411-24

Warner DF, Ndwandwe DE, Abrahams GL, Kana BD, Machowski EE, Venclovas C, Mizrahi V. (2010) Essential roles for imuA′- and imuB-encoded accessory factors in DnaE2-dependent mutagenesis in Mycobacterium tuberculosis. *Proc. Natl. Acad. Sci. USA* 107:13093–13098

Yakimov A, Pobegalov G, Bakhlanova I, Khodorkovskii M, Petukhov M, Baitin D. Blocking the RecA activity and SOS-response in bacteria with a short α-helical peptide. *Nucleic Acids Res.* 45(16):9788-96

Zerulla K, Chimileski S, Näther D, Gophna U, Papke RT, Soppa J. (2014) DNA as a phosphate storage polymer and the alternative advantages of polyploidy for growth or survival. *PLOS One* 9(4):e94819

Zhao G, Gleave ES, Lamers MH. (2017) Single-molecule studies contrast ordered DNA replication with stochastics translesion synthesis. *eLife* 6:e32177